Copyright Warning & Restrictions

The copyright law of the United States (Title 17, United States Code) governs the making of photocopies or other reproductions of copyrighted material.

Under certain conditions specified in the law, libraries and archives are authorized to furnish a photocopy or other reproduction. One of these specified conditions is that the photocopy or reproduction is not to be "used for any purpose other than private study, scholarship, or research." If a, user makes a request for, or later uses, a photocopy or reproduction for purposes in excess of "fair use" that user may be liable for copyright infringement,

This institution reserves the right to refuse to accept a copying order if, in its judgment, fulfillment of the order would involve violation of copyright law.

Please Note: The author retains the copyright while the New Jersey Institute of Technology reserves the right to distribute this thesis or dissertation

Printing note: If you do not wish to print this page, then select "Pages from: first page # to: last page #" on the print dialog screen

ABSTRACT

A NONDESTRUCTIVE METHOD FOR THE DETERMINATION OF FRACTURE ENERGY IN CONCRETE STRUCTURES

by
Been-Jyh Yu

It is generally believed that linear elastic fracture mechanics concepts can not be employed in determining fracture parameters in concrete, and therefore most of the current research effort has focused on applying the principles in yielding fracture mechanics. Despite all these efforts, comparison of results reported by many investigators indicate wide variations in fracture toughness values even for essentially similar materials. The main source of discrepancy in the observed results is the existence of a large process zone at the crack tip. Hence, the amount of energy consumed in advancing the crack will depend on the size of the process zone, and in turn on the specimen size.

Based on these considerations, the objective of this study is to develop a methodology for determining the fracture energy, G_f, for concrete-like materials in a non-destructive manner. The method combines the principles of fracture mechanics and maturity (time-temperature effects) on fracture resistance development of concrete. The technique is based on a novel hypothesis in which the fracture parameters are related to the strength gain characteristics of concrete during the hydration process. The concept was examined with cube, cylinder and three different sizes of three-point-bend notched specimens. The range of tested specimens consisted of samples were cured under three different isothermal temperatures(14°C, 23°C and 35°C). The specimens were tested at six ages from 0.25 to 45 days. The hypothesis is verified through inverse determination of thermodynamic characteristics of concrete for the specimen tested.

Based on the theoretical basis and statistical analysis of about three hundred tests, the results show that the activation energies obtained from the three-point bend test and from compressive tests are similar. And results also illustrate that the maturity method may be used to predict the in-place fracture energy of concrete structure based on its thermal history.

A NONDESTRUCTIVE METHOD FOR THE DETERMINATION OF FRACTURE ENERGY IN CONCRETE STRUCTURES

by
Been-Jyh Yu

A Dissertation
Submitted to the Faculty of
New Jersey Institute of Technology
in Partial Fulfillment of the Requirements for the Degree of
Doctor of Philosophy

Department of Civil and Environmental Engineering

January 1995

APPROVAL PAGE

A NONDESTRUCTIVE METHOD FOR THE DETERMINATION OF FRACTURE ENERGY IN CONCRETE STRUCTURES

Been-Jyh Yu

Prof. Farhad Ansari, Dissertation Advisor — Date
Professor of Civil and Environmental Engineering, NJIT

Prof. Paul C. Chan, Committee Member — Date
Professor of Civil and Environmental Engineering, NJIT

Prof. Edward G. Dauenheimer, Committee Member — Date
Professor and Associate Chairman of Civil and Environmental Engineering, NJIT

Associate Prof. James M. Grow, Committee Member — Date
Professor of Chemistry, NJIT

Prof. William R. Spillers, Committee Member — Date
Professor and Chairman of Civil and Environmental Engineering, NJIT

BIOGRAPHICAL SKETCH

Author: Been-Jyh Yu

Degree: Doctor of Philosophy in Civil Engineering

Date: January 1995

Undergraduate and Graduate Education:

- Doctor of Philosophy in Civil Engineering, New Jersey Institute of Technology, Newark, NJ 1995
- Master of Engineering in Civil Engineering (Structures), Manhattan College, Riverdale, New York, 1988
- Bachelor of Science in Civil Engineering, Tamkang University, Taiwan, R.O.C., 1980

Major: Civil Engineering

Presentation and Publication:

Yu, B.J. (1994), "Nondestructive Determination of Fracture Energy in Concrete Structures", Graduate Seminar, Department of Civil and Environmental Engineering, New Jersey Institute of Technology, Newark, New Jersey, November 9.

Yu, B.J. and Ansari, F. (1995), "Method of Theory for Insitu Nondestructive Determination of Fracture Energy in Concrete Structures", submitted for possible publication in ACI Material Journal.

This dissertation is dedicated to my wife Ko-Chia Yu
for her patience, understanding, and encouragement.

ACKNOWLEDGMENT

I wish to express my sincere gratitude to my supervisor, Professor Farhad Ansari, for his guidance, friendship, and constant support throughout this research.

Special thanks are expressed to Professor Paul C. Chan, Professor Edward G. Dauenheimer, Professor James M. Grow and Professor William R. Spillers for serving as members of the thesis committee.

Appreciation is expressed to Mr. Allyn Luke, assistant to the Chairman for Laboratories, Department of Civil and Environmental Engineering, for his assistance in the experiment and a lot of productive suggestions.

I wish to thank Mr. John Eimess, Mr.Zhaowu Zhang, Mr. Rajendra Navlurkar, Mr. Wei Ma, Mr. Charles Bowen, Mr. Fred Kish, Mr. Hector Illescas, Mr. Vito Nigro, Mr. Lee Loke Fung, Mr. Paul Dencky, Mr. Mauricio Cabrera and Mr. Frank Pelizzi for their helps during the experimental program.

Finally, I wish to express my love to my family for their support and encouragement during this study.

TABLE OF CONTENTS

Chapter **Page**

1 INTRODUCTION 1

1.1 General 1

1.2 Objectives 5

2 LITERATURE REVIEW 6

2.1 Fracture Mechanics of Concrete 6

2.1.1 Fictitious Crack Model (FCM) 7

2.1.2 Crack Band Model (CBM) 14

2.1.3 Two-Parameter Fracture Model (TPFM) 17

2.2 Maturity Method 21

2.2.1 Introduction 22

2.2.2 Maturity Functions 24

2.2.2.1 Linear Temperature Function 24

2.2.2.2 Arrhenius Equation 27

2.2.3 The Equivalent Age Approach 28

2.2.4 Summary 29

3 THEORETICAL DEVELOPMENT 32

3.1 Introduction 32

3.2 The Rate Theory 32

3.3 Theoretical Basis 35

TABLE OF CONTENTS
(Continued)

Chapter **Page**

3.3.1 Fracture Energy Gain Function 35

3.3.2 Fracture Energy Function 36

3.3.3 Analytical Development 41

3.3.3.1 Fracture Energy Gain of Concrete 42

3.3.3.2 The Rate Theory and The Fracture Energy Relationship 43

3.3.4 Activation Energy of Concrete 45

3.3.5 Fracture Energy, Strength, and Activation Energy 46

3.3.6 Rate Constant, Limiting Strength, and the Activation Energy 47

4 EXPERIMENTAL PROGRAM 51

4.1 Introduction 51

4.2 Experimental Procedure 52

4.2.1 Materials and Mixture Proportions 52

4.2.2 Specimens Preparation 52

4.2.2.1 Compressive Test Specimen 52

4.2.2.2 Three-Point Bend Beams 53

4.2.3 Specimens Curing Temperature 53

4.2.4 Specimens Temperature Monitoring 55

4.2.5 Test Schedule 56

4.2.6 Three Point Bend Beam Test and Setup 58

TABLE OF CONTENTS
(Continued)

Chapter	Page
5 RESULTS AND DISCUSSIONS	62
5.1 General	62
5.2 Experimental Results	63
5.2.1 Mortar Curbes and Concrete Cylinders	63
5.2.2 Beam Specimens	76
5.3 Analysis of Results	95
5.3.1 Comparison of Fracture Energy Development Parments	95
5.3.1.1 Fracture Energy	99
5.3.1.2 Limiting Fracture Energy	99
5.3.1.3 Rate Constant	99
5.3.1.4 Datum Age	101
5.3.2 Variation of Rate Constant with Temperature	101
5.3.2.1 Datum Temperature	101
5.3.2.2 Activation Energy	103
5.3.3 Relative Fracture Energy Gain	104
6 CONCLUSIONS	105
APPENDIX A DEVELOPMENT OF FRACTURE FUNCTION	109
APPENDIX B EXPERIMENTAL DATA	112
BIBLIOGRAPHY	187

LIST OF TABLES

Tables **Page**

4.1 Beam specimen sizes and corresponding designations 53

4.2.a Mixing water temperatures (°C) for mortar 54

4.2.b Mixing water temperatures (°C) for concrete 55

4.3 Curing temperature and testing age for mortar cubes 58

4.4 Curing temperature and testing age for concrete specimens 59

5.1 Compressive strength - age data for mortar cubes 64

5.2 Compressive strength - age data for concrete cylinders 65

5.3 Analysis of strength-age mortar data to determine limiting strength 68

5.4 Analysis of strength-age concrete data to determine limiting strength 68

5.5 Analysis of strength-age mortar data to determine rate constant 70

5.6 Analysis of strength-age concrete data to determine rate constant 70

5.7 Constants acquired for linear k(T), and Arrhenius functions 73

5.8 Fracture energy - age data for size A 81

5.9 Fracture energy - age data for size B 82

5.10 Fracture energy - age data for size C 83

5.11 Analysis of fracture energy-age data to determine limiting fracture energy for size A 87

5.12 Analysis of fracture energy-age data to determine limiting fracture energy for size B 87

5.13 Analysis of fracture energy-age data to determine limiting fracture energy for size C 87

LIST OF TABLES
(Continued)

Tables **Page**

5.14 Analysis of fracture energy -age data to determine rate constant for size A..... 91

5.15 Analysis of fracture energy -age data to determine rate constant for size B..... 91

5.16 Analysis of fracture energy -age data to determine rate constant for size C..... 91

5.17 Constants of linear k(T) function and Arrhenius function..... 95

5.18 The value of datum temperature published in various references..... 102

5.19 The value of activation energy published in various references..... 103

LIST OF FIGURES

Figure **Page**

2.1 The principles for division of the deformation properties into a σ-ε diagram and σ-ω diagram, where w is the additional deformation due to formation of a fracture zone 8

2.2 The simplified description of the fracture zone as a "fictitious crack" with width w 9

2.3 (a) The fracture process zone, (b) Fictitious Crack with assumed stress distribution 10

2.4 Stress distribution in front of a crack tip before and after growth of the real crack 12

2.5 Simple approximate assumption for use in numerical calculations 13

2.6 The Cartesian Coordinate for Crack Band Model 15

2.7 Stress - Strain for fracture process zone 16

2.8 Fracture Resistance Stages of Plain Concrete 18

2.9 Three-Point Bend Notched Specimen 20

2.10 Maturity function based on assumption that rate of strength gain varies linearly with temperature 25

2.11 Procedures for using maturity method involve laboratory testing and field measurements 31

3.1 Consequences of Arrhenius' law, (b) Strain rate follow Arrhenius' law 34

3.2 A typical fracture energy - age curve 39

3.3 G_f against dG_f / dt 39

3.4 G_f against $\sqrt{dG / dt}$ 40

3.5 Fracture energy-age function of isothermally cured concrete: Linear Transformations 49

LIST OF FIGURES
(Continued)

Figure **Page**

3.6 (a) Variation of rate constant k(T) with temperature T: Linear & Arrhenius Eq.
(b) ln k(T) vs. $1/T_k$ 50

4.1 Typical curing temperature for beam specimen 57

4.2 Three-point bend test setup 60

4.3 Typical raw experimental data for a 3-point bend beam test 61

5.1 Compressive strength versus age for isothermally cured mortar cubes 66

5.2 Compressive strength versus age for isothermally cured concrete cylinders 66

5.3 Plot of $1/f_c$ versus $1/t$ to evaluate f_{cu} for mortar 67

5.4 Plot of $1/f_c$ versus $1/t$ to evaluate f_{cu} for concrete 67

5.5 Plot of $[f_c / (f_{cu}-f_c)]$ versus t to evaluate k_T and t_o for mortar 69

5.6 Plot of $[f_c / (f_{cu}-f_c)]$ versus t to evaluate k_T and t_o for concrete 69

5.7 Rate constant versus curing temperature for mortar cubes by linear function 71

5.8 Rate constant versus curing temperature for concrete cylinders by linear function 71

5.9 Logarithm of rate constant versus reciprocal of curing temperature in Kelvin
by Arrhenius function for mortar cubes 72

5.10 Logarithm of rate constant versus reciprocal of curing temperature in Kelvin
by Arrhenius function for concrete cylinders 72

5.11 Relative strength versus maturity for isothermally cured mortar cubes 74

5.12 Relative strength versus maturity for isothermally cured concrete cylinders 74

5.13 Relative strength versus equivalent age for isothermally cured mortar cubes 75

5.14 Relative strength versus equivalent age for isothermally cured concrete cylinders ... 75

LIST OF FIGURES
(Continued)

Figure **Page**

5.15 Load versus deflection for size A, curing at 23 °C, age = 28 days 77

5.16 Load versus deflection for size B, curing at 23 °C, age = 28 days 77

5.17 Load versus deflection for size C, curing at 23 °C, age = 28 days 78

5.18 Load versus deflection for size B, tested at very young age 78

5.19 Load versus deflection for size B, tested after about a week 79

5.20 Load versus deflection for size B, tested at mature age 79

5.21 Fracture energy versus age for isothermally cured size A beam 84

5.22 Fracture energy versus age for isothermally cured size B beam 84

5.23 Fracture energy versus age for isothermally cured size C beam 85

5.24 Plot of $1/G_f$ versus $1/t$ to evaluate G_{fu} for size A 85

5.25 Plot of $1/G_f$ versus $1/t$ to evaluate G_{fu} for size B 86

5.26 Plot of $1/G_f$ versus $1/t$ to evaluate G_{fu} for size C 86

5.27 Plot of $[G_f / (G_{fu} - G_f)]$ versus t to evaluate k_T and t_o for size A 89

5.28 Plot of $[G_f / (G_{fu} - G_f)]$ versus t to evaluate k_T and t_o for size B 89

5.29 Plot of $[G_f / (G_{fu} - G_f)]$ versus t to evaluate k_T and t_o for size C 90

5.30 Rate constant versus curing temperature for size A beam by linear function 92

5.31 Rate constant versus curing temperature for size B beam by linear function 92

5.32 Rate constant versus curing temperature for size C beam by linear function 93

5.33 Logarithm of rate constant versus reciprocal of curing temperature in Kelvin by Arrhenius function for size A beam 93

LIST OF FIGURES
(Continued)

Figure **Page**

5.34 Logarithm of rate constant versus reciprocal of curing temperature in Kelvin by Arrhenius function for size B beam 94

5.35 Logarithm of rate constant versus reciprocal of curing temperature in Kelvin by Arrhenius function for size C beam 94

5.36 Relative fracture energy versus maturity for isothermally cured size A beam 96

5.37 Relative fracture energy versus maturity for isothermally cured size B beams 96

5.38 Relative fracture energy versus maturity for isothermally cured size C beams 97

5.39 Relative fracture energy versus equivalent age for isothermally cured size A beams 97

5.40 Relative fracture energy versus equivalent age for isothermally cured size B beams 98

5.41 Relative fracture energy versus equivalent age for isothermally cured size C beams 98

5.42 Limiting fracture energy versus curing temperature 100

6.1 Logarithm of rate constant versus reciprocal of curing temperature in Kelvin 108

3.7 G_f versus dG_f / dt for size A 109

3.8 G_f versus dG_f / dt for size C 110

3.9 G_f versus dG_f / dt for size A 110

3.10 G_f versus dG_f / dt for size C 111

A1a Load versus deflection for size A, curing at 14 °C, age = 1.22 days 112

A1b Load versus deflection for size A, curing at 14 °C, age = 1.22 days 112

LIST OF FIGURES
(Continued)

Figure **Page**

A1c Load versus deflection for size A, curing at 14 °C, age = 1.22 days 113

A2a Load versus deflection for size A, curing at 14 °C, age = 2.04 days 113

A2b Load versus deflection for size A, curing at 14 °C, age = 2.04 days 114

A2c Load versus deflection for size A, curing at 14 °C, age = 2.04 days 114

A3a Load versus deflection for size A, curing at 14 °C, age = 4.03 days 115

A3b Load versus deflection for size A, curing at 14 °C, age = 4.03 days 115

A3c Load versus deflection for size A, curing at 14 °C, age = 4.03 days 116

A4a Load versus deflection for size A, curing at 14 °C, age = 7.25 days 116

A4b Load versus deflection for size A, curing at 14 °C, age = 7.25 days 117

A4c Load versus deflection for size A, curing at 14 °C, age = 7.25 days 117

A5a Load versus deflection for size A, curing at 14 °C, age = 22.04 days 118

A5b Load versus deflection for size A, curing at 14 °C, age = 22.04 days 118

A5c Load versus deflection for size A, curing at 14 °C, age = 22.04 days 119

A6a Load versus deflection for size A, curing at 14 °C, age = 36.0 days 119

A6b Load versus deflection for size A, curing at 14 °C, age = 36.0 days 120

A6c Load versus deflection for size A, curing at 14 °C, age = 36.0 days 120

A7a Load versus deflection for size A, curing at 23 °C, age = 0.5 day..... 121

A7b Load versus deflection for size A, curing at 23 °C, age = 0.5 day..... 121

A7c Load versus deflection for size A, curing at 23 °C, age = 0.5 day..... 122

A8a Load versus deflection for size A, curing at 23 °C, age = 1.3 days 122

LIST OF FIGURES
(Continued)

Figure **Page**

A8b Load versus deflection for size A, curing at 23 °C, age = 1.3 days 123

A8c Load versus deflection for size A, curing at 23 °C, age = 1.3 days 123

A9a Load versus deflection for size A, curing at 23 °C, age = 3.06 days 124

A9b Load versus deflection for size A, curing at 23 °C, age = 3.06 days 124

A9c Load versus deflection for size A, curing at 23 °C, age = 3.06 days 125

A10a Load versus deflection for size A, curing at 23 °C, age = 7.16 days 125

A10b Load versus deflection for size A, curing at 23 °C, age = 7.16 days 126

A10c Load versus deflection for size A, curing at 23 °C, age = 7.16 days 126

A11a Load versus deflection for size A, curing at 23 °C, age = 14.02 days 127

A11b Load versus deflection for size A, curing at 23 °C, age = 14.02 days 127

A11c Load versus deflection for size A, curing at 23 °C, age = 14.02 days 128

A12a Load versus deflection for size A, curing at 23 °C, age = 28.03 days 128

A12b Load versus deflection for size A, curing at 23 °C, age = 28.03 days 129

A12c Load versus deflection for size A, curing at 23 °C, age = 28.03 days 129

A13a Load versus deflection for size A, curing at 35 °C, age = 0.35 day..... 130

A13b Load versus deflection for size A, curing at 35 °C, age = 0.35 day..... 130

A13c Load versus deflection for size A, curing at 35 °C, age = 0.35 day..... 131

A14a Load versus deflection for size A, curing at 35 °C, age = 0.5625 day..... 131

A14b Load versus deflection for size A, curing at 35 °C, age = 0.5625 day..... 132

A14c Load versus deflection for size A, curing at 35 °C, age = 0.5625 day..... 132

LIST OF FIGURES
(Continued)

Figure **Page**

A15a Load versus deflection for size A, curing at 35 °C, age = 1.07 days 133

A15b Load versus deflection for size A, curing at 35 °C, age = 1.07 days 133

A15c Load versus deflection for size A, curing at 35 °C, age = 1.07 days 134

A16a Load versus deflection for size A, curing at 35 °C, age = 4.03 days 134

A16b Load versus deflection for size A, curing at 35 °C, age = 4.03 days 135

A16c Load versus deflection for size A, curing at 35 °C, age = 4.03 days 135

A17a Load versus deflection for size A, curing at 35 °C, age = 9.5 days 136

A17b Load versus deflection for size A, curing at 35 °C, age = 9.5 days 136

A17c Load versus deflection for size A, curing at 35 °C, age = 9.5 days 137

A18a Load versus deflection for size A, curing at 35 °C, age = 20.02 days 137

A18b Load versus deflection for size A, curing at 35 °C, age = 20.02 days 138

A18c Load versus deflection for size A, curing at 35 °C, age = 20.02 days 138

B1a Load versus deflection for size B, curing at 14 °C, age = 1 day 139

B1b Load versus deflection for size B, curing at 14 °C, age = 1 day 139

B1c Load versus deflection for size B, curing at 14 °C, age = 1 day 140

B2a Load versus deflection for size B, curing at 14 °C, age = 2 days 140

B2b Load versus deflection for size B, curing at 14 °C, age = 2 days 141

B2c Load versus deflection for size B, curing at 14 °C, age = 2 days 141

B3a Load versus deflection for size B, curing at 14 °C, age = 4.1 days 142

B3b Load versus deflection for size B, curing at 14 °C, age = 4.1 days 142

LIST OF FIGURES
(Continued)

Figure **Page**

B3c Load versus deflection for size B, curing at 14 °C, age = 4.1 days..... 143

B4a Load versus deflection for size B, curing at 14 °C, age = 10 days..... 143

B4b Load versus deflection for size B, curing at 14 °C, age = 10 days 144

B4c Load versus deflection for size B, curing at 14 °C, age = 10 days..... 144

B5a Load versus deflection for size B, curing at 14 °C, age = 22 days..... 145

B5b Load versus deflection for size B, curing at 14 °C, age = 22 days 145

B5c Load versus deflection for size B, curing at 14 °C, age = 22 days 146

B6a Load versus deflection for size B, curing at 14 °C, age = 38 days..... 146

B6b Load versus deflection for size B, curing at 14 °C, age = 38 days 147

B6c Load versus deflection for size B, curing at 14 °C, age = 38 days..... 147

B7a Load versus deflection for size B, curing at 23 °C, age = 0.56 day..... 148

B7b Load versus deflection for size B, curing at 23 °C, age = 0.56 day..... 148

B7c Load versus deflection for size B, curing at 23 °C, age = 0.56 day..... 149

B8a Load versus deflection for size B, curing at 23 °C, age = 1.21 days..... 149

B8b Load versus deflection for size B, curing at 23 °C, age = 1.21 days 150

B8c Load versus deflection for size B, curing at 23 °C, age = 1.21 days..... 150

B9a Load versus deflection for size B, curing at 23 °C, age = 2.95 days..... 151

B9b Load versus deflection for size B, curing at 23 °C, age = 2.95 days 151

B9c Load versus deflection for size B, curing at 23 °C, age = 2.95 days..... 152

B10a Load versus deflection for size B, curing at 23 °C, age = 7.16 days..... 152

LIST OF FIGURES
(Continued)

Figure **Page**

B10b Load versus deflection for size B, curing at 23 °C, age = 7.16 days..... 153

B10c Load versus deflection for size B, curing at 23 °C, age = 7.16 days..... 153

B11a Load versus deflection for size B, curing at 23 °C, age = 14.02 days..... 154

B11b Load versus deflection for size B, curing at 23 °C, age = 14.02 days..... 154

B11c Load versus deflection for size B, curing at 23 °C, age = 14.02 days..... 155

B12a Load versus deflection for size B, curing at 23 °C, age = 28.0 days..... 155

B12b Load versus deflection for size B, curing at 23 °C, age = 28.0 days..... 156

B12c Load versus deflection for size B, curing at 23 °C, age = 28.0 days..... 156

B13a Load versus deflection for size B, curing at 35 °C, age = 0.25 day..... 157

B13b Load versus deflection for size B, curing at 35 °C, age = 0.25 day..... 157

B13c Load versus deflection for size B, curing at 35 °C, age = 0.25 day..... 158

B14a Load versus deflection for size B, curing at 35 °C, age = 0.55 day..... 158

B14b Load versus deflection for size B, curing at 35 °C, age = 0.55 day..... 159

B14c Load versus deflection for size B, curing at 35 °C, age = 0.55 day..... 159

B15a Load versus deflection for size B, curing at 35 °C, age = 1.55 days..... 160

B15b Load versus deflection for size B, curing at 35 °C, age = 1.55 days..... 160

B15c Load versus deflection for size B, curing at 35 °C, age = 1.55 days..... 161

B16a Load versus deflection for size B, curing at 35 °C, age = 4.26 days..... 161

B16b Load versus deflection for size B, curing at 35 °C, age = 4.26 days..... 162

B16c Load versus deflection for size B, curing at 35 °C, age = 4.26 days..... 162

LIST OF FIGURES
(Continued)

Figure **Page**

B17a Load versus deflection for size B, curing at 35 °C, age = 9.05 days..... 163

B17b Load versus deflection for size B, curing at 35 °C, age = 9.05 days..... 163

B17c Load versus deflection for size B, curing at 35 °C, age = 9.05 days..... 164

B18a Load versus deflection for size B, curing at 35 °C, age = 20.2 days..... 164

B18b Load versus deflection for size B, curing at 35 °C, age = 20.2 days..... 165

B18c Load versus deflection for size B, curing at 35 °C, age = 20.2 days..... 165

C1a Load versus deflection for size C, curing at 14 °C, age = 1.1 days..... 166

C1b Load versus deflection for size C, curing at 14 °C, age = 1.1 days 166

C2a Load versus deflection for size C, curing at 14 °C, age = 2.1 days..... 167

C2b Load versus deflection for size C, curing at 14 °C, age = 2.1 days 167

C3a Load versus deflection for size C, curing at 14 °C, age = 4.0 days..... 168

C3b Load versus deflection for size C, curing at 14 °C, age = 4.0 days 168

C4a Load versus deflection for size C, curing at 14 °C, age = 9.0 days..... 169

C4b Load versus deflection for size C, curing at 14 °C, age = 9.0 days 169

C5a Load versus deflection for size C, curing at 14 °C, age = 18.0 days..... 170

C5b Load versus deflection for size C, curing at 14 °C, age = 18.0 days 170

C6a Load versus deflection for size C, curing at 14 °C, age = 36.0 days..... 171

C6b Load versus deflection for size C, curing at 14 °C, age = 36.0 days 171

C7a Load versus deflection for size C, curing at 23 °C, age = 0.65 day 172

C7b Load versus deflection for size C, curing at 23 °C, age = 0.65 day..... 172

LIST OF FIGURES
(Continued)

Figure **Page**

C7c Load versus deflection for size C, curing at 23 °C, age = 0.65 day 173

C8a Load versus deflection for size C, curing at 23 °C, age = 1.0 day 173

C8b Load versus deflection for size C, curing at 23 °C, age = 1.0 day 174

C8c Load versus deflection for size C, curing at 23 °C, age = 1.0 day 174

C9a Load versus deflection for size C, curing at 23 °C, age = 3.0 days 175

C9b Load versus deflection for size C, curing at 23 °C, age = 3.0 days 175

C9c Load versus deflection for size C, curing at 23 °C, age = 3.0 days 176

C10a Load versus deflection for size C, curing at 23 °C, age = 7.0 days 176

C10b Load versus deflection for size C, curing at 23 °C, age = 7.0 days 177

C10c Load versus deflection for size C, curing at 23 °C, age = 7.0 days 177

C11a Load versus deflection for size C, curing at 23 °C, age = 14.0 days 178

C11b Load versus deflection for size C, curing at 23 °C, age = 14.0 days 178

C11c Load versus deflection for size C, curing at 23 °C, age = 14.0 days 179

C12a Load versus deflection for size C, curing at 23 °C, age = 28.0 days 179

C12b Load versus deflection for size C, curing at 23 °C, age = 28.0 days 180

C12c Load versus deflection for size C, curing at 23 °C, age = 28.0 days 180

C13a Load versus deflection for size C, curing at 35 °C, age = 0.29 day 181

C13b Load versus deflection for size C, curing at 35 °C, age = 0.29 day 181

C14a Load versus deflection for size C, curing at 35 °C, age = 0.51 day 182

C14b Load versus deflection for size C, curing at 35 °C, age = 0.51 day 182

LIST OF FIGURES
(Continued)

Figure **Page**

C15a Load versus deflection for size C, curing at 35 °C, age = 1.03 days..... 183

C15b Load versus deflection for size C, curing at 35 °C, age = 1.03 days..... 183

C16a Load versus deflection for size C, curing at 35 °C, age = 4.28 days..... 184

C16b Load versus deflection for size C, curing at 35 °C, age = 4.28 days..... 184

C17a Load versus deflection for size C, curing at 35 °C, age = 9.0 days..... 185

C17b Load versus deflection for size C, curing at 35 °C, age = 9.0 days 185

C18a Load versus deflection for size C, curing at 35 °C, age = 23.01 days..... 186

C18b Load versus deflection for size C, curing at 35 °C, age = 23.01 days..... 186

CHAPTER 1

INTRODUCTION

1.1 General

Application of fracture mechanics for concrete is important for a variety of reasons, including: determination of structural size and geometry effects upon the nominal stress at failure of structural components and systems, computation of post-peak load deflection diagram for computation of energy absorption capacity and structural ductility, and use of energy criterion for more realistic portrayal of failure stress and strains in concrete.

Classical linear elastic fracture mechanics (LEFM), which has been successfully applied to metallic materials is however limited when applied to concrete. Concrete is characteristically heterogeneous. Because of the heterogeneity, the cracking process is associated with the development of a microcracking zone or fracture process zone in front of the crack tip and along the main crack surface. This behavior does not conform with LEFM.

Fracturing process is associated with three elementary fracture modes: mode I or the opening mode, mode II known as the planar shear mode and mode III as the antiplane shear mode. Modes I and II are planar symmetric and antisymmetric, while mode III is associated with local displacements that are skew symmetric with respect to both x-y and x-z planes.. In general fracture is a linear combination of these three modes.

Much of the effort is being devoted to develop fracture mechanics methods for the analysis of cracked concrete structures. Different parameters have been proposed to

describe the fracture behavior in concrete subjected to mode I deformation, such as the fracture toughness, K_{IC}, the critical-strain energy-release rate, G_{IC}, the fracture energy, G_f, the J integral, the critical crack tip opening displacement, $CTOD_c$ and the crack resistance, R.

Several models have been proposed to explain the fracture process as well as the size dependency in concrete. Hillerborg (1976) has proposed a fictitious crack model which is also known as a damage zone model. In this model, the tensile stress is assumed not to fall to zero immediately after the attainment of its limiting value, but to decrease with increasing crack widths. The fracture energy, G_f, which is defined as the area under post-peak stress versus the crack opening displacement curve, the modulus of elasticity, E, uniaxial tensile strength, σ_t, are the material properties required to describe the tensile fracture behavior of concrete.

Bazant and Oh (1983) introduced the concept of crack band theory for fracture of concrete. The fracture front is modeled as a blunt smeared crack band. The material fracture properties are characterized by three parameters G_f, σ_t and w_c, the effective width of crack band (fracture process zone). Results are similar to those obtained from fictitious crack model if the same values of G_f and σ_t are used in the crack band model. Instead of using the value of G_f determined from the area under σ-COD curve, Bazant, Kim, and Pheiffer (1984) have used an R-curve analysis to determine the fracture energy, G_f, for the crack band model.

Jenq and Shah (1984) have proposed a two parameter fracture model. The two parameters are the critical stress intensity factor calculated at the tip of the effective crack

and the elastic critical crack opening displacement. Based on their test results the two parameters are found to be size independent.

Fracture energy G_f has been considered to be a reliable fracture mechanics parameter which can describe the process of cracking in concrete. The parameter G_f is defined as the energy absorbed to create a unit area of fracture surface. To determine the fracture energy, the RILEM committee TC50 has put forward a recommendation. This Recommendation specifies a method for the determination of the fracture energy (G_f) of mortar and concrete by means of a stable three-point bend test on notched beams.

To meet rapid construction schedules, form removal, application of post-tensioning, termination of curing, and the removal of reshores must be carried out as early as is possible and safe. Since concrete is a brittle material, those operations, if performed, prior to attainment of sufficient fracture energy would cause cracking which might lead to a catastrophical failure. The determination of in-place fracture energy to enable these operations to proceed safely at the earliest possible time requires the use of reliable in-place tests.

In-place tests, which by nature of their applications ought to be nondestructive, are used to obtain information about the properties of concrete as it exists in a structure. A number of Nondestructive Evaluation (NDE) test methods are currently available for the in-situ determination of strength and other properties in concrete structure. The most widely used NDE methods for insitu estimation of strength are the surface hardness (the rebound hammer), probe penetration, pullout, ultrasonic pulse velocity, maturity, and cast-in-place cylinder techniques.

In this dissertation, a testing methodology is developed for insitu nondestructive determination of fracture energy, G_f, in concrete elements and structures. The method combines the principles of fracture mechanics and time-temperature effects on fracture resistance development of concrete. "Maturity" is the term used to represent quantitatively the cumulative effects of temperature and time on strength development in concrete. The present methodology employs the maturity concept in order to relate the time-temperature effects to the gain in fracture energy with time. To date, there are no available testing techniques for the determination of fracture energy in large concrete structures. Current fracture mechanics testing methodologies for concrete are limited to small size laboratory specimens. The present technique will have the potential for use as the only NDE standard for the determination of G_f in all types of elements, including large concrete structures.

1.2 Objectives

The primary objective of this dissertation is to develop a methodology for the determination of the in-place fracture energy, G_f, for concrete-like materials in a non-destructive manner. In doing so, the findings of this study prove that in direct correspondence with strength, the increase in development of fracture resistance in concrete is rate dependent. The experimental and analytical developments lead to the determination of activation energy. Depending on the cement type, and mixture proportions, the activation energy can be considered material constant that pertains to the exothermic chemical process during hydration of concrete. Indirect determination of this material constant, the activation energy, through the present fracture tests validates the proposed hypothesis.

CHAPTER 2

LITERATURE REVIEW

In this dissertation, the principles of fracture mechanics and maturity method (time-temperature effects) are combined for the development of the proposed in-place NDE methodology. In this context, the purpose of this chapter is to review the fracture mechanics models pertinent to concrete. Moreover, the underlying principles (time-temperature effects) governing the maturity rule as applied to the estimation of concrete strength will be reviewed. The modifications to the maturity rule for application to fracture testing of concrete will be explained in the subsequent chapters.

2.1 Fracture Mechanics of Concrete

Application of linear elastic fracture mechanics (LEFM) to concrete was first attempted by Kaplan (1961). Since then, fracture testing of concrete has developed tremendously during the 1980's. A large number of experimental testing techniques and specimen types have been tried and the developments have crystallized into some effective methods. The Fictitious Crack Model, FCM, (Hillerborg et al., 1976), the Crack Band Model, CBM, (Bazant, et al., 1979, 1983) and the Two-Parameter Fracture Model, TPFM, (Jeng and Shah, 1985a, 1985b) are among the most widely employed fracture models.

2.1.1 Fictitious Crack Model (FCM)

The fundamental idea of FCM is best demonstrated by means of a tension test, Figure 2.1. The test is assumed to be deformation-controlled and stable, so that it is possible to follow the descending branch of the stress-deformation curve all the way down to zero load.

The specimen is assumed to be homogenous and to have a constant cross section area. The deformation is measured along two equal gauge lengths A and B as shown in the diagram. Curves A and B coincide until the maximum load is reached. On further deformation a fracture zone forms somewhere in the specimen. This fracture zone has a limited width in the direction of the stress. As the fracture zone develops the force will decrease due to the formation of microcracks and the corresponding weakening of the material. The decreasing load results in a decrease in deformation everywhere outside of the fracture zone, corresponding to the unloading curve in the stress-strain diagram. No more fracture zone can form, as the load decreases.

In Figure 2.1a it is assumed that the whole fracture zone falls within gauge length A. The deformations within gauge length B can then be described by means of a stress-strain curve, including the unloading branch. The deformation within gage length A includes also the deformation of the fracture zone. The additional deformation, w, due to the fracture zone is the difference between the descending branches of curves A and B.

It is possible to describe the deformation properties of the test piece by means of two diagrams:

1. The stress-strain (σ-ε) diagram, including the unloading branch, Figure 2.1c.
2. The stress-deformation (σ-w) diagram for the fracture zone, Figure 2.1d.

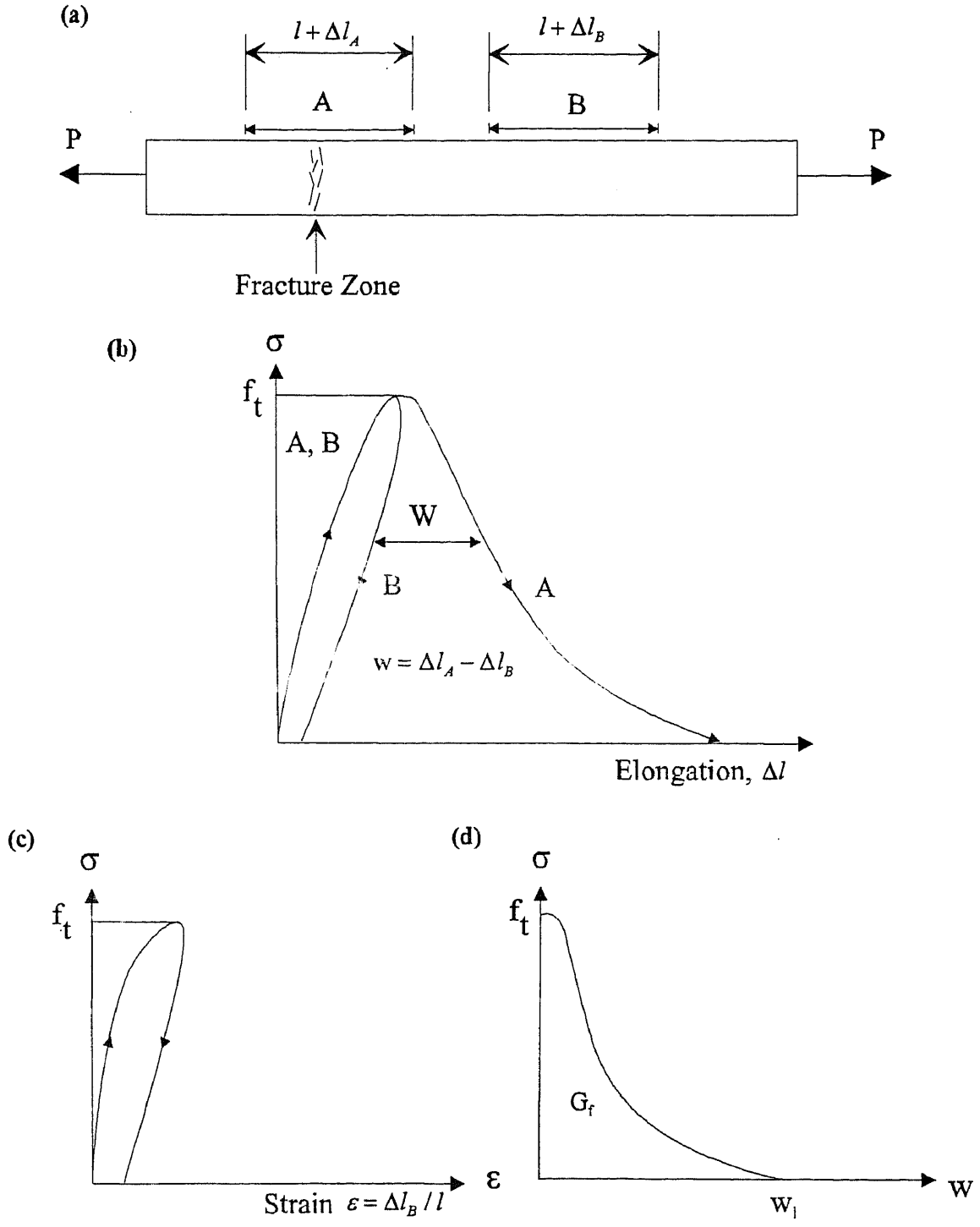

Figure 2.1 The principles for division of the deformation properties into a σ-ε diagram and σ-ω diagram, where w is the additional deformation due to formation of a fracture zone(Hillerborg, 1983)

The application of the fictitious crack model (FCM) to the description of the tensile test is shown in Figure 2.2.

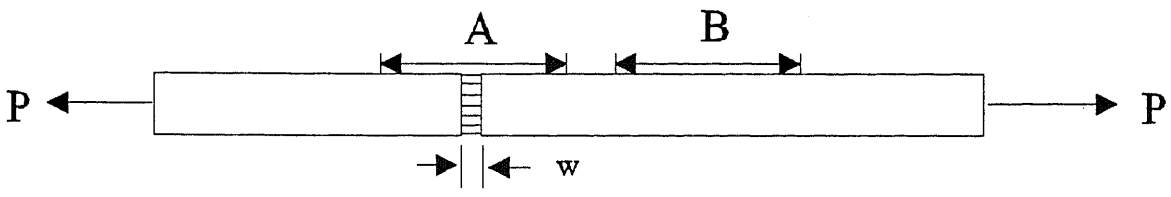

Figure 2.2 The simplified description of the fracture zone as a "fictitious crack" with width w (Hillerborg, 1983)

When using the Fictitious Crack Model, the fracture zone in front of a crack tip is replaced by a crack that is able to transfer stress, called fictitious crack, (Figure 2.3.) (Petersson, 1981). According to the σ-w curve(Figure 2.1d), the stress is a function of the fictitious crack width. The stress transferring capability of the fictitious crack normally decreases when the crack width increases.

During a tensile test to complete separation, energy is absorbed inside and outside of the fracture zone. With the FCM, the energy absorbed in the fictitious crack is given by:

$$A\int_{o}^{w_1}\sigma\ dw = AG_f \qquad (2.1)$$

where A = cross sectional area,

w_1 = crack separation value at $\sigma = 0$,

G_f = area below the σ-w curve, Figure 2.1.d.

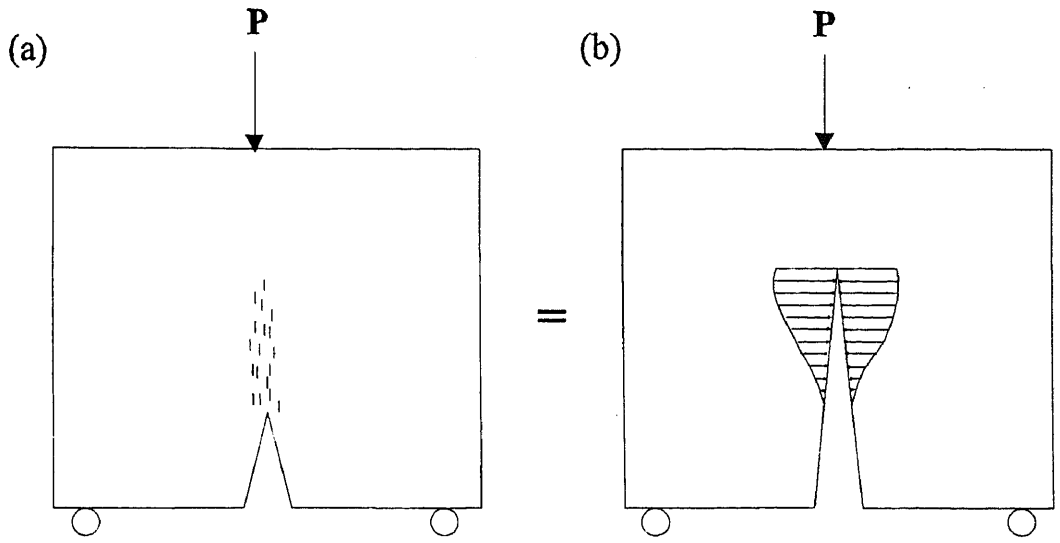

Figure 2. 3 (a) The fracture process zone, (b) Fictitious Crack with assumed stress distribution (Petersson, 1981)

G_f is the absorbed energy per unit crack area for the complete separation of the crack surfaces. It should be noted that the crack area in question is the projected area, rather than the total area of the irregular crack surface. The energy absorption outside the fictitious crack is determined in the usual way as the volume of the specimen times the area below the σ-ε curve, Figure 2.1c. For a purely elastic material, this energy absorption is zero.

The FCM is not only applicable to the tension test, but also to more complicated stress situations. Of primary interest is in its application to the analysis of stability and growth of a crack. For example, as shown in Figure 2.4 consider the stress distribution in front of a notch or a crack tip in a beam under the action of a growing imposed deformation (or load). The fracture zone that has developed is described as the fictitious crack. Within the fictitious crack the relationship between the stress, σ, and the crack width, w, is given by the σ-w curve. In the region away from the fracture process zone (fictitious crack), the σ-ε relationship for the material is valid. As the deformation is increased, the stresses in front of the fictitious crack tip is also increased. No stress is assumed to be higher than the tensile strength f_t. As soon as a stress has reached f_t, any increase in deformation causes the development of a fictitious crack at that point. Thus the stress at the fictitious crack tip is f_t as long as the fictitious crack grows.

The FCM has a very general applicability. It can be used to analyze the formation and growth of fracture zones and cracks, whether the fracture starts from a crack, a notch, an irregularity or a plain surface. It can also be used where shrinkage or temperature strains act and for non-isotropic materials.

Finite element (FEM) analysis is necessary to implement the model. In FEM calculations it is very time-consuming and hence expensive to use non-linear σ-ε and σ-w curves. It is however relatively inexpensive to use stepwise linear σ-w curves. The simplest possible assumptions regarding σ-ε and σ-w curves to be used in FEM analyses are according to Figure 2.5, i. e., straight line approximations for both curves. Most analyses performed so far have been based on these assumptions.

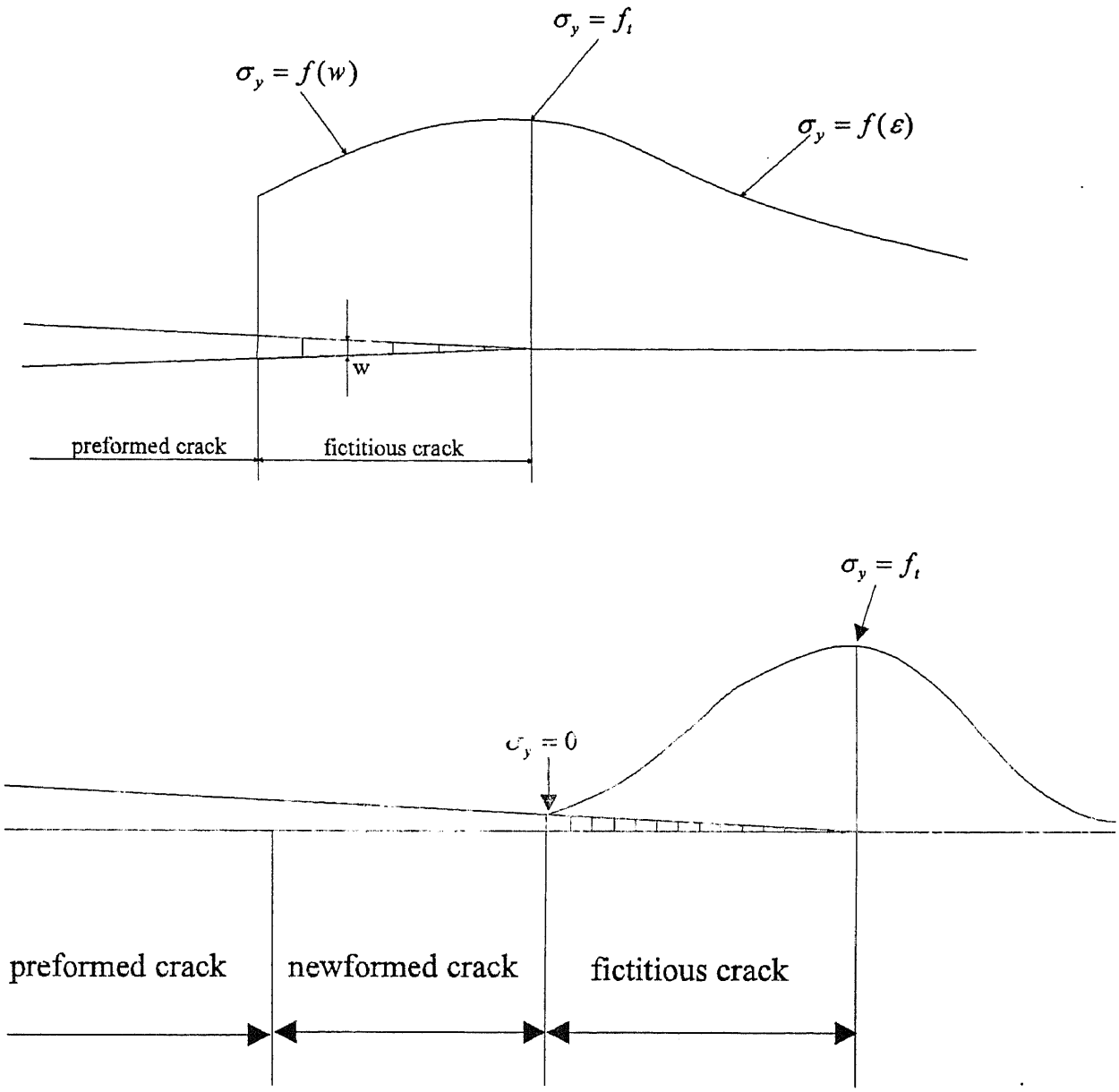

Figure 2.4 Stress distribution in front of a crack tip before and after growth of the real crack(Hillerborg, 1983)

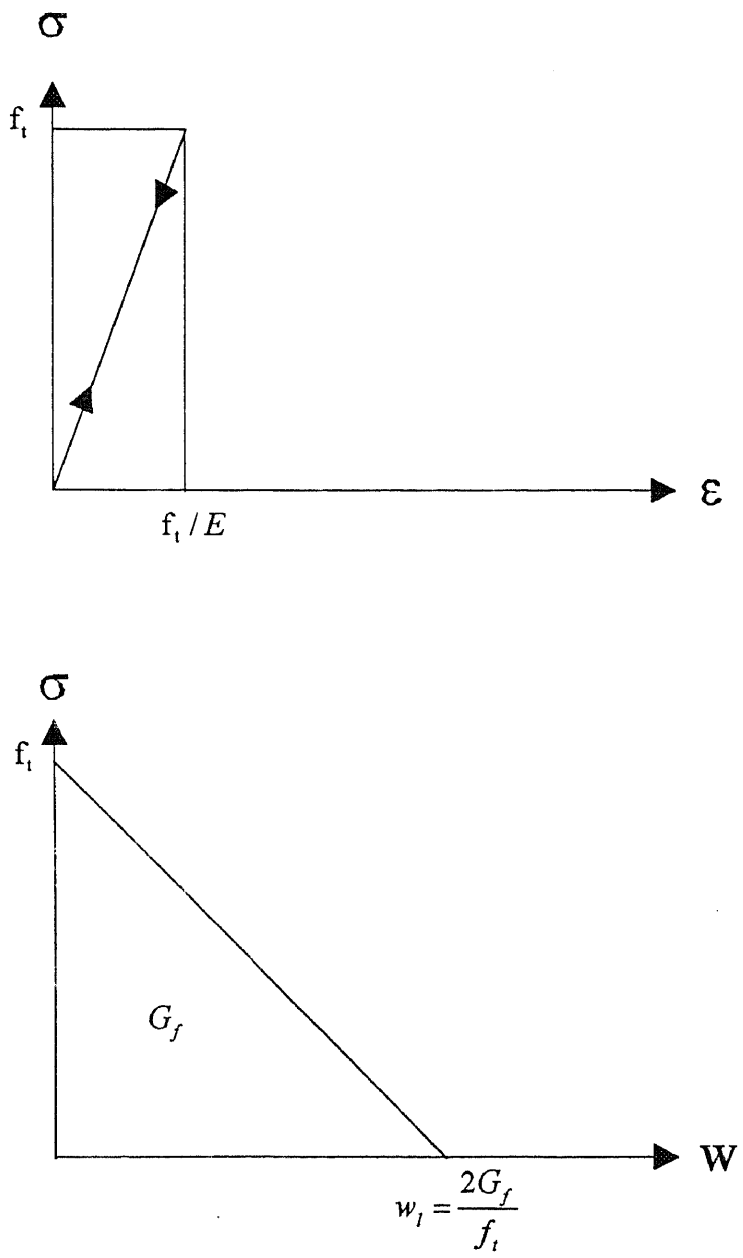

Figure 2.5 Simple approximate assumption for use in numerical calculations (Hillerborg, 1983)

2.1.2 Crack Band Model (CBM)

The basic idea for the crack band theory is to characterize the material behavior in the fracture process zone in a smeared manner through a strain-softening constitutive relation, and to impose a fixed width w_c of the front of the strain-softening zone (crack band),which is assumed to represent a material property.

The fracture energy, G_f, which is defined as the energy consumed in the formation and opening of all microcracks per unit area of plane (x,y) (Figure 2.6 & 2.7a) :

$$G_f = w_c \int_0^{\varepsilon_f} \sigma_z \, d\varepsilon_f \tag{2.3}$$

Referring to Figure 2.7b:

$$G_f = w_c \, (f_t' \, \varepsilon_o) / 2, \quad \varepsilon_o = f_t' / C_f \tag{2.4}$$

where w_c = the effective width of the fracture process zone (or crack band) over which the microcracks are assumed to be uniformly spread,

ε_f = the fracture strain, i. e., the additional strain caused by the opening of the microcracks,

f_t' = the direct tensile strength, and

$\varepsilon_o = \delta_f / w_c$, ($\delta_f$ = sum of the openings of individual microcracks), is the strain at the end of strain-softening and σ_z is zero ,

C_f = the slope of strain-softening curve (Figure 2.7b).

The pre-peak and post-peak behavior are both described by a stress-strain relationship, which the pre-peak modules is E and the post-peak modules is E_t (≤ 0) (Figure 2.7c). If G_f, f_t',and w_c are known from experimental measurements. The width of crack-band w_c can be used to relate the stress-strain response to the fracture energy:

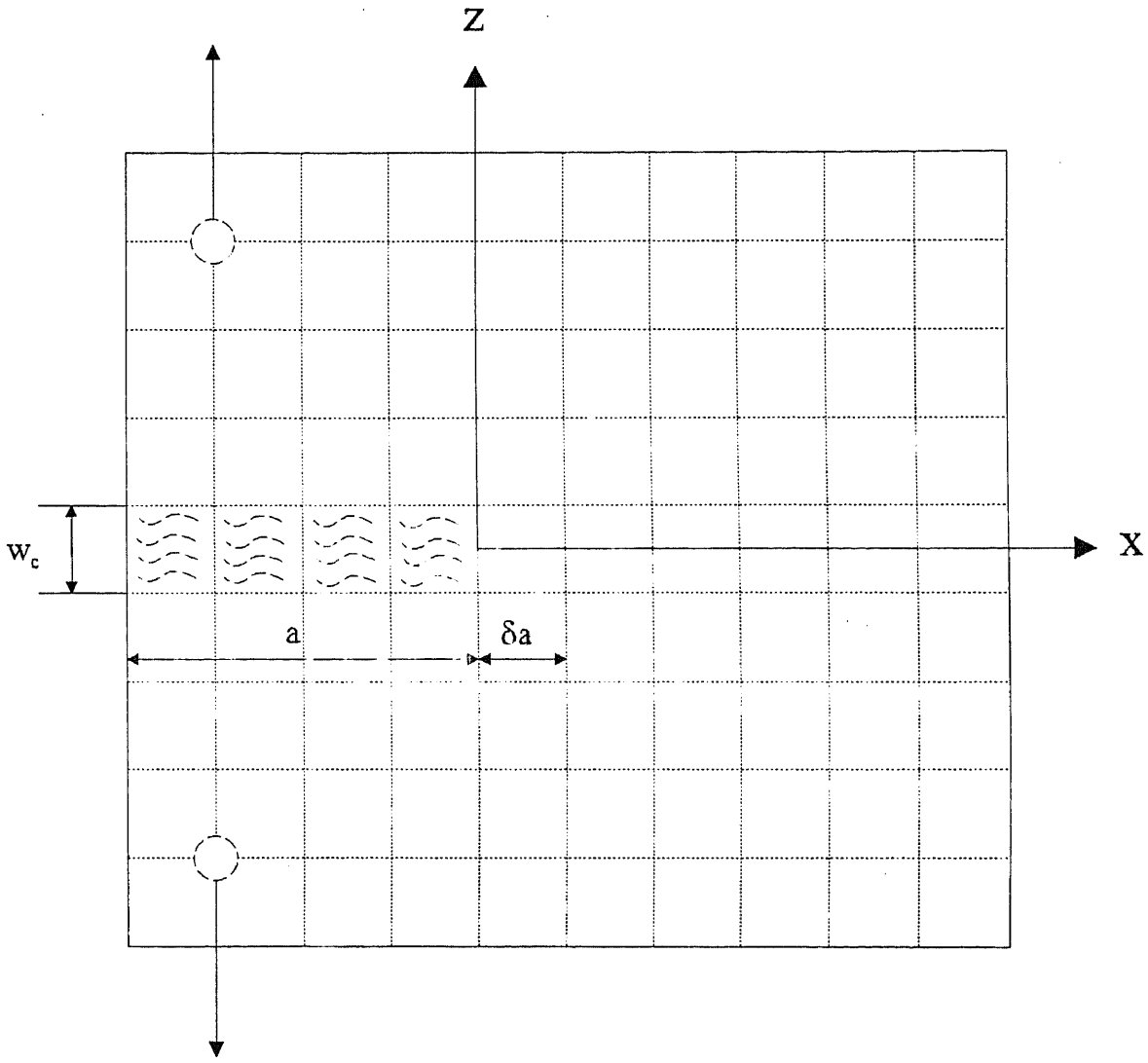

Figure 2.6 The Cartesian Coordinate for Crack Band Model (Bazant, 1983)

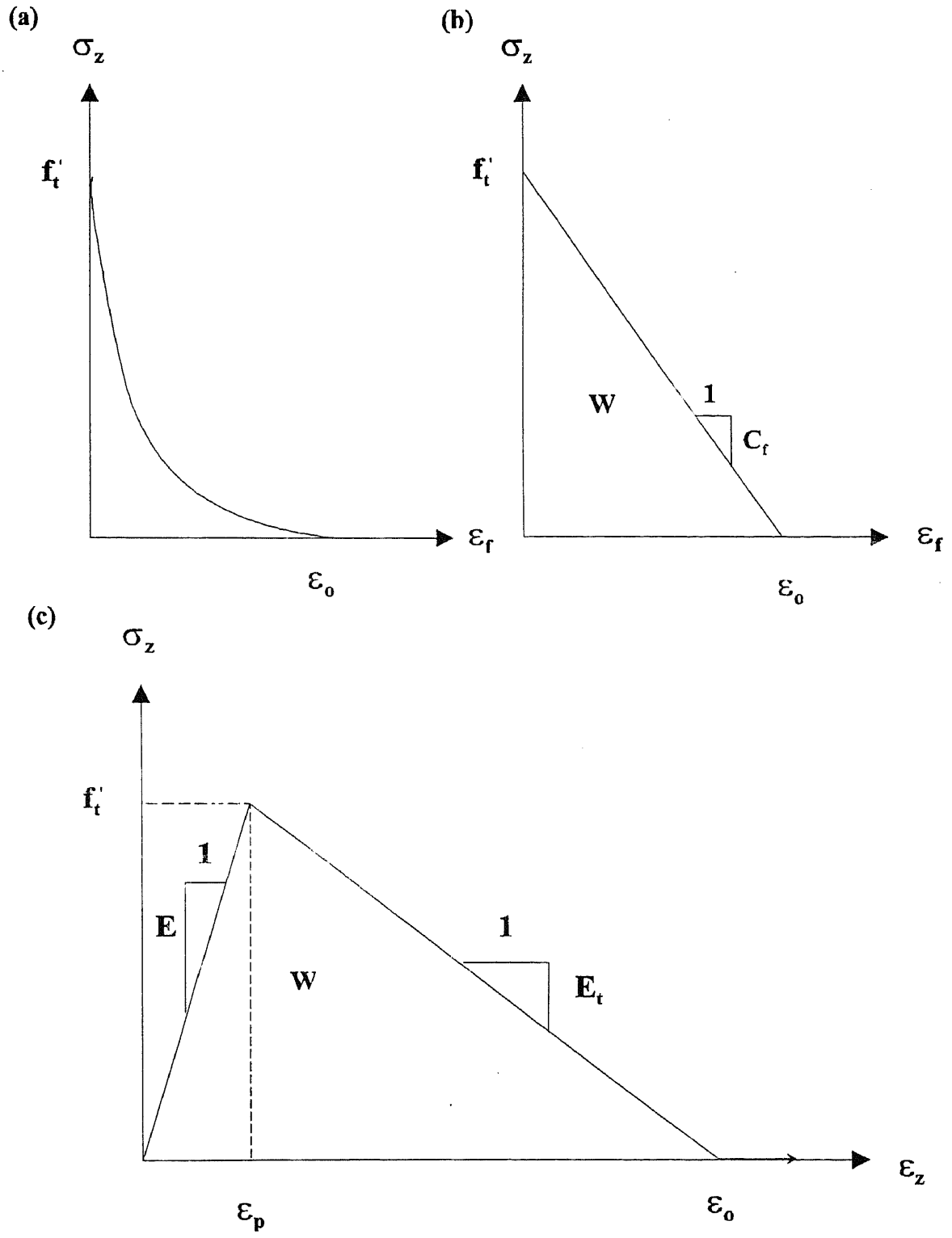

Figure 2.7 Stress - Strain for fracture process zone
(Bazant, 1983)

$$G_f = w_c \int_0^{\infty} \sigma_z \, d\varepsilon_f = \frac{1}{2}\left(\frac{1}{E} - \frac{1}{E_t}\right) f_t'^2 w_c \qquad (2.4)$$

Both the Fictitious Crack Model and the Crack Band Model, mentioned above, irrespective of the approaches adopted, require a complete stress-crack opening relationship.

2.1.3 Two-Parameter Fracture Model (TPFM)

Unlike the fictitious crack model and crack band model, the two-parameter model of Jenq and Shah (1985), does not require a post-peak (strain softening) constitutive law, yet it can describe the nonlinear slow crack growth prior to peak load The two parameters are the critical stress intensity factor K_{IC}^S and the critical crack tip opening displacement $CTOD_C$ relationship shown in Figure 2.8. This relationship is essentially linear on the ascending portion of the curve from P = 0 up to about the load corresponding to half the maximum load P_m. At this stage, the crack tip opening displacement is negligible and K_I is less than 0.5 K_{IC}^S(Figure 2.8a). As the load P exceed the value of $0.5P_m$, inelastic displacement and slow crack growth occur during the nonlinear range (Figure 2.8b). At the critical point (Figure 2.8c), the crack tip opening displacement reaches a critical value and $K_I = K_{IC}^S$. For standard plain concrete beams tested in three-point bending, the critical point can be approximated between the point of P_m and the point of 0.95 P_m on the descending branch of the P-CMOD plot.

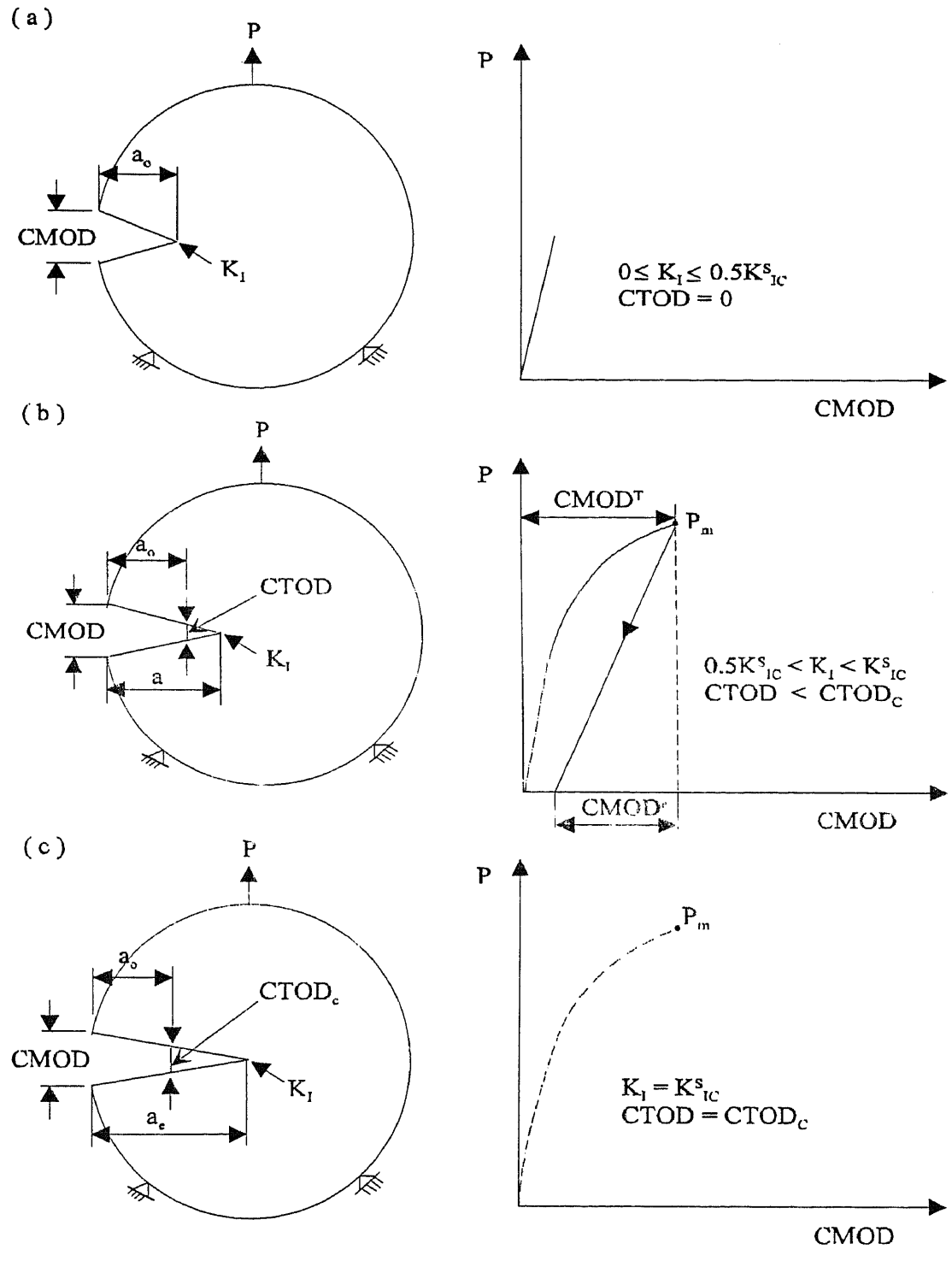

Figure 2.8 Fracture Resistance Stages of Plain Concrete
(Jenq and Shah, 1985)

Since the model is based on the LEFM concept, for each specimen geometry tested, one needs to be able to calculate K_I, CMOD, and COD, all functions of the applied load (P), crack growth (a), Young's modulus of elasticity (E), and the specimen geometry. General LEFM based equations for three-point bend notched beam specimens are presented by Tada et al., (1976) as follows (see Figure 2.9) :

Stress Intensity Factor (K_I) :

$$K_I = \frac{6P}{bd}\sqrt{\pi a}F(\frac{a}{d}) \tag{2.5}$$

$$F(\frac{a}{d}) = \frac{1}{\sqrt{\pi}}\frac{1.99 - A(1-A)(2.15 - 3.93A + 2.7A^2)}{(1+2A)(1-A)^{3/2}} \tag{2.6}$$

Crack Mouth Opening Displacement (CMOD) :

$$CMOD = \frac{24Pa}{bdE}V_1(\frac{a}{d}) \tag{2.7}$$

$$V_1(\frac{a}{d}) = 0.76 - 2.28A + 3.87A^2 - 2.04A^3 + \frac{0.66}{(1-A)^2} \tag{2.8}$$

Crack Opining Displacement (COD) :

$$COD(x) = CMOD\{(1-\frac{x}{a})^2 + (-1.149A + 1.081)[\frac{x}{a} - (\frac{x}{a})^2]\}^{1/2} \tag{2.9}$$

where E = Young's modulus; A = a / d; x = the distance measured from the crack mouth location toward the crack tip.

In the Two-Parameter Fracture Model the maximum applied load and the corresponding elastic $CMOD_e$ are all directly obtained from the experiments. With known specimen geometry and the Young's modulus, the effective elastic crack length a_e can be calculated from the LEFM formula using measured $CMOD_e$ and the measured maximum load. However, it is not a simple task to calculate a_e using the LEFM formula. Iteration

or trial and error method has to be adopted to obtain a_e. With the calculated effective crack length, K_{IC}^{S} and $CTOD_C$ can be obtained. These two values should be specimen size-independent as recommended in the TPFM. The validity of these values for the two parameter model even in the cases of beams possessing different span to beam depth ratios has yet to be established.

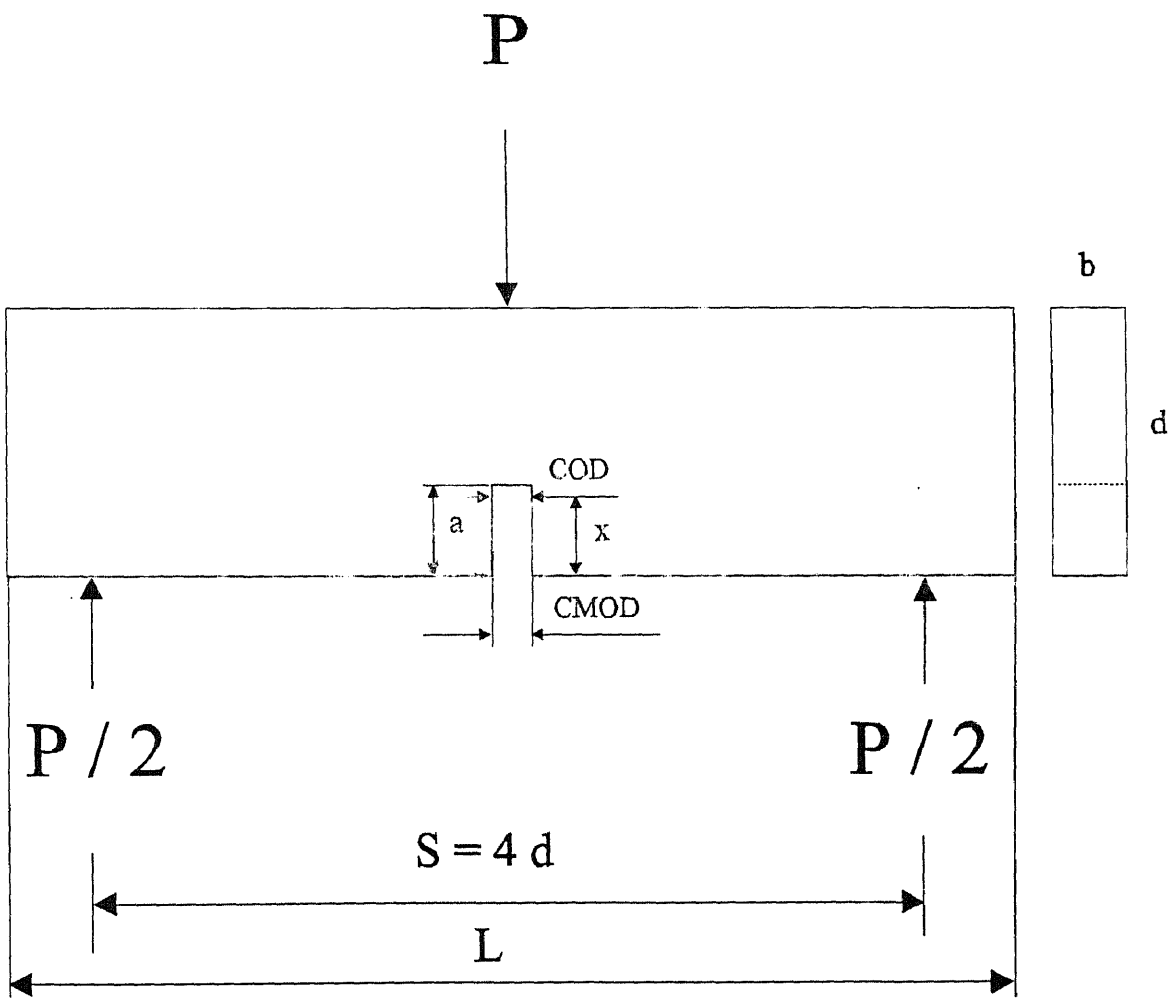

Figure 2.9 Three-Point Bend Notched Specimen (Jenq, 1985b)

2.2 Maturity Method

Fracture mechanics when applied to concrete members subjected to tensile loading, should be able to analyze the formation and growth of cracks. One way of quantifying the tensile stress or the tensile toughness is by means of the fracture energy, G_f. At present time, all methods to determine G_f of concrete rely on some form of destructive testing. For instance, it is recommended to extract drilled core specimens from existing concrete members. These specimens are then tested either in direct tension or three-point bend test to determine G_f. Disadvantage of such schemes is damage to structures due to extration of large pieces of materials from structures, since large beams are needed for valid fracture tests for example for concrete containing 1/2 inch maximum aggregate size a 4x4x34 inch size specimen is required. For this reason, there is a great urgency in developing an NDE technique for measuring the fracture energy, G_f, of concrete.

The maturity method is a technique to estimate in-place strength which accounts for the effects of temperature and time on strength development. Knudsen worked with the degree of hydration of cement rather than concrete strength. He demonstrated (1980, 1982) that the general strength-age, (f_c-t), equation

$$f_c = f_{cu} \frac{k_T(t - t_o)}{1 + k_T(t - t_o)} \tag{2.10}$$

is valid for strength development and any other property of concrete that is directly related to the extent of cement hydration, where

f_c = compressive strength,

f_{cu} = limiting compressive strength at infinite age,

k_T = rate constant,

t = age, and

t_o = datum age, age when strength development is assumed to begin.

And Carino(1984) prenested the following general strength-gain function

$$f_c = f_{cu} \frac{F(t,T)}{1+F(t,T)} \tag{2.11}$$

where F(t,T) is a time-temperature function.

In chapters to follow, it will be demonstrated that the maturity concept is also applicable to in-place determination of fracture energy,G_f, in concrete. The principles underlying the basis for the maturity method as related to the relationship between time-temperature and strength will be reviewed in this section.

2.2.1 Introduction

Concrete gains strength gradually as a result of exothermic chemical reactions (hydration) between Portland cement and water. For a specific concrete mixture, strength at any age is related to the degree of cement hydration. An increase in the curing temperature accelerates the hydration process. The rate of hydration, and therefore, the strength development of a given concrete mixture, will be a function of the concrete curing temperature. Thus, the strength of concrete depends on its time-temperature history assuming that sufficient moisture is always present for hydration. If there is insufficient moisture in concrete for hydration, strength development ceases.

The basic principle of maturity method is that the strength varies as a function of both time and temperature. The thermal history of the concrete and a so-called maturity function are used to compute a maturity value that quantifies the combined effects of time

and temperature. The strength of a particular concrete mixture is expressed as a function of its maturity by means of a strength-maturity relationship.

"Maturity" is the term used to represent quantitatively the cumulative effects of temperature and time on strength development in concrete. It is computed from the time-temperature history of the concrete. Early publications relating the development of strength in concrete to maturity date back to 1950's(Saul, 1951, McIntosh, 1949 and Nurse, 1949). According to Saul, the combined effects of time and temperature on strength development can be described by the single factor "maturity" (Saul, 1951), which was calculated as:

$$M = \int_0^t (T - T_o)dt \qquad (2.12)$$

where M = temperature-time factor (often called "maturity"),

T = average temperature of concrete during time interval Δt, °C,

T_0= datum temperature, °C, which is the lowest temperature at which strength gain is observed

Saul also proposed the "maturity concept" which states that samples of the same concrete will have equal strength if they have equal maturity, irrespective of their actual time temperature history (Saul, 1951). The concept has been viewed as a useful and simple means to account approximately for the complex effects of time and temperature on strength development.

2.2.2 Maturity Functions

The maturity function is a mathematical expression that converts the thermal history of the concrete to a maturity value. Several such functions have been proposed and are reviewed in Malhotra (1971), RILEM (1981) and Malhotra and Carino (1991). The key feature of a maturity function is the expression used to represent the influence of temperature on the rate of strength development. The maturity value can be expressed either as a temperature-time factor or as the equivalent age.

2.2.2.1 Linear Temperature Function

In one case it is assumed that the rate of strength development is a linear function of temperature as follows:

$$k(T) = B\,(T - T_o) \tag{2.13}$$

where $k(T)$ = a function of temperature, or the rate constant, and

B = a constant, the slope of the straight line.

And this leads to the simple maturity function shown in Figure 2.10. In this case, the maturity index at any age equals the area between the temperature curve and a datum temperature T_o of the concrete. The term temperature-time factor is used for this area and is calculated as follows:

$$M = B \sum_{0}^{t} (T_a - T_o)\,\Delta t \tag{2.14}$$

where M = temperature-time factor (often called "maturity"),

t = age, days,

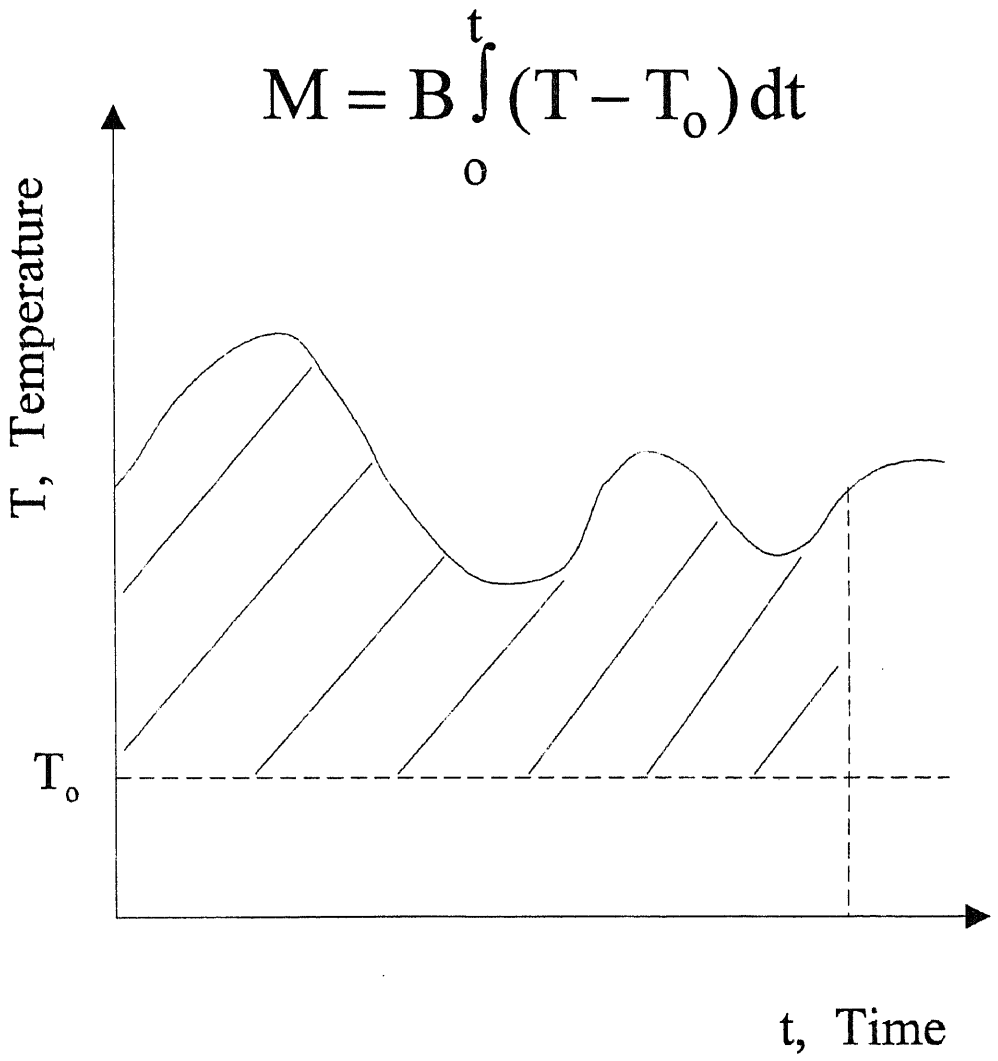

Figure 2. 10 Maturity function based on assumption that rate of strength gain varies linearly with temperature

T_a = average temperature of concrete during time interval Δt, °C,

T_o = datum temperature, °C.

This equation has become known as the Nurse-Saul function. Saul recommended a datum temperature of -10.5°C (13°F). As per ASTM C 1074-87, the maturity value computed according to Eq. (2.11) is termed the "temperature-time factor". Saul was the first to state that, under special conditions, sample of a given concrete having equal maturity will have approximately equal strength, independent of the in-place temperature history. The special conditions were that the concrete should not be heated too rapidly during the start of the steam curing cycle in particular reference to prestressing operations. He also recognized that at an early age curing temperature has more influence on strength development than time. But at later ages, temperature is less important than time. Thus, Saul-function widely used today with datum temperature value equal to -10°C. Note that a datum temperature of -10°C is appropriate only for the case of low activation energy and 0 to 20 °C temperature range.

Based on Eqs. 2.10 through 2.13, the time-temperature function(or called maturity function) can be expressed as follows:

$$M(t,T) = \int_{t_o}^{t} B(T - T_o)dt = \int_{0}^{t} B(T - T_o)dt - \int_{0}^{t_o} B(T - T_o)dt \qquad (2.15)$$

where M(t,T) is a time-temperature function. If the two terms on the right hand side of equation 2.15 are called M and M_o, the maturity function is

$$M(t,T) = B\,(M - M_o) \qquad (2.16)$$

Substituting equation 2.16 into equation 2.11, the strength - maturity relationship can be obtained as:

$$f_c = f_{cu} \frac{B(M - M_o)}{1 + B(M - M_o)} \tag{2.17}$$

2.2.2.2 Arrhenius Equation

The accuacy of the strength gain equation(Eq. 2.10) depends on the accuracy of the rate constant expression, and review of technical literature reveals that the Arrhenius equation provides a better function for the rate constant in terms of temperature. In European practice, Arrhenius equation is empolyed for the development of time-temperature function in the maturity method and is given by:

$$k(T) = A \exp(-\frac{Q}{RT_k}) \tag{2.18}$$

where A = a constant, or a factor,

T_k = temperature (°K),

R = universal gas constant (= 8.3144 J / °K-mole), and

Q = activation energy (kJ/mol).

The time-temperature function can be expressed as

$$M(t,T) = \int_0^t A \exp(-\frac{Q}{RT_k})\, dt \tag{2.19}$$

As known by Carino (1984), Arrhenius equation is a better representation of k(T) than the linear equation (2.13) when a wide variation in the concrete temperature is expected. Maturity number at a particular age is computed as follows:

$$M = A\sum_{o}^{t} \exp(-\frac{Q}{RT_k})\Delta t \qquad (2.20)$$

In equation (2.10), k_T is the value of the temperature function k(T) while concrete is isothermally cured. Based on equation (2.10), the relationship between the strength and age is a hyperbola with initial slope at t_o equal to $k_T f_{cu}$. The initial development of strength gain is dependent on k_T which is the so called rate constant. Thus, the temperature function, or the rate constant, k(T) is a key feature of the strength gain function.

2.2.3 The Equivalent Age Approach

Instead of expressing strength gain in terms of the temperature-time factor, an alternative approach is the use of the "equivalent age" method suggested by Rastrup (1954). Accordly (ASTM C 1074-87, 1989), the equivalent age is defined as the number of days or hours at a specified standard temperature required to produce a maturity value equal to the value achieved by a curing period at temperatures different from the specified temperature. In the equivalent age approach the actual age of concrete is transformed to its equivalent age at a specified temperature by means of a maturity function. The equivalent age concept is a convenient method for using other functions to account for the combined effects of time and temperature on strength development.

There are several different equations to compute an equivalent age depending upon the maturity function. For example, The maturity function (Eq. 2.12) can be used to transform temperature-time history to an equivalent age of curing at a standard temperature as follows:

$$t_e = \frac{\Sigma(T_a - T_o)\Delta t}{(T_s - T_o)} \tag{2.21}$$

where t_e = equivalent age at a standard temperature Ts.

Equation (2.21) can be written as follows:

$$t_e = \Sigma \alpha \, \Delta t \tag{2.22}$$

where

$$\alpha = \frac{(T - T_o)}{(T_s - T_o)} \tag{2.23}$$

The ratio α, which is called the "age conversion factor", has a simple interpretation: it converts a curing interval Δt to the equivalent curing interval at the standard reference temperature.

By using equivalent age approach based on Arrhenius equation, the strength-maturity relationship can be expressed as follows:

$$f_c = f_{cu} \frac{k_s(t - t_o)}{1 + k_s(t - t_o)} \tag{2.24}$$

where k_s is the value of the rate constant at the standare temperature.

2.2.4 Summary

The maturity method is intended for estimating strength development of concrete. First, a strength-maturity relationship should be developed in laboratory by measuring compressive strength and temperature history of cylinders on the concrete mixture to be used. Second, the temperature history of the concrete sample, for which strength is to be estimated, is recorded from the time of concrete placement to the time when the strength

estimation is desired. Third, the recorded temperature history is used to calculate the maturity of the concrete sample. Finally, using the calculated maturity and the strength-maturity relationship, the strength of the concrete sample is estimated. Strength estimates are based on two important assumptions: 1) there is always sufficient water for continued hydration, and 2) the concrete in the structure is the same as that used to develop the strength-maturity relationship.

The basic principle in applying the maturity method is illustrated in Figure 2.11. Two phases are involved:

(1) laboratory testing

- Mortar test is to determine datum temperature and activation energy.
- Based on the datum temperature or activation energy and recored cylinder temperature, the strength-maturity relationship is established by cylinder test.

(2) field measurement of the in-place concrete temperature history.

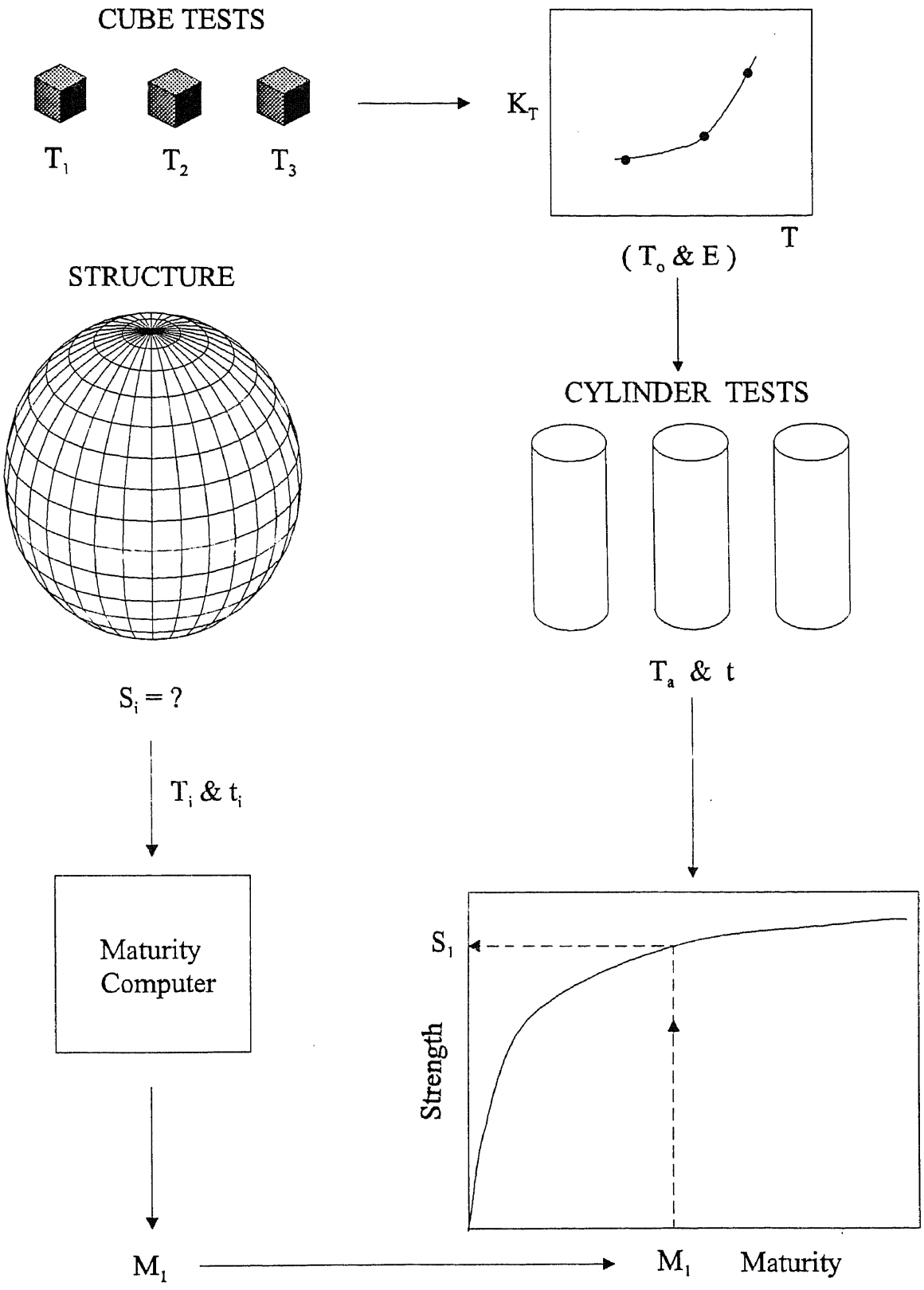

Figure 2. 11 Procedures for using maturity method involve laboratory testing and field measurements

CHAPTER 3

THEORETICAL DEVELOPMENT

3.1 Introduction

A testing methodology for insitu nondestructive determination of fracture energy, G_f, is developed in this study. The validity of the procedure is justified through the theoretical basis given in this section.

The rate theory in term of Arrhenius law is applied to explain the fracture energy gain of concrete. The derivations follow the same pattern as those developed in the formulation of time-temperature relationships for the rate of strength gain in concrete. However, time-temperature relationships are employed in an inverse manner to arrive at values for the activation energy of concrete through fracture experiments. Applicability of the maturity method is justified if, for all practical purpose, the activation energy evaluated from fracture tests equals the activation energy of concrete from strength tests or hydration studies.

3.2 The Rate Theory

Arrhenius Law which has been employed for nonlinear representation of the rate constant as a function of temperature in strength-maturity relations has great generality. It applies not only to the rate of strength gain in concrete, but to the rate of creep, oxidation, corrosion, and even to the rate at which bacteria multiplies. The Arrhenius or the rate law

states that the rate of a process increase exponentially with temperature(Figure 3.1a). For example, the rate of steady-state creep, $\dot{\varepsilon}$ varies with temperature as:

$$\dot{\varepsilon} = A e^{-Q/RT_k} \tag{3.1}$$

or the rate constant, k(T), in the maturity rule for in-place determination of strength in concrete as:

$$k(T) = A e^{-Q/RT_k} \tag{3.2}$$

where in both Eqs. (3.1) and (3.2):

A = a constant, or a factor,

T_k = temperature (°K),

R = universal gas constant (= 8.3144 J / °K-mole), and

Q = activation energy (kJ/mol), the energy which the reacting molecules must acquire before they can react.

According to Eqs. (3.1) and (3.2) the activation energy is the slope of the linear relationship between the natural logarithm of the rate of process(rate constant, creep rate, etc.) and the inverse of absolute temperature, 1/T. As an example, this is illustrated in Figure 3.1b for the steady state creep.

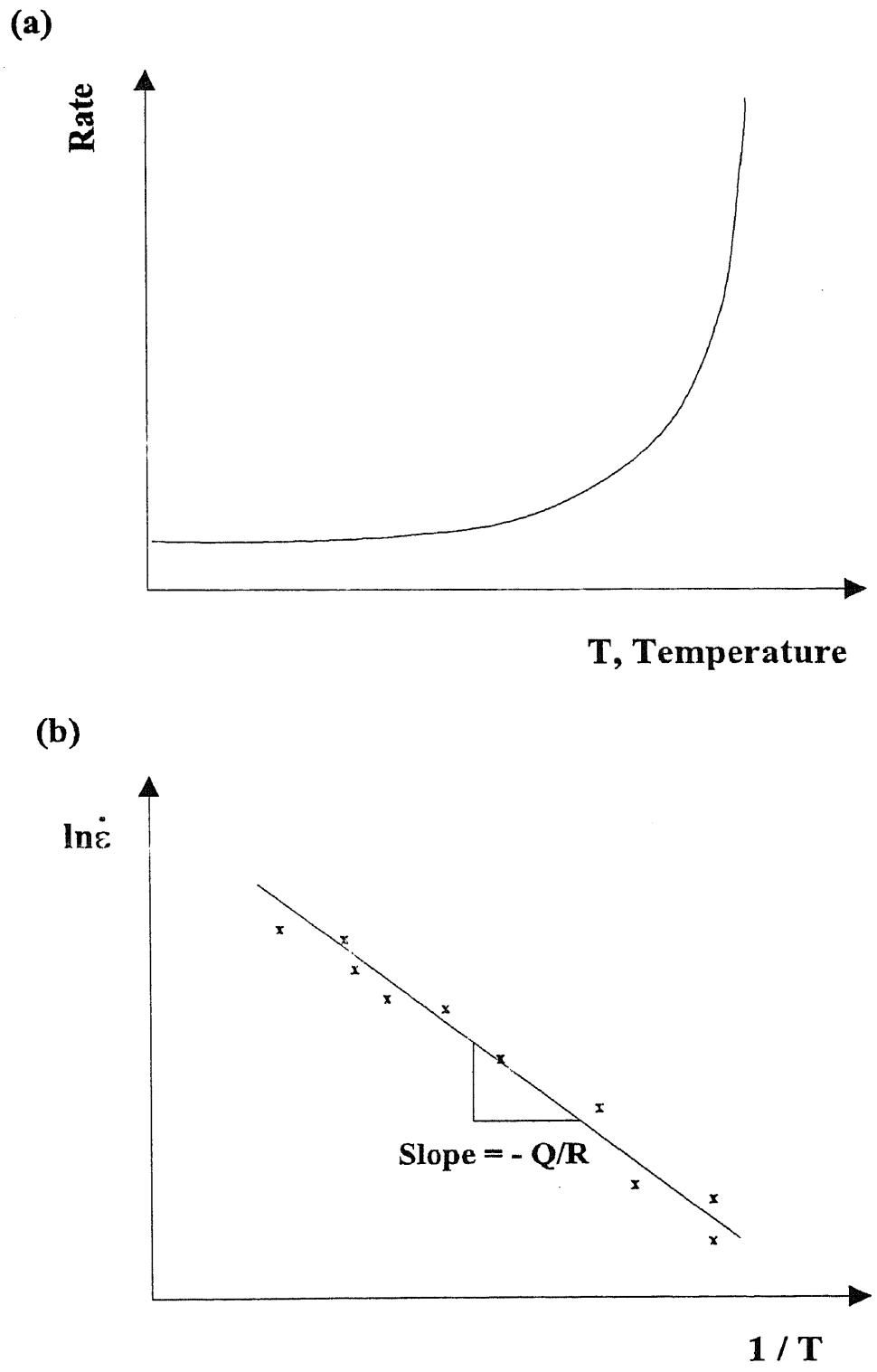

Figure 3. 1 (a) Consequences of Arrhenius' law,
(b) Strain rate follow Arrhenius' law (Ashby, 1980)

3.3 Theoretical Basis

3.3.1 Fracture Energy Gain Function

Concrete gains rigidity and resistance to fracture at the end of induction period, approximately 2.5 to 3.5 hours after the mixing. Temperature and moisture conditions play an important role in the rate of strength-gain in concrete. Bernhardt (1956) explained the rate of strength gain, at any age t, as a function of current strength, f_c, and the temperature T:

$$\frac{df_c}{dt} = k(T) \cdot g(f_c) \tag{3.3}$$

where k(T) is a function of temperature and $g(f_c)$ is a function of strength. Bernhardt went on to empirically obtain the strength function $g(f_c)$ which enabled him to develop the following general strength-age relationship:

$$f_c = f_{cu} \{F(t,T) / [1 + F(t,T)]\} \tag{3.4}$$

where the general form of the time-temperature function F(t,T) is the integral of the temperature function between time t_o (the end of induction period, time at which strength is equal to zero) and t, as follows:

$$F(t,T) = \int_{t_o}^{t} k(T)\, dt \tag{3.5}$$

Assuming that eq. (3.2) holds not only for strength development but for any other properly of concrete that is directly related to the extent of cement hydration, then it is possible to develop a general fracture energy gain function similar to that of eq. (3.4). It is also possible to develop such a relationship for the fracture energy provided that, under isothermal conditions, the relationship between the fracture energy and age is hyperbolic,

and the function $g(G_f)$ can be determined. $g(G_f)$ is then employed for the following relationship describing the rate of fracture energy gain as a function of fracture energy and temperature:

$$\frac{dG_f}{dt} = k(T) \cdot g(G_f) \tag{3.6}$$

Rearranging terms in eq. (3.6) results in:

$$\frac{dG_f}{g(G_f)} = k(T)\,dt \tag{3.7}$$

We need to integrate eq. (3.7) to determine G_f:

$$\int_{o}^{G_f} \frac{dG_f}{g(G_f)} = \int_{t_o}^{t} k(T)\,dt \tag{3.8}$$

provided that we have already determined the function $g(G_f)$, it will then be possible to evaluate G_f through eq. (3.8) as follows:

$$G_f = f\left(\int_{t_o}^{t} k(T)\,dt\right) \tag{3.9}$$

where, $f\left(\int_{t_o}^{t} k(T)\,dt\right)$ is a function of k(T) and age after integration of eq. (3.8). Eq. (3.9) is the fracture energy-gain function. It is necessary to determine the function of fracture energy $g(G_f)$ in order to expedite the integration in eq. (3.8).

3.3.2 Fracture Energy Function

Bernhardt's formulation for the rate of strength-gain, as described earlier in Eq. (3.3), involves two distinct functions: the function of temperature, k(T), and the function of strength $g(f_c)$ respectively. The intuitive meanings of these two functions as explained by

Bernhardt were that; k(T) indicates the intensity of hardening at the given temperature, and $g(f_c)$ may be regarded as the remaining magnitude of strength to be gained. As a result, the value of $g(f_c)$ is maximum and equal to the limiting or final strength of concrete, f_{cu}, at the end of induction period(2.5 to 3.5 hours after mixing), and equal to zero at the time when the limiting strength is achieved. Accordingly, and based on empirical evidence, Bernhardt arrived at the following relationship for $g(f_c)$:

$$g(f_c) = f_{cu}[1 - (\frac{f_c}{f_{cu}})]^2 \qquad (3.10)$$

Developments leading to the form of Eq. (3.10) stem from the hyperbolic nature of the strength-age function for isothermally cured concretes.

Experimental results in the present study indicated that the increase in fracture energy with age also follows a hyperbolic pattern similar to that for strength. Therefore, it is reasonable to hypothesize that the fracture energy function will have the same form as the one developed for strength in Eq. (3.10). Consequently, the fracture energy gain rates, $\frac{dG_f}{dt}$, are numerically evaluated from the experimental fracture energy versus age data (Figs. 3.2 and 3.3 for size B beam). As it turns out, the relationship between the fracture energy and $\sqrt{\frac{dG_f}{dt}}$ is linear (Fig. 3.4). The figures of G_f against $\frac{dG_f}{dt}$ and G_f against $\sqrt{\frac{dG_f}{dt}}$ for size A and size C beam are given in appendix A.

As shown in the inset of Figure 3.4, the y-intercept corresponds to the limiting or the ultimate fracture energy of concrete (G_{fu}). The x-intercept is the square root of

fracture energy gain rate at maximum, and it can be evaluated by taking the square roots from both sides of Eq. (3.6):

$$\sqrt{\frac{dG_f}{dt}} = \sqrt{k(T)}\sqrt{g(f_c)} \tag{3.11}$$

Since for the case of isothermal curing, the rate constant, k(T), is constant, at x-intercept, the function $g(G_f)$ must have its maximum value in order for $\sqrt{\frac{dG_f}{dt}}$ to be maximum. Moreover $g(G_f)$ represents the remaining magnitude of the fracture energy to be gained, and the x-intercept of Figure 3.4 corresponds to time t_o, when the concrete starts gaining rigidity. Therefore at time t_o:

$$g(G_f) = G_{fu} \tag{3.12}$$

which means at time t_o concrete needs to attain all its fracture energy. And the x-intercept value in Figure 3.4 is:

$$\sqrt{\frac{dG_f}{dt}} = \sqrt{k(T)}\sqrt{G_{fu}} \tag{3.13}$$

at y-intercept (when $G_f = 0$). Hence, the straight line relationship between the fracture energy, and the square root of fracture energy gain rate is given as:

$$G_f = -\frac{G_{fu}}{\sqrt{k(T)}\sqrt{G_{fu}}}\sqrt{\frac{dG_f}{dt}} + G_{fu} \tag{3.14}$$

Eq. (3.14) leads to:

$$\frac{dG_f}{dt} = k(T)G_{fu}\left(1 - \frac{G_f}{G_{fu}}\right)^2 \tag{3.15}$$

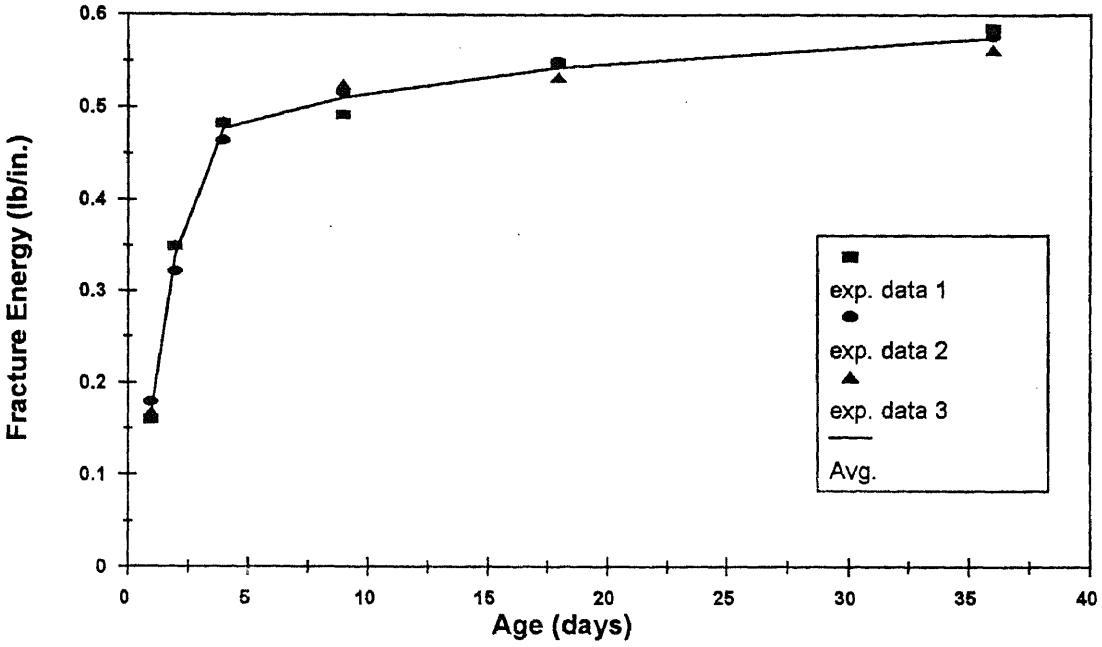

Figure 3. 2 A typical fracture energy - age curve

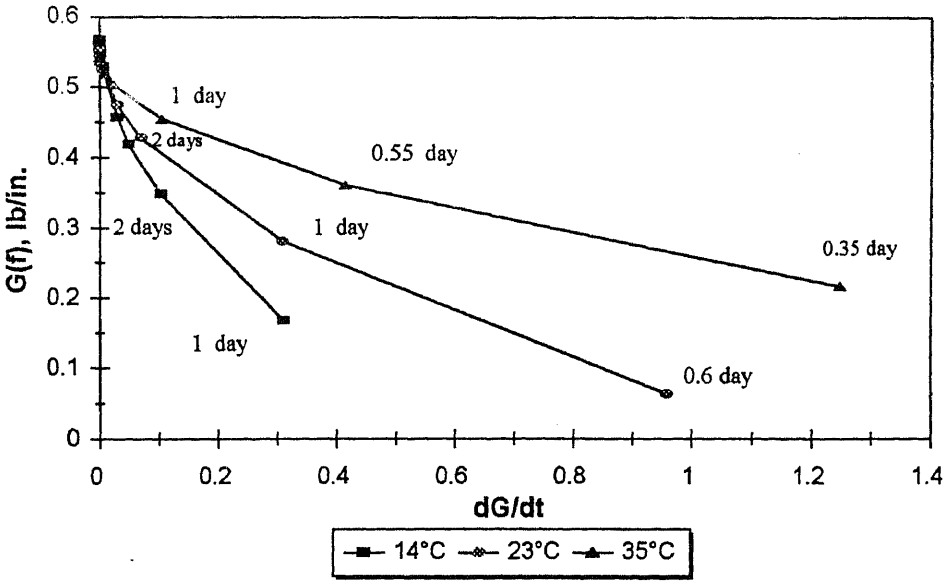

Figure 3.3 G_f against dG_f / dt

Comparison of Eqs. (3.6) and (3.15) yields the fracture energy function:

$$g(G_f) = G_{fu}(1-\frac{G_f}{G_{fu}})^2 \tag{3.16}$$

Eq. (3.16) is of the same form given for strength function in Eq. (3.10).

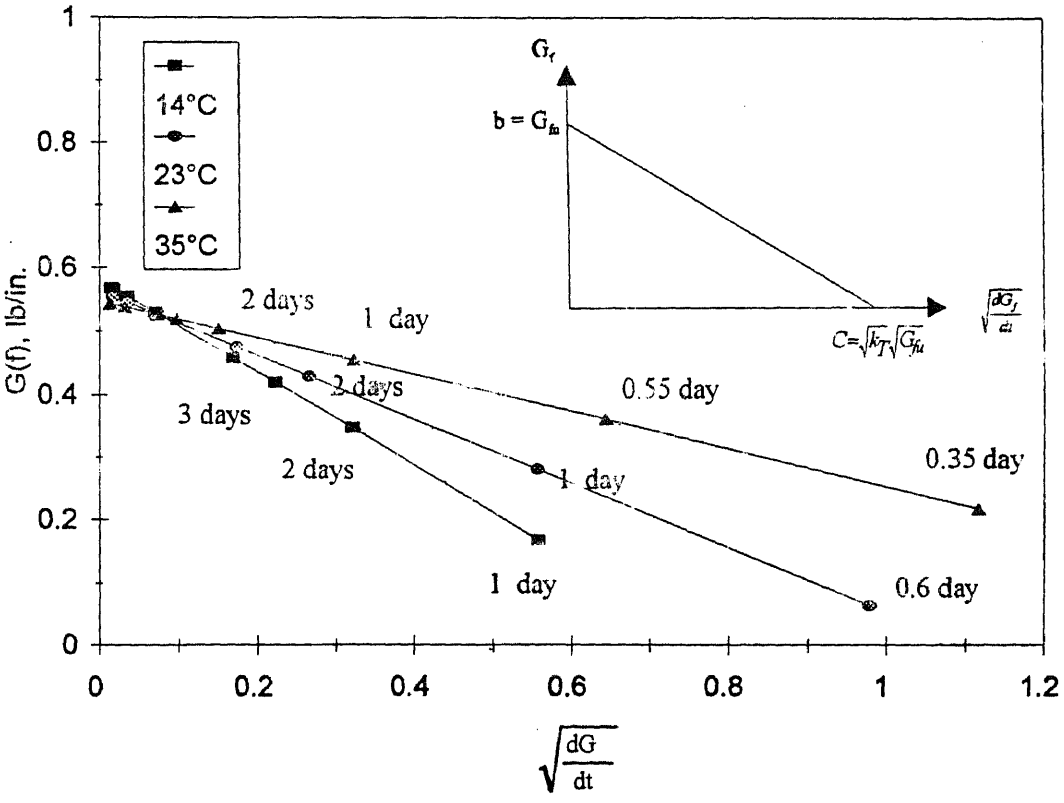

Figure 3.4 G_f against $\sqrt{dG/dt}$

3.3.3 Fracture Energy Gain of Concrete

The formulation of a mathematical expression to describe the fracture energy development of concrete is discussed first. The fracture energy function is proposed as follows:

$$g(G_f) = G_{fu}(1-\frac{G_f}{G_{fu}})^2 \tag{3.16}$$

where G_{fu} is the limiting fracture energy at infinite age. Assuming that the limiting fracture energy, G_{fu}, is independent of curing temperature, substitution of $g(G_f)$ from Eq. (3.16) into Eq. (3.8) and rearranging terms leads to:

$$\int_0^{G_f} \frac{dG_f}{g(G_f)} = \int_{t_0}^{t} k(T)dt \tag{3.17}$$

$$\int_0^{G_f} \frac{dG_f}{(1-G_f/G_{fu})^2} = \int_{t_0}^{t} G_{fu}\, k(T)\, dt \tag{3.18}$$

where t_o, datum age, is the age when fracture energy development is assumed to begin, and it can be given in days.

The integral on the right side of Equation (3.17) was suggested as the general form of the maturity function, the time-temperature function, and denoted M(t,T) with

$$M(t,T) = \int_{t_0}^{t} k(T)dt \tag{3.19}$$

where M(t,T) = the maturity function, or a function of the time and temperature.

The integral on the left side of Equation (3.18) may be evaluated as follows:

$$\int_0^{G_f} \frac{dG_f}{(1-\frac{G_f}{G_{fu}})^2} = \frac{G_{fu}^2}{(G_{fu}-G_f)}\Bigg|_0^{G_f} = \frac{G_{fu}G_f}{G_{fu}-G_f} \tag{3.20}$$

Substituting Equation (3.19) into the right side of Equation (3.18), and Equation (3.18) becomes:

$$G_{fu} \int_{t_o}^{t} k(T)dt = G_{fu} \cdot M(t,T) \tag{3.21}$$

Substitution of Equations (3.20) and (3.21) in (3.18) yields,

$$\frac{G_f}{G_{fu} - G_f} = M(t,T) \tag{3.22}$$

By rearranging terms, Equation (3.22) will have the following form:

$$G_f = G_{fu} \cdot M(t,T) - G_f \cdot M(t,T) \tag{3.23}$$

$$G_f [\ 1 + M(t,T)\ ] = G_{fu} \cdot M(t,T) \tag{3.24}$$

and it is possible to arrive at the following fracture energy development relationship:

$$G_f = G_{fu}\ [\frac{M(t,T)}{1+M(t,T)}] \tag{3.25}$$

This is the basic form of the fracture energy-maturity relationship, the general fracture energy gain function, in terms of the time-temperature function. The time-temperature function has different forms depending upon curing conditions and the nature of temperature function k(T).

3.3.3.1 Isothermal conditions

For the special case of constant concrete curing temperature, the temperature function k(T) has a constant value, k_T. Therefore, the general fracture energy-age function reduces to a simple expression:

$$G_f = G_{fu}\frac{k_T(t-t_0)}{1+k_T(t-t_0)} \tag{3.26}$$

where k_T is the value of the temperature function, or the rate constant, at the constant concrete temperature T.

As it will be shown later by this study, there is not a single fracture energy-age function for a given concrete mixture, because different initial concrete temperatures will result in different values of G_{fu}. Nevertheless, it is proposed that there is a unique relative fracture energy versus age function:

$$\frac{G_f}{G_{fu}} = \frac{k_T(t-t_0)}{1+k_T(t-t_0)} \tag{3.27}$$

3.3.3.2 Variable temperature conditions

When the curing temperature is not constant, the temperature function k(T) is not constant. First, the simplest case is to assume a linear relationship as follows :

$$k(T) = B(T - T_o) \tag{3.28}$$

where T_o = datum temperature, temperature corresponding to k(T) = 0, and

B = a constant, the slope of the straight line.

Substituting equation 3.28 into equation 3.19, the maturity function can be expressed as:

$$M(t,T) = \int_{t_o}^{t} B(T-T_o)dt = \int_{0}^{t} B(T-T_o)dt - \int_{0}^{t_o} B(T-T_o)dt \tag{3.29}$$

If the two terms on the right hand side of equation 3.29 are called M and M_o, the maturity function is

$$M(t,T) = B(M - M_o) \tag{3.30}$$

Substituting equation 3.30 into equation 3.25, the fracture energy - maturity relationship can be obtained as:

$$G_f = G_{fu} \frac{B(M - M_o)}{1 + B(M - M_o)} \tag{3.31}$$

Next, since hydration is an exothermic chemical reaction, it is reasonable to assume that the rate constant should vary with temperature according to the Arrhenius equation, equation 3.2, i.e.,

$$k(T) = A \exp\left(-\frac{Q}{RT_k}\right)$$

An alternative to expressing fracture energy gain in terms of the time-temperature function is to use the equivalent age approach. Equivalent age represents the age at a standard curing temperature, T_s (°K), which results in the same maturity as under the actual curing temperature. Mathematically, equivalent age t_e is defined as follows

$$t_e = \int_0 \frac{k(T)}{k_s} dt \tag{3.32}$$

where t_e = equivalent age at the standard temperature, T_s,

k_s = value of the rate constant at the standard temperature.

The ratio $k(T) / k_s$ has been termed the age conversion factor,

$$\alpha = \frac{k(T)}{K_s} \tag{3.33}$$

and the relative fracture energy gain can be expressed in terms of equivalent age:

$$\frac{G_f}{G_{fu}} = \frac{K_s \alpha (t - t_o)}{1 + K_s \alpha (t - t_o)} \tag{3.34}$$

By using the Arrhenius equation, the age conversion factor is

$$\alpha = \exp[-\frac{Q}{R}(\frac{1}{T_k} - \frac{1}{T_s}) \tag{3.35}$$

The equivalent age expression becomes as follow:

$$t_e = \sum_0^t \exp\{-\frac{Q}{R}[\frac{1}{T_k} - \frac{1}{T_s}]\}\Delta t \tag{3.36}$$

3.3.4 Activation Energy of Concrete

The Arrhenius equation is used to describe the relationship between the rate constant and curing temperature. In this case, the important parameter is the activation energy, which defines the temperature sensitivity of the rate constant. The value of activation energy depends on the cement chemistry, the cement fineness, and the type and quantity of cement replacements and admixtures. Typical published values of activation energy for ordinary portland cement are between 42 and 47 kJ/mol(Gauthier, 1982, Regourd, 1980b and Roy, 1982).

The value of the activation energy for a particular concrete can be determined in several ways. One approach is to make and cure concrete specimens at several different temperatures and analyze the strength-age data by transforming the hyperbolic strength-age relations into linear equations and regression analysis as described later in this section. However, there are alternative possibilities. It has been firmly established that the degree of hydration of cement correlates with the mechanical strength of concrete (Alexander, 1969; Seki, 1969). Therefore it is possible to determine the activation energy from hydration studies of cement paste. This approach is supported by the work of others (Regourd, 1980a and b; Gauthier, 1982) who have shown that the activation energies

based upon heats of hydration are the same as those based upon the mechanical strength of mortars. Another approach is to measure the chemical shrinkage of cement pastes (Geiker, 1982 and 1983).

3.3.5 Fracture Energy, Strength, and Activation Energy

The work presented herein suggests the use of maturity method for in-place estimation of fracture energy in concrete structures. As shown in Figure 3.2, the fracture energy-age relationship has the same hyperbolic form as the one for strength-age of concrete employed in the maturity method. However, the mere similarity between the general form of these relationships does not provide sufficient justification for the applicability of the maturity method in estimating the in-place fracture energy.

As discussed in the previous section, in using a time-temperature function the activation energy of concrete which is an important parameter for the rate constant of concrete mixture must be known. It was further discussed that several method are available for the determination of activation energy including the methods based on hydration studies of cement paste and regression analysis of the strength-age data. Typical values of activation energy (42-47 kJ/mol) can also be used for cases where accuracy of strength prediction is not crucial.

The proof for the applicability of the maturity method in estimating the fracture energy of concrete will be in arriving at similar activation energies for the same concrete by using the fracture energy-age date in a similar manner as the strength-age relationship for the evaluation of activation energy. Experimental results from tests on more than 150

beams of various dimensions (3 different sizes) in this study proved the above mentioned hypothesis. In the following section, the strength-age approach for the determination of activation energy from experimental results will be reviewed. An exact similar approach will be employed for the determination of activation energy from fracture energy-age data.

3.3.6 Rate Constant, Limiting Strength, and the Activation Energy

The hyperbolic strength-maturity relationship which was independently proposed by Bernhardt(1956), and Goral(1956) was later on adopted by committee 209 of the American Concrete Institute to estimate concrete strength at different ages(ACI, 1971). To evaluate the hyperbolic function for the given strength-age data for each curing temperature values of three parameters, namely f_{cu}, k_T, and t_o need to be evaluated. Similarly, to evaluate the hyperbolic function for the given fracture energy-age data, G_{fu}, k_T, and t_o need to be evaluated at each curing temperature. Several approaches are available for evaluating the above-mentioned parameters from the experimental data, including the least-square fit(Carino), and the trial and error approach. Knudsen's approach(Knudsen, 1980) is the most simplistic approach in arriving at the three parameters, and will be described in the following. In Knudsen's approach, the approximation $t \approx (t\text{-}to)$ simplifies the parameter evaluation procedure.

For the case of strength evaluation, equation 2.10 can be rewritten as follows:

$$\frac{1}{f_c} = \frac{1}{f_{cu}} + \frac{1}{k_T f_{cu}} \frac{1}{t} \tag{3.37}$$

In this dissertation the sane approach is applied for fracture energy:

$$\frac{1}{G_f} = \frac{1}{G_{fu}} + \left(\frac{1}{k_T G_{fu}} \frac{1}{t}\right) \tag{3.38}$$

Thus, a plot of $1/G_f$ versus $1/t$ is a straight line, and the inverse of the intercept is the limiting fracture energy G_{fu} (Figure 3.5a). Having estimated the value of G_{fu}, equation 3.26 can be written in the following form to estimate k_T and t_o

$$\frac{G_f}{G_{fu} - G_f} = -k_T t_o + k_T t \tag{3.39}$$

Then, a plot of $\frac{G_f}{G_{fu} - G_f}$ versus t is a straight line having a slope k_T and a t-axis intercept of t_o (Figure 3.5b).

As the rate constant obeys the Arrhenius equation, there should be a linear relationship between ln k(T) and the reciprocal of the absolute temperatures. A plot of the natural logarithm (ln) of the rate constant, k(T), against the reciprocal of the absolute temperature, $1/T_k$, is a straight line as shown in figure 3.6b. The slope of this line is the value of the activation energy divided by the gas constant. This approach will be employed for both strength-age, and fracture energy-age data. It will be shown that the activation energies computed from both sets of data are equivalent.

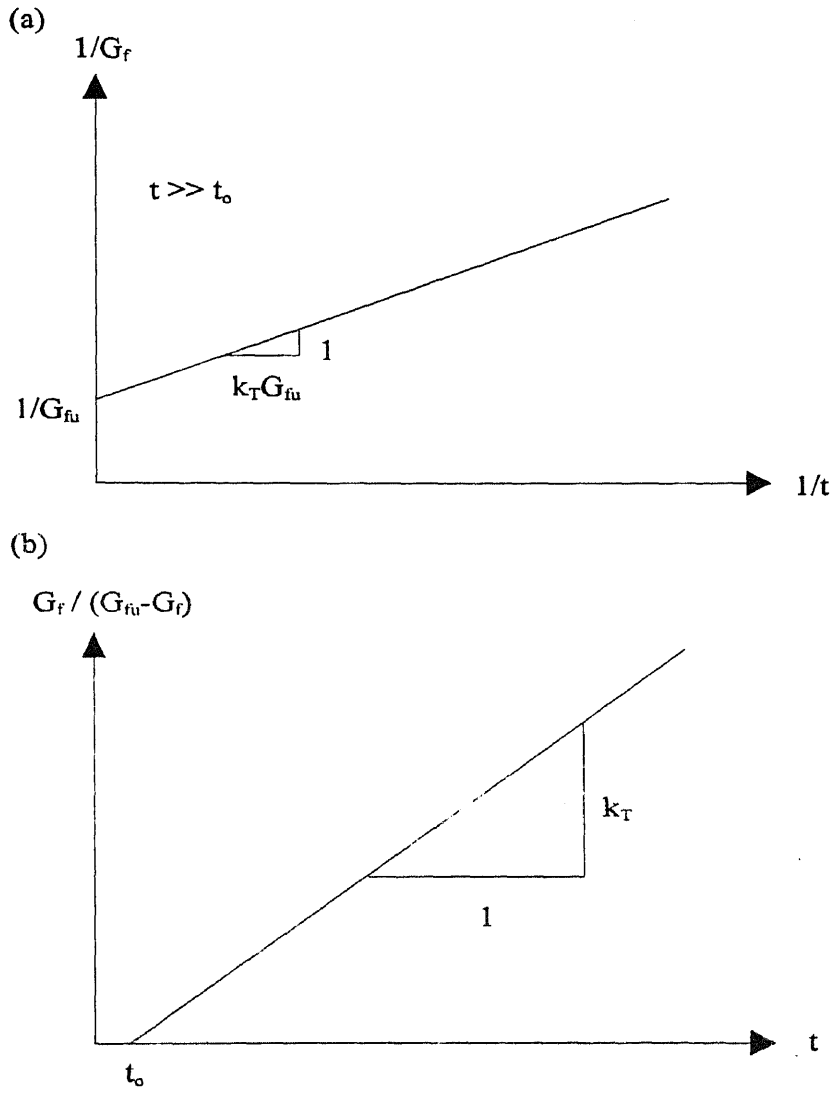

Figure 3.5 Fracture energy-age function of isothermally cured concrete: Linear Transformations

(a)

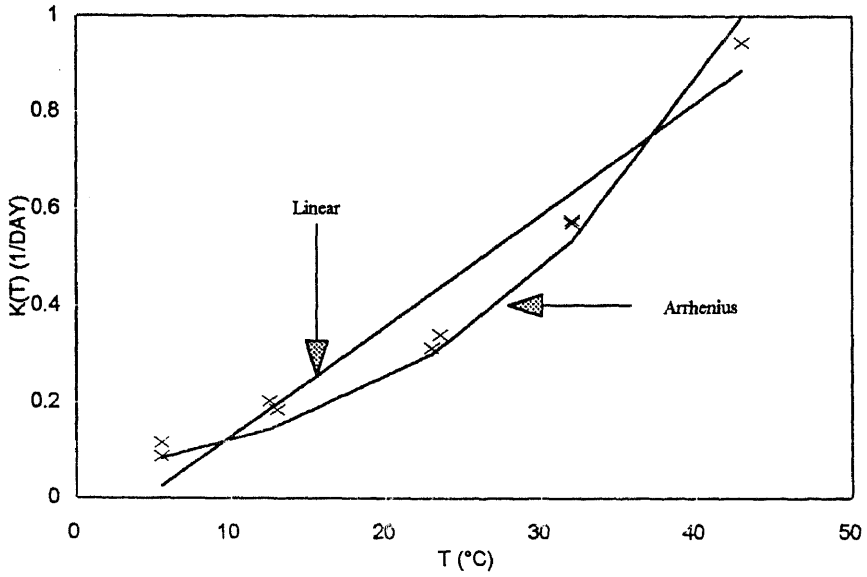

(b)

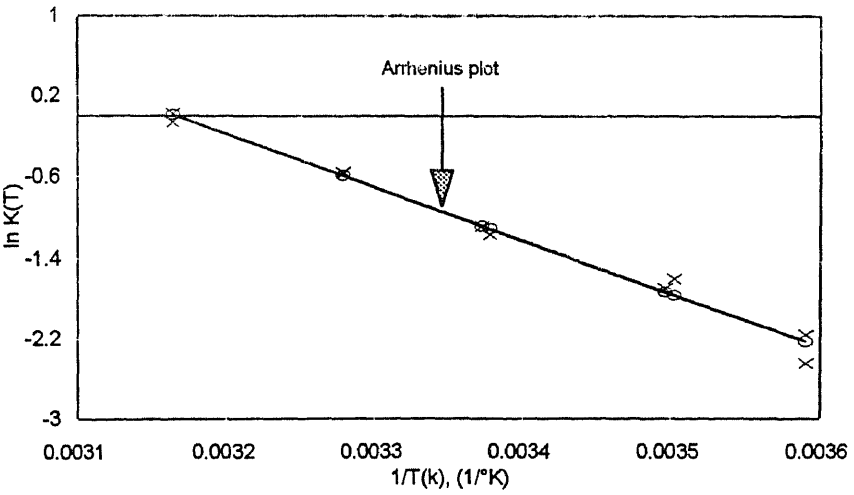

Figure 3.6 (a) Variation of rate constant k(T) with temperature T: Linear & Arrhenius Eq.
(b) ln k(T) vs. $1/T_k$ (Carino, 1991)

CHAPTER 4

EXPERIMENTAL PROGRAM

4.1 Introduction

The test program was designed for compression cylinder and cube and the three-point bend beam tests. Compression tests were performed according to ASTM C 109 for cubes and C 39 for cylinders. Three-point bend test on notched beams were employed for the determination of fracture energy. The dimensions of the beam were selected according to the recommendations by RILEM Committee T50 (1985). The fracture energy, G_f, was estimated using the FCM formula given by the RILEM Committee T50 (1985) which is given as:

$$G_f = \frac{w_0 + mgw_1}{A_{lig}} \tag{4.1}$$

where w_0 = area under the load-deflection curve of three-point bend test,

m = mass of the specimen between supports,

g = acceleration due to gravity,

A_{lig} = projection of the fracture zone on a plane perpendicular to the beam axis, and

w_1 = deformation at the final failure of the beam.

4.2 Experimental Procedure

4.2.1 Materials and Mixture Proportions

Concrete and mortar mixtures were proportioned with a water-cement ratio of 0.5. Type I portland cement was employed for the mortar and concrete mixtures. Granite was used as the coarse aggregate with 3/8" nominal maximum size. Fine aggregate was natural river sand. The mix proportion by weight of concrete was designed to be 1:2:2.7:0.5, corresponding to Cement : Sand : Aggregate : Water. The mix proportion by weight of mortar was designed to be 1:2.7:0.5, corresponding to Cement : Sand : Water.

4.2.2 Specimens Preparation

4.2.2.1 Compressive Test Specimens

For the concrete, cylindrical specimens were prepared using 3" x 6" plastic molds and then were cast along with beam specimens. Molds were filled in two layers, tamping each layer 15 times with a 3/8" diameter steel rod. For the mortar, cubic specimens were prepared using 2" x 2" x 2" steel molds. Molds were filled in two layers and each layer was tamped 16 times with a hard rubber tamper. Three to eight hours after casting, cubes, cylinders and beams were immersed carefully into water bath and allowed to cure. All the mortar cubes were demolded at the time of the first strength test. Cylinders were demolded at the same time as the beam specimens.

4.2.2.2 Three-Point Bend Beams

The testing program involved experimentation with three different sizes of specimens. Size B beam dimensions were chosen according to the recommendations by RILEM Committee T50. Smaller size A and larger size C specimens were selected for comparison. Specimen sizes and designations are given in Table 4.1. All beams were pre-notched with a notch to depth ratio of 0.5.

Table 4.1 Beam specimen sizes and corresponding designations.

TYPE	width (b) (in)	depth(d) (in)	span(S) (in)	length(L) (in)
A	3	3	18	20
B	4	4	32	34
C	4	6	38	40

4.2.3 Specimens Curing Temperature

To obtain the desired curing temperatures for specimens as quickly as possible, it was necessary to control the temperature of the aggregates for the concrete to be mixed. As this study was carried out in the laboratory , cements and aggregates were stored in room

temperature. The approximate temperature of the laboratory was about 23 °C. For specimens to be cured at 14 °C, cements and aggregates were stored in an air conditioned room at 14 °C.

To obtain a fresh mortar and concrete temperature close to the intended curing temperature values of 14°C, 23°C and 35°C respectively, the temperature of the mixing water was varied. The following thermodynamic formula was employed to arrive at the mixing water temperatures (Portland Cement Association, 1988) :

$$T = \frac{0.22(T_a W_a + T_c W_c) + T_w W_w}{0.22(W_a + W_c) + W_w} \tag{4.2}$$

where T = desired temperature of fresh mortar and concrete,

T_a , T_c , T_w = temperature of aggregates, cement, and mixing water, respectively

W_a, W_c, W_w = weight of aggregates, cement, and mixing water, respectively.

Calculated mixing water temperatures are given in Table 4.2

Table 4.2.a Mixing water temperatures (°C) for mortar.

Fresh Mortar (Temp. Desired)	Temp. of Cement & Aggregates	Temp. of Mixing Water (Calculated)	Temp. of Mixing Water (Used)
14	14	14	14
23	23	23	23
35	23	54.5	54.5

Table 4. 2.b Mixing water temperatures (°C) for concrete.

Fresh Concrete (Temp. Desired)	Temp. of Cement & Aggregates	Temp. of Mixing Water (Calculated)	Temp. of Mixing Water (Used)
14	14	14	14
23	23	23	23
35	23	65	65

4.2.4 Specimens Temperature Monitoring

Temperature of mortar and concrete specimens were monitored via thermocouples embedded within the samples during curing. For mortar cubes, temperatures of three samples per a batch of 30 specimens were monitored. Concrete mixing process involved production of 3 beams, and 3 cylinders per batch. Temperatures for 2 beams, and 2 cylinders per each concrete batch were monitored. Temperatures were monitored at 2 minutes intervals for the first 12 hours, and half hour to one hour intervals thereafter. Thermocouples were of type T manufactured by the Omega Engineering, INC. Temperature histories for each batch were acquired via an EXP-16 Universal Expansion Interface, analog input multiplexer, connected to the DAS-8 data acquisition board in a

personal computer. Based on the temperature data, it was found that the concrete and mortar specimens reached the bath temperature within 2 to 3 hours after the start of mixing. Figure 4.1 illustrates typical curing temperature data for a specimen in a curing chamber. As shown in Figure 4.1, specimen temperatures deviate from the intended values by about 3 to 4°C at the first few hours after mixing.

4.2.5 Test Schedule

This study required testing of about three hundred and fifty concrete and mortar specimens. To obtain similar strength-age and fracture energy-age data it is necessary to test the specimen at approximately equal maturities. Based on the maturity concept, samples of the same concrete will have equal strength if they have equal maturity, irrespective of their actual time-temperature histories. To determine the test age, a preliminary investigation was carried out with mortar cube tests. Based on preliminary tests, ASTM C1074-87, and tests by others (Carino, 1984), the testing age for specimens which were cured at 23 °C were determined. The test-age schedule was established first for the specimens at 23°C, and test ages for 14°C and 35°C specimens were determined on the basis of equal maturity values corresponding to the 23 °C reference temperature. Tables 4.3 and 4.4 list the testing age schedule used for the three different curing temperatures.

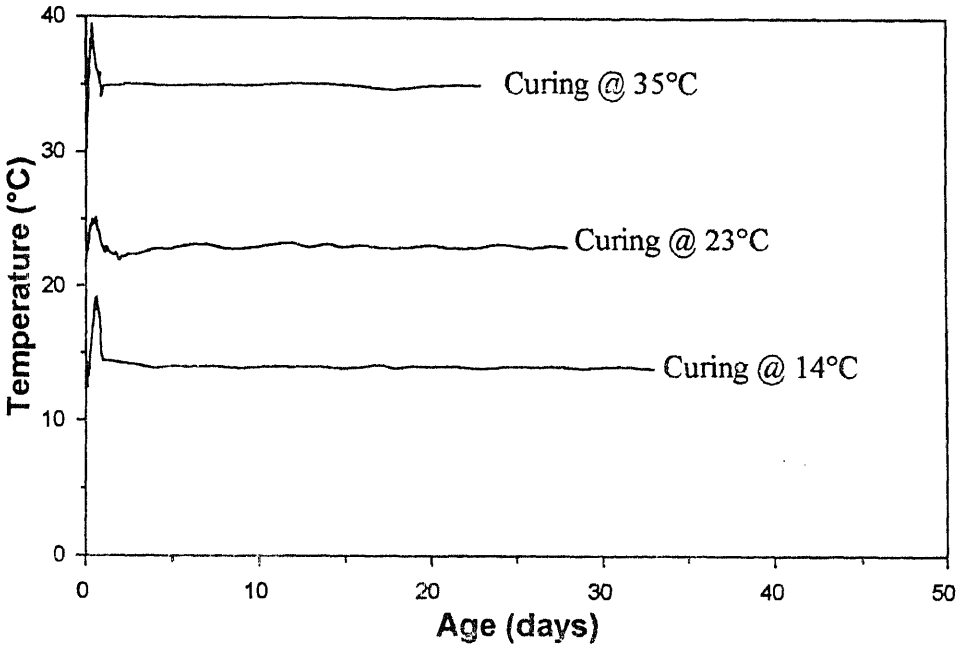

Figure 4.1 Typical curing temperature for beam specimen

4.2.6 Three Point Bend Beam Test and Setup

All samples were tested on an MTS system closed-loop servo controlled hydraulic testing machine. The closed-loop system enabled the use of CMOD control under which the CMOD was increased at a rate of 50 μ inch per second. Load point displacements(center point deflections) were measured by a Linear Variable Differential Transformer(LVDT). To eliminate displacements associated with the support settlement, the setup shown in Figures 4.2 were employed for measuring the load point displacements. This mode of control causes a controlled failure of the sample allowing all parameters of interest to be measured. Data including Time, Load, CMOD and LVDT were recorded using a Metrabyte DAS-20 data acquisition and control board running the Labtech Notebook data acquisition program. Typical experimental raw data from a beam test are depicted in Figure 4.3.

Table 4. 3 Curing temperatures and testing age for mortar cubes

Curing Temperature	No. of Specimen[a]	Approximate Testing Age (days)	Total No. of Specimens
14°C	3	1, 2, 3, 7, 11, 22, 46	21
23°C	3	0.6, 1, 2, 4, 7, 14, 28	21
35°C	3	0.4, 0.8, 1, 2, 3, 9, 18	21

[a]Number of replicate tests at each age.

Table 4.4 Curing temperatures and testing age for concrete specimens

Specimen Type	Curing Temperature (°C)	No. of Specimen*	Testing Age (days)	Total No. of Specimens
A	14	3	1.22, 2, 4, 7, 22, 36	18
	23	3	0.5, 1.3, 3, 7, 14, 28	18
	35	3	0.35, 0.56, 1 , 4, 9, 20	18
B	14	3	1, 2, 4, 10, 22, 38	18
	23	3	0.56, 1.2, 3, 7, 14, 28	18
	35	3	0.25, 0.55, 1.6, 4, 9, 20	18
C	14	2	1.1, 2.1, 4, 9, 18, 36	12
	23	3	0.65, 1, 3, 7, 14, 28	18
	35	2	0.29, 0.51, 1, 4.28, 9, 20	12
Cylinder**	14	3	1, 2, 4, 7, 10, 20, 38, 45	24
	23	3	0.55, 0.7, 1, 3, 7, 14, 28	21
	35	3	0.375, 0.56, 1, 2, 4, 9, 20 ,23	24

* Number of replicate tests per testing age.
**Companion 3x6 cylinders from the same batch as in beams.

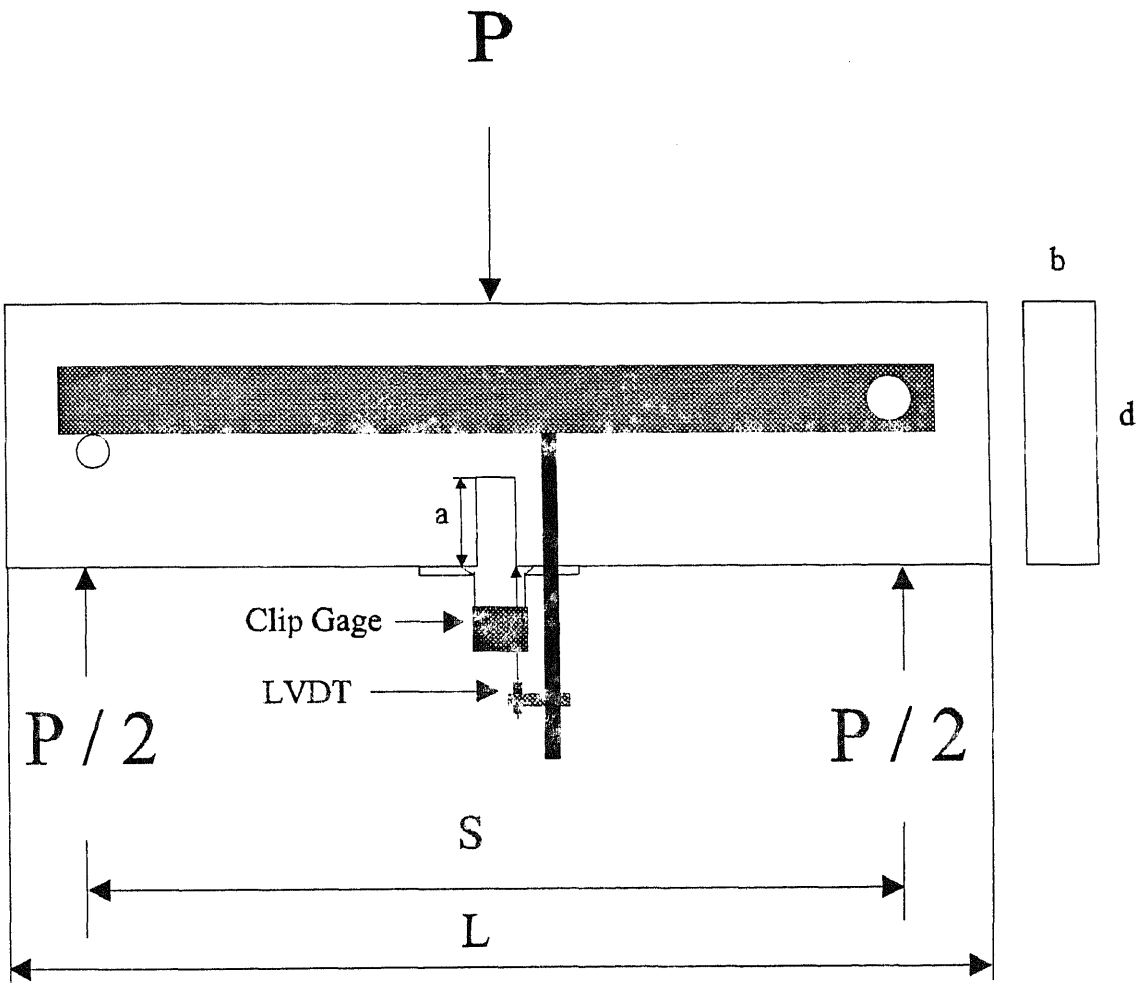

Figure 4.2 Three-Point Bend Test Setup

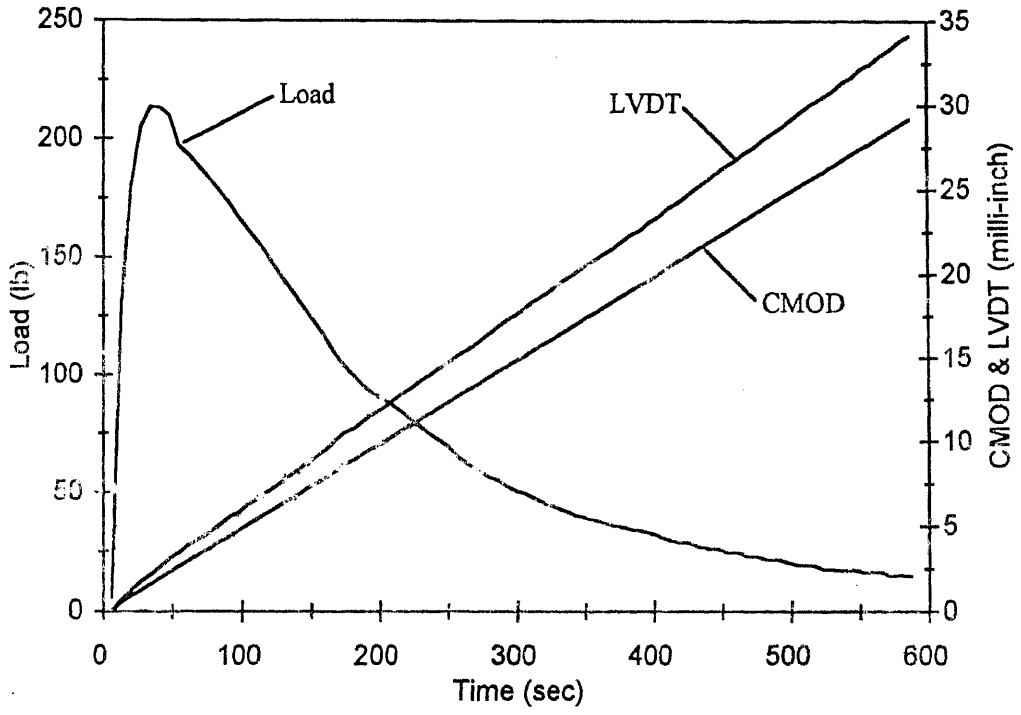

Figure 4.3 Typical raw experimental data for a 3-point bend beam test

CHAPTER 5

RESULTS AND DISCUSSIONS

5.1 General

This dissertation aims to develop a nondestructive technique to estimate the relative fracture energy gain of concrete based upon its time-temperature history. This nondestructive method is proposed and the basic fracture energy development parameters are calculated on the basis of the fracture energy - age data from one hundred and fifty beam specimens. The experimental procedures were outlined in Chapter 4. This chapter presents the experimental results, analysis of results and a discussion of the observed trends.

Experimental data was analyzed to study the effect of the curing temperature on the parameters governing the fracture energy development in concrete mixtures. Basic constants for the hyperbolic model including the limiting fracture energy, the rate constant, and age at initial hardening for specimens cured at constant temperatures of approximately 14 °C, 23 °C and 35 °C are given. The fracture energy - age data, Tabulated results of analyzed data, and representative plots for the various sizes of tested specimens are given in this chapter.

The strength - age data are also analyzed for the evaluation of basic constants for the hyperbolic model, which are the limiting strength, the rate constant, and the initial age. Once the rate constant values at various temperatures are determined, the relationship between the rate constant and the curing temperature is evaluated by the linear as well as

the Arrhenius time-temperature models. Finally, the relative strength development is expressed in terms of maturity and equivalent age.

5.2 Experimental Results

5.2.1 Mortar Cubes and Concrete Cylinders

The strength - age test results for mortar cubes and concrete cylinders are summarized in Table 5.1 and 5.2. Coefficients of variations given in these tables are based on test results of three specimens. Average strength versus age data for mortar cubes and concrete cylinders are in Figures 5.1 and 5.2. For each curing temperature, the strength-age data can be represented by Eq. 2.10. The three parameters for each curing temperature, namely the limiting strength f_{cu}, the rate constant k_T, and the initial age t_o were evaluated based on the data in Tables 5.1 and 5.2. The method introduced by Knudsen (1980) was employed. To determine f_{cu}, data at later ages are considered and the approximation $t \approx (t-t_o)$ is made. This will results Eq. 3.37 as follows:

$$\frac{1}{f_c} = \frac{1}{f_{cu}} + \frac{1}{k_T f_{cu}} \frac{1}{t}$$

a plot of $1/f_c$ versus $1/t$ is a straight line, and the inverse of the intercept is the limiting strength f_{cu} (Figures 5.3 and 5.4). The regression analysis results for mortar and concrete tests are given in Table 5.3 and 5.4. In these tables, N represents the number of data points-working from the latest to the earliest ages-that were used in estimating f_{cu}. The criterion was to use the number of points that produced the lowest estimated standard error in the intercept ($1/f_{cu}$), and that is why the N-values differed.

Table 5.1 Compressive strength - age data for mortar curbs

Isothermal curing Temperature, (°C)	Age, (days)	Strength, (psi)	Coefficient of Variation, %
14	0.75	430	1
	1.12	1130	4
	1.65	2160	3
	2.95	4165	2
	5.70	5550	1
	9.91	6650	4
	21.00	7360	3
	45.00	7800	1
23	0.75	2140	2
	1.00	3220	2
	2.00	4647	2
	4.00	5252	2
	7.00	6323	5
	14.00	6879	2
	28.00	7348	2
35	0.31	635	2
	0.63	3436	1
	1.00	3791	3
	2.00	4810	1
	4.00	5508	3
	7.00	5843	1
	12.00	6300	2
	20.00	6700	1

Table 5.2 Compressive strength - age data for concrete cylinders

Isothermal curing Temperature, (°C)	Age, (days)	Strength, (psi)	Coefficient of Variation, %
14	1.00	436	5
	1.25	1126	2
	2.00	2999	7
	4.10	4624	1
	7.30	5300	4
	9.00	5698	1
	10.00	5811	2
	22.00	6086	2
	38.00	6462	2
	45.00	6584	5
23	0.55	722	2
	0.70	1899	1
	1.00	2724	2
	3.00	3759	4
	7.00	5261	4
	14.00	5554.8	2
	28.00	6057	3
35	0.37	1740	4
	0.56	2408	3
	0.70	3250	4
	1.00	3718	1
	2.00	3915	3
	4.00	4480	4
	9.00	5094	5
	20.00	5433	2
	23.00	5535	1

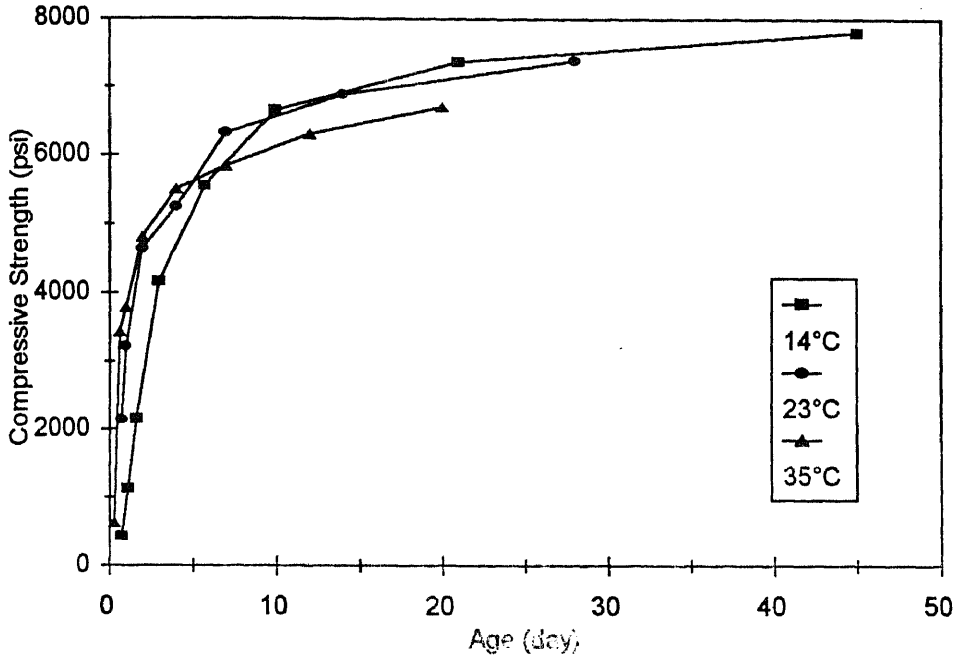

Figure 5.1 Compressive strength versus age for isothermally cured mortar cubes

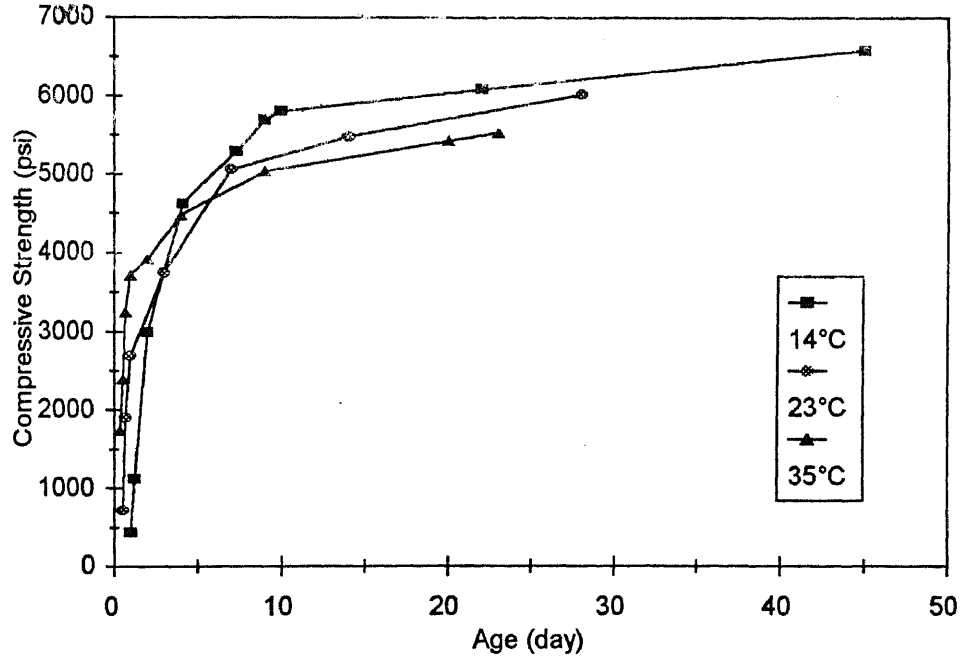

Figure 5.2 Compressive strength versus age for isothermally cured concrete cylinders

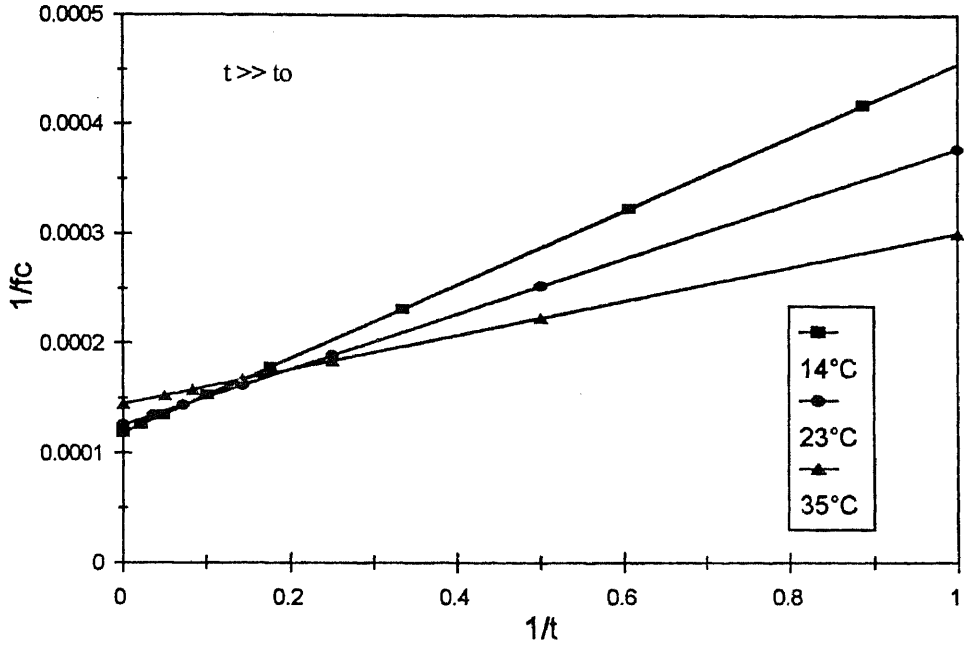

Figure 5.3 Plot of $1/f_c$ versus $1/t$ to evaluate f_{cu} for mortar

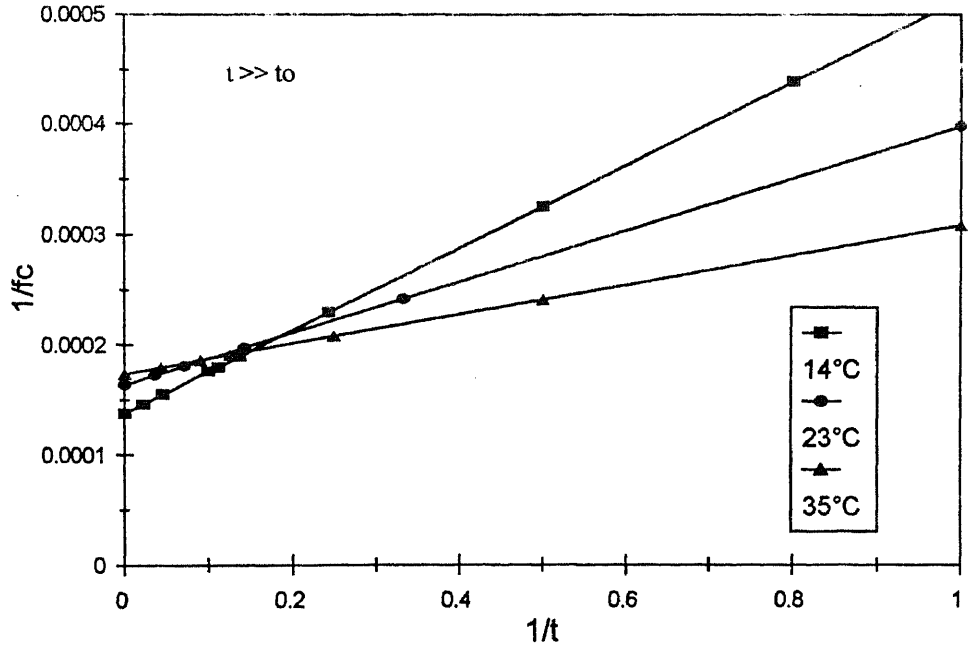

Figure 5.4 Plot of $1/f_c$ versus $1/t$ to evaluate f_{cu} for concrete

Table 5.3 Analysis of strength-age mortar data to determine limiting strength

Temperature (°C)	N*	$1/f_{cu}$ (10^{-6} psi^{-1})	Standard Error (10^{-6} psi^{-1})	f_{cu} (psi)
14	4	119	2.6	8370
23	4	126	3.1	7945
35	4	145	4.1	6915

* N represents the number of data points-working from the latest to the earliest ages- that were used in estimation f_{cu}.

Table 5.4 Analysis of strength-age concrete data to determine limiting strength

Temperature (°C)	N*	$1/f_{cu}$ (10^{-6} psi^{-1})	Standard Error (10^{-6} psi^{-1})	f_{cu} (psi)
14	6	147	3.5	6798
23	3	161	6.9	6207
35	3	171	1.2	5863

* N represents the number of data points-working from the latest to the earliest ages- that were used in estimation f_{cu}.

Estimation of k_T and t_o is evaluated from Eq. 2.10 as follows:

$$\frac{f_c}{f_{cu} - f_c} = -k_T t_o + k_T t \tag{5.1}$$

Thus a plot of $f_c/(f_{cu} - f_c)$ versus t is a straight line, its slope is k_T and the t-intercept is t_o (Figures 5.5 and 5.6). The results of this second series of regression analyses are given in Tables 5.5 and 5.6. In this case the data points used were those from the earliest to later ages, and the number was based of the lowest standard error for the estimate of k_T.

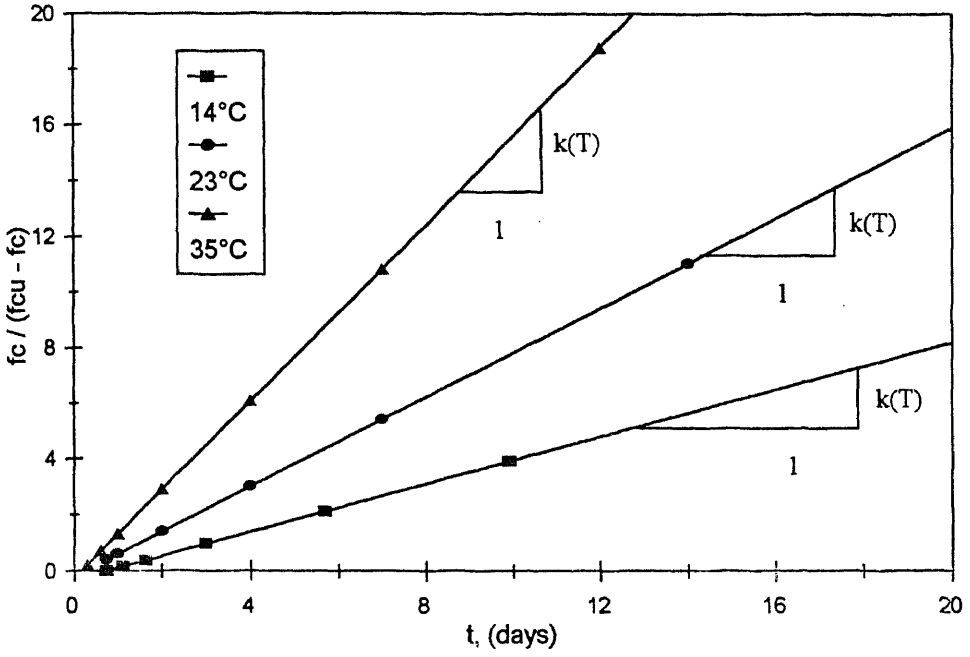

Figure 5.5 Plot of $[f_c / (f_{cu} - f_c)]$ versus t to evaluate k_T and t_o for mortar

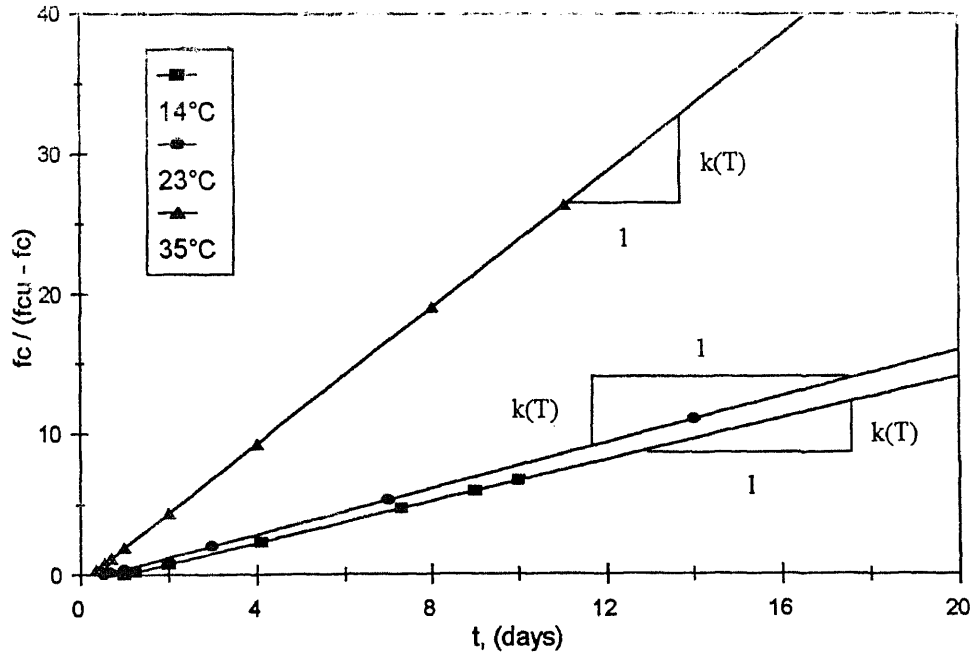

Figure 5.6 Plot of $[f_c / (f_{cu} - f_c)]$ versus t to evaluate k_T and t_o for concrete

Table 5.5 Analysis of strength-age mortar data to determine rate constant

Temperature (°C)	N*	$k_T t_o$	Standard Error	k_T (day^{-1})	Standard Error (day^{-1})	t_o (day)
14	4	0.32	0.05	0.43	0.03	0.73
23	3	0.18	0.08	0.80	0.09	0.23
35	3	0.26	0.31	1.58	0.64	0.16

* N represents the number of data points-working from the earliest to the latest ages- that were used in estimation k_T.

Table 5.6 Analysis of strength-age concrete data to determine rate constant

Temperature (°C)	N*	$k_T t_o$	Standard Error	k_T (day^{-1})	Standard Error (day^{-1})	t_o (day)
14	3	0.69	0.04	0.74	0.05	0.94
23	3	0.47	0.10	1.19	0.30	0.40
35	3	0.56	0.17	2.47	0.72	0.23

* N represents the number of data points-working from the earliest to the latest ages- that were used in estimation k_T.

Examination of the variation of the rate constant with temperature for the mortar and the concrete tests are based on the data in Tables 5.5 and 5.6. Figures 5.7 and 5.8 illustrate the variation of rate constant with temperature for mortar and concrete samples respectively. In Figures 5.9 and 5.10 the natural logarithms of k_T are plotted against the reciprocal of absolute temperature. The best-fit linear function and the best-fit Arrhenius equation were determined for k(T). Analysis of data in Figures 5.9 and 5.10 the datum temperature T_o and the activation energy Q were obtained. Values of T_o and Q are summarized in Table 5.7. Values of Q are expressed by rounding to the nearest whole number.

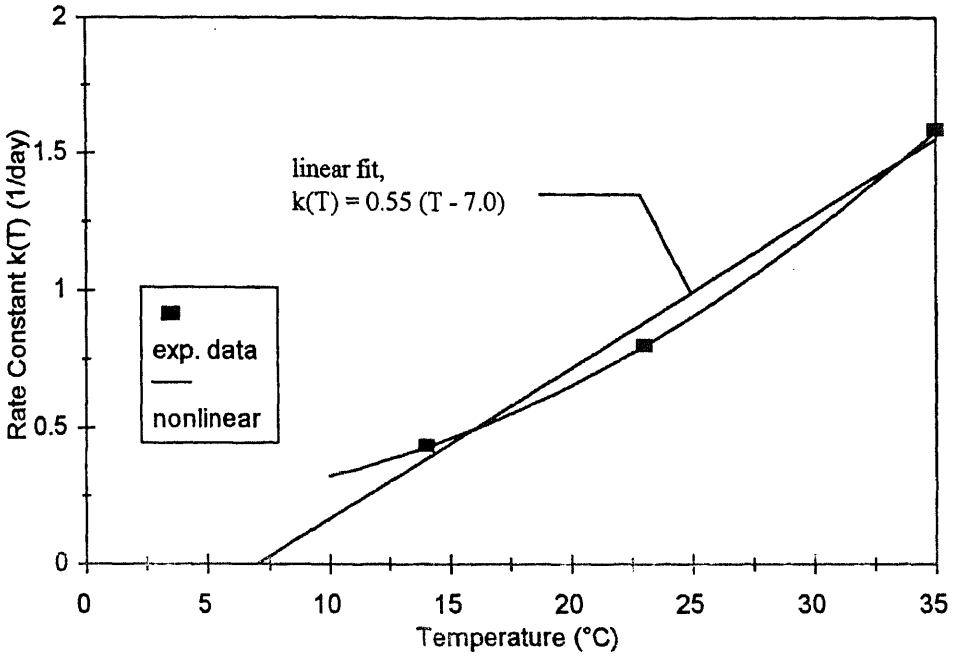

Figure 5.7 Rate constant versus curing temperature for mortar cubes by linear function

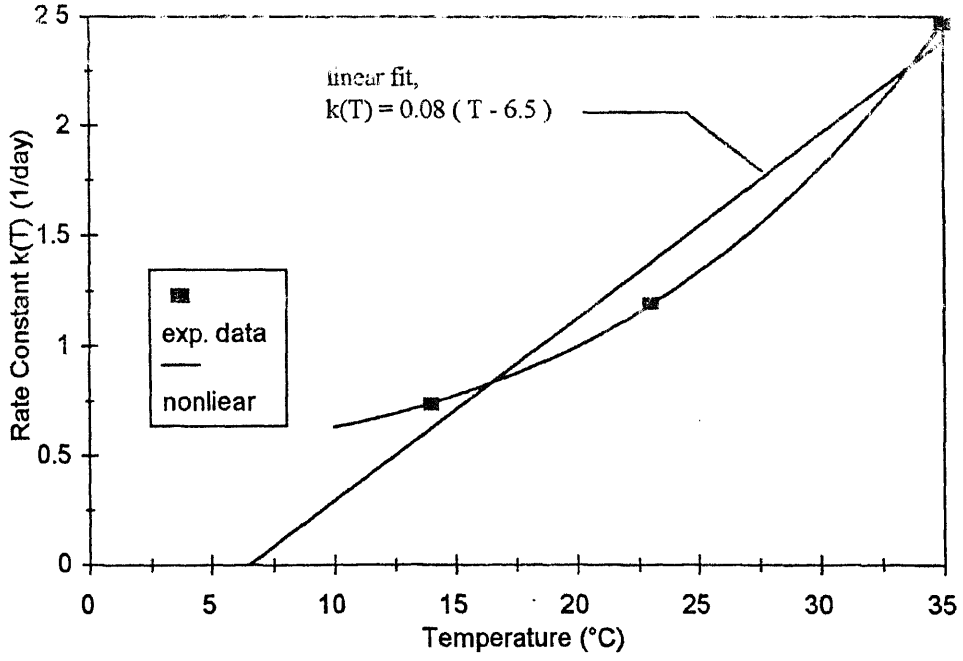

Figure 5.8 Rate constant versus curing temperature for concrete cylinders by linear function

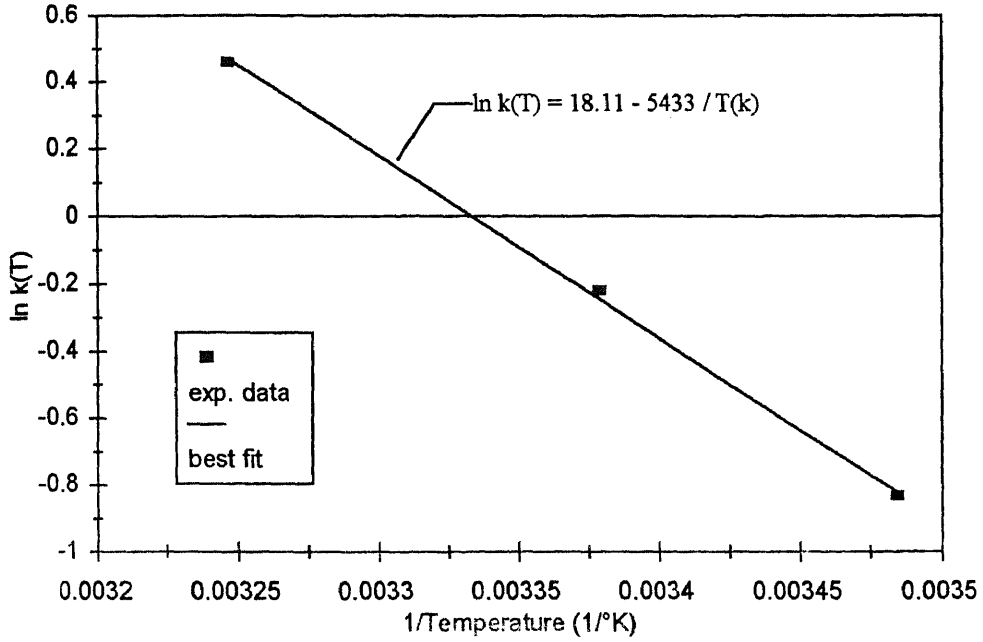

Figure 5.9 Logarithm of rate constant versus reciprocal of curing temperature in Kelvin by Frrhenius function for mortar cubes

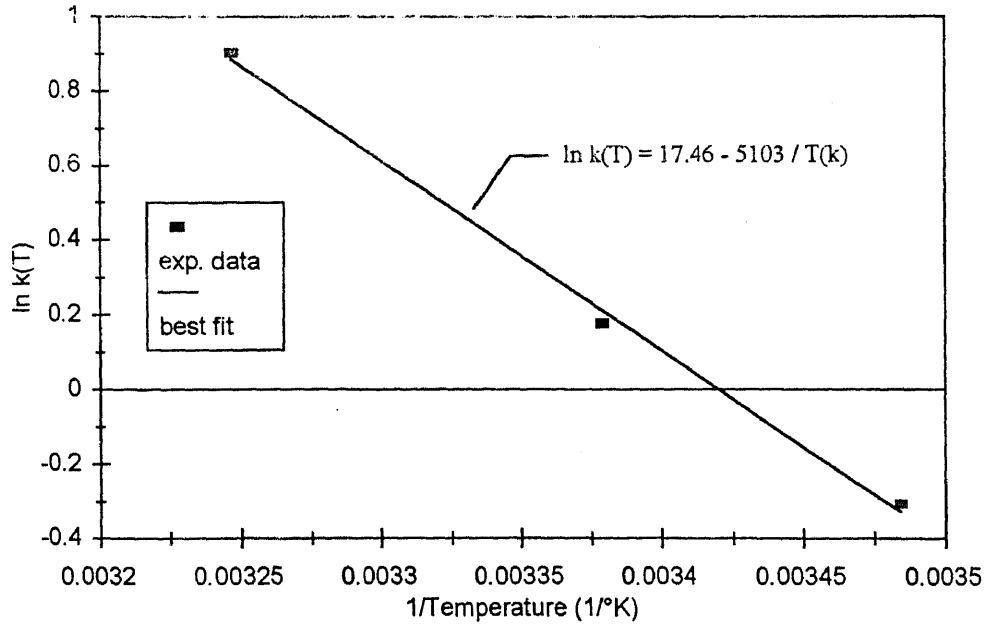

Figure 5.10 Logarithm of rate constant versus reciprocal of curing temperature in Kelvin by Frrhenius function for concrete cylinders

Table 5.7 Constants acquired for linear k(T), and Arrhenius functions

Material	Datum Temperature To (°C)	Activation Energy Q (kJ/mole)
Mortar	7.0	45
Concrete	6.5	42

Based on the evaluated parameters, f_{cu}, k_T, t_o, T_o and Q, it is possible to fit the hyperbolic model to experimental data(Figs. 5.11 through 5.12). As pointed out by Carino (1984), since curing temperature affects the limiting strength, data have been presented in terms of relative strength (f_c/f_{cu}). Alternatively, Figures 5.13 through 5.14 depict relative strength versus the equivalent age at a standard temperature 23°C. The hyperbolic model (Eq. 2.10) was employed to fit the data in Figures 5.13 through 5.14.

The difference between the two models (Figs. 5.11 and 5.12 versus Figs. 5.13 and 5.14) is:

To describe strength gain under variable temperature conditions, a maturity function is needed to account for the effect of time and temperature. It has been shown that the product of the rate constant and age is the general form of the maturity function. Thus the key element in arriving at a valid maturity function is describing the relationship between the rate constant and the curing temperature.

For the plot of relative strength versus maturity, the rate constant is assumed to be a linear function of temperature and the resulting maturity function is the traditional Nurse-Saul function. However, Carino (1984) has shown that, over a wide temperature

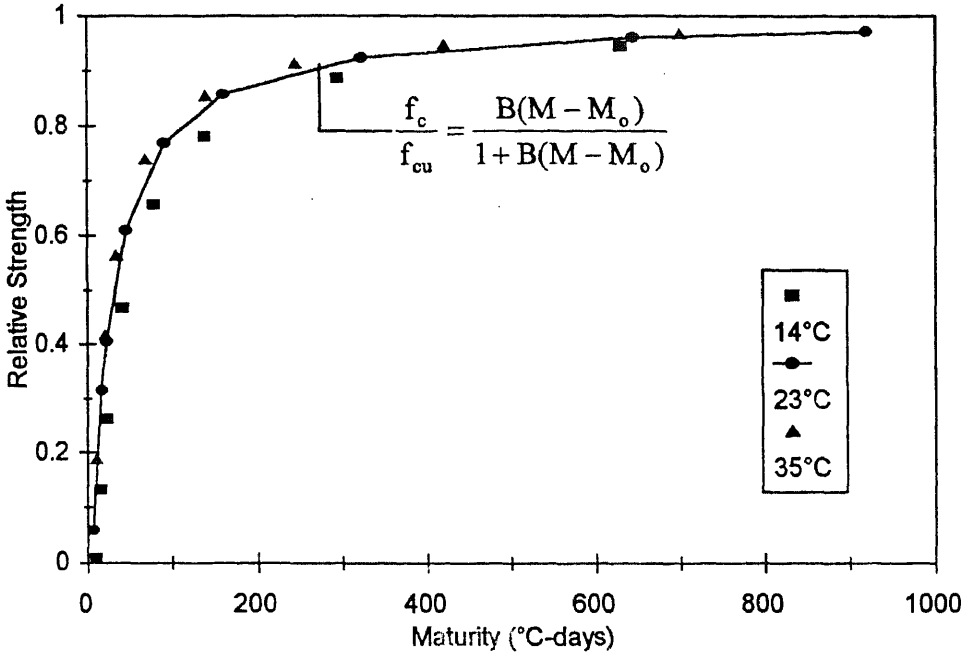

Figure 5.11 Relative strength versus maturity for isothermally cured mortar cubes

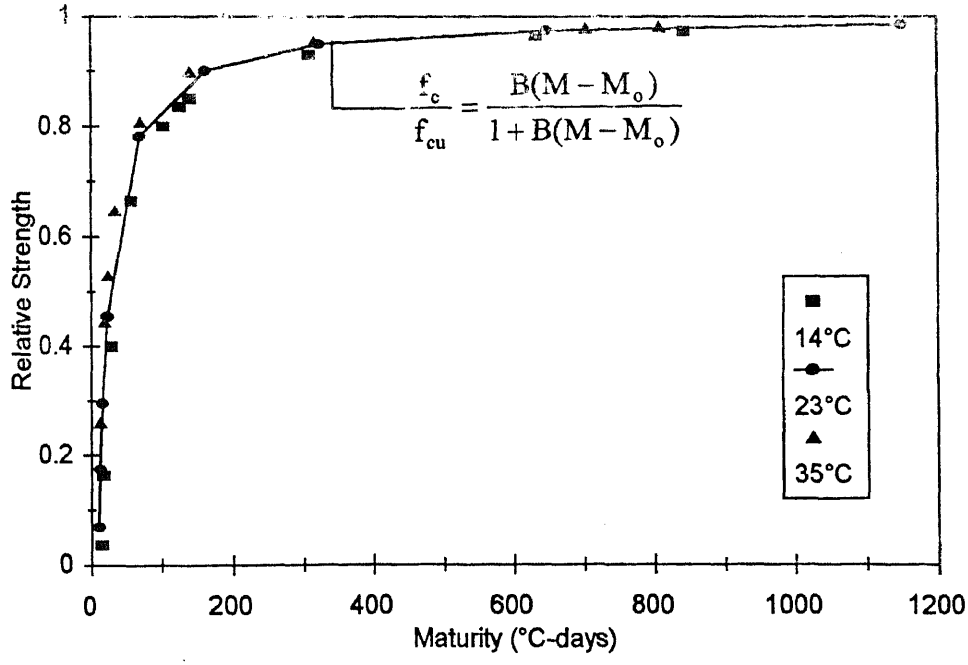

Figure 5.12 Relative strength versus maturity for isothermally cured concrete cylinders

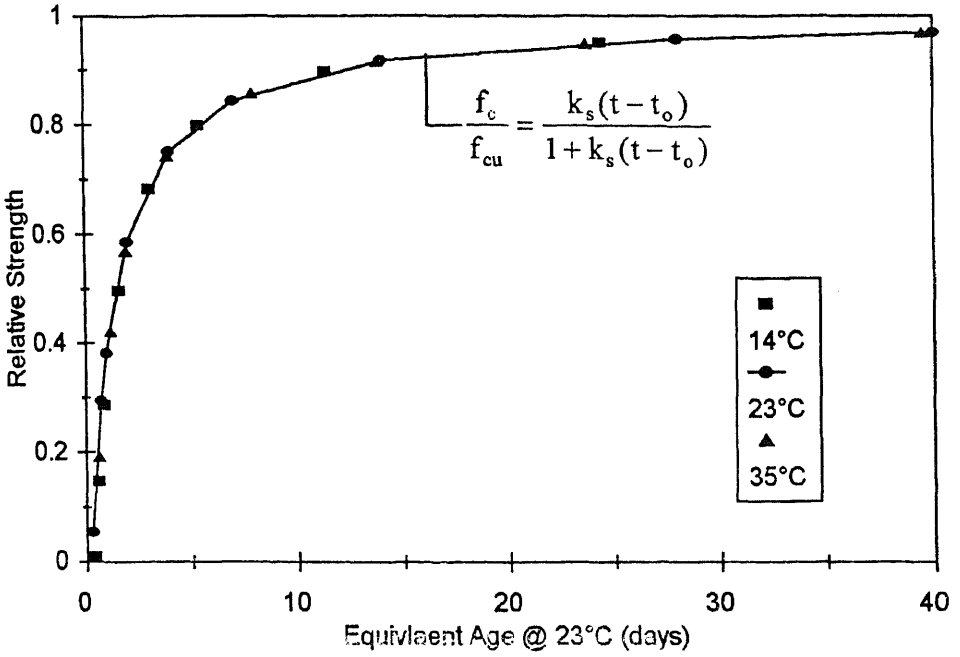

Figure 5.13 Relative strength versus equivalent age for isothermally cured mortar cubes

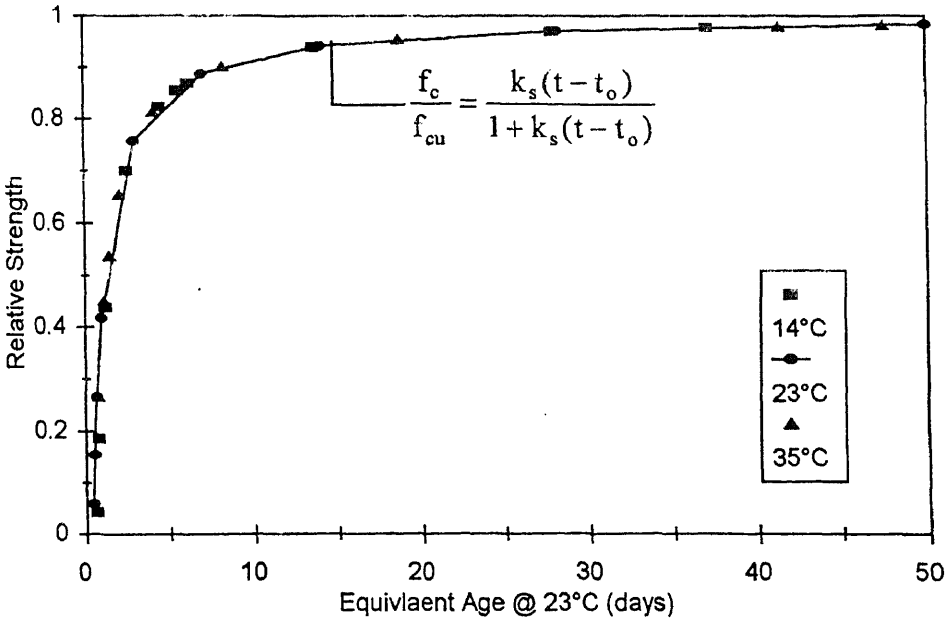

Figure 5.14 Relative strength versus equivalent age for isothermally cured cocrete cylinders

range, the rate constant is not a linear function of temperature. Therefore, the Nurse-Saul function is inherently approximate and will either overestimate or underestimate the effects of temperature on strength gain. The key parameter of this approach is the datum temperature. It must be emphasized that the computed values of the datum temperature are applicable only over the temperature range 14 to 35°C.

For the plot of relative strength versus equivalent age, the rate constant is assumed to be a nonlinear function, Arrhenius equation, which can better represent the effect of temperature on strength development over wide temperature range. For the Arrhenius equation, the activation energy is the parameter which defines the temperature sensitivity of the rate constant. The equivalent age approach is the most flexible technique to represent maturity. In this case, the age factor is used to convert a curing time interval at any temperature to an equivalent time interval at a reference temperature. The age factor is simply the ratio of the value of the rate constant at any temperature to its value at the reference temperature.

5.2.2 Beam Specimens

As shown earlier in table 4.4, for each of the three isothermal curing temperatures, beam specimens were tested at six different testing age. Figures 5.15 through 5.17 represent typical load-deflection curves for beam specimens tested in this study. Load-deflection diagrams for all the beams tested in this study are given in appendix A. Figures 5.18 through 5.20 illustrate the effect of curing temperature and testing age on load deflection

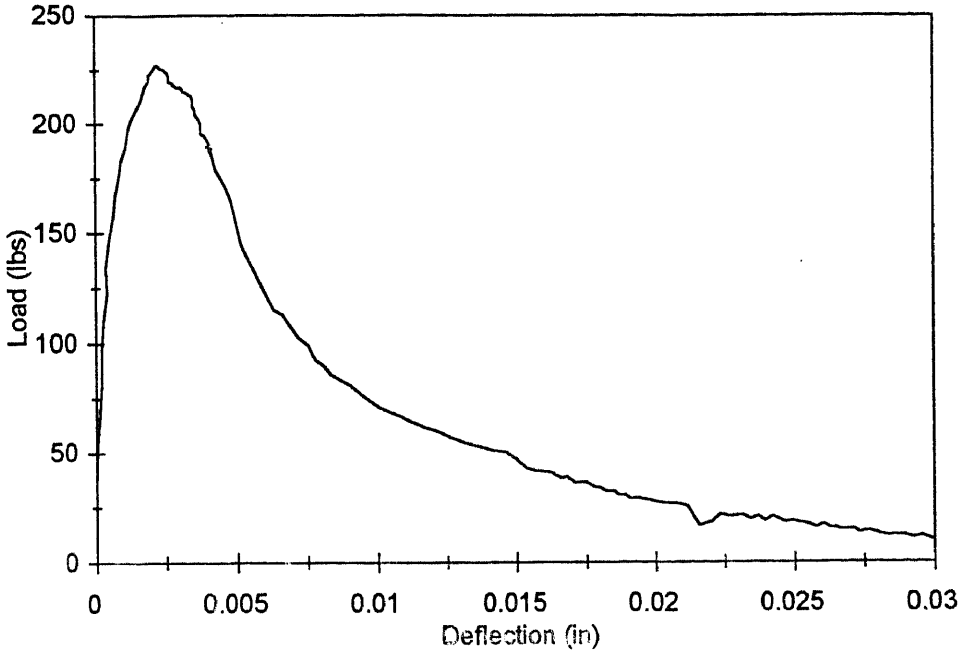

Figure 5.15 Load versus deflection, size A, , curing at 23°C, age = 28 days

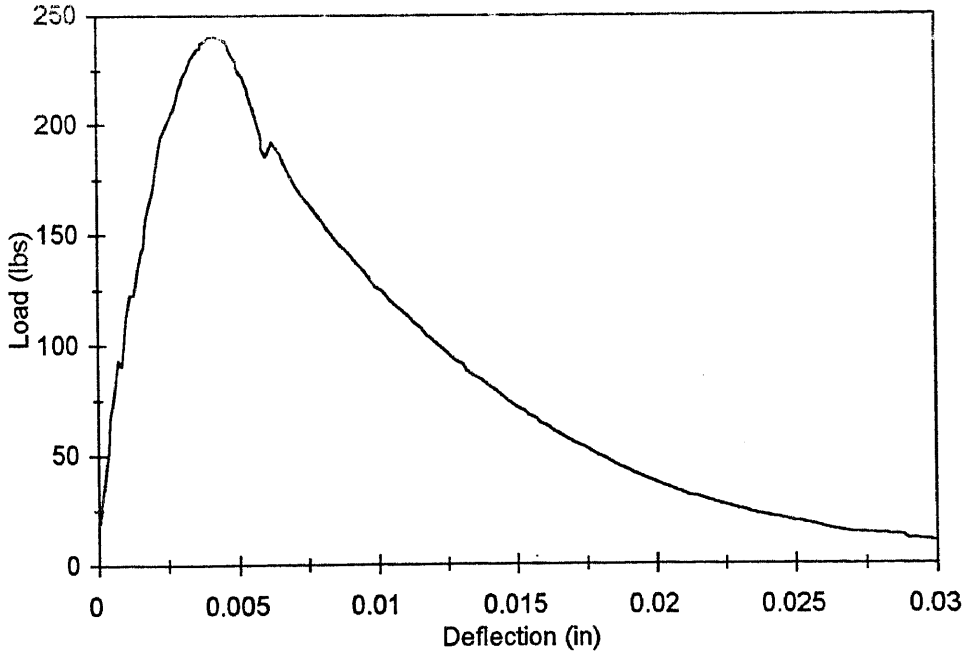

Figure 5.16 Load versus deflection, size B, , curing at 23°C, age = 28 days

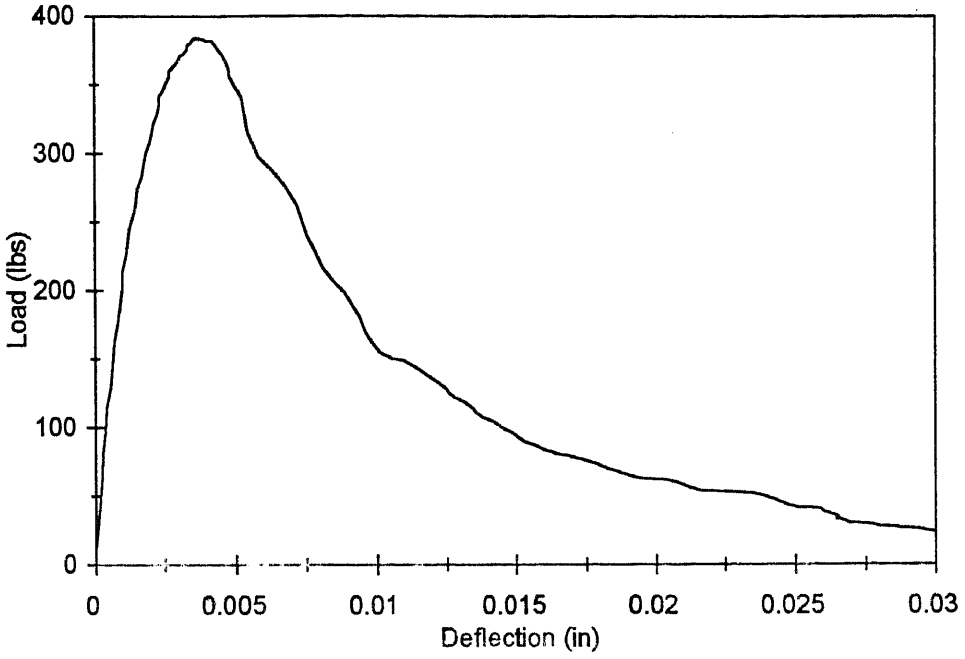

Figure 5.17 Load versus deflection, size C, , curing at 23°C, age = 28 days

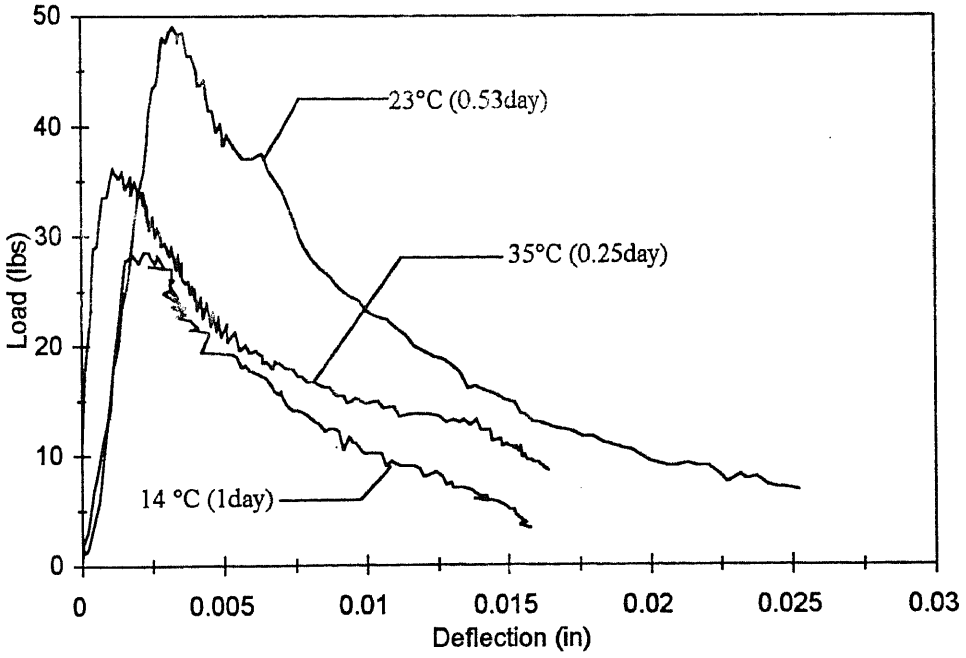

Figure 5.18 Load versus deflection for size B, tested at very young age

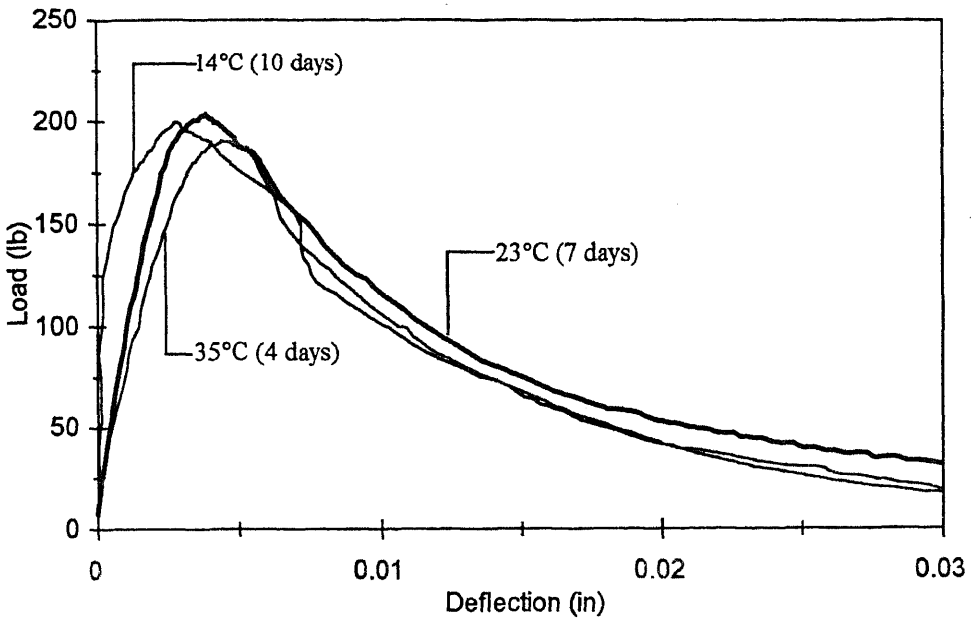

Figure 5.19 Load versus deflection for size B, tested after about a week

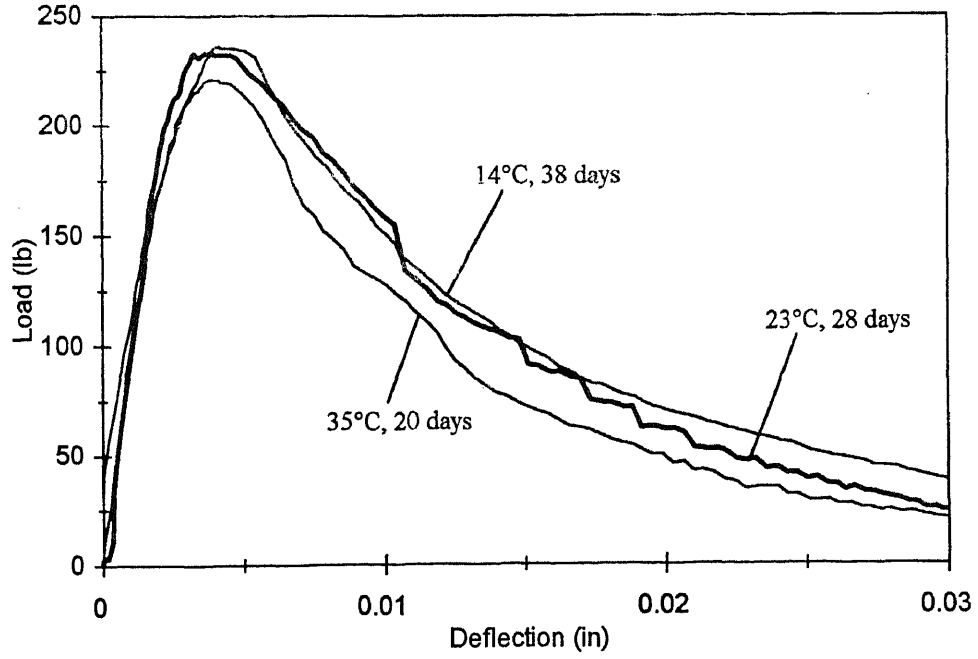

Figure 5.20 Load versus deflection for size B, tested at mature age

behavior of size B beam specimens. Fracture energies were calculated for all 150 specimens according to equation 4.1. Average fracture energies of all beams are summarized in Tables 5.8 through 5.10. The coefficient of variation of fracture energy at early ages is higher as compared to that of fracture energy at mature ages. This is due to difficulties involved in proper testing of very young concretes.

Average fracture energy versus age data are shown in Figures 5.21 through 5.23. For each curing temperature, the fracture energy versus age data can be represented by Eq. 3.26. The hyperbolic equation can be transformed into linear equations. The three parameters for each curing temperature, namely the limiting fracture energy G_{fu}, the rate constant k_T, and the datum age t_o were evaluated based on the data in Tables 5.8 through 5.10 by using the linear transformations (Eqs. 3.38 and 3.39). To determine G_{fu}, data at later ages are considered and the approximation $t \approx (t-t_o)$ is made. This will results Eq. 3.38 as follows:

$$\frac{1}{G_f} = \frac{1}{G_{fu}} + \left(\frac{1}{k_T G_{fu}} \frac{1}{t}\right)$$

a plot of $1/G_f$ versus $1/t$ is a straight line, and the inverse of the intercept is the limiting fracture energy (Figures 5.24 through 5.26). The regression analysis results for three size beams are given in Tables 5.11 through 5.13. In these tables, N represents the number of data points-working from the latest to the earliest ages-that were used in estimating G_{fu}. The criterion was to use the number of points that produced the lowest estimated standard error in the intercept ($1/ G_{fu}$), and that is why the N-values differed.

Table 5.8 Fracture energy - age data for size A

Isothermal curing Temperature, (°C)	Age, (days)	Average Fracture Energy (lb/in)	Coefficient of Variation, %
14	1.22	0.21	12
	2.04	0.35	6
	4.03	0.49	6
	7.25	0.51	3
	22.04	0.56	4
	36.00	0.59	4
23	0.50	0.20	10
	1.30	0.37	9
	3.06	0.50	8
	7.16	0.53	3
	14.02	0.56	4
	28.03	0.58	3
35	0.35	0.22	10
	0.56	0.38	3
	1.07	0.46	8
	4.03	0.53	2
	9.50	0.56	2
	20.02	0.57	4

Table 5.9 Fracture energy - age data for size B

Isothermal curing Temperature, (°C)	Age, (days)	Average Fracture Energy (lb/in)	Coefficient of Variation, %
14	1.00	0.17	5
	2.00	0.35	4
	4.10	0.48	2
	10.00	0.53	3
	22.00	0.55	2
	38.00	0.56	2
23	0.56	0.22	6
	1.21	0.34	9
	2.95	0.48	5
	7.16	0.52	1
	14.02	0.54	1
	28.00	0.59	1
35	0.25	0.18	1
	0.55	0.38	1
	1.55	0.50	4
	4.26	0.51	3
	9.05	0.54	4
	20.20	0.58	2

Table 5.10 Fracture energy - age data for size C

Isothermal curing Temperature, (°C)	Age, (days)	Average Fracture Energy (lb/in)	Coefficient of Variation, %
14	1.10	0.20	1
	2.10	0.33	1
	4.00	0.47	1
	9.00	0.51	5
	18.00	0.54	2
	36.00	0.57	1
23	0.65	0.22	6
	1.00	0.38	4
	3.00	0.45	8
	7.00	0.51	1
	14.00	0.54	1
	28.00	0.57	2
35	0.29	0.22	4
	0.51	0.37	3
	1.03	0.46	1
	4.28	0.50	3
	9.00	0.54	2
	23.01	0.56	3

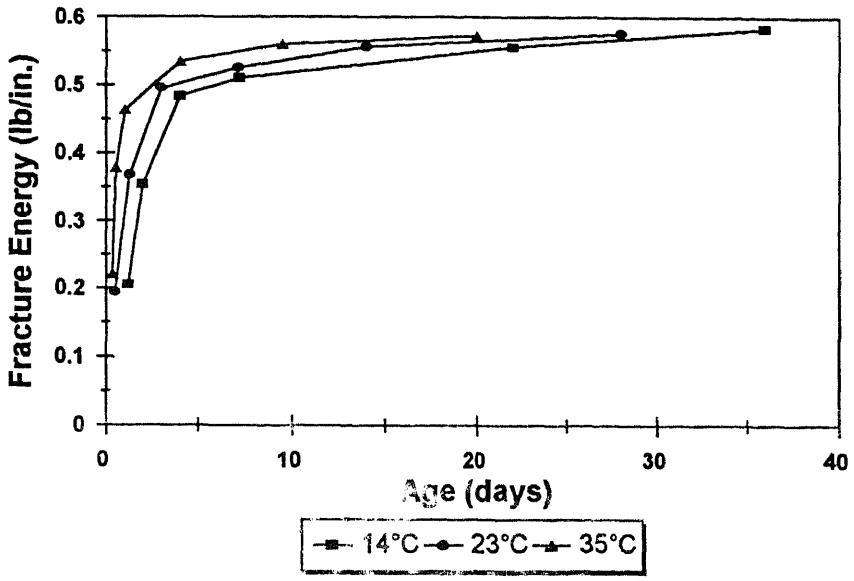

Figure 5.21 Fracture energy versus age for isothermally cured size A

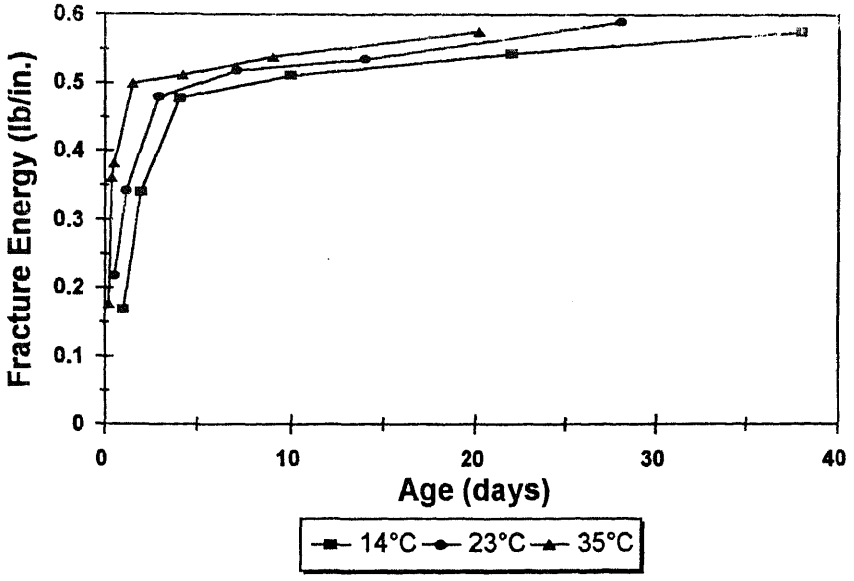

Figure 5.22 Fracture energy versus age for isothermally cured size B

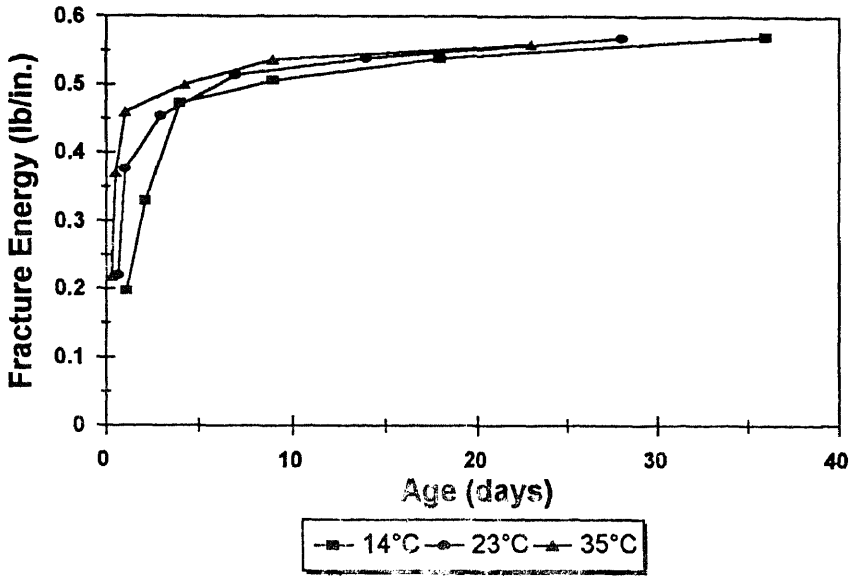

Figure 5.23 Fracture energy versus age for isothermally cured size C

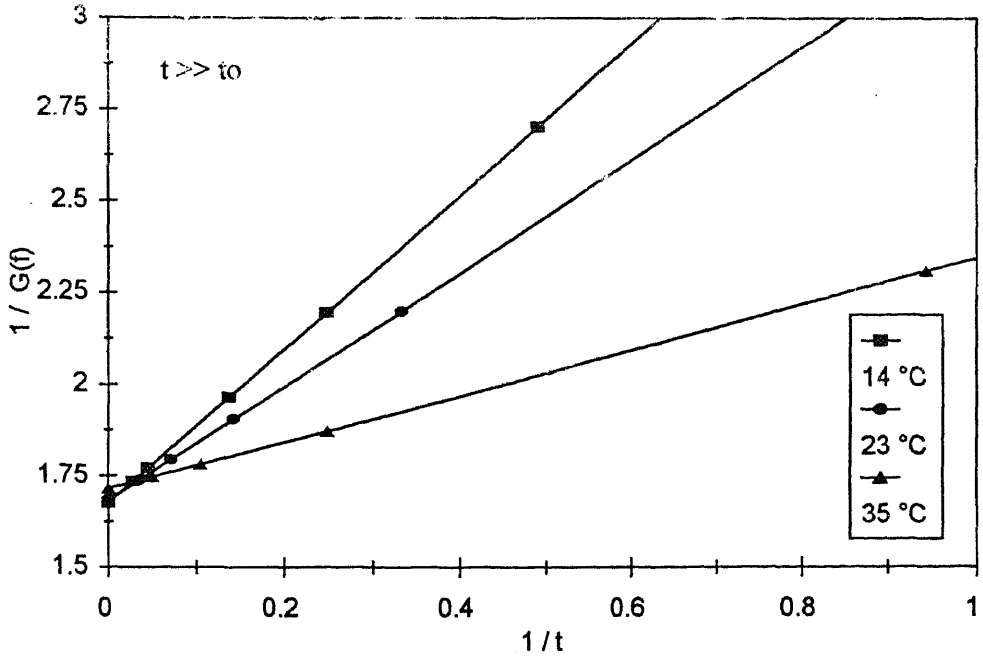

Figure 5.24 Plot of $1/G_f$ versus $1/t$ to evaluate G_{fu} for size A

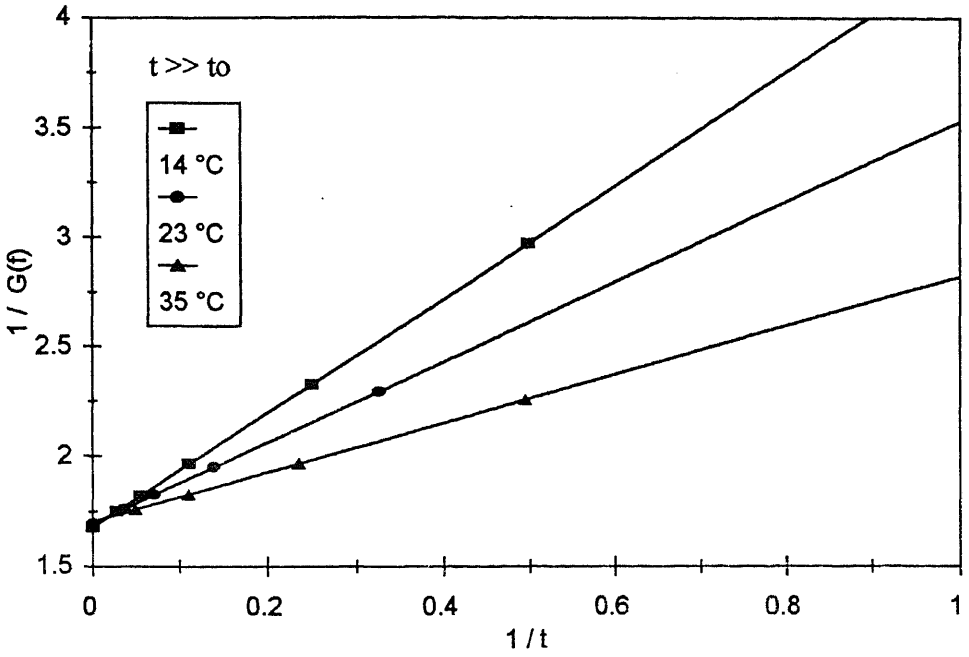

Figure 5.25 Plot of $1/G_f$ versus $1/t$ to evaluate G_{fu} for size B

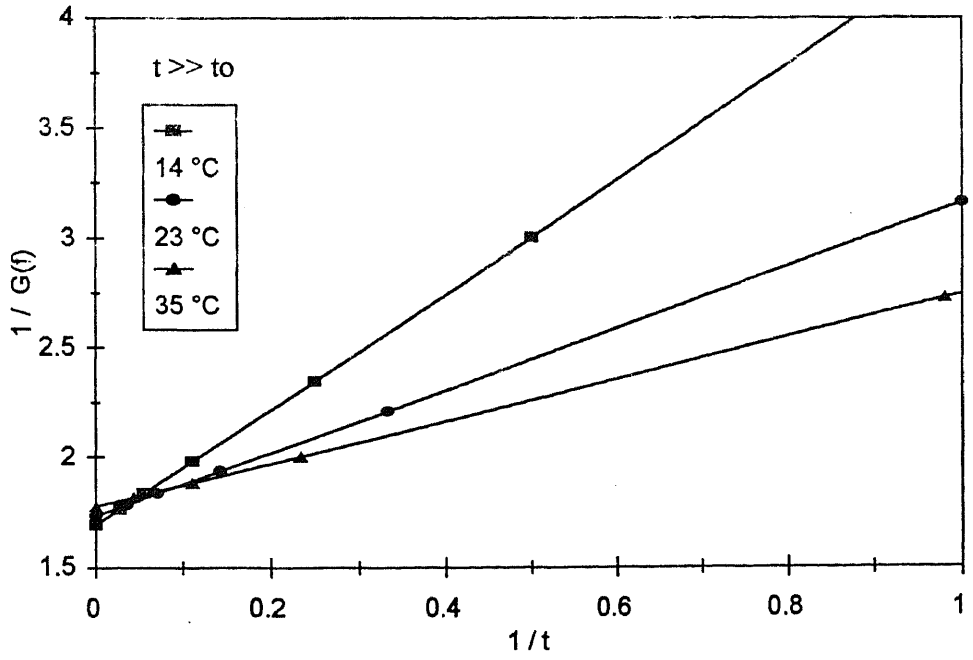

Figure 5.26 Plot of $1/G_f$ versus $1/t$ to evaluate G_{fu} for size C

Table 5.11 Analysis of fracture energy-age data to determine limiting fracture energy for size A

Temperature (°C)	N*	$1/G_{fu}$ $(lb/in)^{-1}$	Standard Error $(lb/in)^{-1}$	G_{fu} (lb/in)
14	3	1.68	0.04	0.60
23	3	1.68	0.01	0.59
35	3	1.72	0.01	0.58

* N represents the number of data points-working from the latest to the earliest ages- that were used in estimation G_{fu}.

Table 5.12 Analysis of fracture energy-age data to determine limiting fracture energy for size B

Temperature (°C)	N*	$1/G_{fu}$ $(lb/in)^{-1}$	Standard Error $(lb/in)^{-1}$	G_{fu} (lb/in)
14	3	1.68	0.22	0.60
23	3	1.70	0.07	0.59
35	3	1.70	0.04	0.59

* N represents the number of data points-working from the latest to the earliest ages- that were used in estimation G_{fu}.

Table 5.13 Analysis of fracture energy-age data to determine limiting fracture energy for size C

Temperature (°C)	N*	$1/G_{fu}$ $(lb/in)^{-1}$	Standard Error $(lb/in)^{-1}$	G_{fu} (lb/in)
14	3	1.69	0.03	0.59
23	3	1.72	0.03	0.58
35	3	1.74	0.01	0.58

* N represents the number of data points-working from the latest to the earliest ages- that were used in estimation G_{fu}.

Estimation of k_T and t_o are based on Eq. 3.39 as follows:

$$\frac{G_f}{G_{fu} - G_f} = -k_T t_o + k_T t$$

Thus a plot of G_f / (G_{fu} - G_f) versus t is a straight line having a slope k_T and a t-axis intercept of t_o (Figures 5.27 through 5.29). The results of this second series of regression analyses are given in Tables 5.14 through 5.16. In this case the data points used were those from the earliest to later ages, and the number was based of the lowest standard error for the estimate of k_T.

Examination of the variation of the rate constant with temperature for mortar and concrete tests are based on the data in Tables 5.14 through 5.16. Figures 5.30 through 5.32 illustrate the variation of rate constant with temperature for size A, B, and C beams respectively. In Figures 5.33 through 5.35 the natural logarithms of k_T are plotted against the reciprocal of absolute temperature. The best-fit linear function and the best-fit Arrhenius equation were determined for k(T). Analysis of data in Figures 5.33 through 5.35 the datum temperature T_o and the activation energy Q were obtained. Values of T_o and Q are summarized in Table 5.17. Values of Q are expressed by rounding to the nearest whole number.

Based on the evaluated parameters, G_{fu}, k_T, t_o, T_o and Q, it is possible to fit the hyperbolic model to experimental data (Figs. 5.36 through 5.38). As pointed out earlier, since curing temperature affects the limiting fracture energy, data have been presented in terms of relative strength (G_f / G_{fu}). Alternatively, Figures 5.43 through 5.45 depict relative strength versus the equivalent age at a standard temperature 23°C. The hyperbolic model (Eq. 3.26) was employed to fit the data in Figures 5.39 through 5.41.

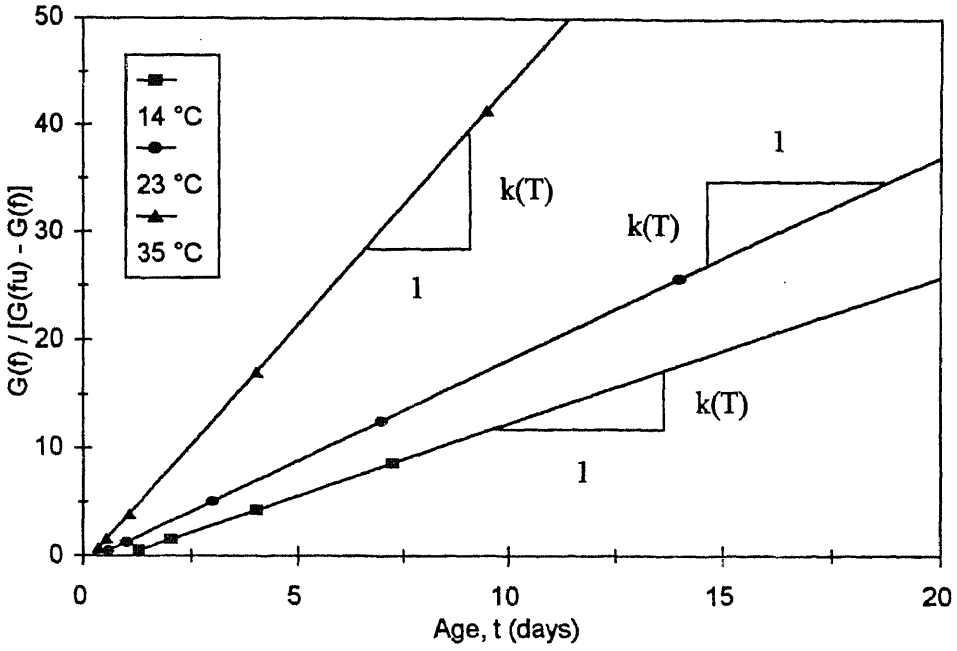

Figure 5.27 Plot of $[G_f / (G_{fu}-G_f)]$ versus t to evaluate k_T and t_o for size A

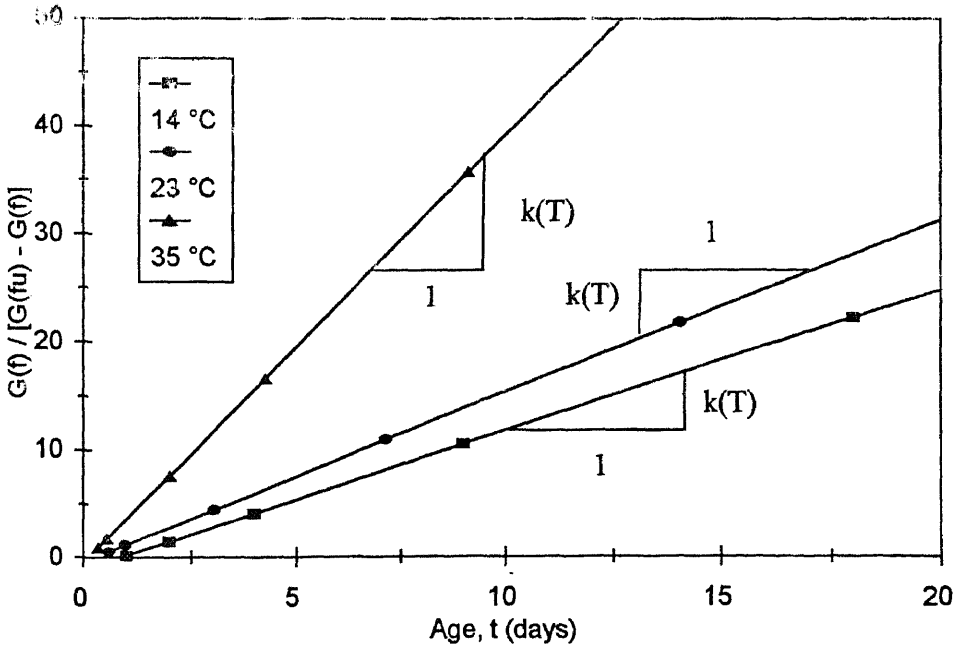

Figure 5.28 Plot of $[G_f / (G_{fu}-G_f)]$ versus t to evaluate k_T and t_o for size B

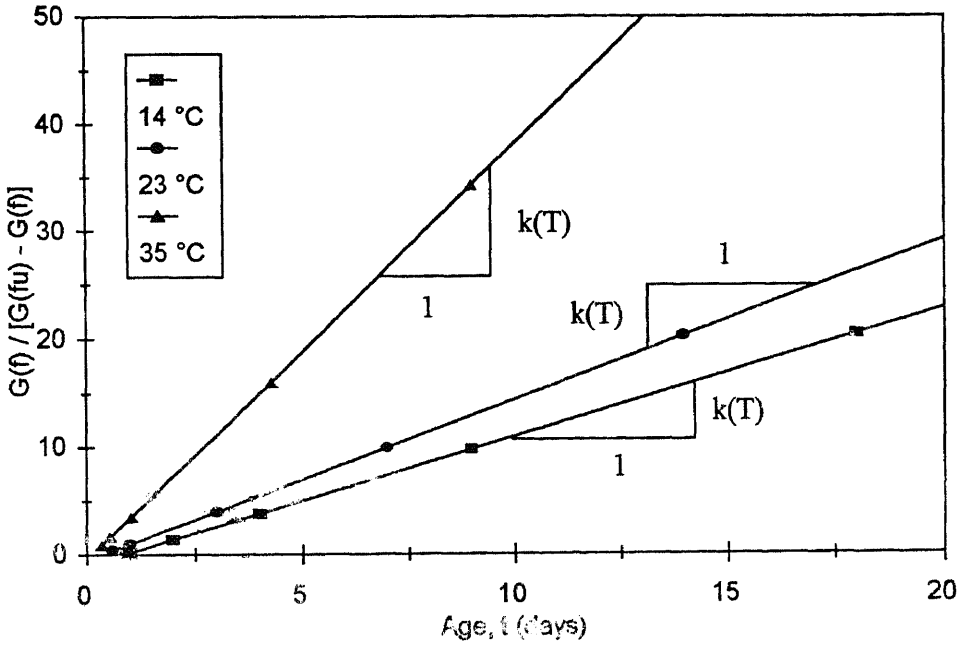

Figure 5.29 Plot of $[G_f / (G_{fu}-G_f)]$ versus t to evaluate k_T and t_o for size C

Table 5.14 Analysis of fracture energy -age data to determine rate constant for size A

Temperature (°C)	N*	$k_T t_o$	Standard Error	k_T (day^{-1})	Standard Error (day^{-1})	t_o (day)
14	3	1.20	0.13	1.35	0.06	0.89
23	3	0.59	0.27	1.87	0.15	0.31
35	3	0.82	0.22	4.44	0.0.4	0.18

* N represents the number of data points-working from the earliest to the latest ages- that were used in estimation k_T.

Table 5.15 Analysis of fracture energy -age data to determine rate constant for size B

Temperature (°C)	N*	$k_T t_o$	Standard Error	k_T (day^{-1})	Standard Error (day^{-1})	t_o (day)
14	3	0.95	0.22	1.23	0.10	0.77
23	3	0.40	0.17	1.58	0.10	0.25
35	3	0.46	0.16	4.00	0.17	0.11

* N represents the number of data points-working from the earliest to the latest ages- that were used in estimation k_T

Table 5.16 Analysis of fracture energy -age data to determine rate constant for size C

Temperature (°C)	N*	$k_T t_o$	Standard Error	k_T (day^{-1})	Standard Error (day^{-1})	t_o (day)
14	3	0.98	0.32	1.19	0.16	0.82
23	3	0.42	0.10	1.48	0.06	0.28
35	3	0.43	0.18	3.85	0.33	0.11

* N represents the number of data points-working from the earliest to the latest ages- that were used in estimation k_T.

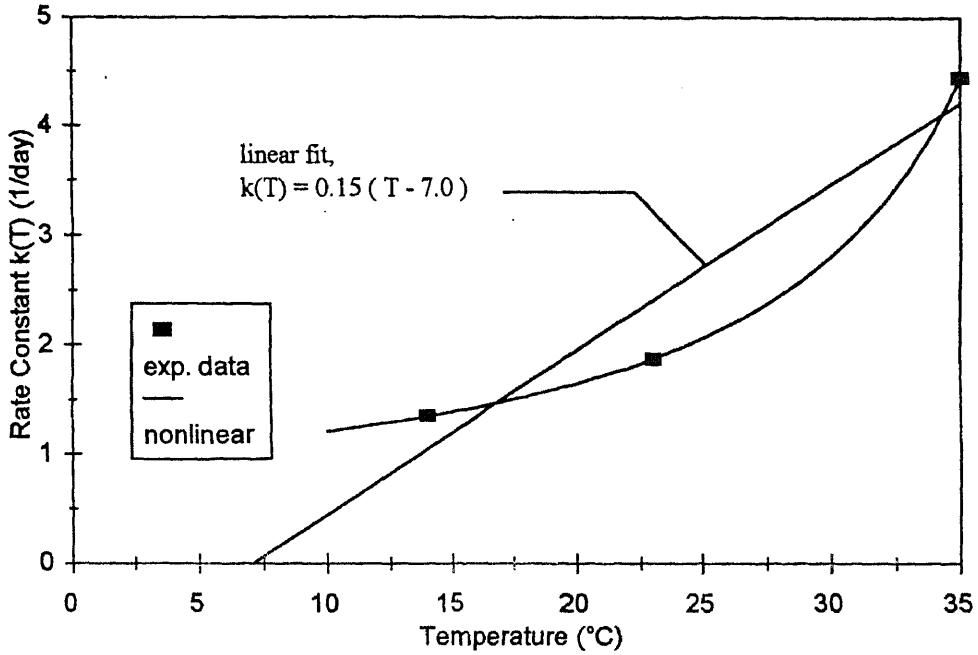

Figure 5.30 Rate constant versus curing temperature for size A beam by linear function

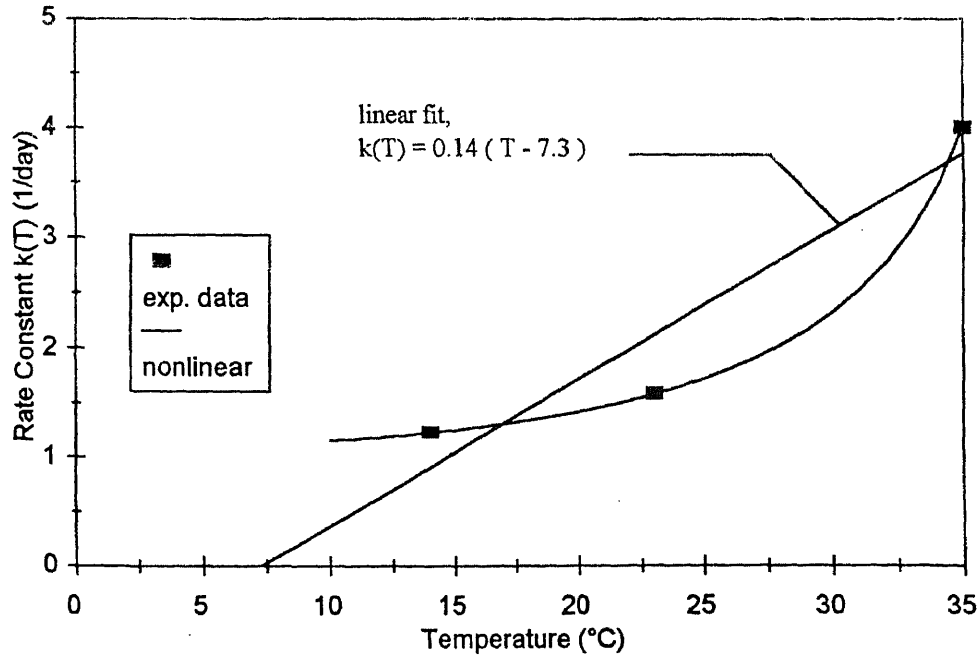

Figure 5.31 Rate constant versus curing temperature for size B beam by linear function

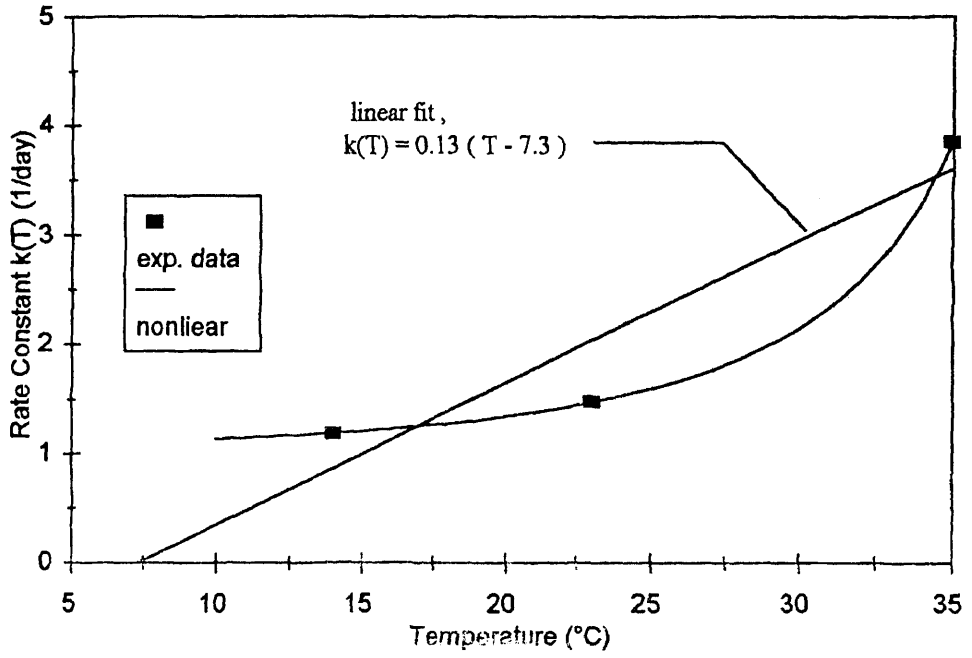

Figure 5.32 Rate constant versus curing temperature for size C beam by linear function

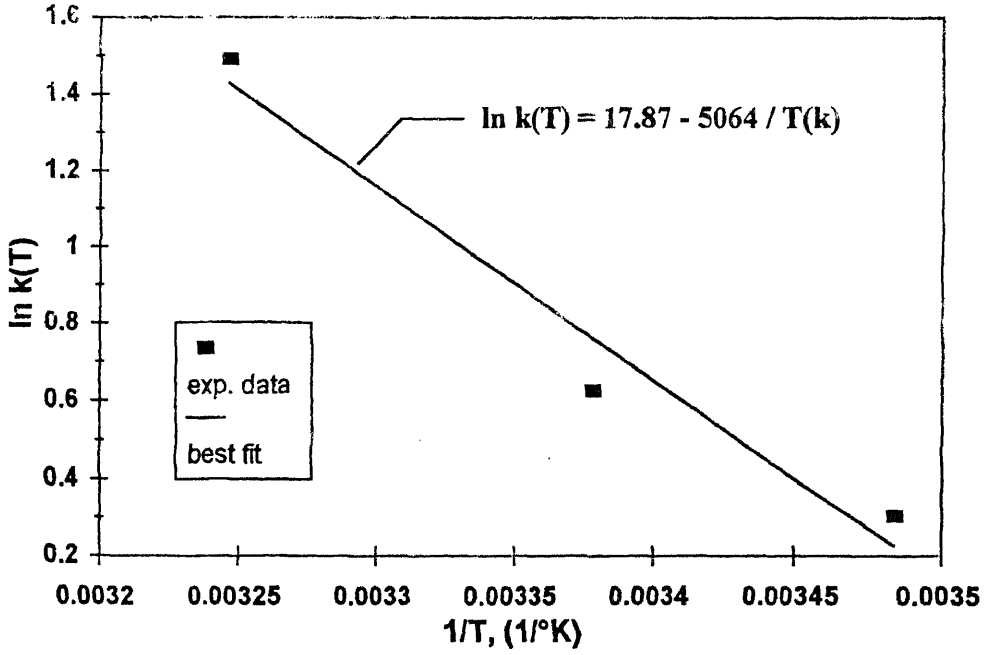

Figure 5.33 Logarithm of rate constant versus reciprocal of curing temperature in Kelvin by Arrhenius function for size A beam

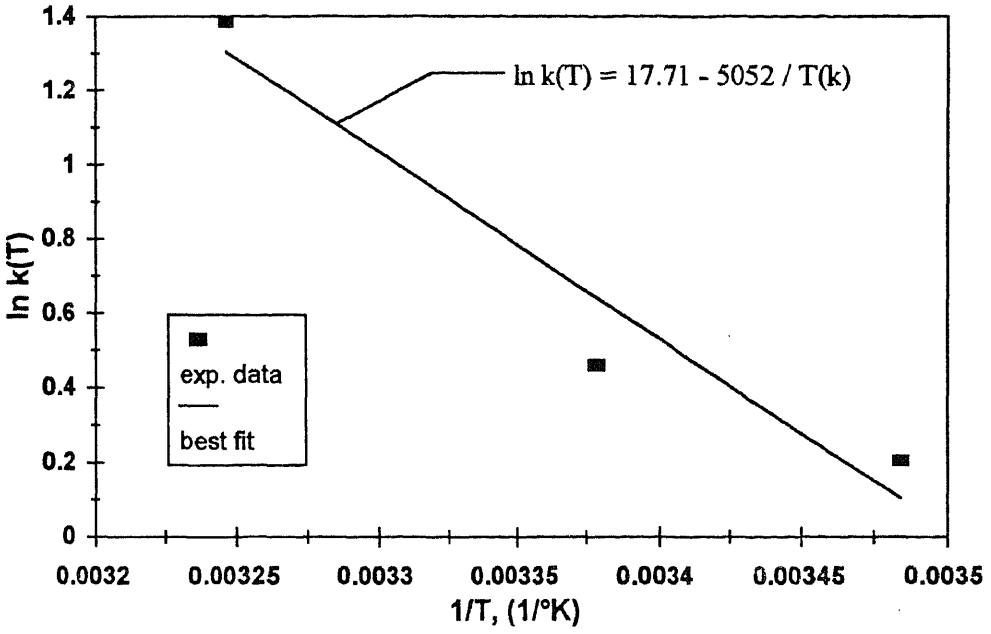

Figure 5.34 Logarithm of rate constant versus reciprocal of curing temperature in Kelvin by Arrhenius function for size B beam

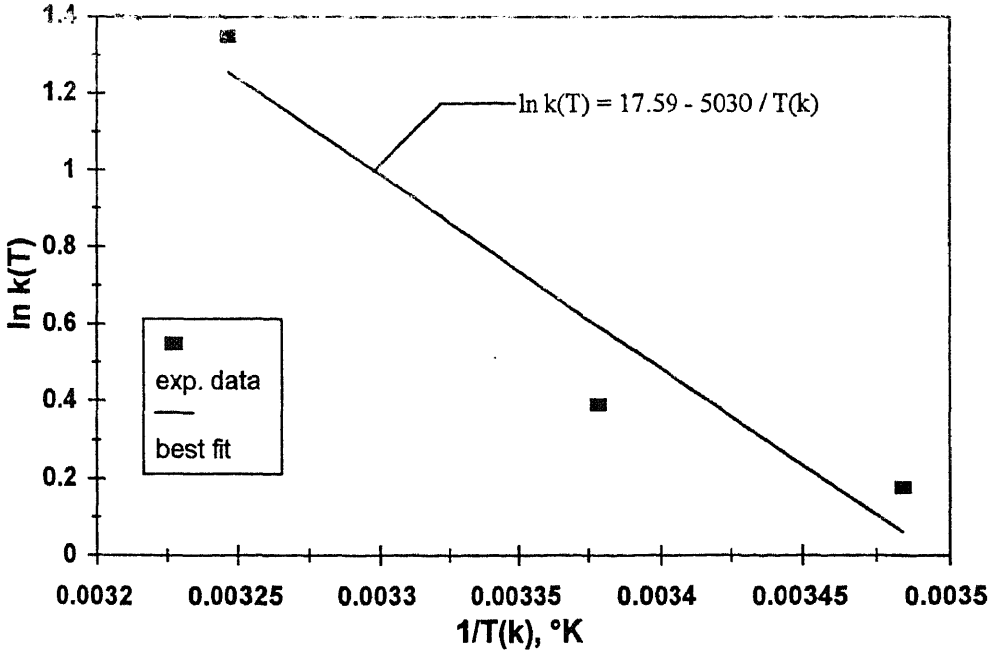

Figure 5.35 Logarithm of rate constant versus reciprocal of curing temperature in Kelvin by Arrhenius function for size C beam

Table 5.17 Constants of linear k(T) function and Arrhenius function

Material	Datum Temperature To (°C)	Activation Energy Q (kJ/mole)
Mortar	7.00	45
Concrete	6.50	42
Size A	7.04	42
Size B	7.27	42
Size C	7.34	42

5.3 Analysis of Results

5.3.1 Comparison of Fracture Energy Development Parameters

Comparison of compressive strength and fracture energy data presented in the preceding section indicates the existence of a strong similarity in fracture energy, and strength gain characteristics. For instance, results shown in Figures 5.1, 5.2 and 5.21 through 5.23 imply that in direct corollary with the strength gain relationship, the fracture energy gain function is also hyperbolic. The fracture energy age data were analyzed using the hyperbolic model Eq. 3.26. The fracture energy development parameters which include

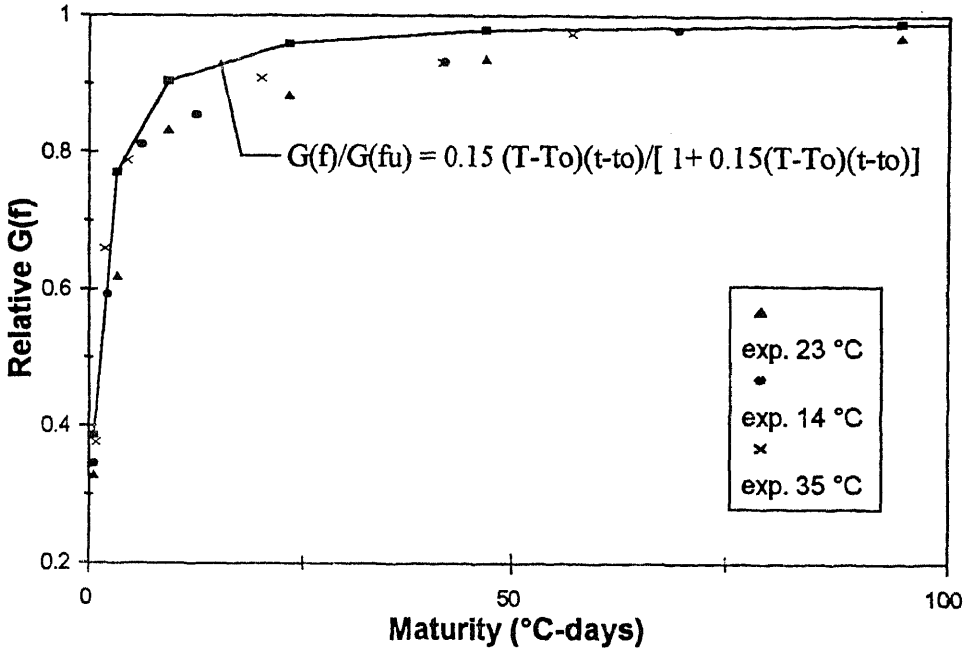

Figure 5.36 Relative fi acture energy versus maturity for isothermally cured size A beams

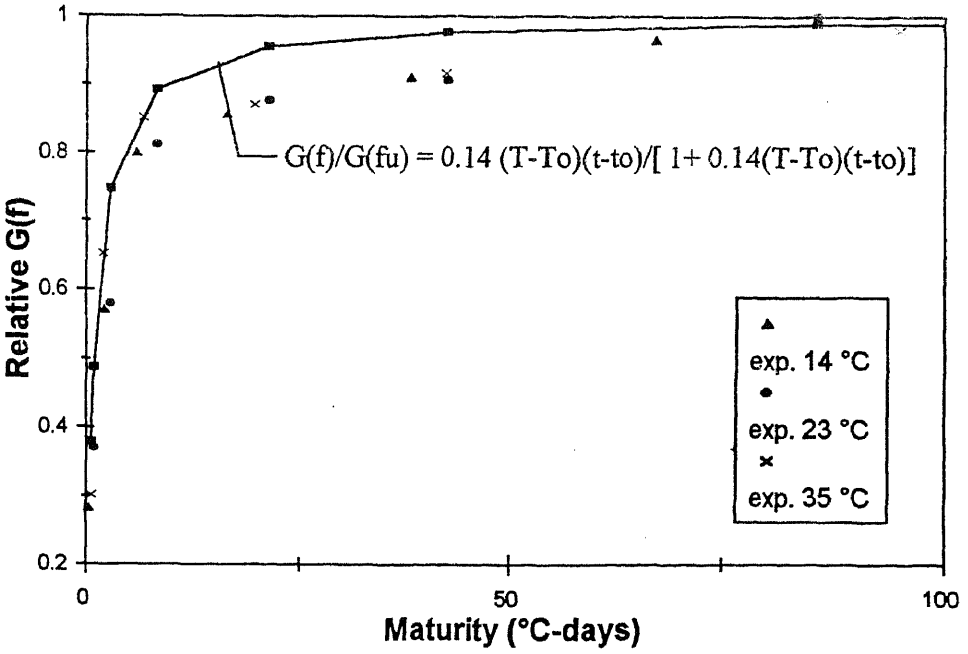

Figure 5.37 Relative fracture energy versus maturity for isothermally cured size B beams

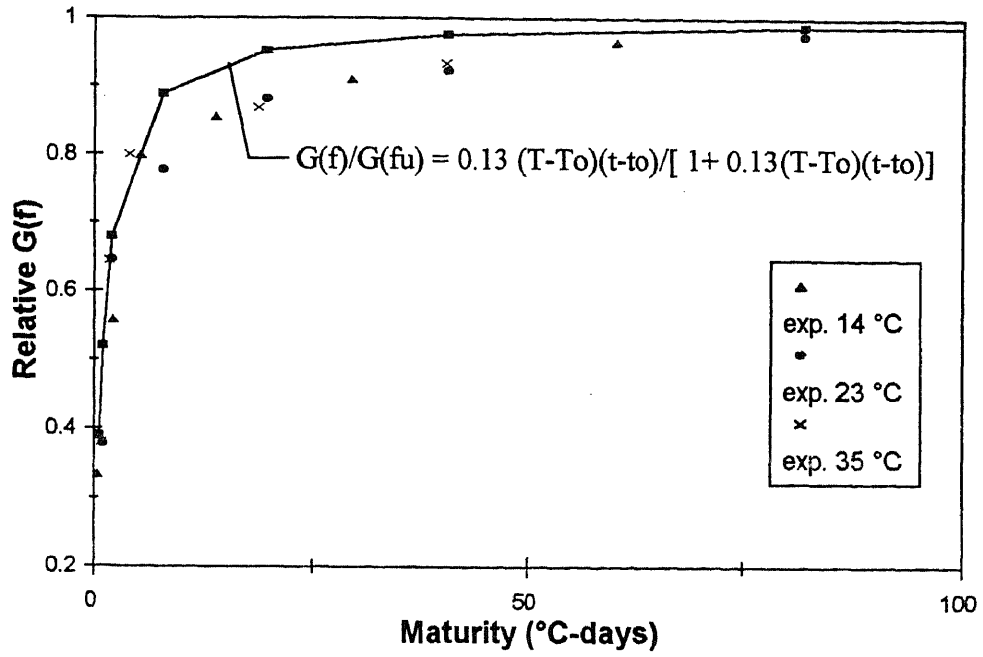

Figure 5.38 Relative fracture energy versus maturity for isothermally cured size C beams

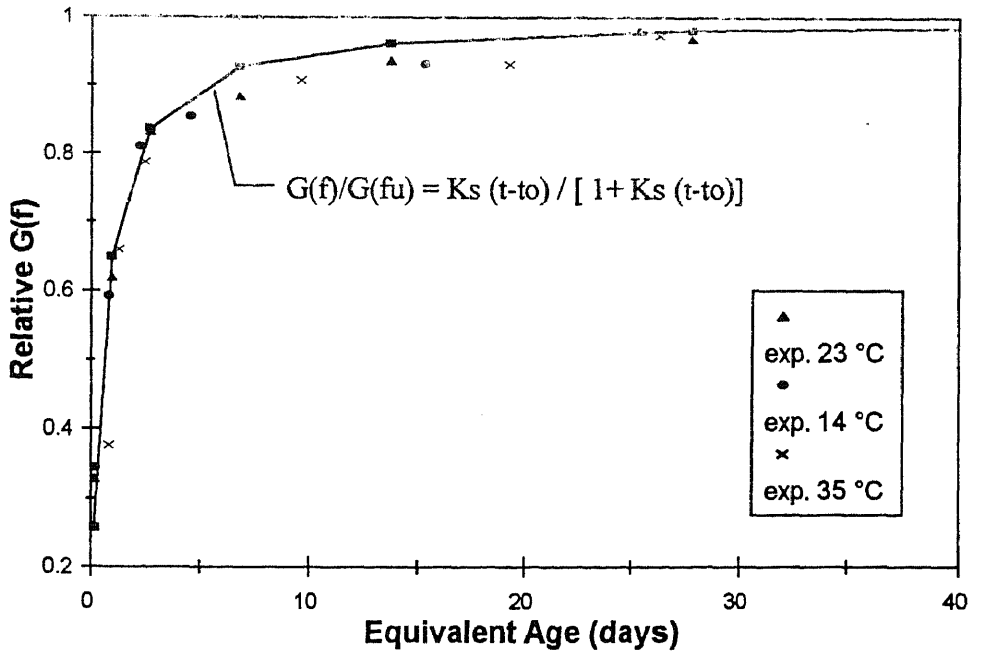

Figure 5.39 Relative fracture energy versus equivalent age for isothermally cured size A beams

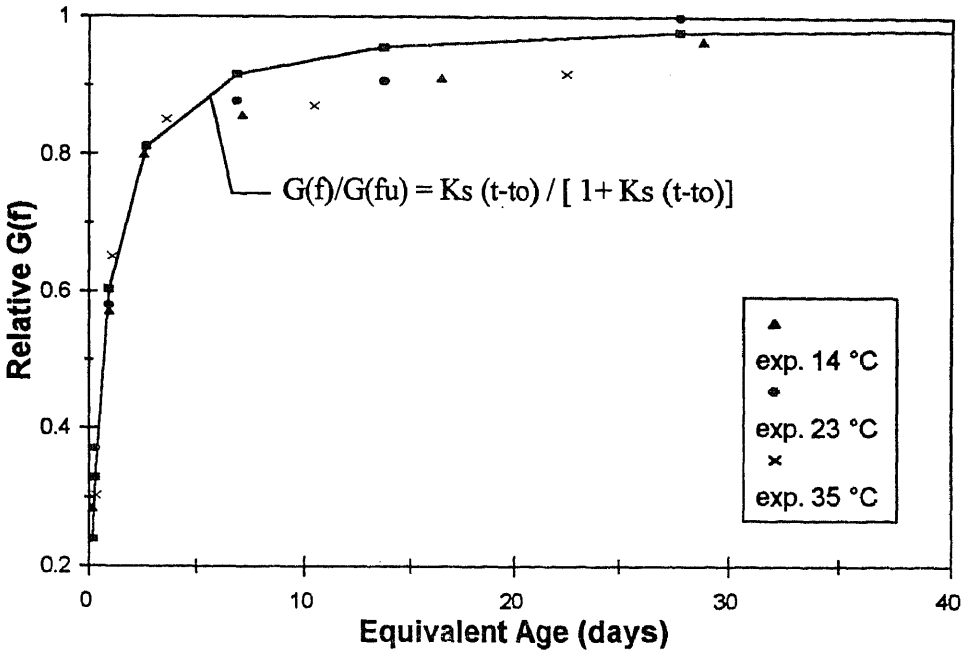

Figure 5.40 Relative fracture energy versus equivalent age for isothermally cured size B beams

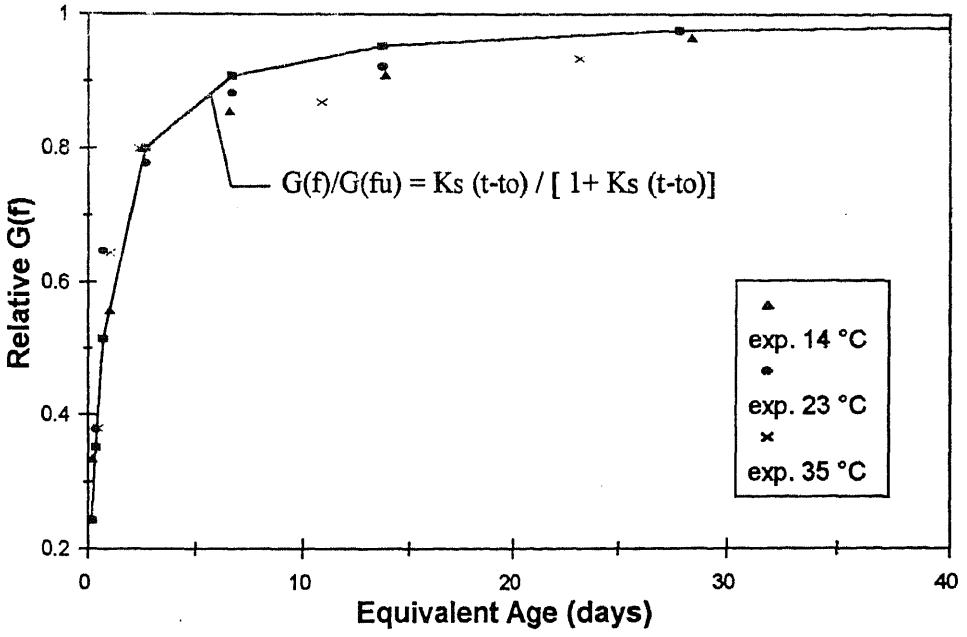

Figure 5.41 Relative fracture energy versus equivalent age for isothermally cured size C beams

the limiting fracture energy G_{fu}, the rate constant k_T, and the initial age t_o were obtained for all beams and are shown in Tables 5.11 through 5.16. The fracture energy-gain parameters are discussed separately as follows.

5.3.1.1 Fracture Energy

The gain in fracture energy as a function of age for the three curing temperatures are presented in Figures 5.21 through 5.23. As seen in the Figures 5.21 through 5.23, the fracture energy exhibit faster gains at early ages for higher curing temperatures, and higher final values at lower temperatures.

5.3.1.2 Limiting Fracture Energy

The limiting fracture energy, G_{fu}, is the computed asymptotic value of the fracture energy at late ages based on the assumption that fracture energy - gain obeys linear transformations (Eq. 5.1) and the hyperbolic model (Eq. 3.26). As shown in Figure 5.42 shows that the limiting fracture energy decreases as the curing temperature of concrete increases.

5.3.1.3 Rate Constant

In the hyperbolic fracture energy-age equation 3.26, the rate constant, k_T, is the initial slope at t_o divided by the limiting fracture energy. Figures 5.30 through 5.32 show that the rate constant is a function of the curing temperature, and they increase with curing temperature. The k_T values calculated based on fracture energy, G_f, which are obtained

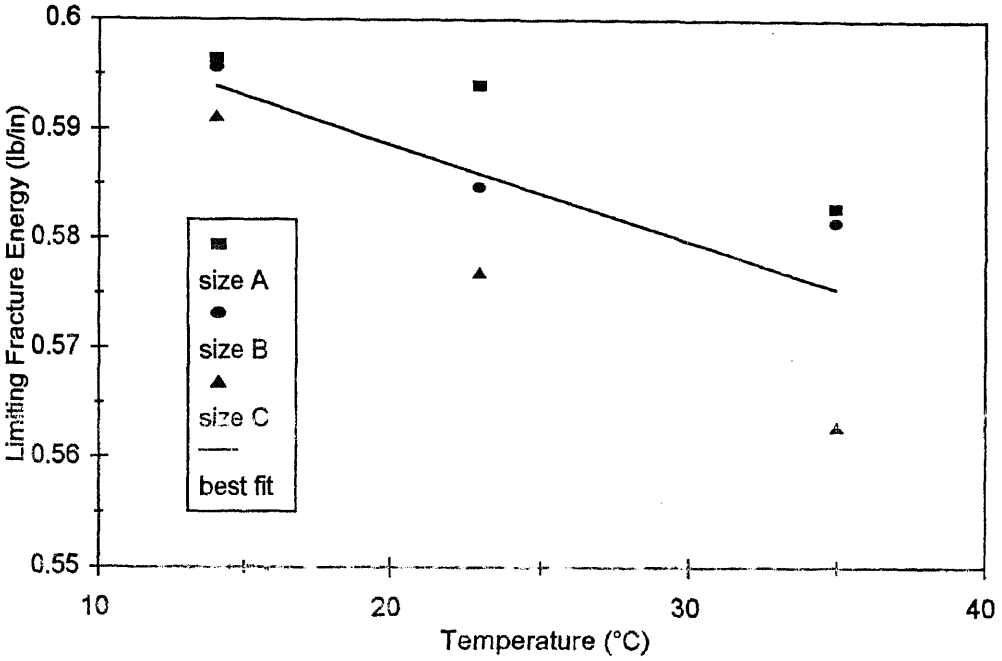

Figure 5.42 Liniting fracture energy versus curing temperature

from load-deflection curves of three-point bend tests are higher than those based on compressive strength, f_c.

5.3.1.4 Datum Age

Datum age, (Initial age), t_o, is age at the end of induction period, when the fracture energy development is assumed to begin. The datum age of concrete decreases as the curing temperature increase. The datum age does not appear to be significantly different for the cubes, cylinders or beams.

5.3.2 Variation of Rate Constant with Temperature

5.3.2.1 Datum Temperature

Figures 5.30 through 5.32 indicate the variation of rate constant with curing temperature and are fitted in the linear. In the linear function, the datum temperature, T_o, is the temperature corresponding to a rate constant equal to zero. The values of datum temperature are shown in Table 5.17. For a given concrete mixture, in which the rate constant varies in a non-linear manner with temperature, the value of datum temperature depends upon the temperature range being considered. In this study, the temperature range for the best fit values of the datum temperature are 14 °C to 35 °C. There are some published values of datum temperature and listed on Table 5.18 . None of the datum temperature calculated in this study, equaled to -10 °C which the value used in the traditional maturity function.

Table 5.18 The value of datum temperature published in various references

Reference	Cement	datum temperature T_o(°C)
Saul, 1951	Concrete with Type I cement	-10.0
Carino, 1984	Mortar with Type I cement	4.0
Carino, 1984	Concrete with Type I cement	4.5
Tank, 1988	Mortar with Type I cement	7.0 - 11.0
Tank, 1988	Mortar with Type II cement	6.0 - 9.0
Tank, 1988	Mortar with Type III cement	6.0 - 6.0
Tank, 1988	Concrete with Type I cement	8.0 - 11.0
Tank, 1988	Concrete with Type II cement	6.0 - 9.0
Tank, 1988	Concrete with Type III cement	7.0

5.3.2.2 Activation Energy

The rate constants vary with temperature according to the Arrhenius equation(Figures 5.33, 5.34 and 5.35). Therefore, the activation energy, Q, is an important parameter of the temperature function. Values of the activation energy as calculated from strength-age and fracture energy-age data are given in Tables 5.7 and 5.17. Both strength-age and fracture energy-age data yielded similar activation energies for concrete.

Published activation energy values are listed in Table 5.19 . Activation energies obtained in this study for mortar and concrete mixtures with type I cement are within the range of the published values.

Table 5.19 The value of Activation energy published in various references

Reference	Cement	Activation Energy Q (kJ/mole)
Carino, 1984	Mortar with Type I cement	43.7
Carino, 1984	Concrete with Type I cement	40.8
Gauthier, 1982	Ordinary portland cement	42.0 - 47.0
Geiker, 1982	Ordinary portland cement	61.0
Geiker, 1982	Rapid Hardening cement	57.0
Tank, 1988	Mortar with Type I cement	44.0 - 62.0
Tank, 1988	Concrete with Type I cement	46.0 - 61.0

5.3.3 Relative Fracture Energy Gain

It is shown that the limiting fracture energy of a concrete mixture is affected by the early-age curing temperature history. Thus there is no unique fracture energy versus maturity function for a given concrete. However, there is a unique relative fracture energy versus maturity function.

Based on time-temperature function, the relative fracture energy can be plotted in two way. First, the traditional maturity function is used with a datum temperature shown in Table 5.17. The resulting relative fracture energy versus maturity plot are presented in Figures 5.36 through 5.38. Alternatively, the relative fracture energy can be plotted versus the equivalent age at standard temperature by using an activation energy given in Table 5.17. The resulting relative fracture energy versus equivalent age plot are presented in Figure 5.39 through 5.41.

Because curing temperature affects the limiting fracture energy, the data have been presented in terms of relative fracture energy and the results presented in Figures 5.36 through 5.41. show that the shape of the relative fracture energy versus the time-temperature function (maturity or equivalent age) is independent of the curing temperature. In addition, it has been shown that by using the correct datum temperature, the traditional maturity function can describe relative fracture energy gain almost as precisely as equivalent age based on the Arrhenius equation.

CHAPTER 6

CONCLUSIONS

The overall objective of this dissertation was to develop a methodology for determining the in-place fracture energy for concrete-like materials in a nondestructive manner. The method combines the principles of fracture mechanics and time-temperature effects on the fracture energy development of concrete. This nondestructive test has been developed based on the theoretical basis given here and on the basis of experimental data on 150 beam specimens, 162 cylinders and 63 cubes. The relative fracture energy-gain of concrete is related to the maturity or the equivalent age by means of a hyperbolic function and three parameters. The three parameters are the limiting fracture energy, G_{fu}, the rate constant, k_T, and datum age, t_o. The effect of major variables on the fracture energy development parameters are studied by statistical analysis of isothermally cured fracture energy-gain data.

To verify the equivalency of activation energy values obtained from fracture and compressive tests, mortar cubes and concrete cylinders were also tested in compression. Comparison of results from mortar cubes, concrete cylinders and three-point bend beams indicated that similar activation energy values are obtained in beam and cylinder tests for the same concrete mixture. This proves that the maturity method is also applicable determination of fracture energy in structures.

The followings conclusions from this study and are summarized as follows:

1. In the theoretical development, the fracture energy gain of concrete under isothermal conditions can be described by a hyperbolic curve which is defined by three parameters: (i) t_o, the age when fracture energy development is assumed to begin, (ii) k_T, a rate constant, which is the initial slope of the curve, and (iii) G_{fu}, the limiting fracture energy. These three parameters are temperature dependent and can be obtained from fracture energy tests by using linear regression analyses.
2. The rate constant, k_T, values calculated based on compressive strength, f_c, are lower than based on fracture energy, G_f, obtained from load-deflection curve of three-point bent tests. This is because the rate of increase of f_c with age is lower than the rate of increase of G_f with age. However, it is interesting to note that the activation energy, Q, calculated from these two tests are almost the same. Values of k_T when plotted on a logarithm scale against $1/T_k$ yield straight lines which are parallel(Figure 6.1) yielding equal slopes. This slope is magnitude of activation energy divided by the gas constant(= 8.3144 J/°K-mole).
3. Due to the fact that the early age curing temperature affects the limiting fracture energy, there is not a unique fracture energy versus maturity function curve for a given concrete mixture. However, there is a unique relative fracture energy versus maturity function curve for all concretes.
4. Activation energy results confirmed the notion that fracture tests can be used as an alternate technique for obtaining the activation energy of concrete.

5. The results of comparison of datum temperature and activation energy appear to confirm the notion that tests of concrete cylinders can provide the datum temperature T_o or activation energy Q requires to develop the time-temperature function of the beam tests.
6. The fracture energy-maturity relationship for concrete was established by conducting laboratory three-point bend tests on the concrete mix used.
7. Based on the maturity concept an insitu nondestructive method for the determination of the fracture energy for concrete has been developed. The fracture energy in any concrete element or structures can be determined based on the fracture energy-maturity relationship in a similar manner as to the maturity tests for strength.

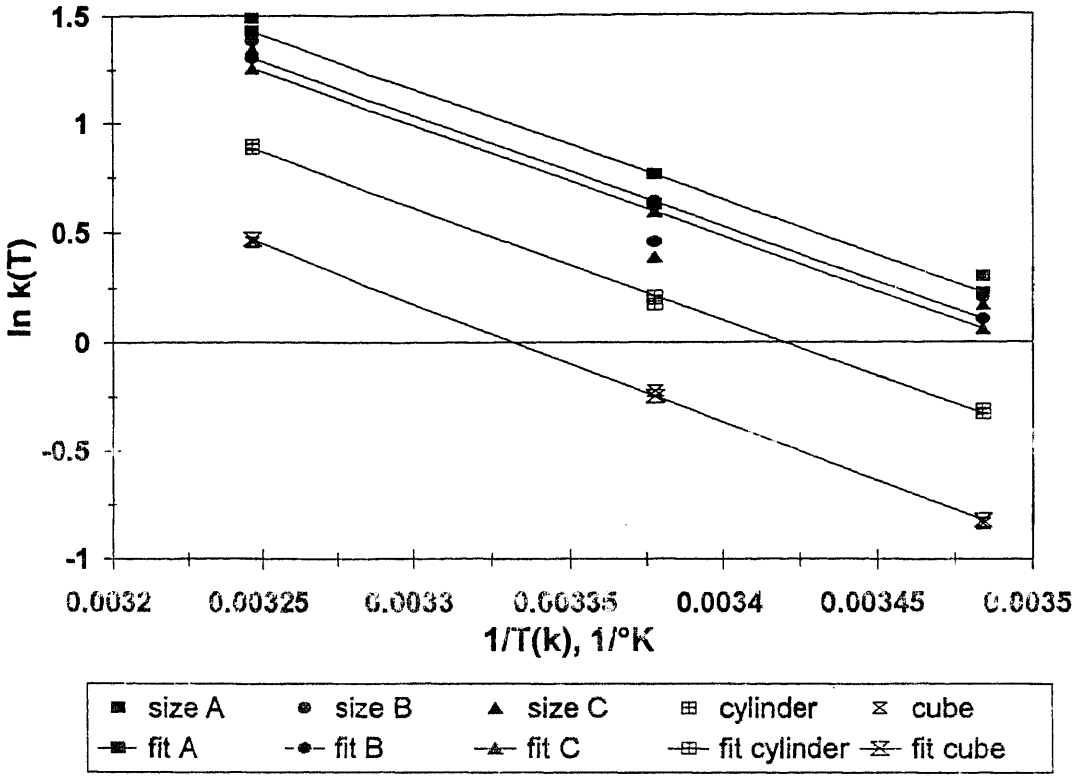

Figure 6.1 Logarithm of rate constant versus reciprocal of curing temperature in Kelvin

APPENDIX A

DEVELOPMENT OF FRACTURE ENERGY FUNCTION

Figures corresponding to the empirical procedure employed for the determination of the fracture energy function $g(G_f)$ in chapter 3.3.2.

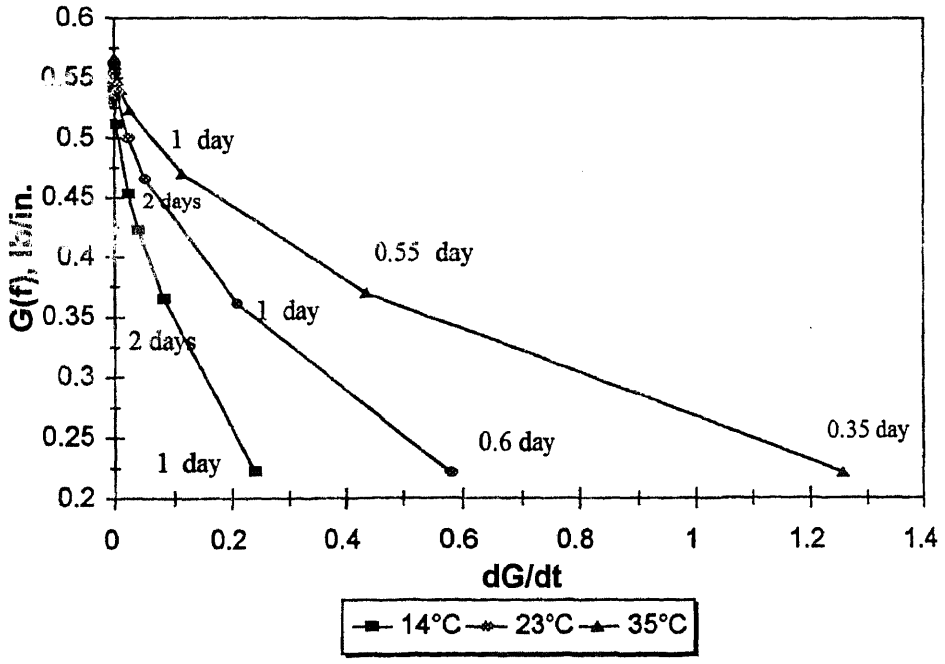

Figure 3.7 G_f versus dG_f/dt for size A

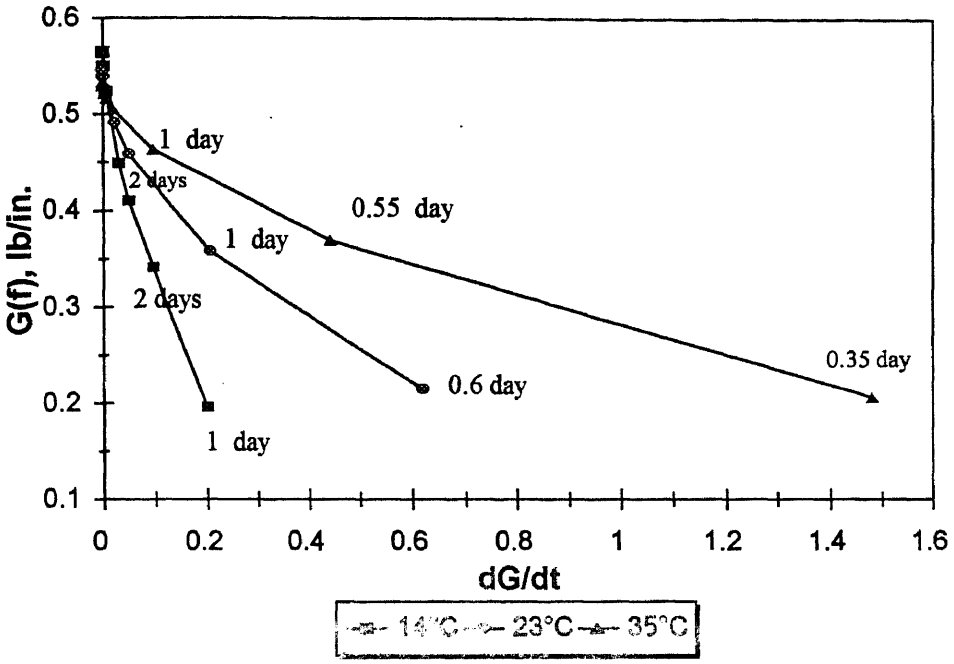

Figure 3.8 G_f versus dG_f/dt for size C

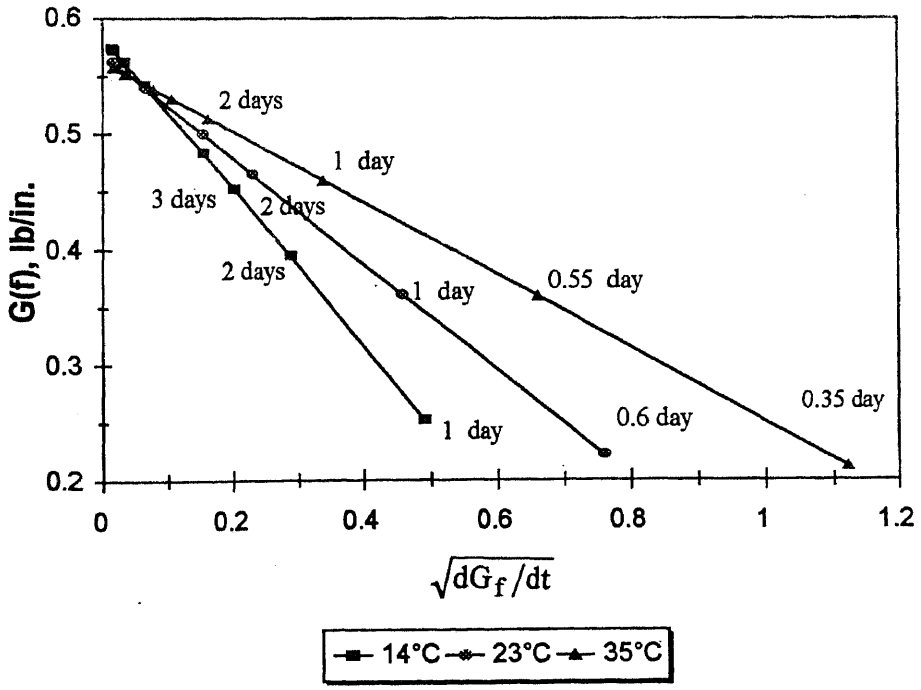

Figure 3.9 G_f vs. $\sqrt{dG_f/dt}$ for size A

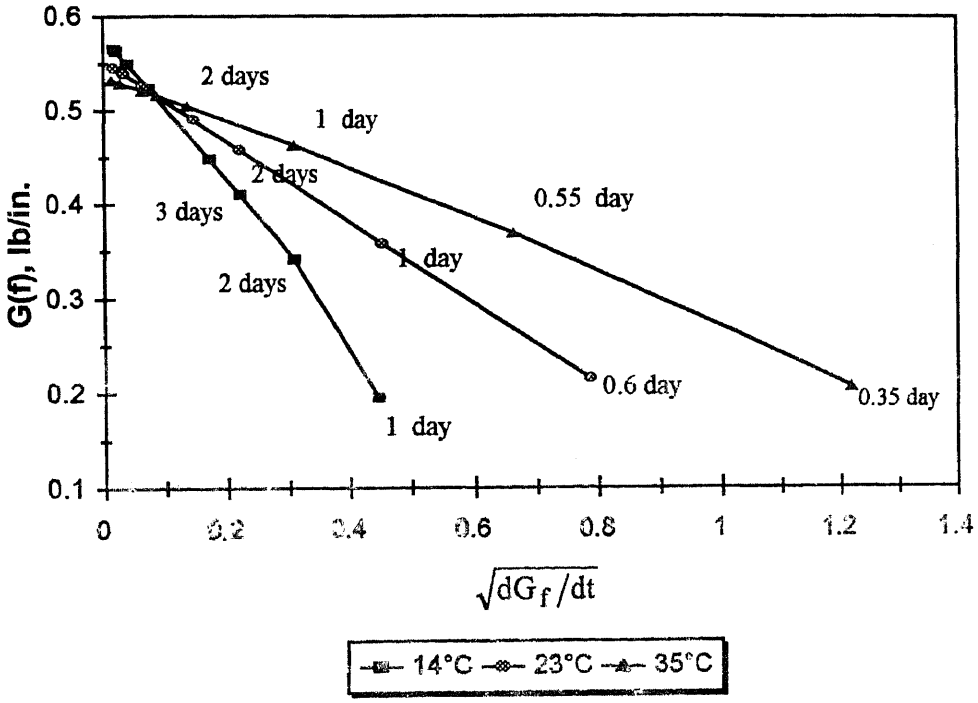

Figure 3.10 G_f vs. $\sqrt{dG_f/dt}$ for size C

APPENDIX B

EXPERIMENTAL DATA

Load deflection diagrams for all the beams tested in this study.

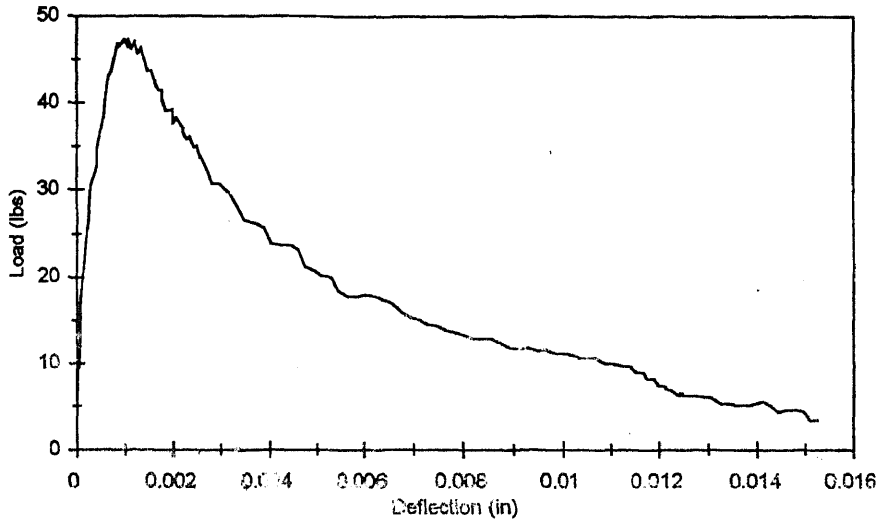

Figure A1a Load versus deflection for size A, curing at 14°C, age = 1.22 days

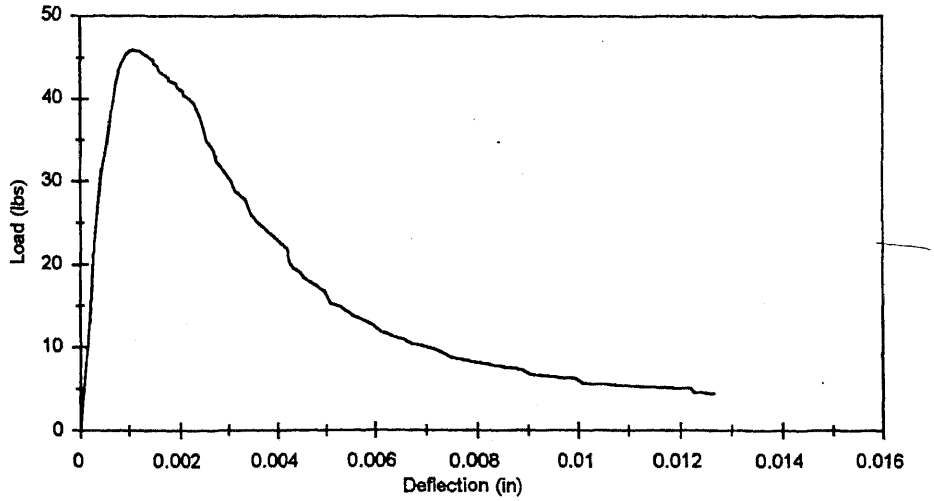

Figure A1b Load versus deflection for size A, curing at 14°C, age = 1.22 days

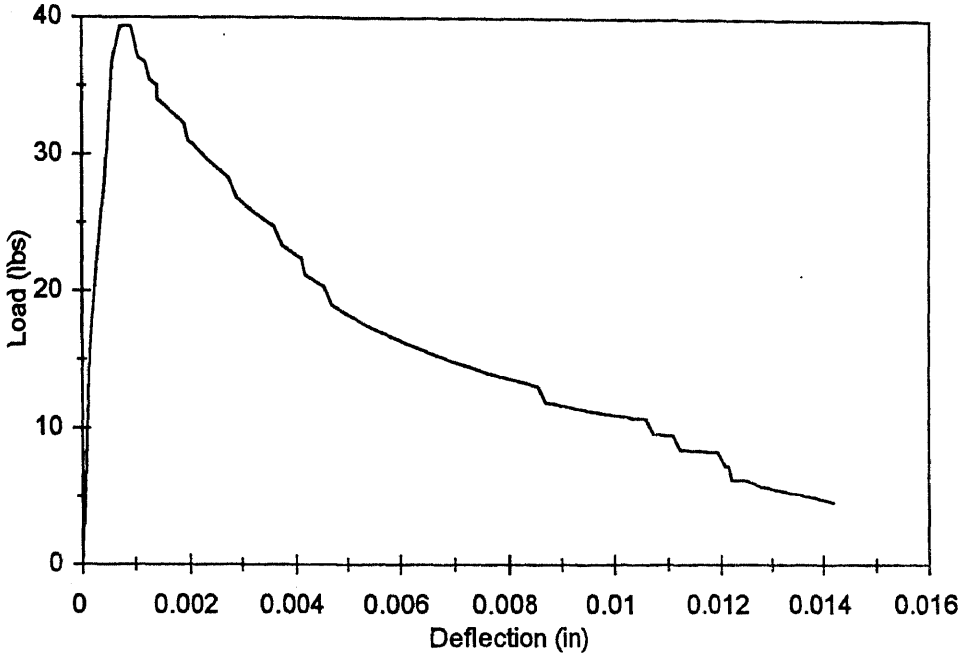

Figure A1c Load versus deflection for size A, curing at 14°C, age = 1.22 days

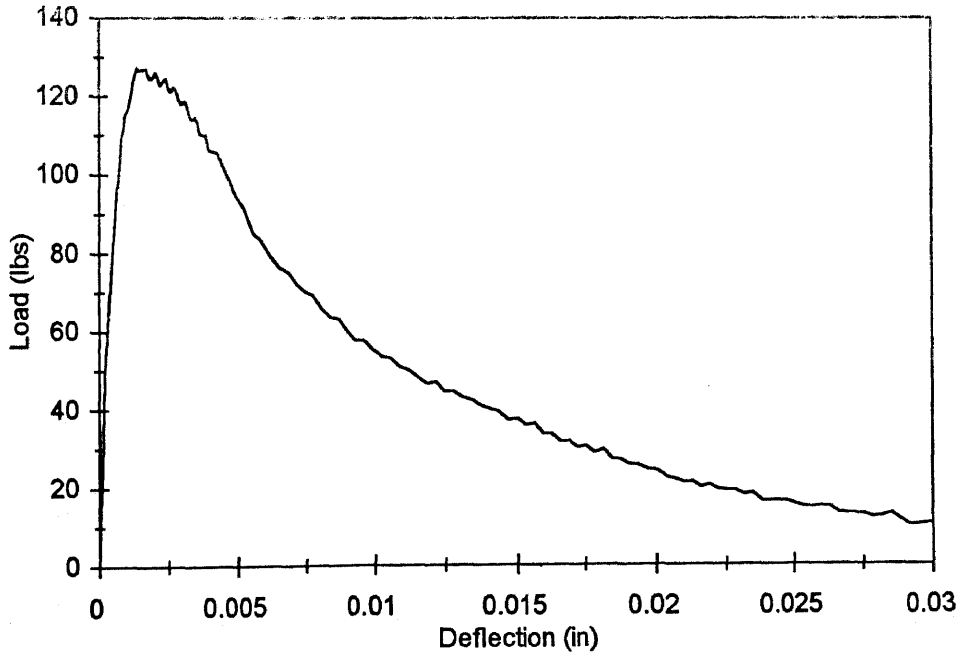

Figure A2a Load versus deflection for size A, curing at 14°C, age = 2.04 days

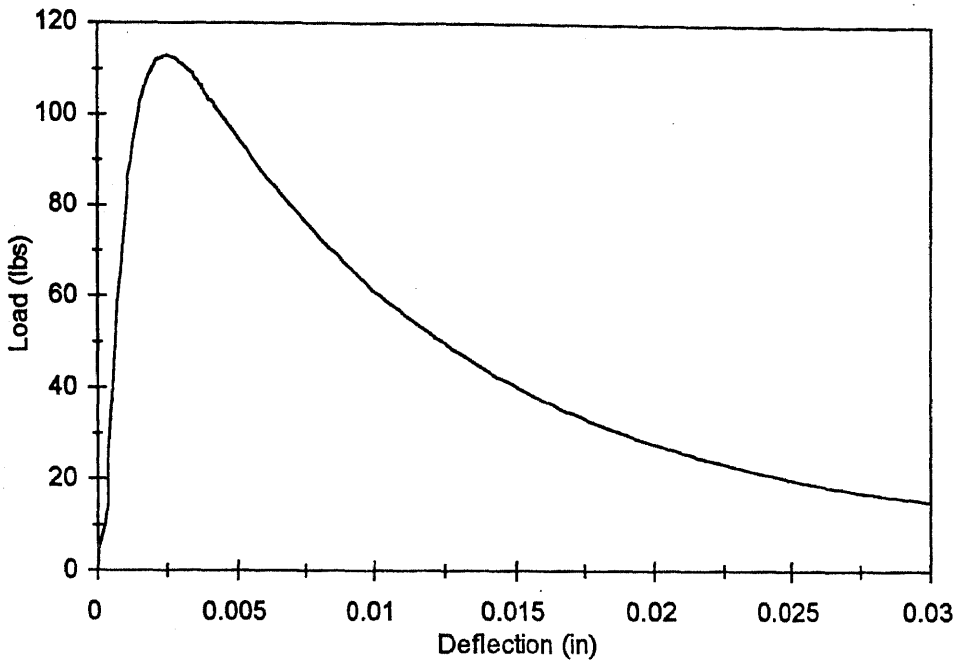

Figure A2b Load versus deflection for size A, curing at 14°C, age = 2.04 days

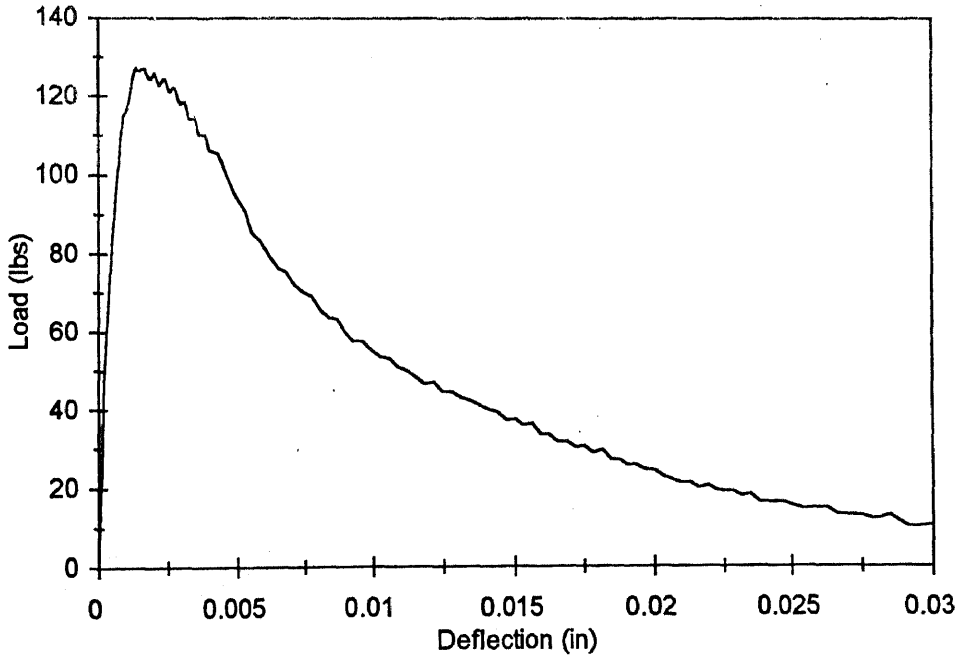

Figure A2c Load versus deflection for size A, curing at 14°C, age = 2.04 days

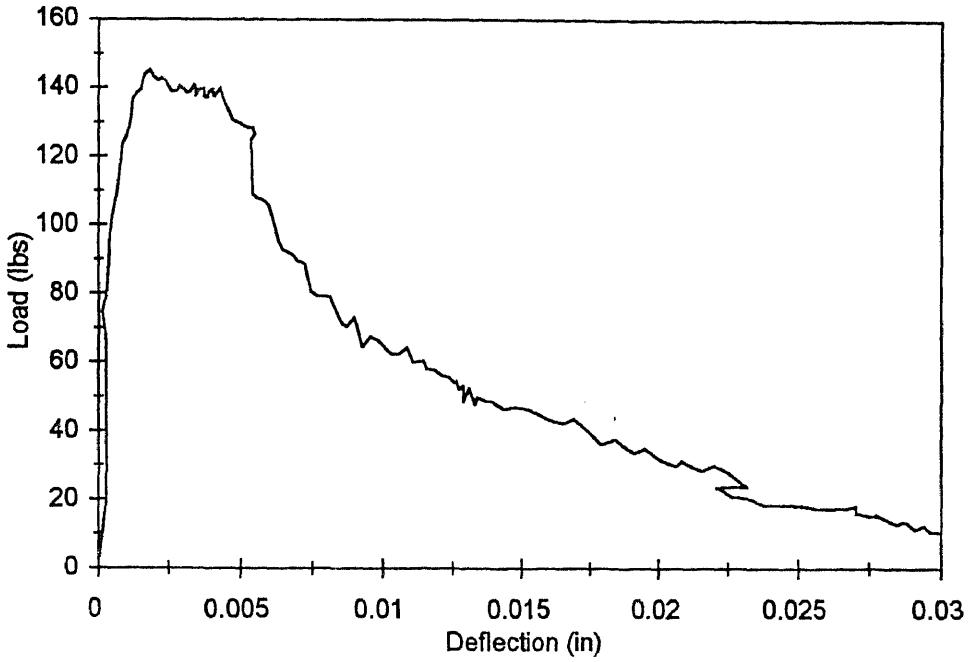

Figure A3a Load versus deflection for size A, curing at 14°C, age = 4.03 days

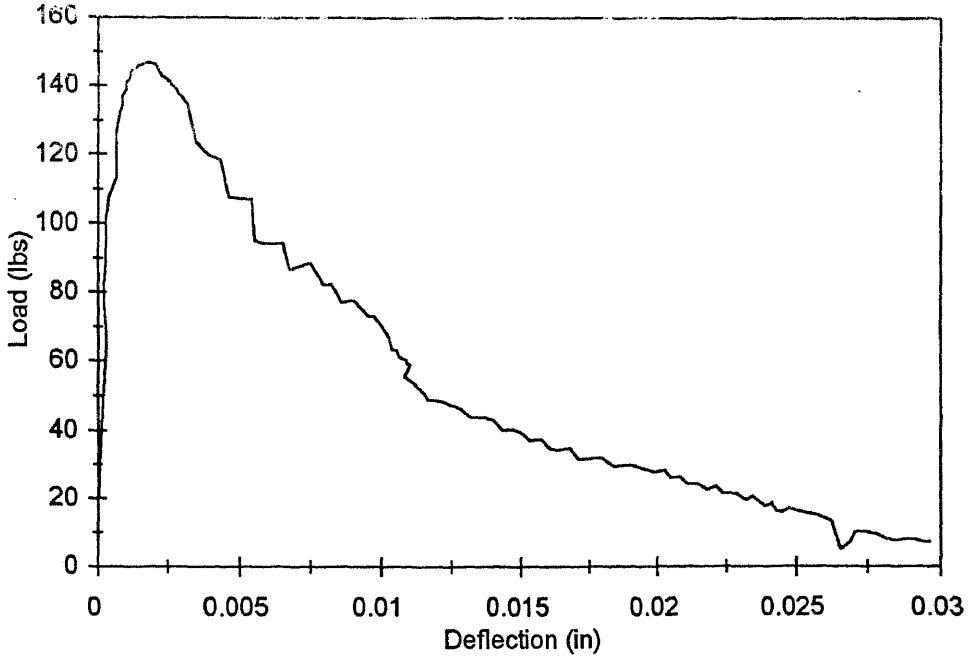

Figure A3b Load versus deflection for size A, curing at 14°C, age = 4.03 days

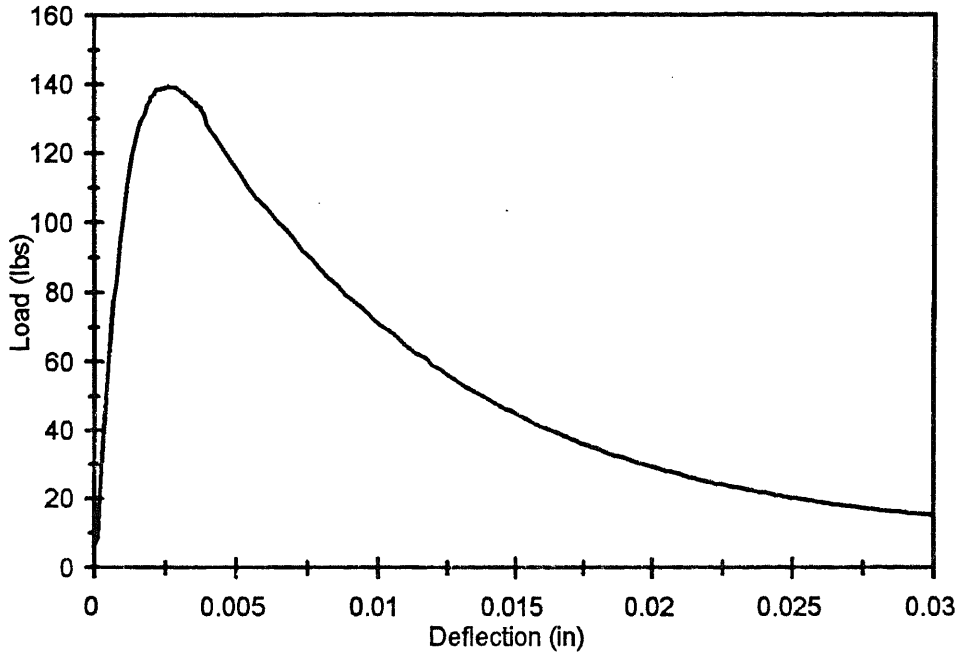

Figure A3c Load versus deflection for size A, curing at 14°C, age = 4.03 days

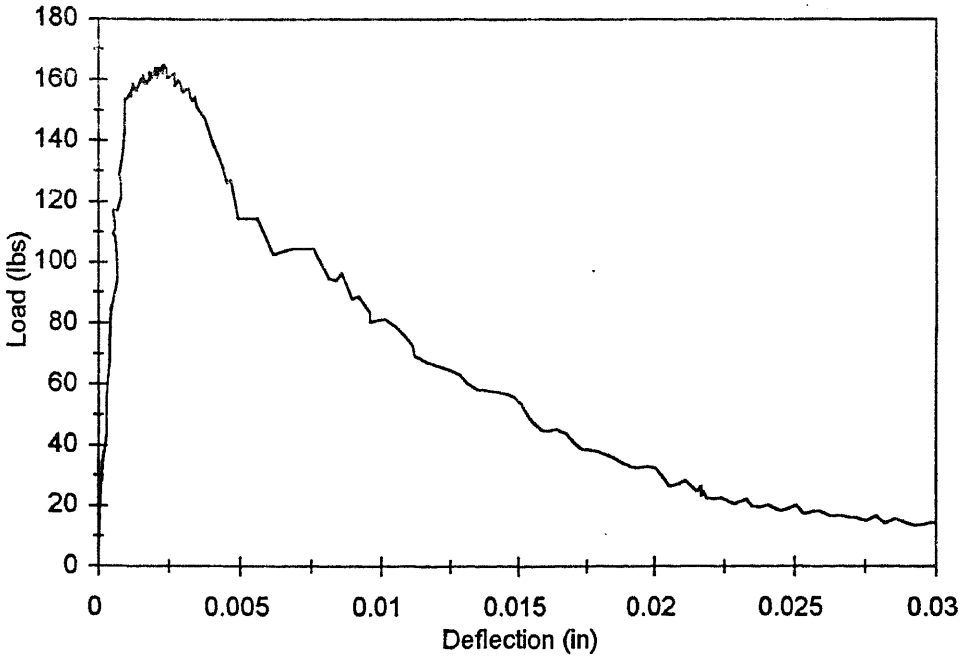

Figure A4a Load versus deflection for size A, curing at 14°C, age = 7.25 days

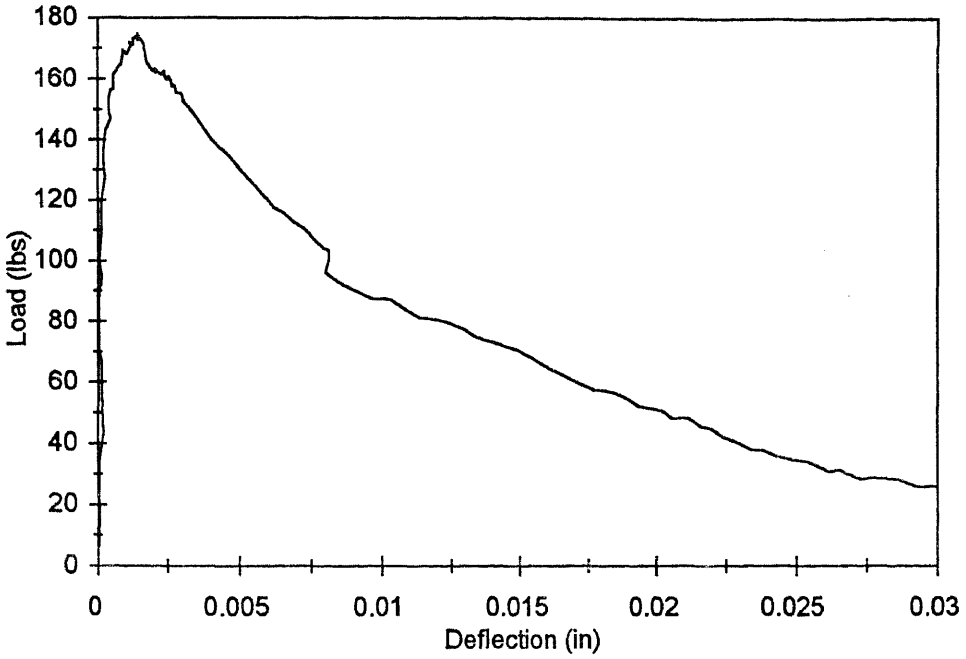

Figure A4b Load versus deflection for size A, curing at 14°C, age = 7.25 days

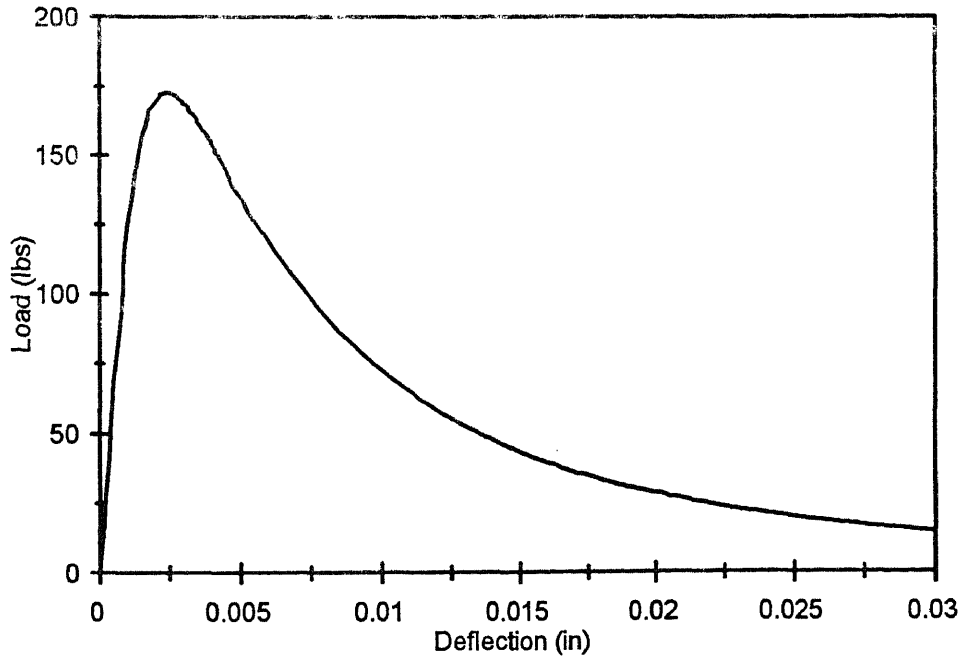

Figure A4c Load versus deflection for size A, curing at 14°C, age = 7.25 days

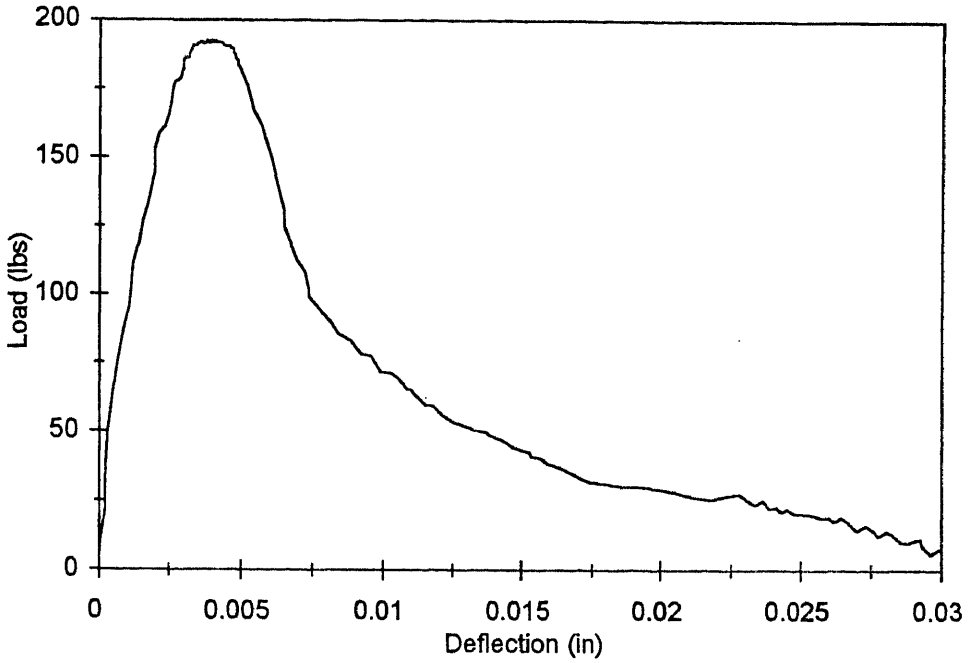

Figure A5a Load versus deflection for size A, curing at 14°C age = 22.04 days

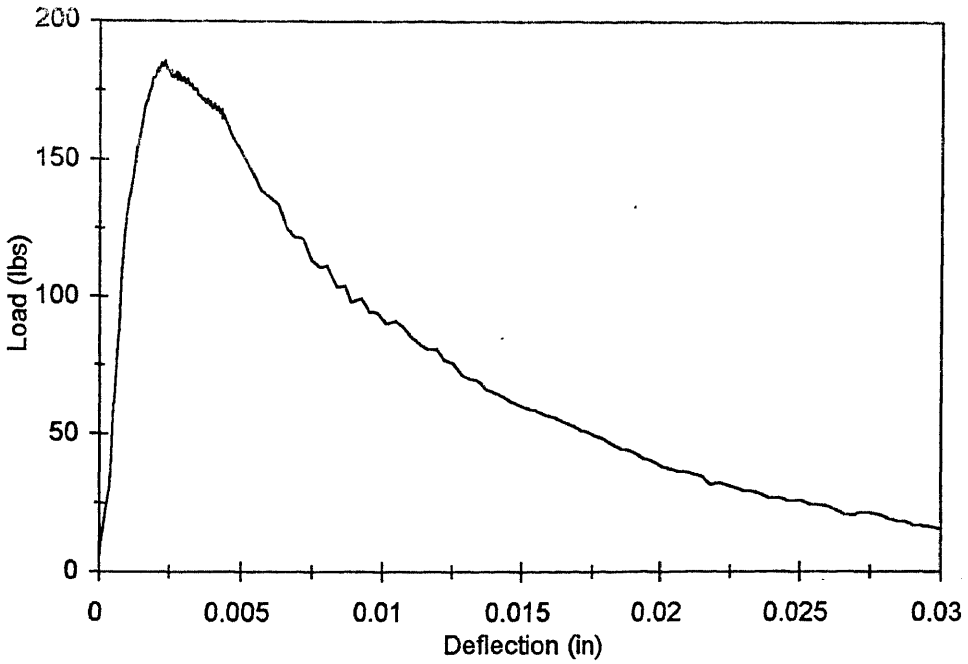

Figure A5b Load versus deflection for size A, curing at 14°C age = 22.04 days

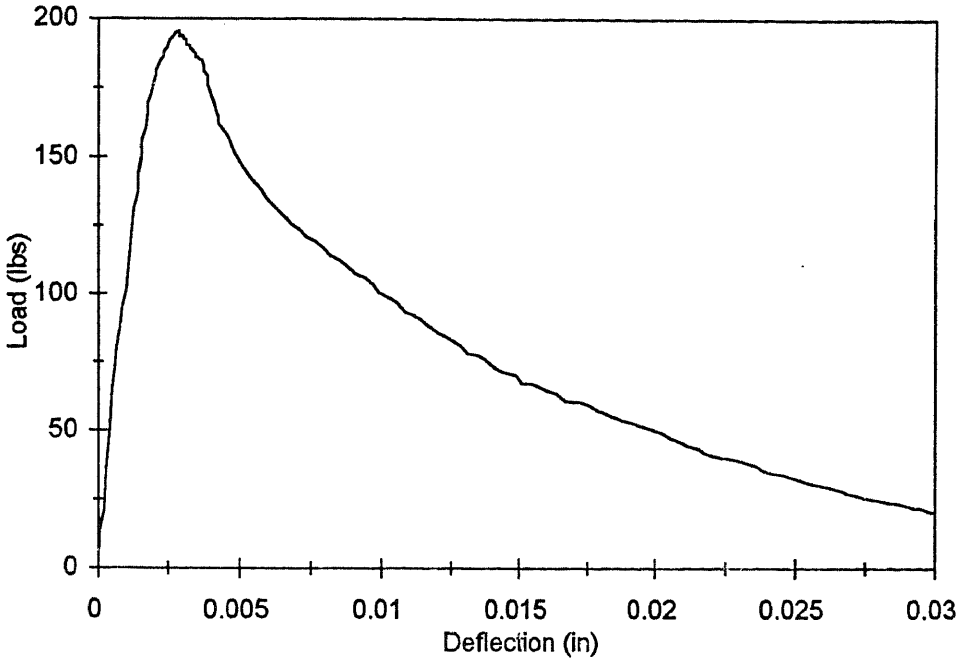

Figure A5c Load versus deflection for size A, curing at 14°C age = 22.04 days

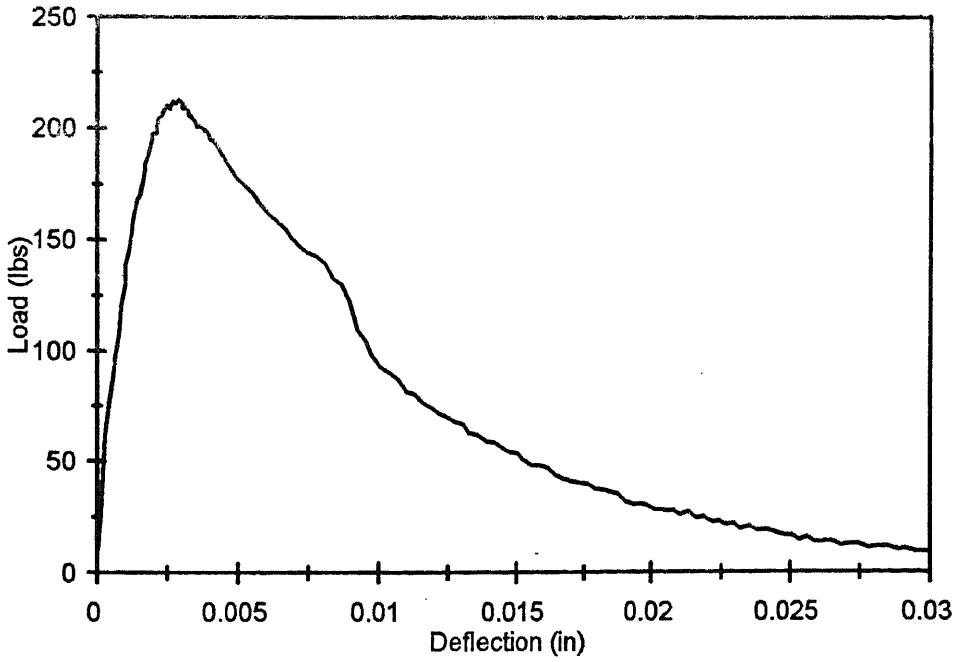

Figure A6a Load versus deflection for size A, curing at 14°C age = 36 days

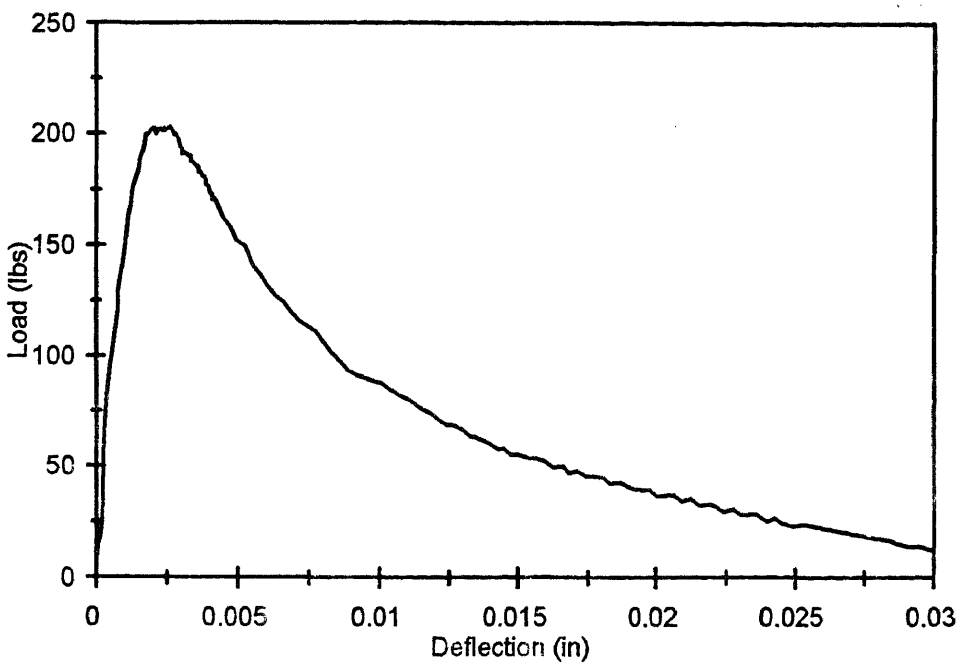

Figure A6b Load versus deflection for size A, curing at 14°C age = 36 days

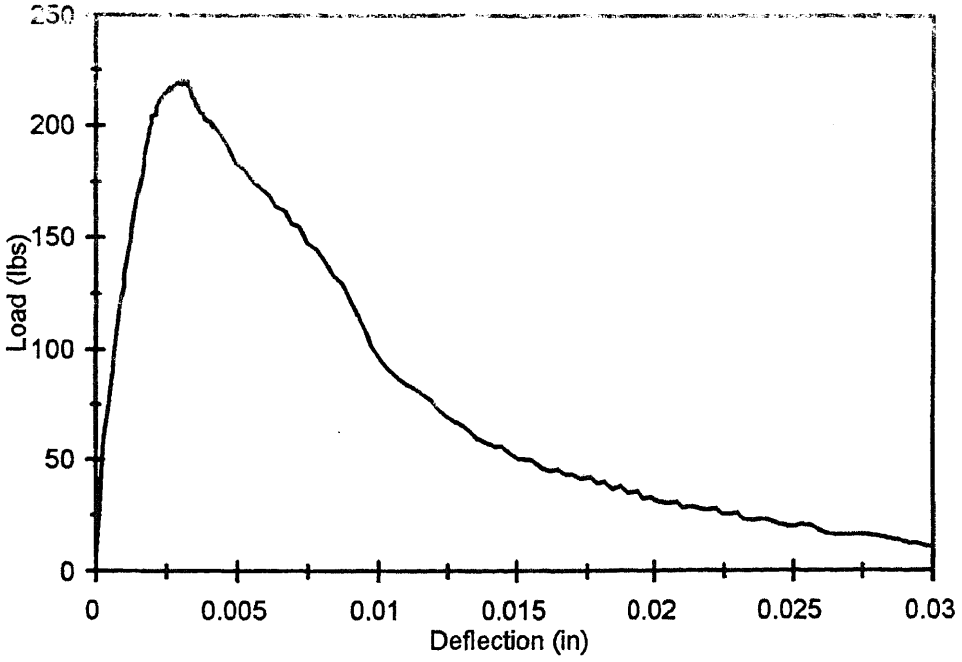

Figure A6c Load versus deflection for size A, curing at 14°C age = 36 days

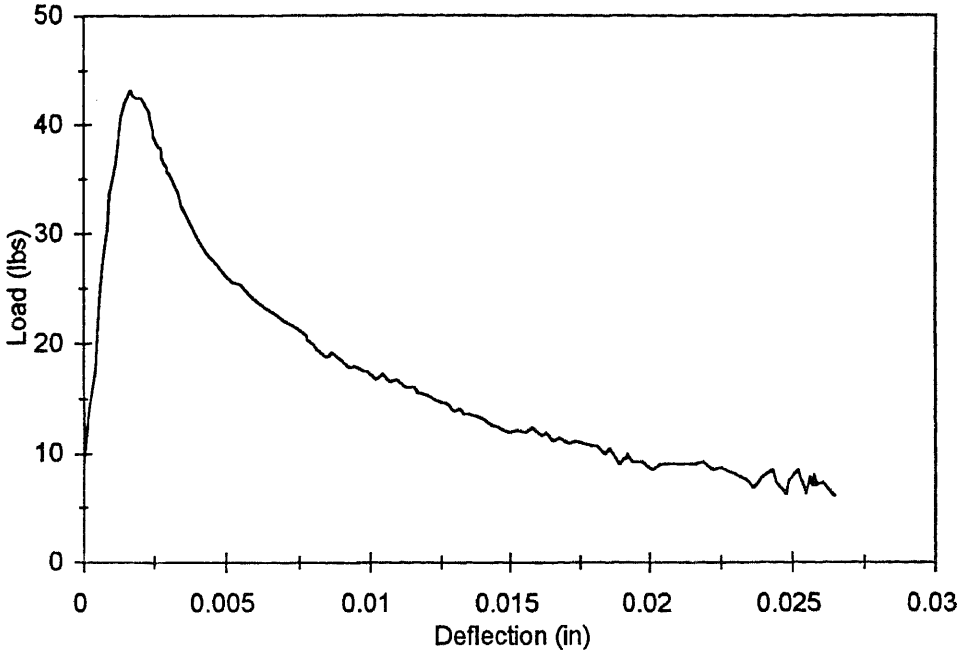

Figure A7a Load versus deflection for size A, curing at 23°C, age = 0.5 day

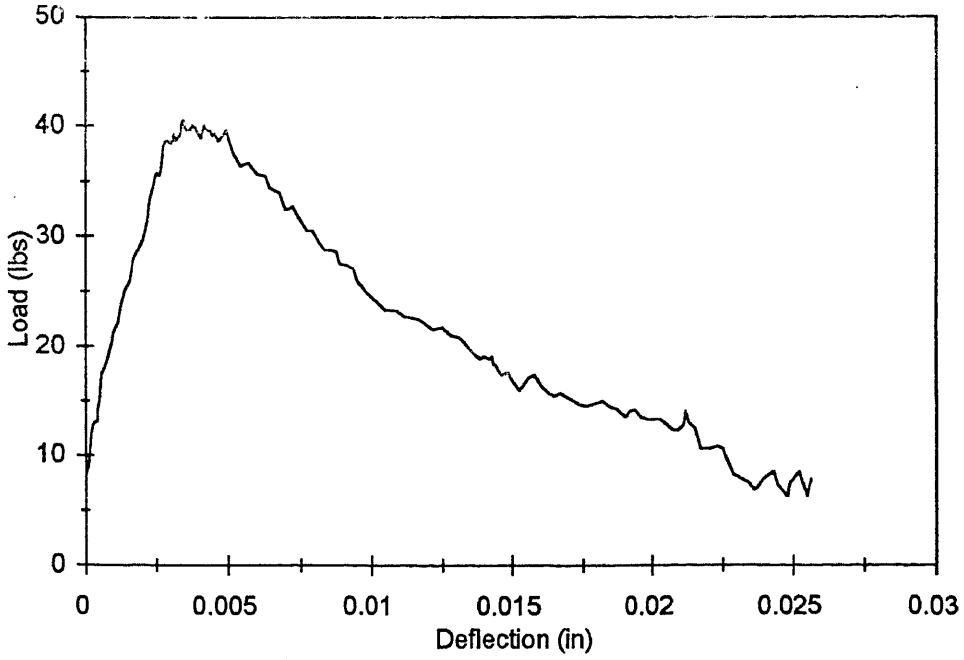

Figure A7b Load versus deflection for size A, curing at 23°C, age = 0.5 day

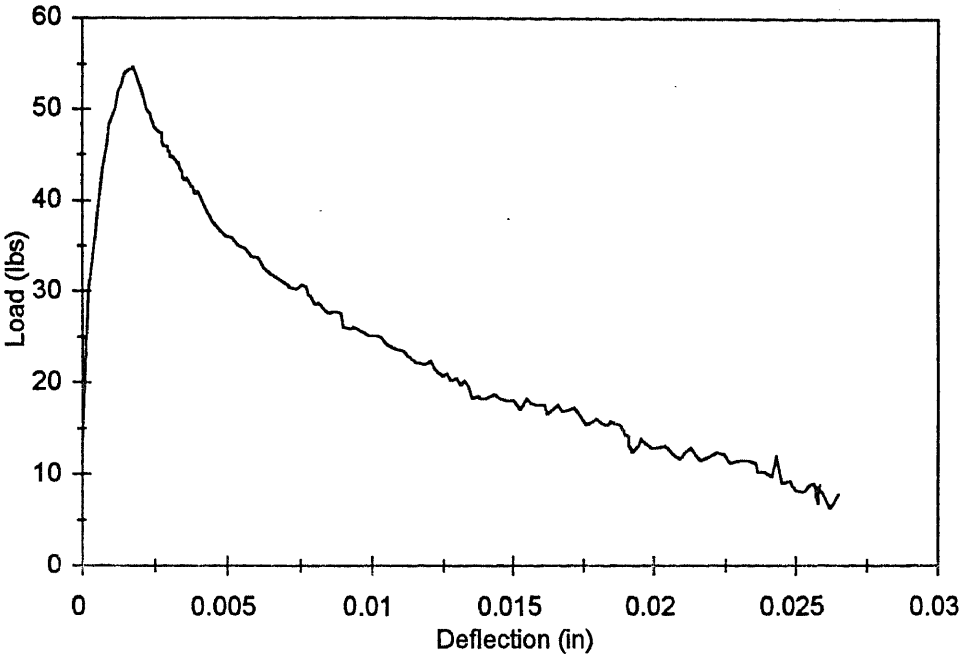

Figure A7c Load versus deflection for size A, curing at 23°C, age = 0.5 day

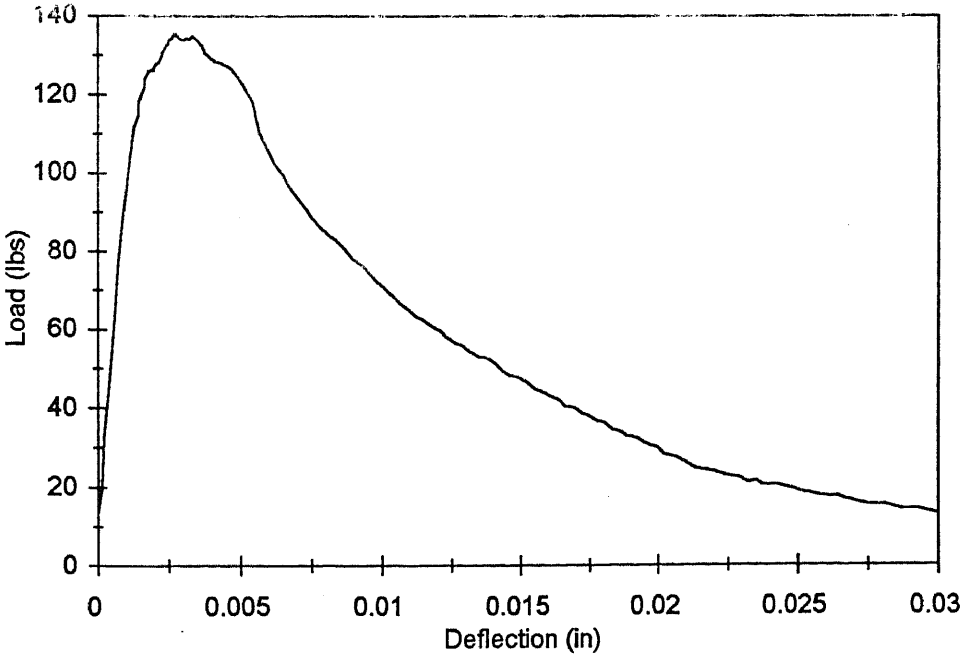

Figure A8a Load versus deflection for size A, curing at 23°C, age = 1.3 days

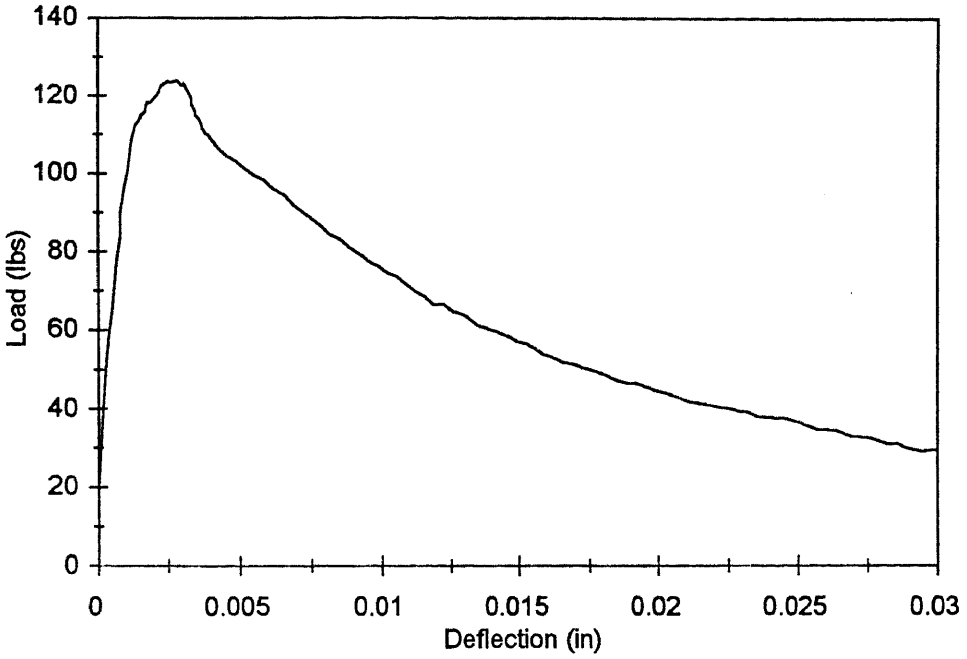

Figure A8b Load versus deflection for size A, curing at 23°C, age = 1.3 days

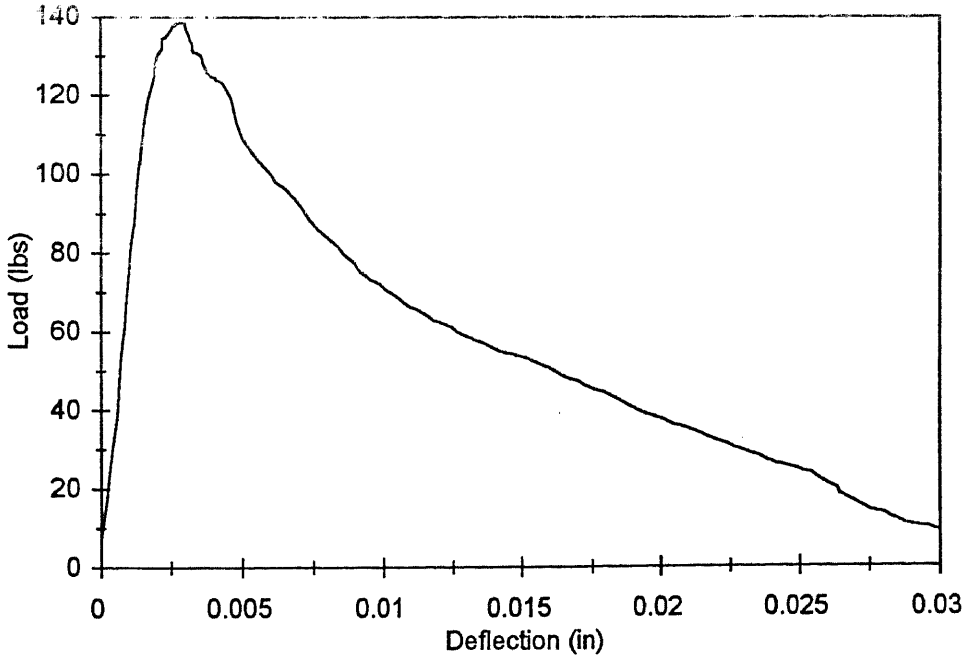

Figure A8c Load versus deflection for size A, curing at 23°C, age = 1.3 days

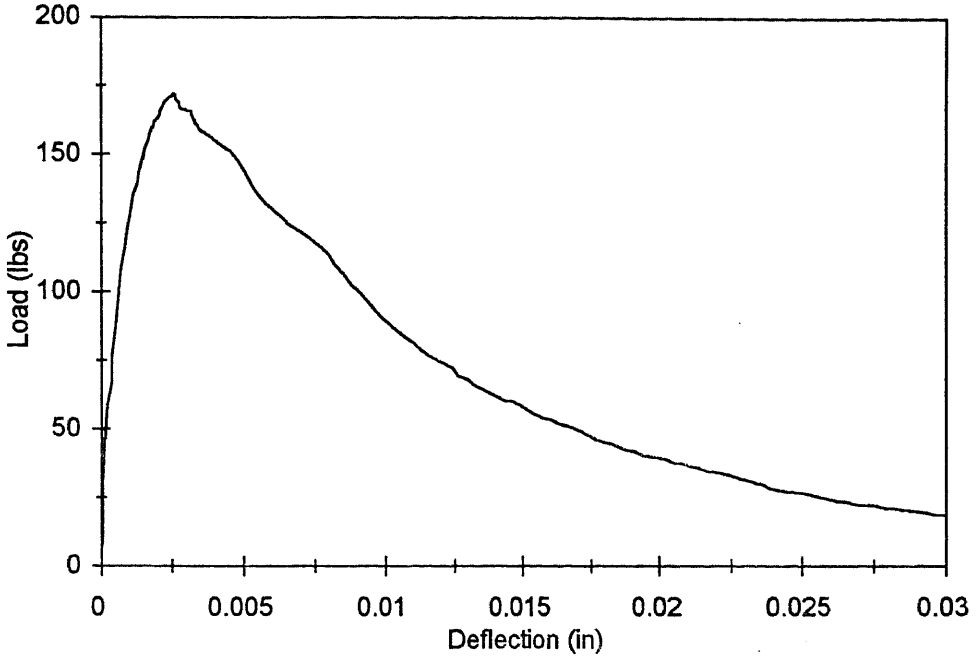

Figure A9a Load versus deflection for size A, curing at 23°C, age = 3.06 day

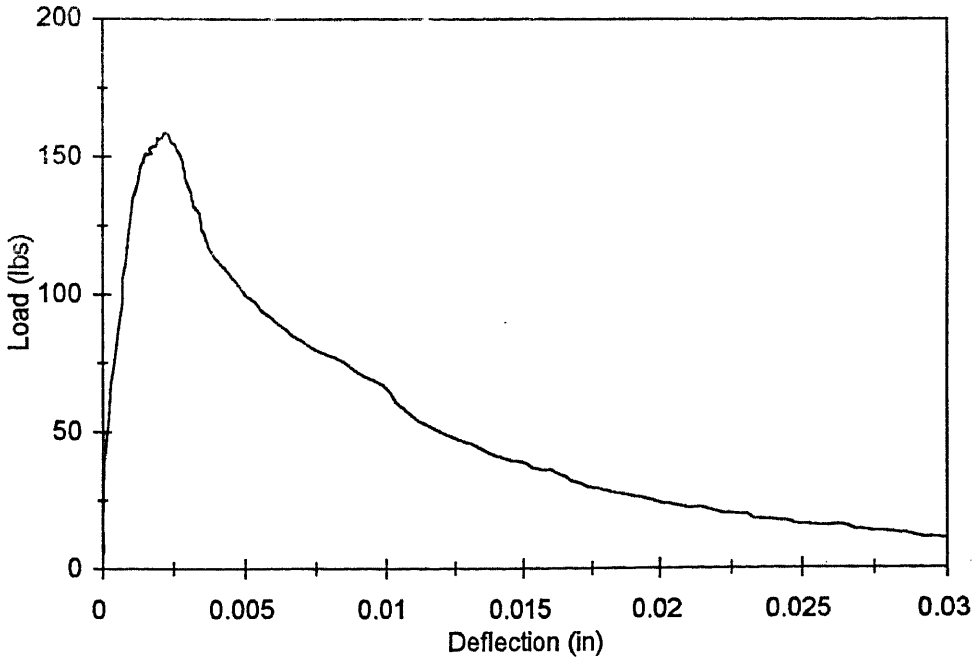

Figure A9b Load versus deflection for size A, curing at 23°C, age = 3.06 day

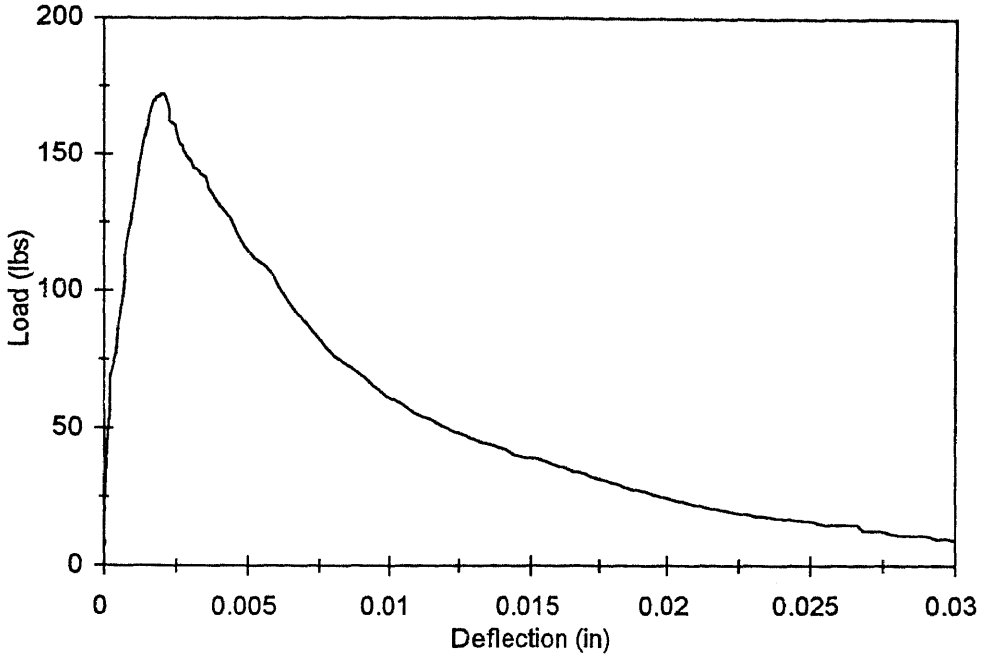

Figure A9c Load versus deflection for size A, curing at 23°C, age = 3.06 day

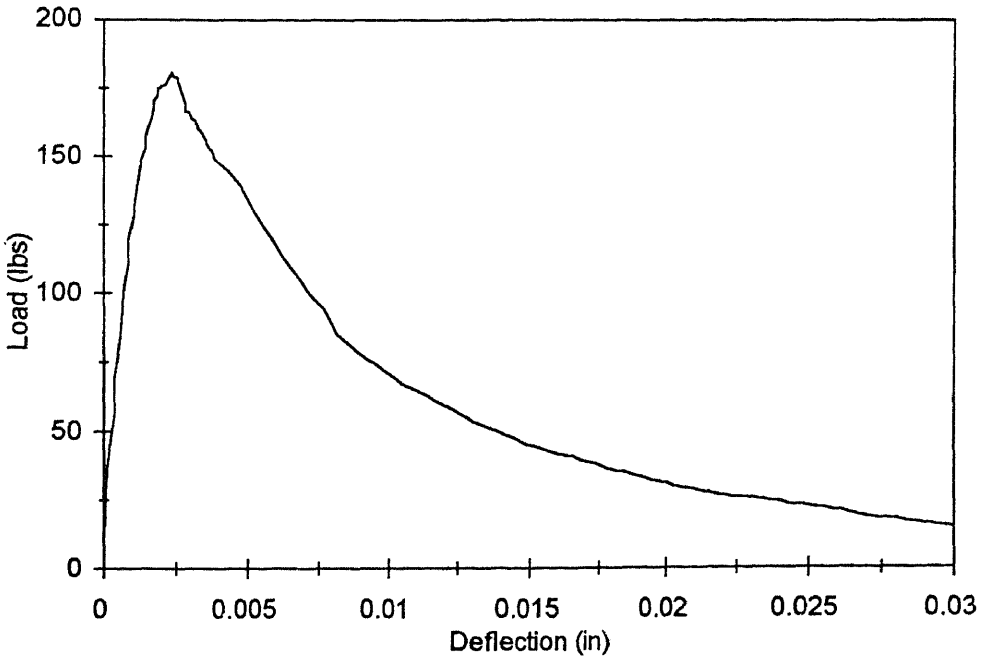

Figure A10a Load versus deflection for size A, curing at 23°C, age = 7.16 day

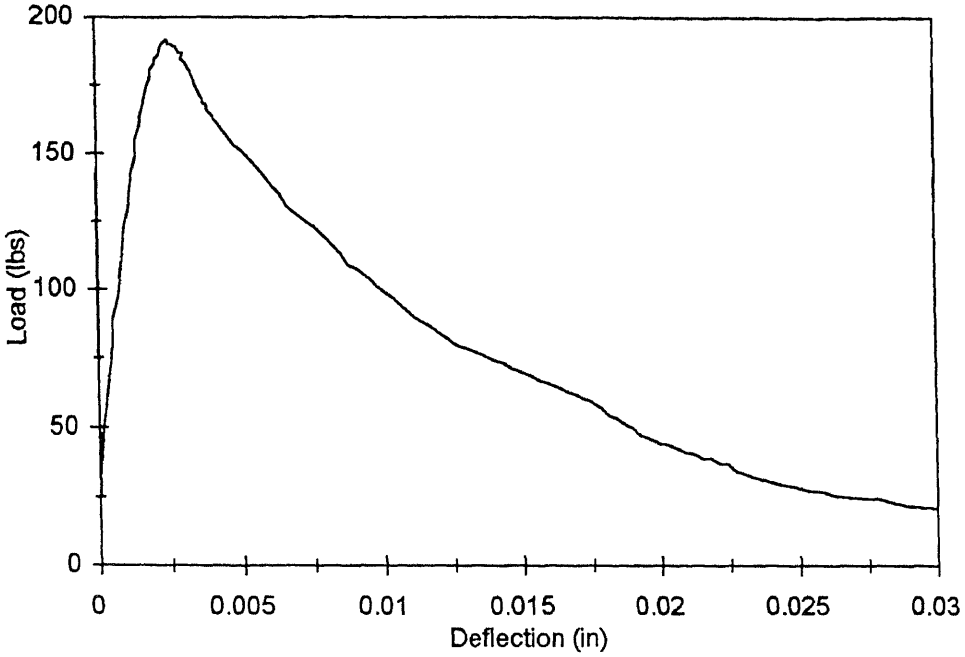

Figure A10b Load versus deflection for size A, curing at 23°C, age = 7.16 day

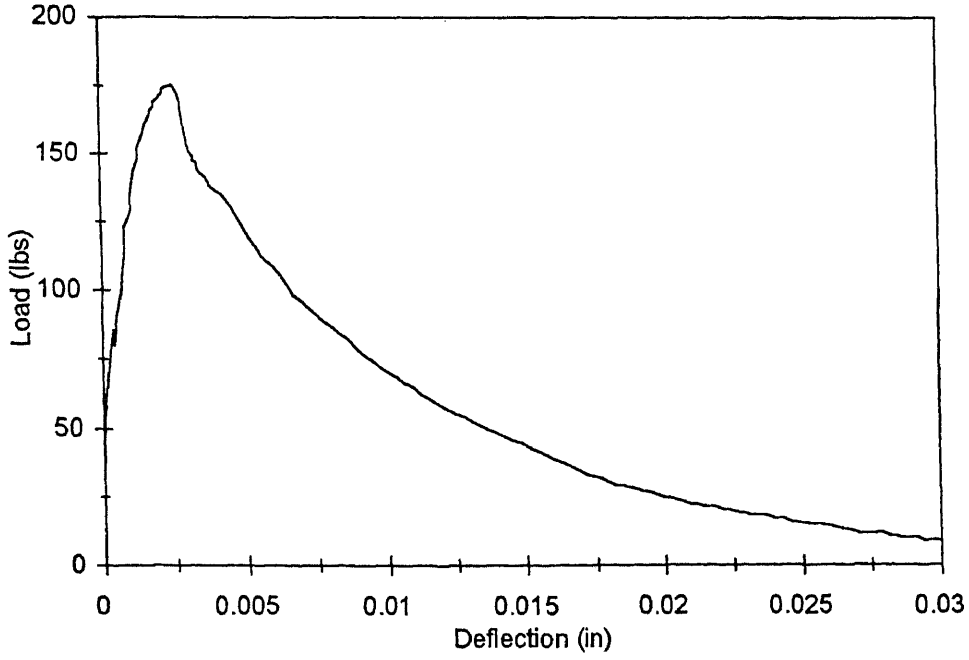

Figure A10c Load versus deflection for size A, curing at 23°C, age = 7.16 day

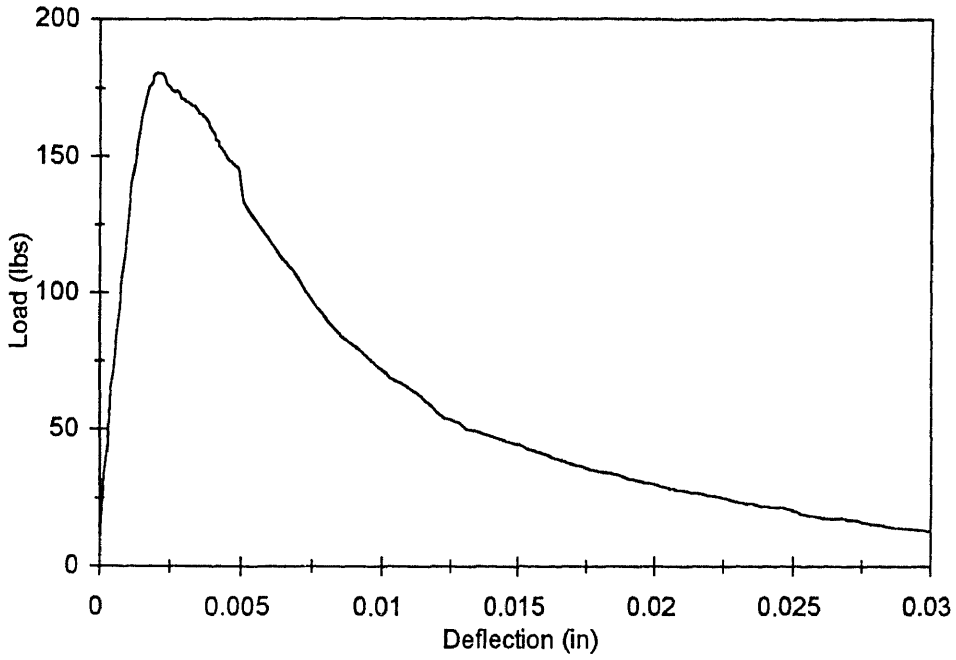

Figure A11a Load versus deflection for size A, curing at 23°C, age = 14.02 day

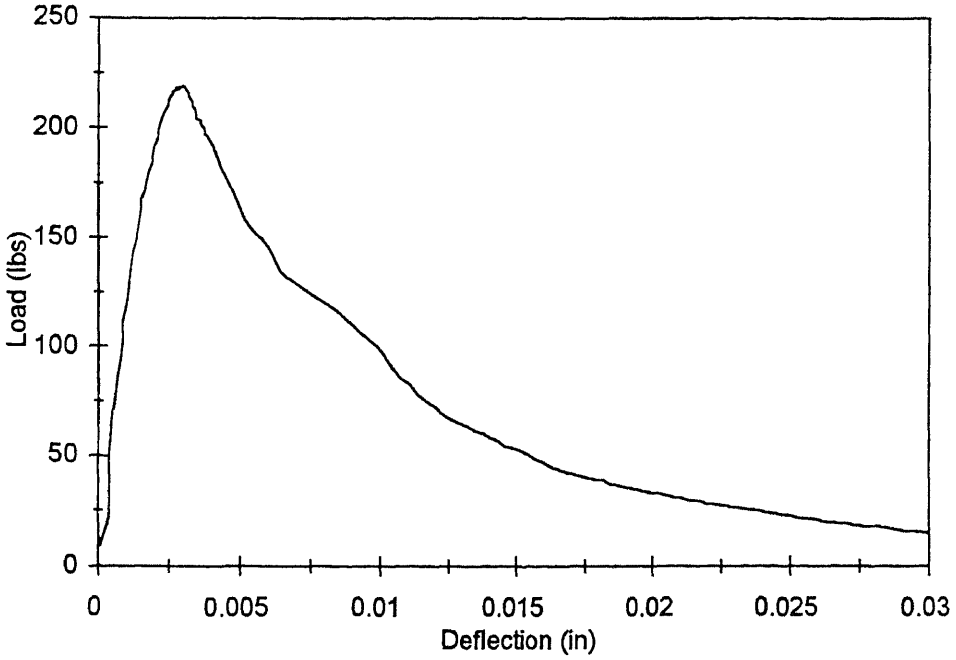

Figure A11b Load versus deflection for size A, curing at 23°C, age = 14.02 day

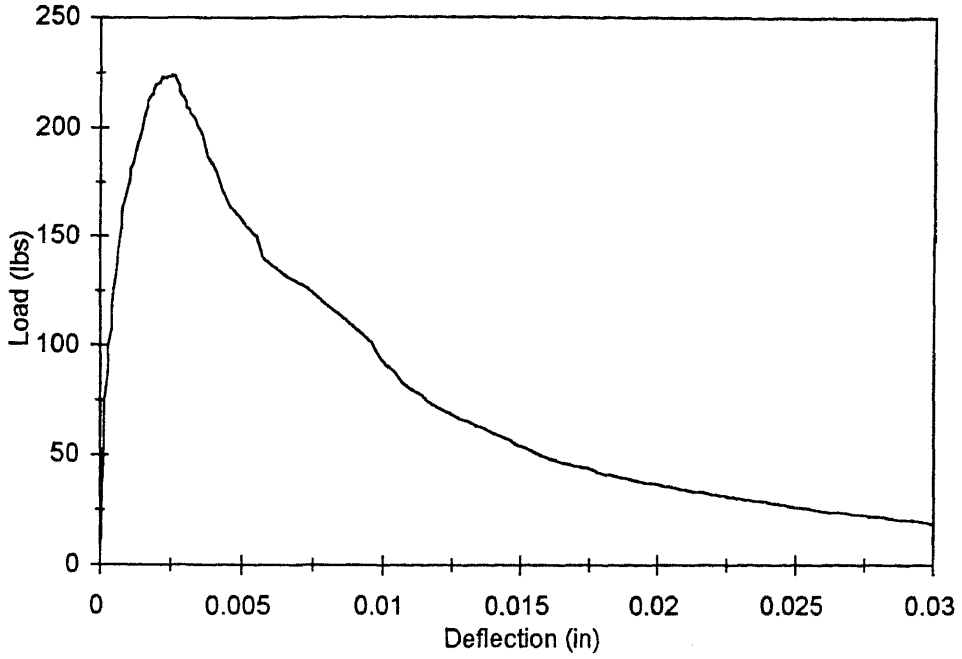

Figure A11c Load versus deflection for size A, curing at 23°C, age = 14.02 day

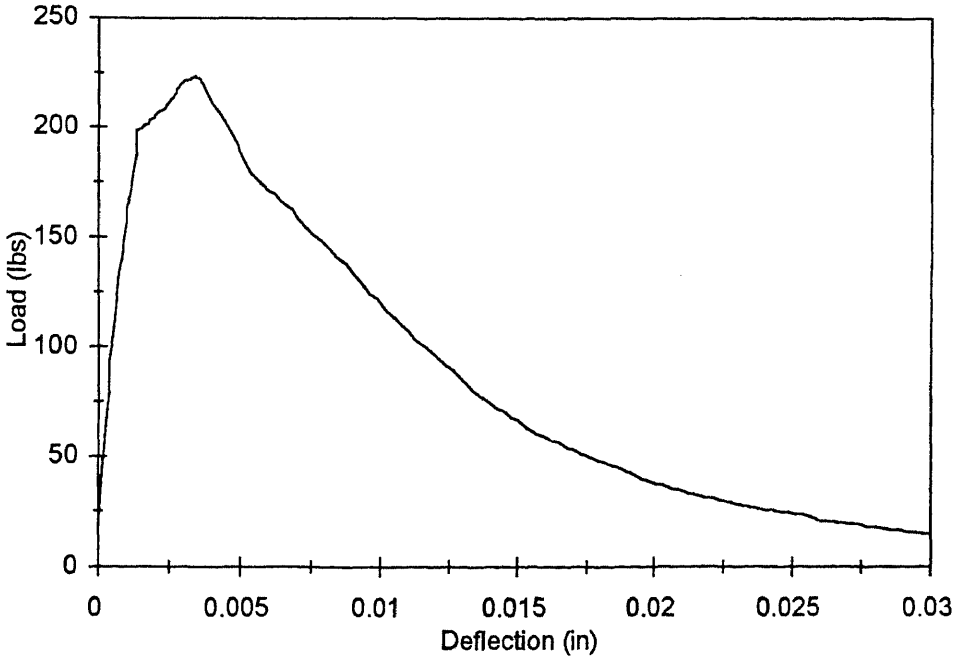

Figure A12a Load versus deflection for size A, curing at 23°C, age = 28.03 days

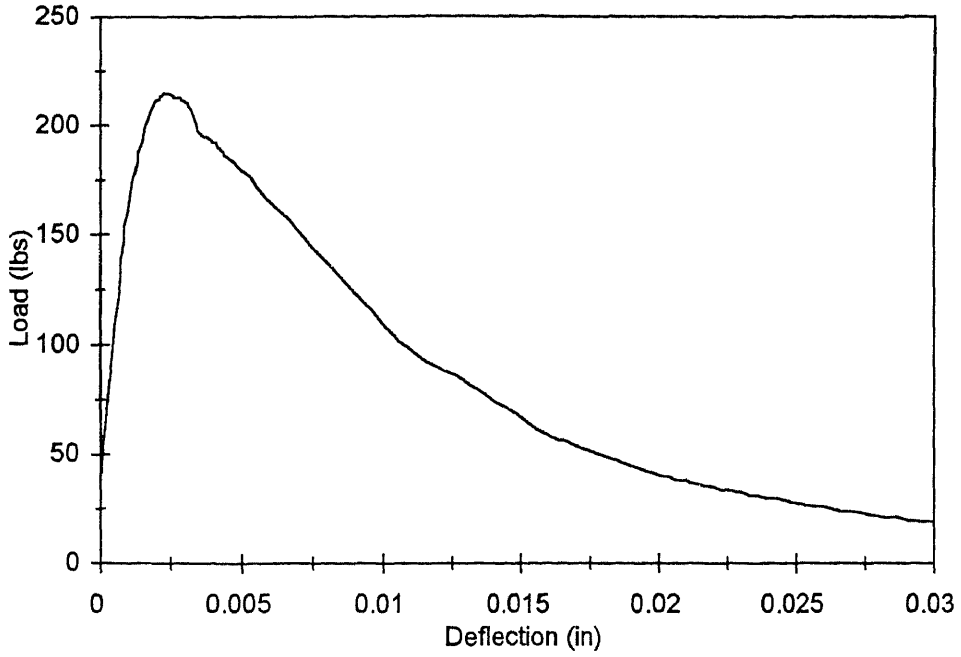

Figure A12b Load versus deflection for size A, curing at 23°C, age = 28.03 days

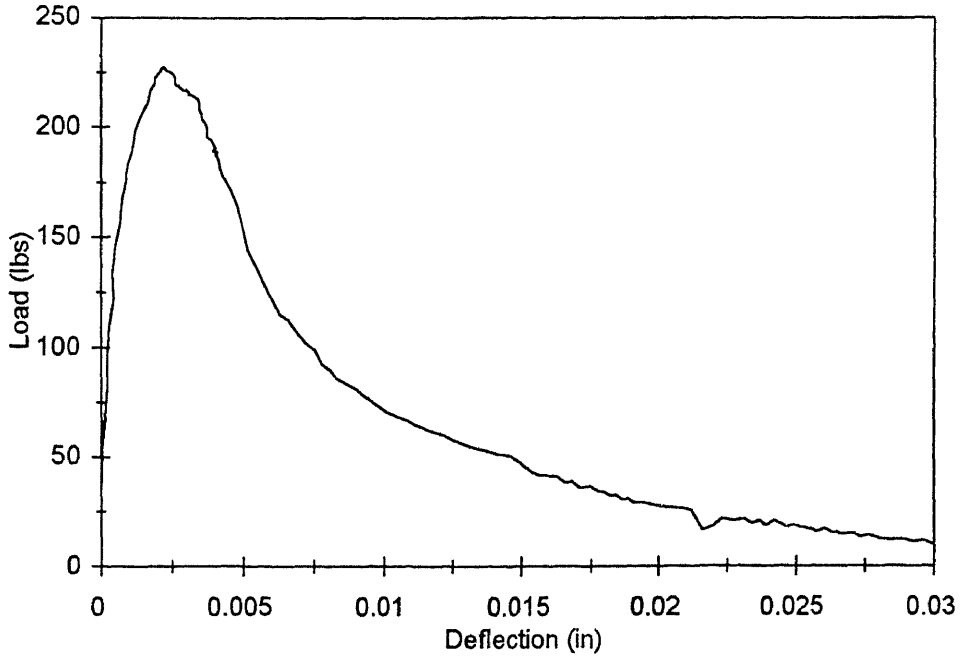

Figure A12c Load versus deflection for size A, curing at 23°C, age = 28.03 days

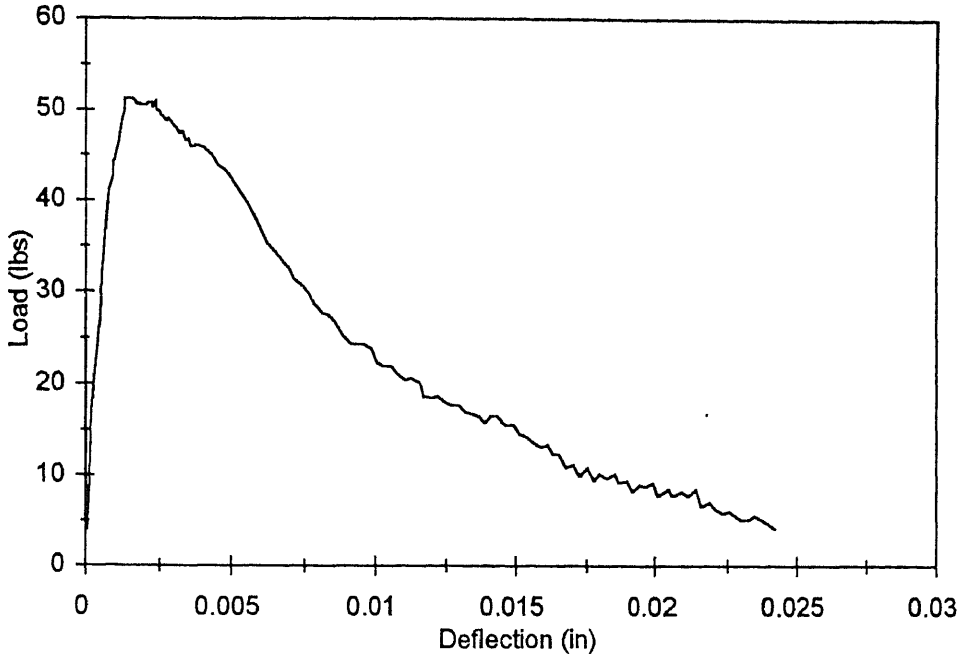

Figure A13a Load versus deflection for size A, curing at 35°C, age = 0.35 day

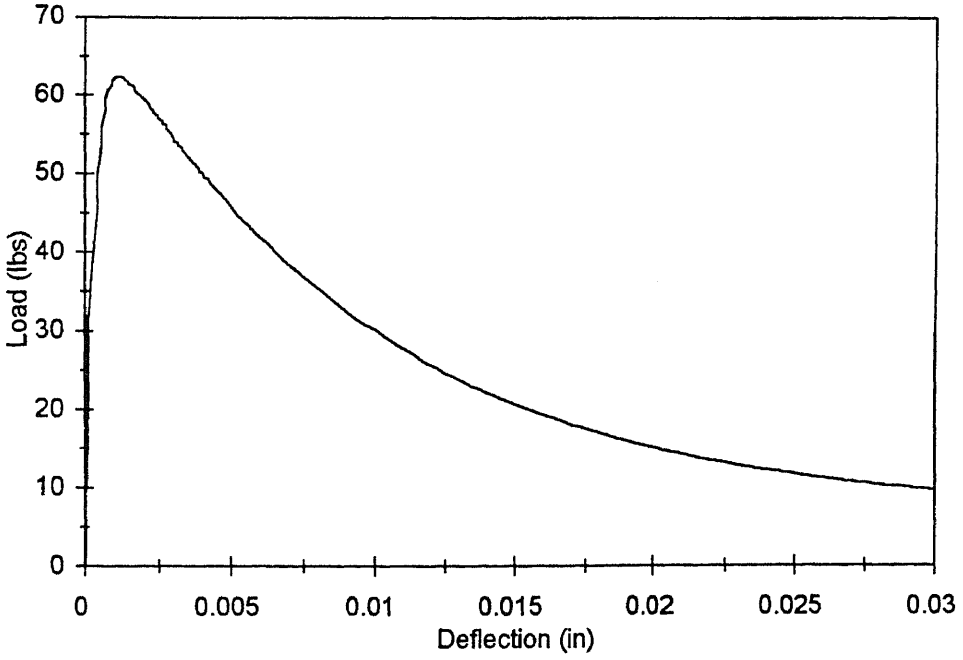

Figure A13b Load versus deflection for size A, curing at 35°C, age = 0.35 day

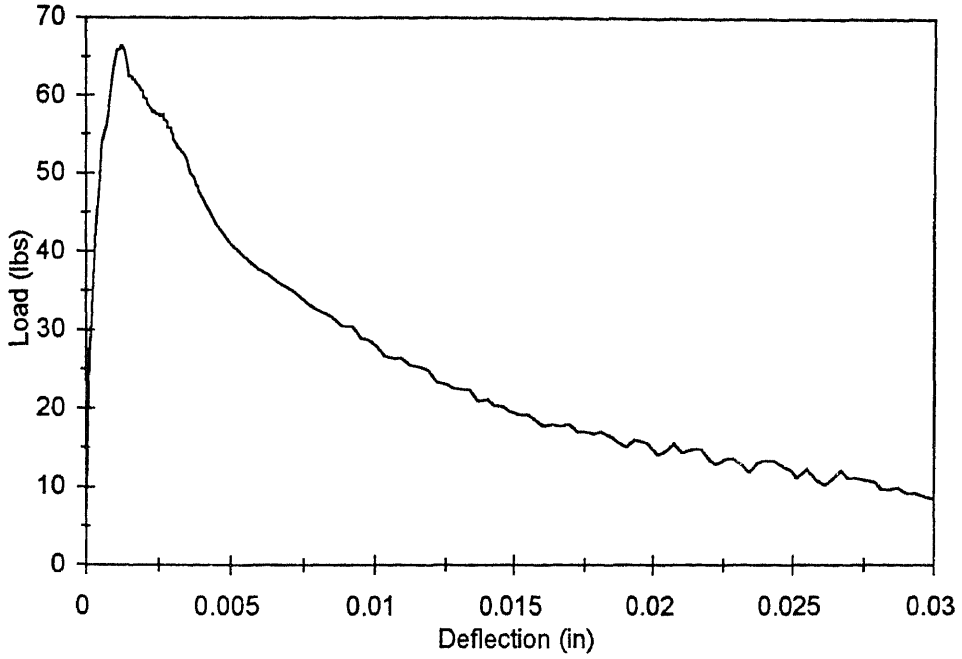

Figure A13c Load versus deflection for size A, curing at 35°C, age = 0.35 day

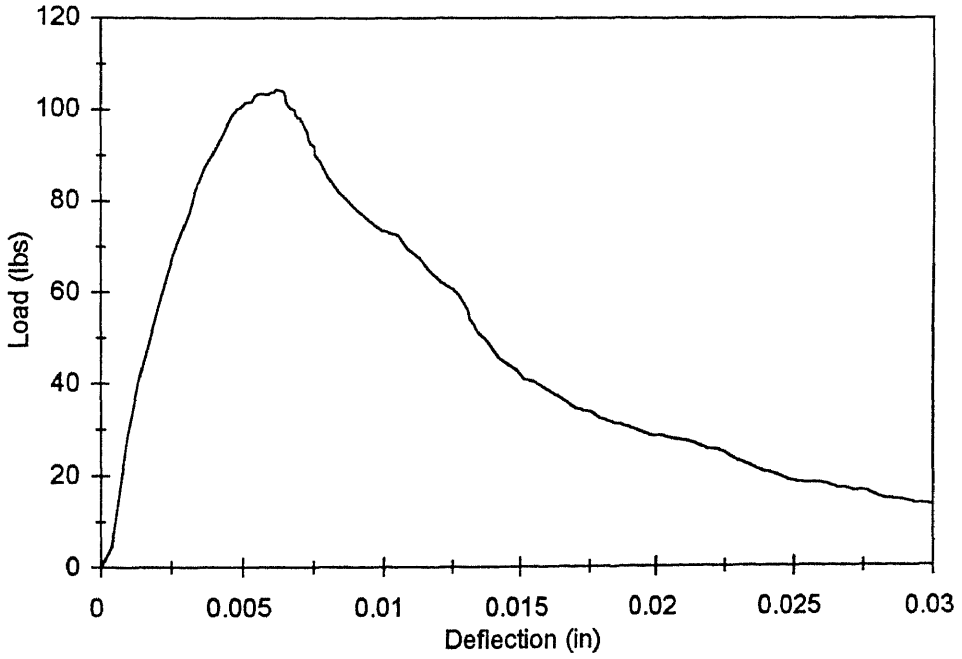

Figure A14a Load versus deflection for size A, curing at 35°C, age = 0.5625 day

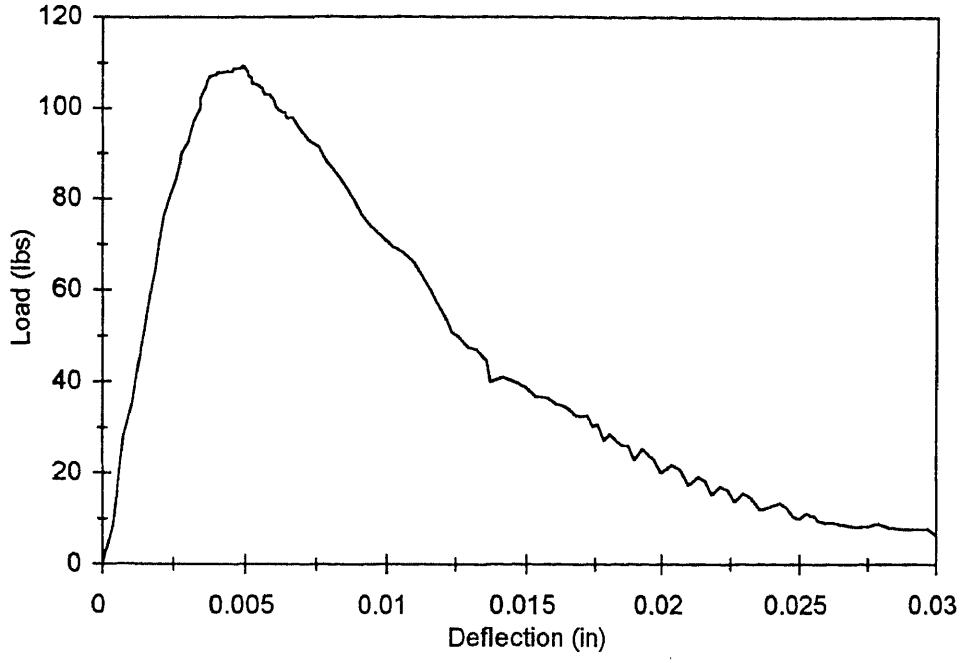

Figure A14b Load versus deflection for size A, curing at 35°C, age = 0.5625 day

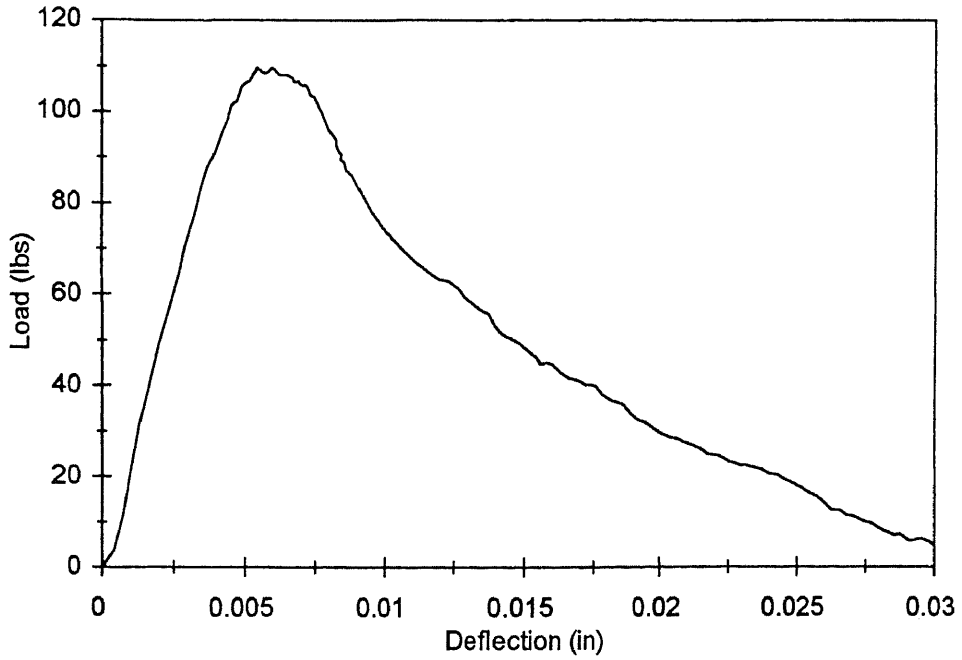

Figure A14c Load versus deflection for size A, curing at 35°C, age = 0.5625 day

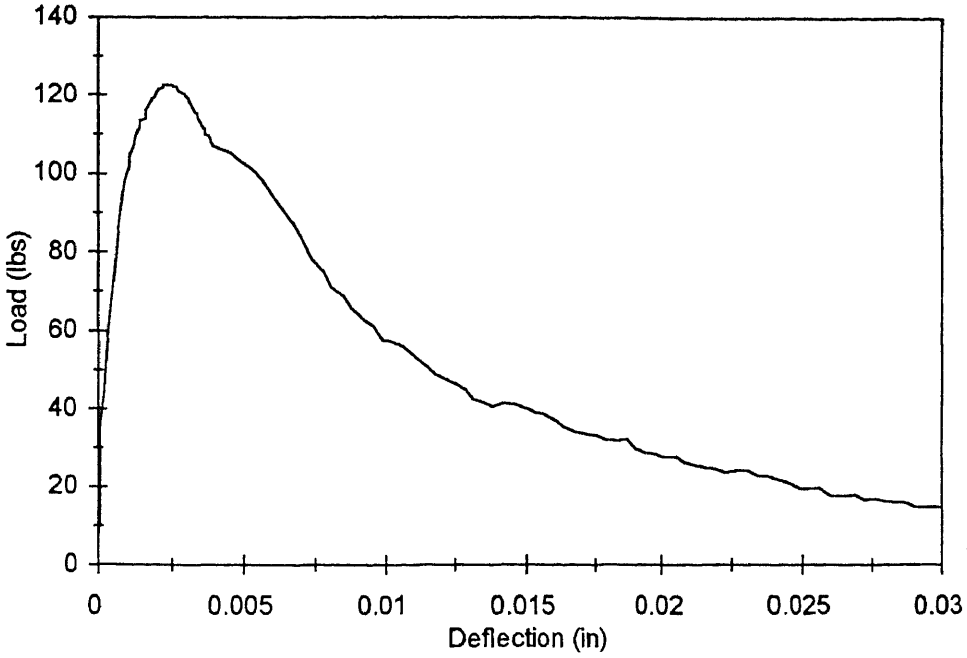

Figure A15a Load versus deflection for size A, curing at 35°C, age = 1.07 days

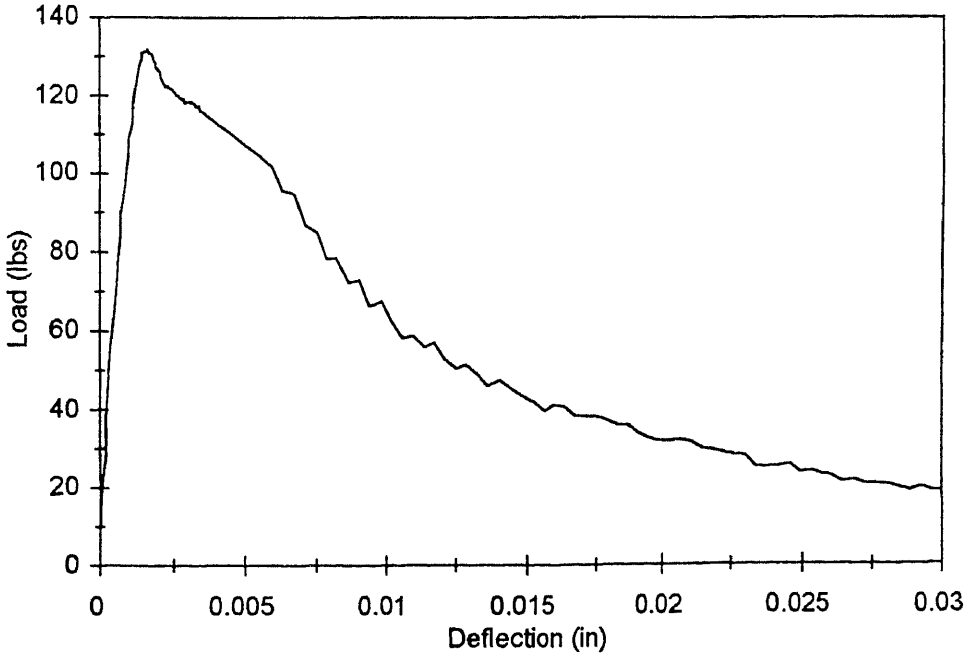

Figure A15b Load versus deflection for size A, curing at 35°C, age = 1.07 days

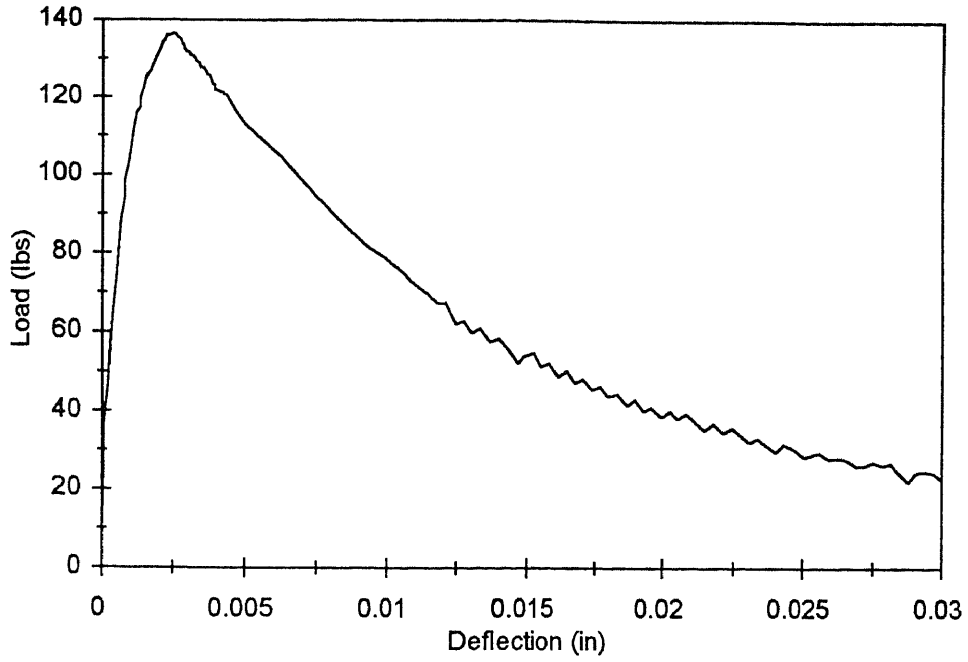

Figure A15c Load versus deflection for size A, curing at 35°C, age = 1.07 days

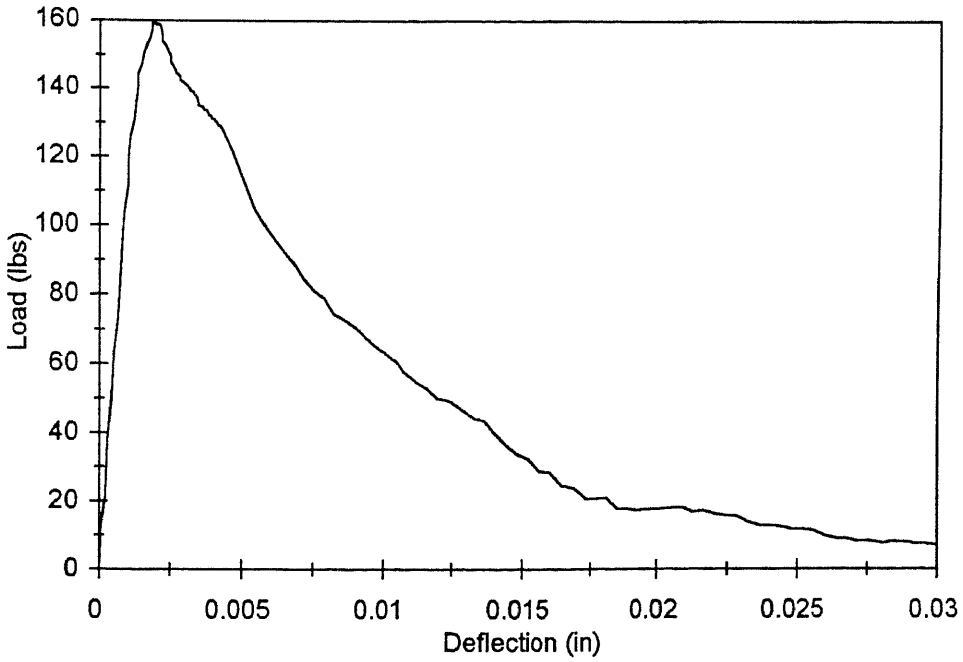

Figure A16a Load versus deflection for size A, curing at 35°C, age = 4.03 days

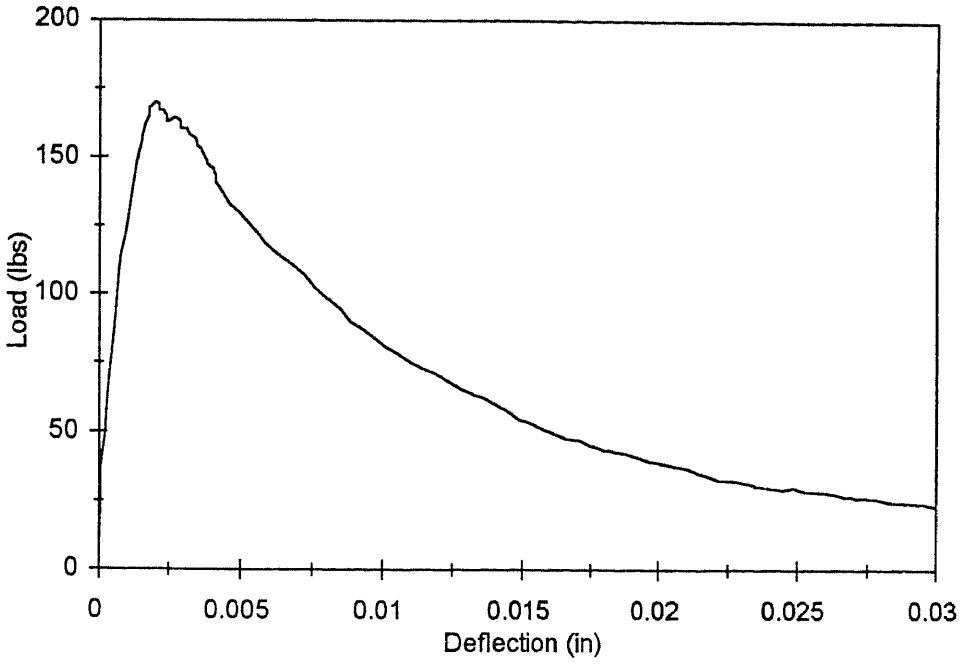

Figure A16b Load versus deflection for size A, curing at 35°C, age = 4.03 days

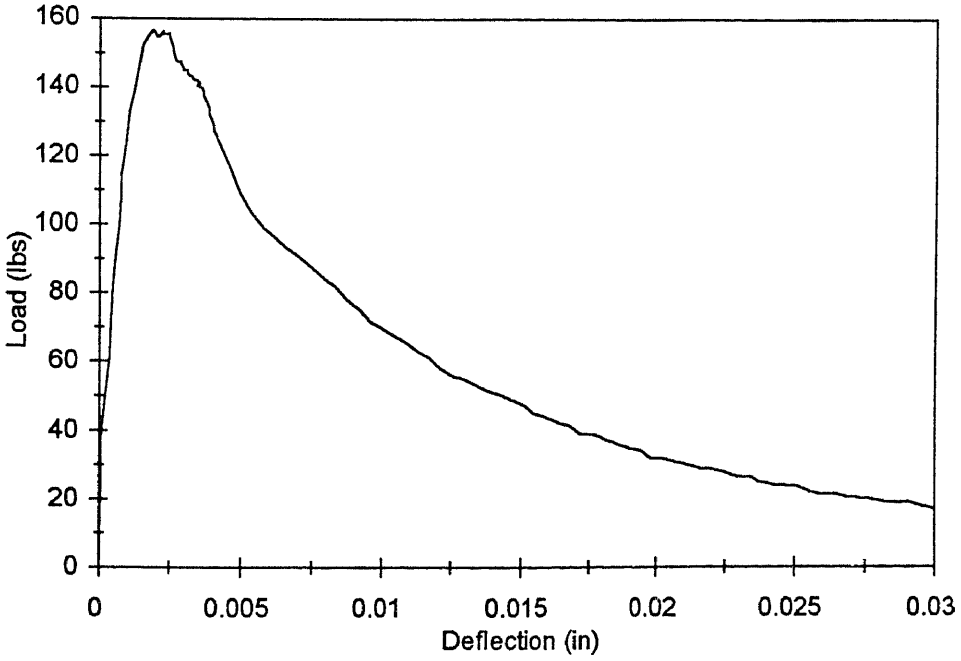

Figure A16c Load versus deflection for size A, curing at 35°C, age = 4.03 days

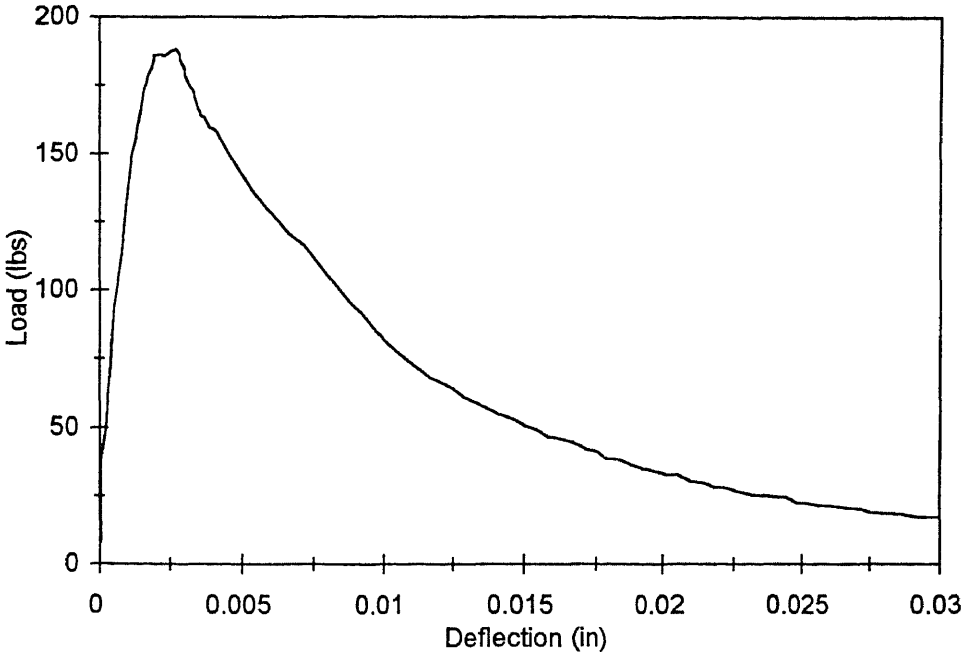

Figure A17a Load versus deflection for size A, curing at 35°C, age = 9.5 days

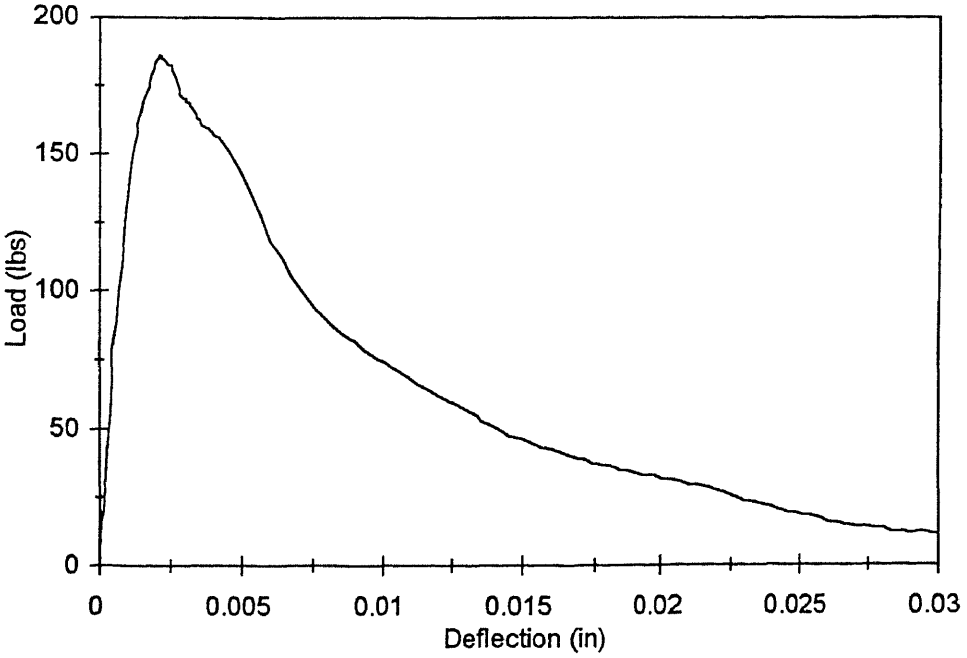

Figure A17b Load versus deflection for size A, curing at 35°C, age = 9.5 days

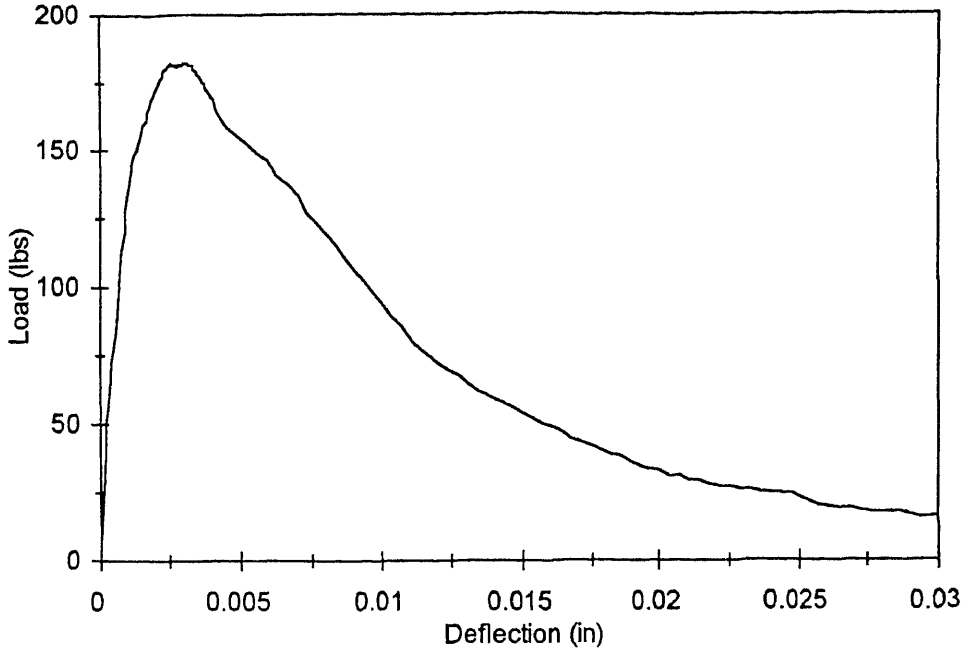

Figure A17c Load versus deflection for size A, curing at 35°C, age = 9.5 days

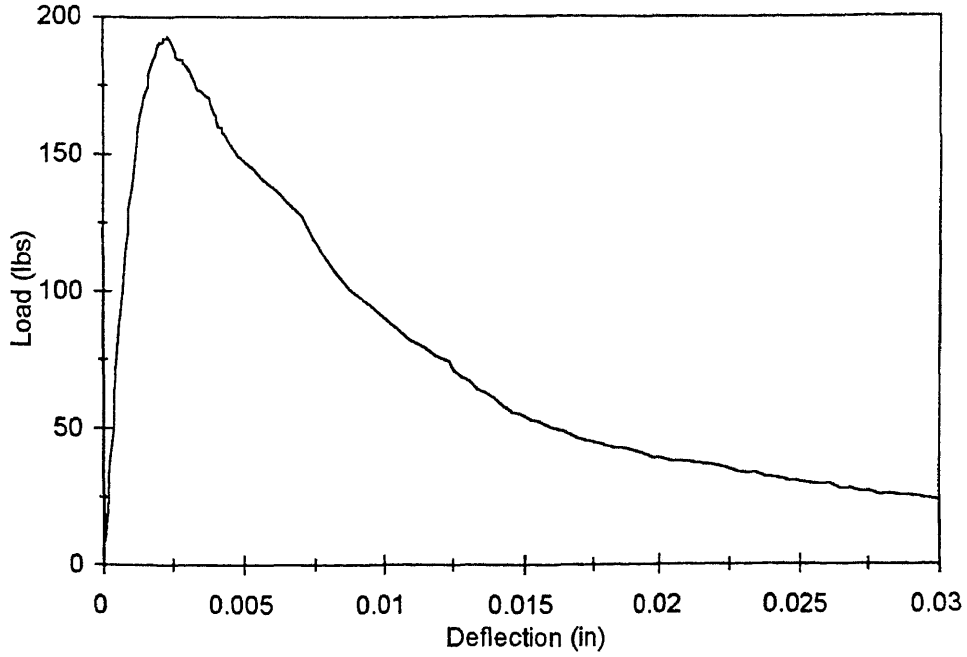

Figure A18a Load versus deflection for size A, curing at 35°C, age = 20.02 days

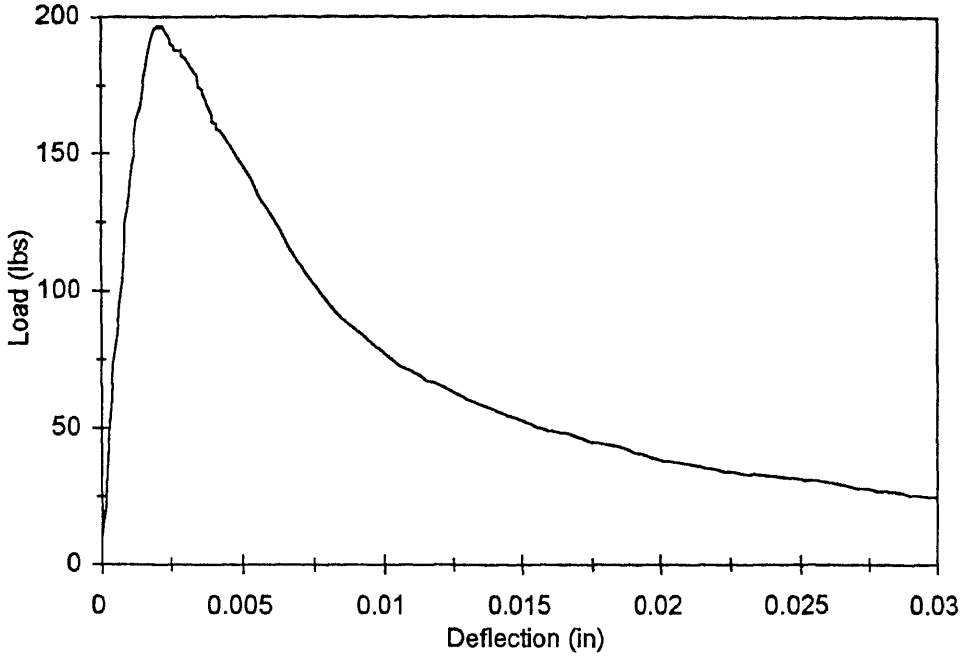

Figure A18b Load versus deflection for size A, curing at 35°C, age = 20.02 days

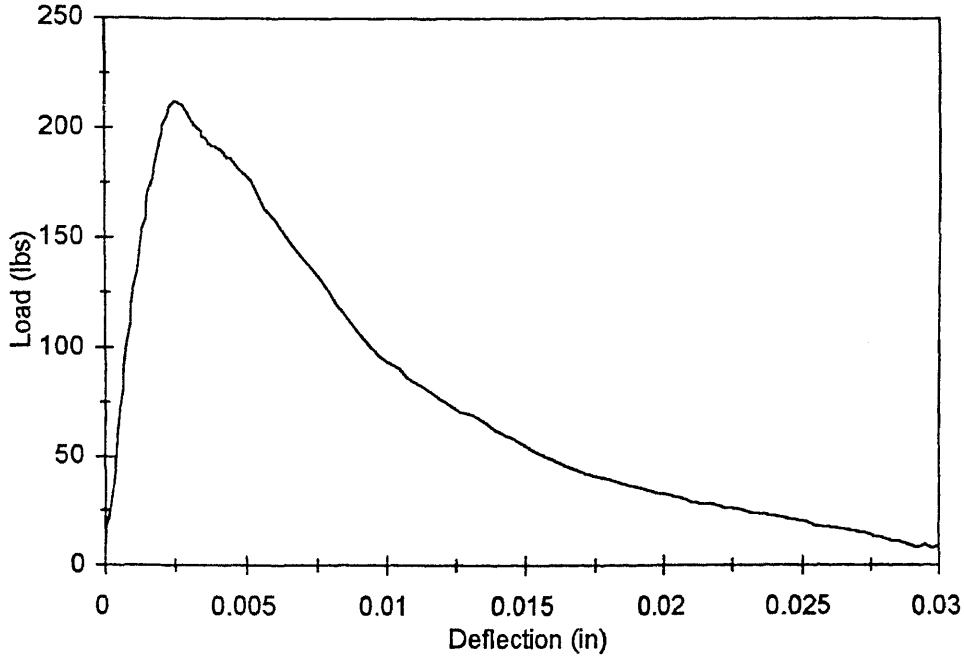

Figure A18c Load versus deflection for size A, curing at 35°C, age = 20.02 days

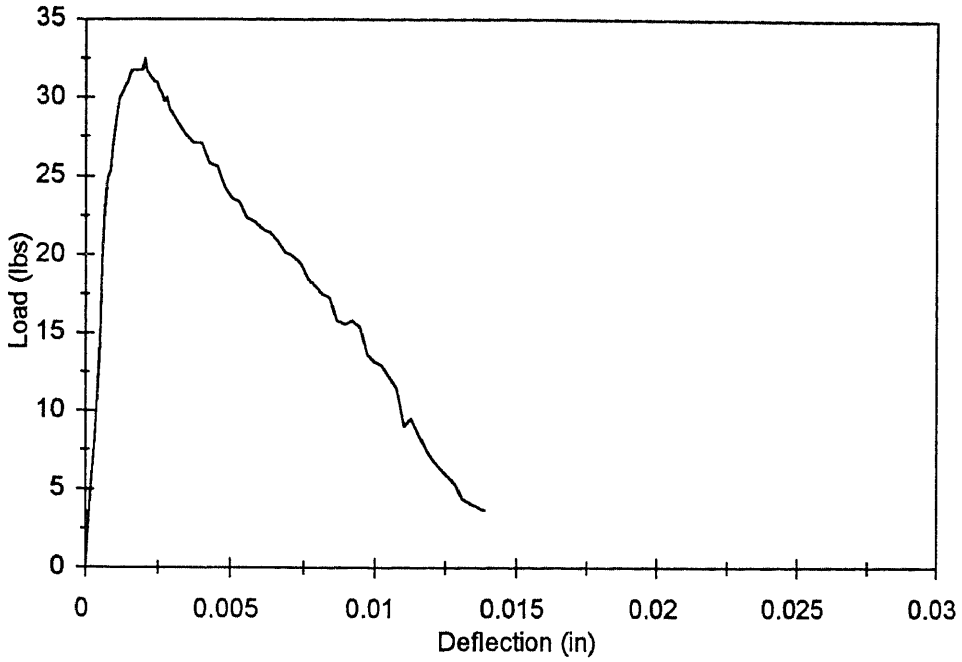

Figure B1a Load versus deflection for size B, curing at 14°C, age = 1 day

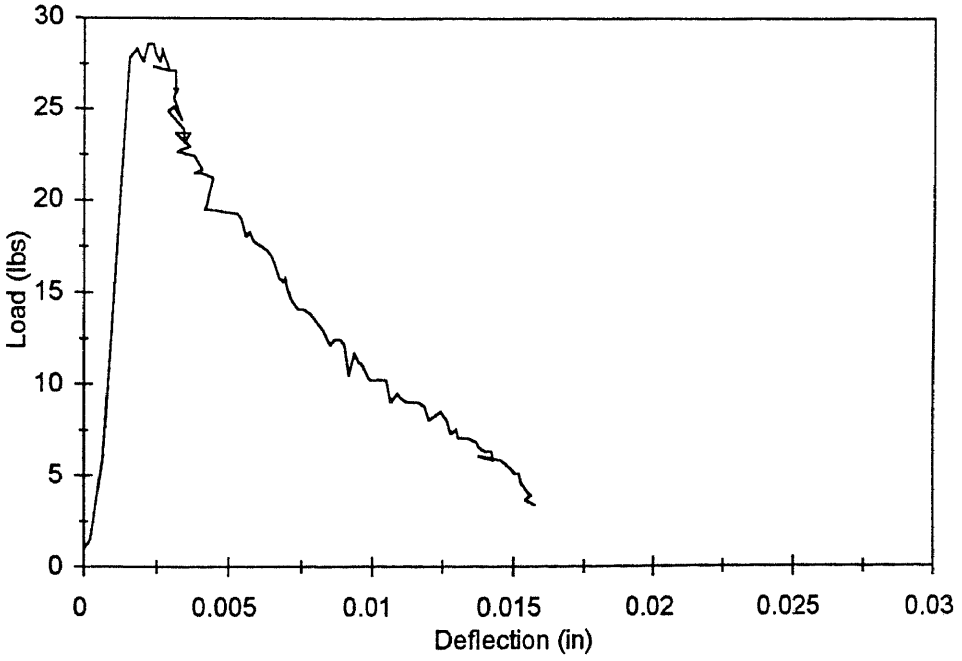

Figure B1b Load versus deflection for size B, curing at 14°C, age = 1 day

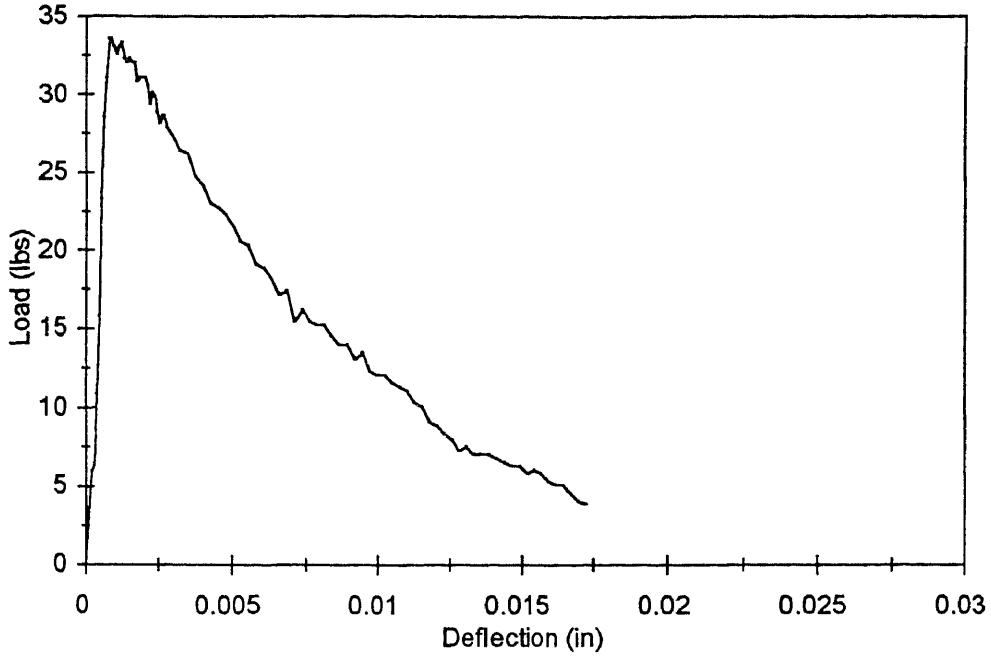

Figure B1c Load versus deflection for size B, curing at 14°C, age = 1 day

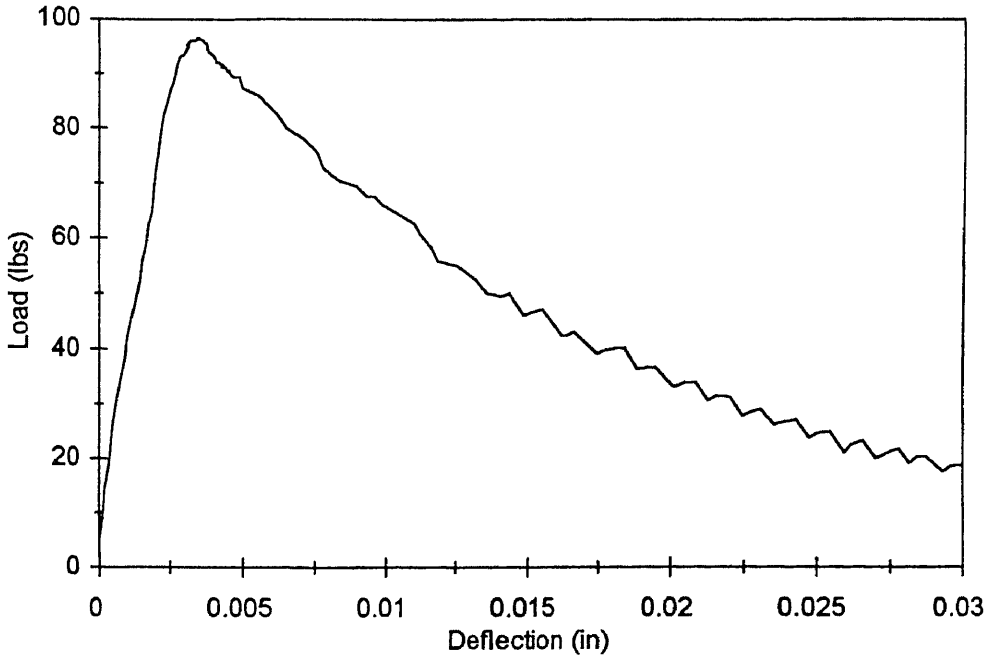

Figure B2a Load versus deflection for size B, curing at 14°C, age = 2 days

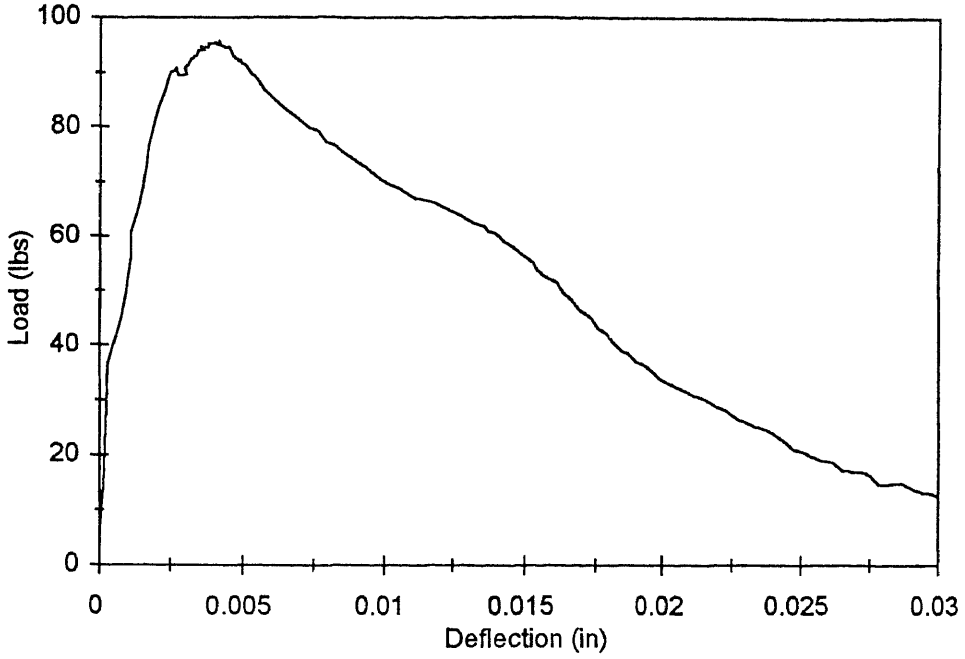

Figure B2b Load versus deflection for size B, curing at 14°C, age = 2 days

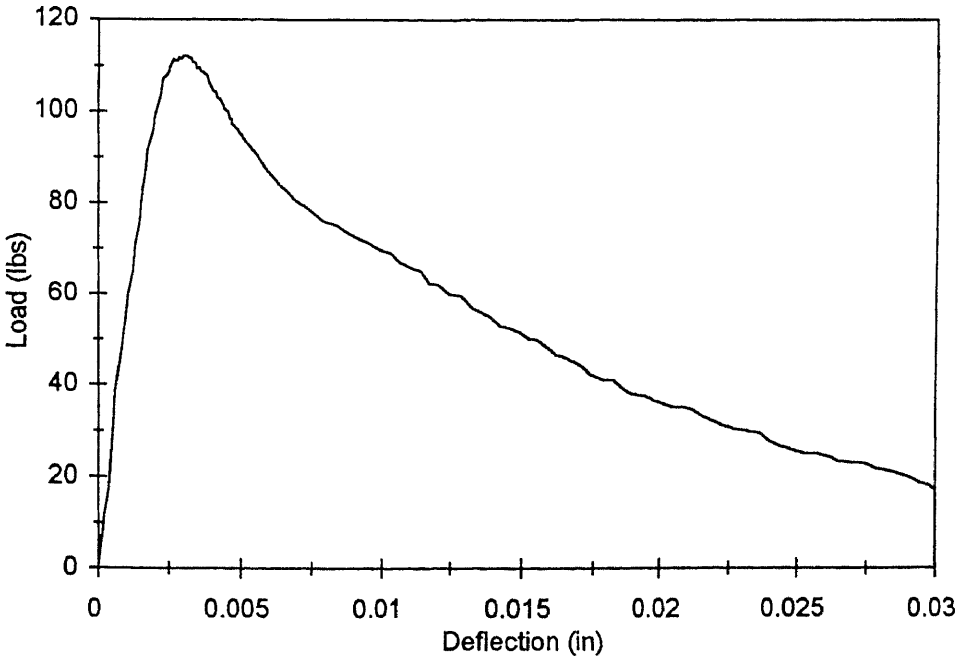

Figure B2c Load versus deflection for size B, curing at 14°C, age = 2 days

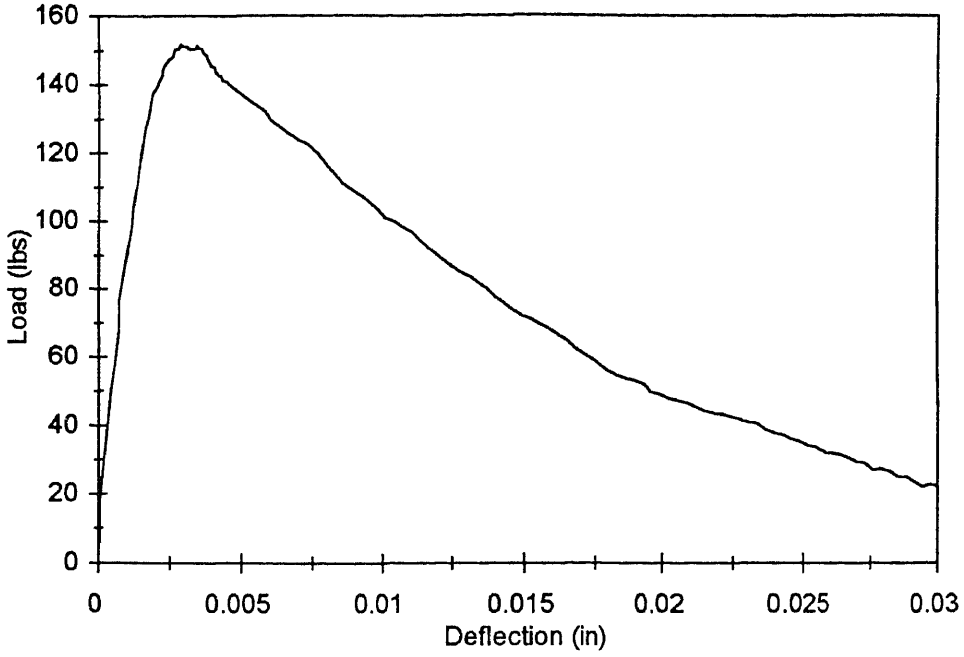

Figure B3a Load versus deflection for size B, curing at 14°C, age = 4.1 day

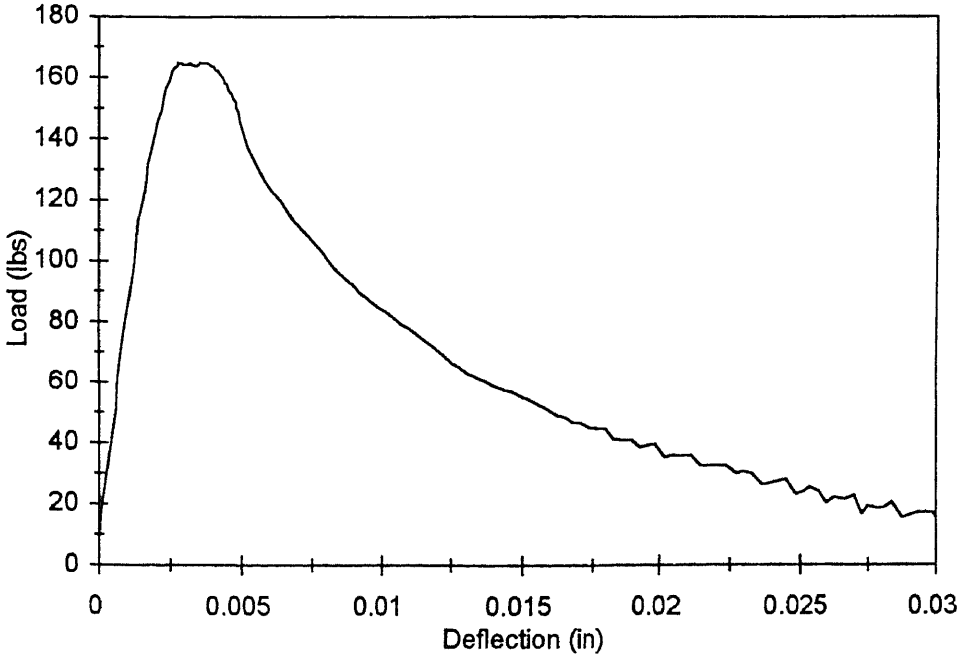

Figure B3b Load versus deflection for size B, curing at 14°C, age = 4.1 day

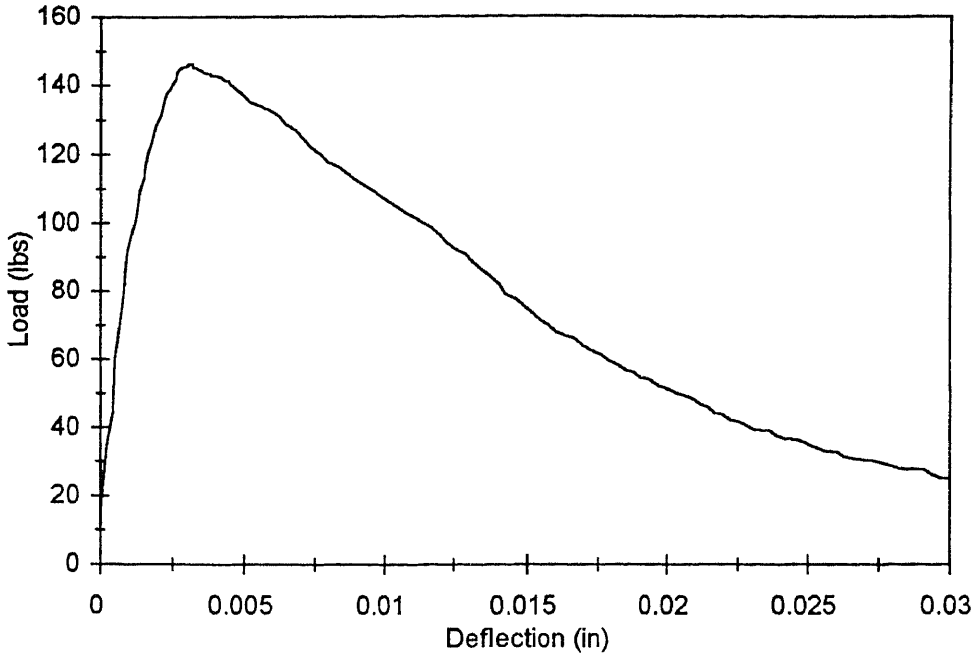

Figure B3c Load versus deflection for size B, curing at 14°C, age = 4.1 day

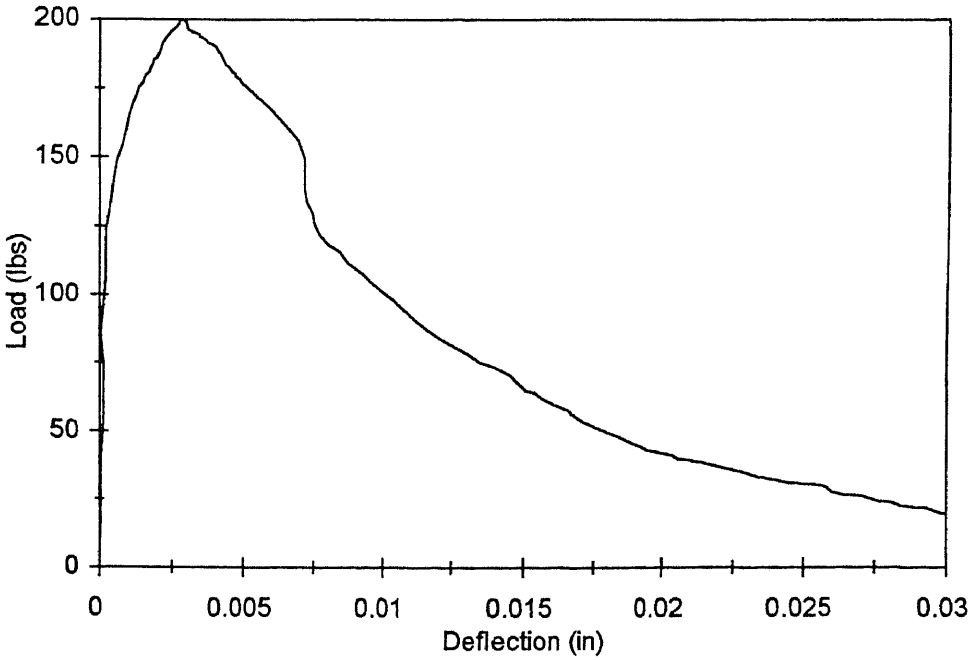

Figure B4a Load versus deflection for size B, curing at 14°C, age = 10 day

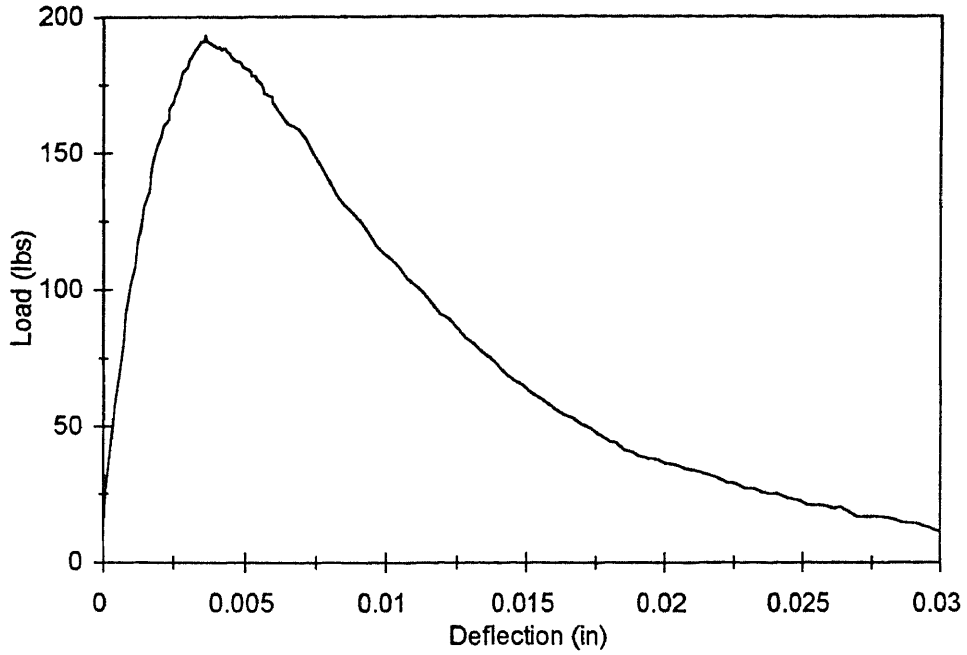

Figure B4b Load versus deflection for size B, curing at 14°C, age = 10 day

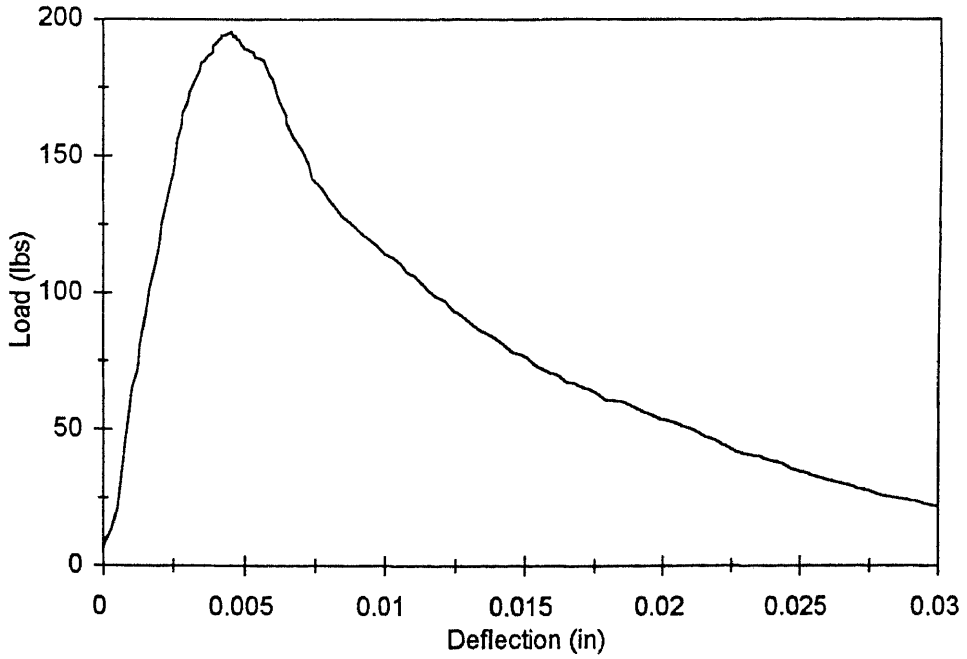

Figure B4c Load versus deflection for size B, curing at 14°C, age = 10 day

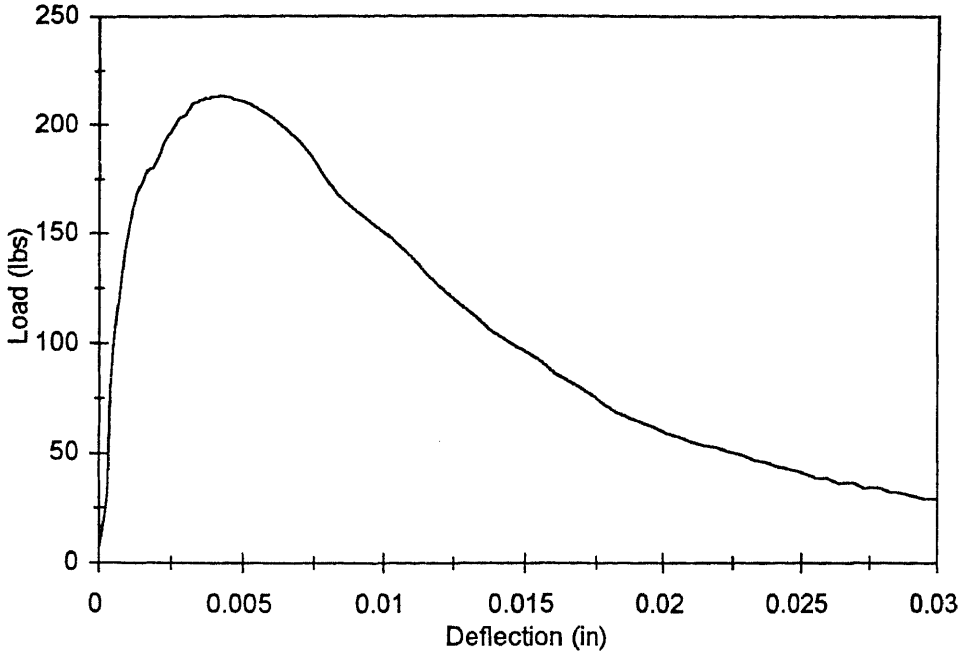

Figure B5a Load versus deflection for size B, curing at 14°C, age = 22 days

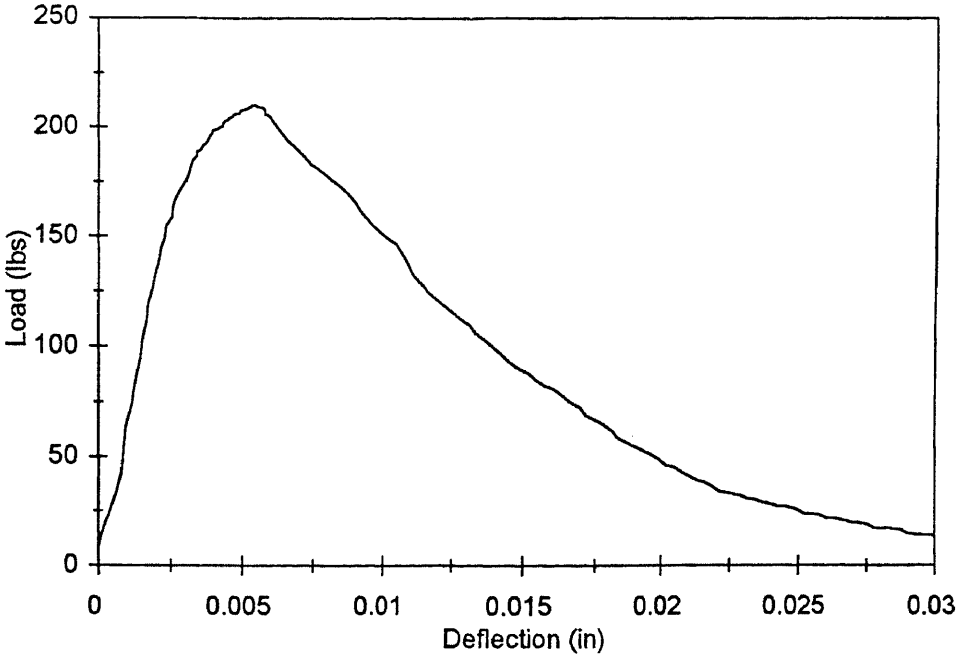

Figure B5b Load versus deflection for size B, curing at 14°C, age = 22 days

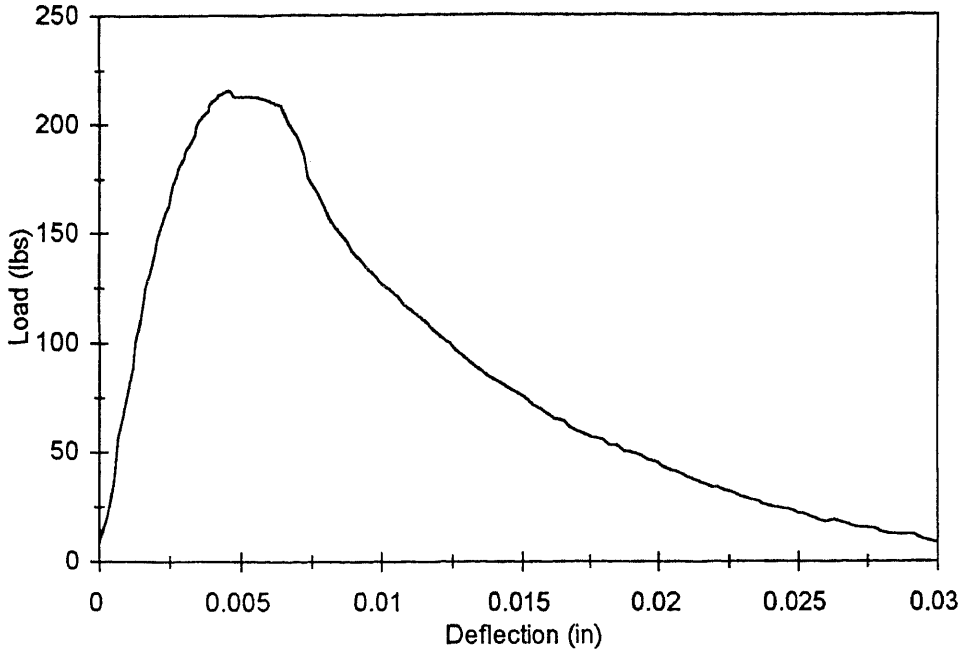

Figure B5c Load versus deflection for size B, curing at 14°C, age = 22 days

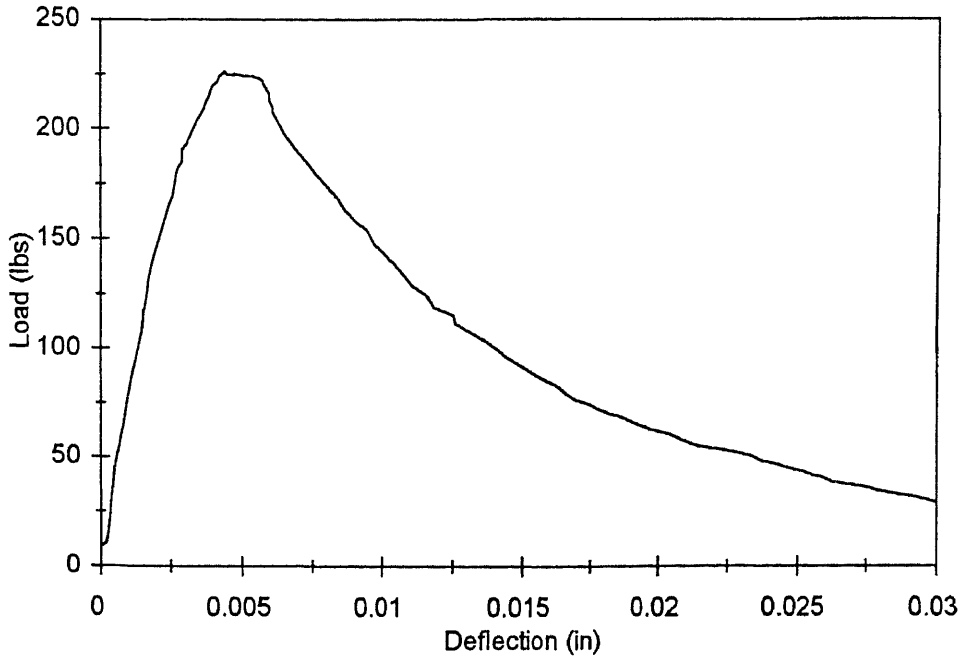

Figure B6a Load versus deflection for size B, curing at 14°C, age = 38 days

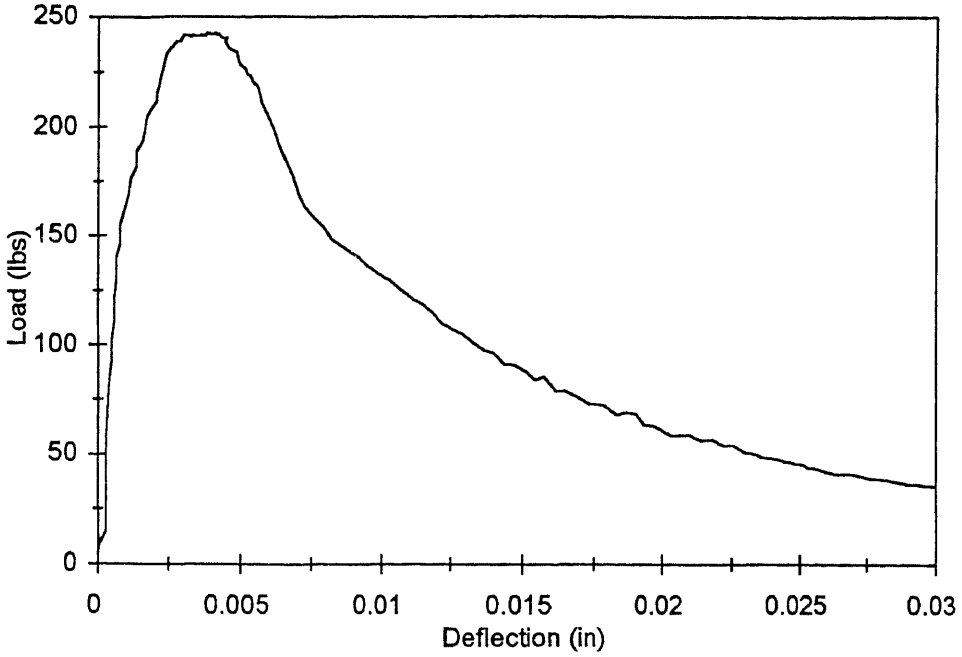

Figure B6b Load versus deflection for size B, curing at 14°C, age = 38 days

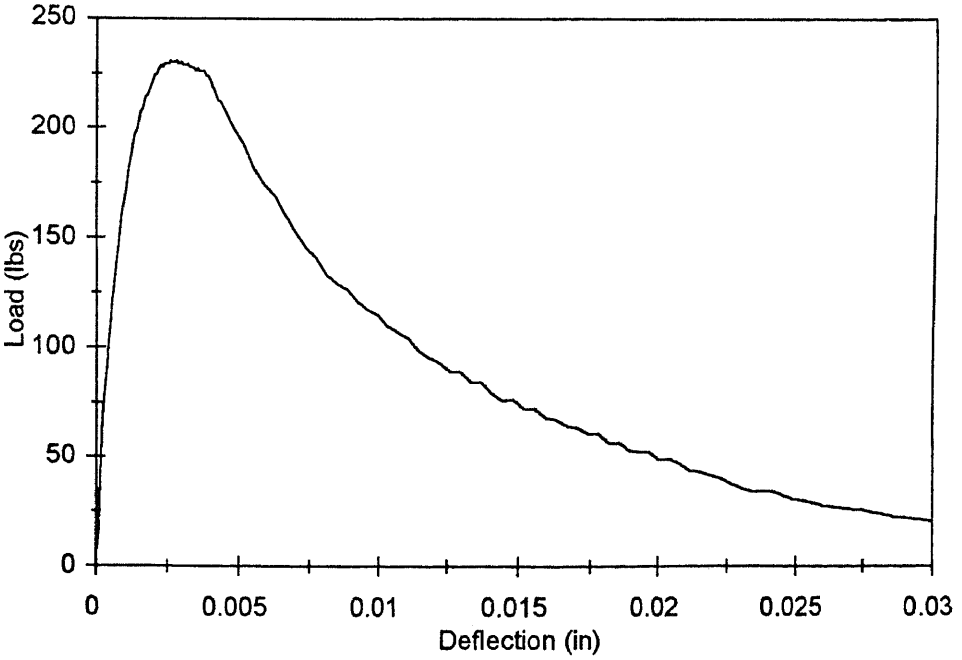

Figure B6c Load versus deflection for size B, curing at 14°C, age = 38 days

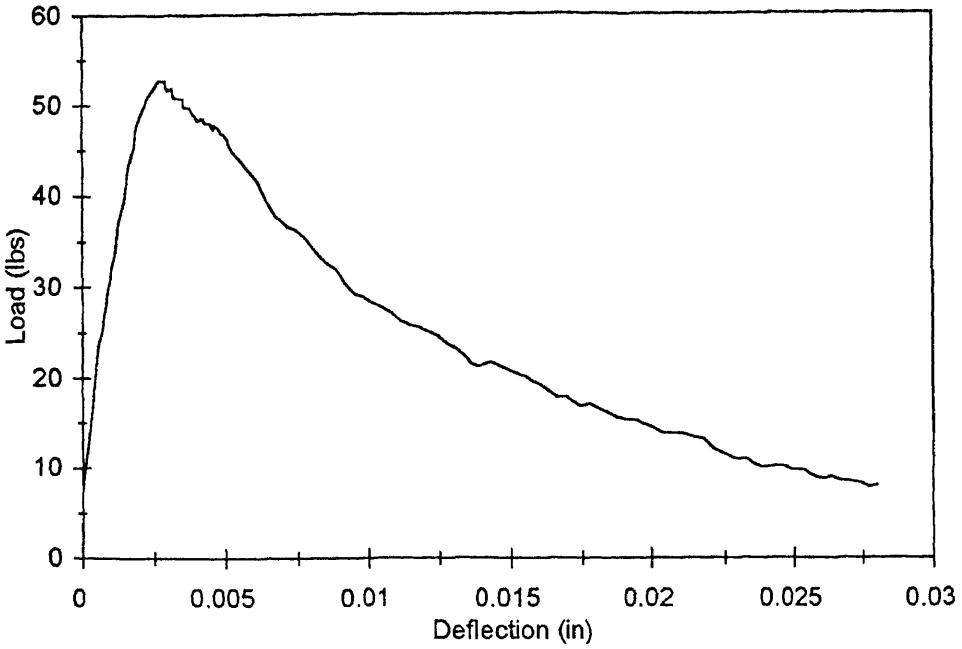

Figure B7a Load versus deflection for size B(T= 23°C, t = 0.56 day)

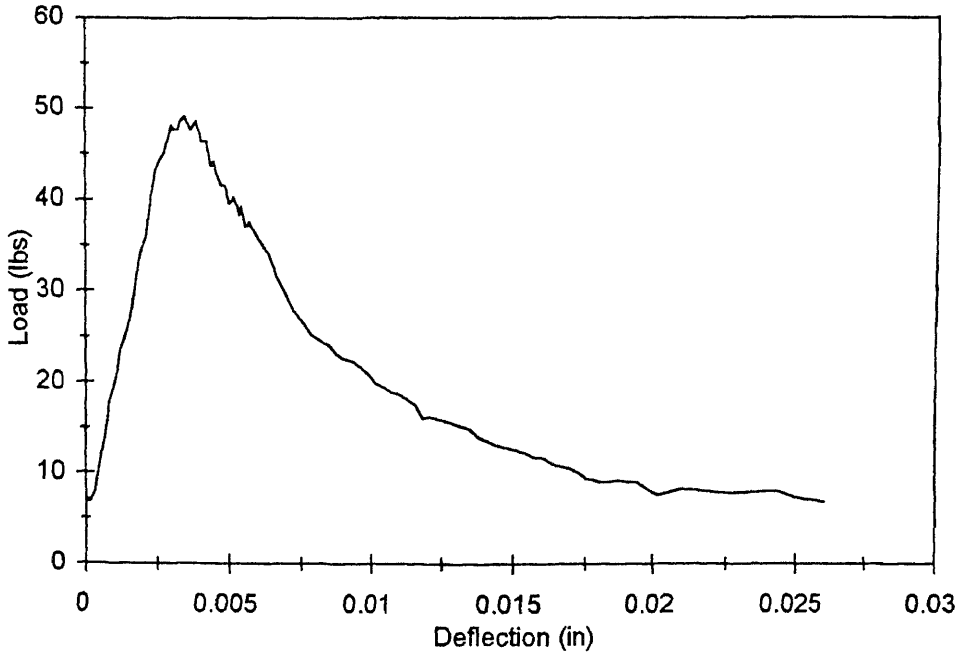

Figure B7b Load versus deflection for size B(T= 23°C, t = 0.56 day)

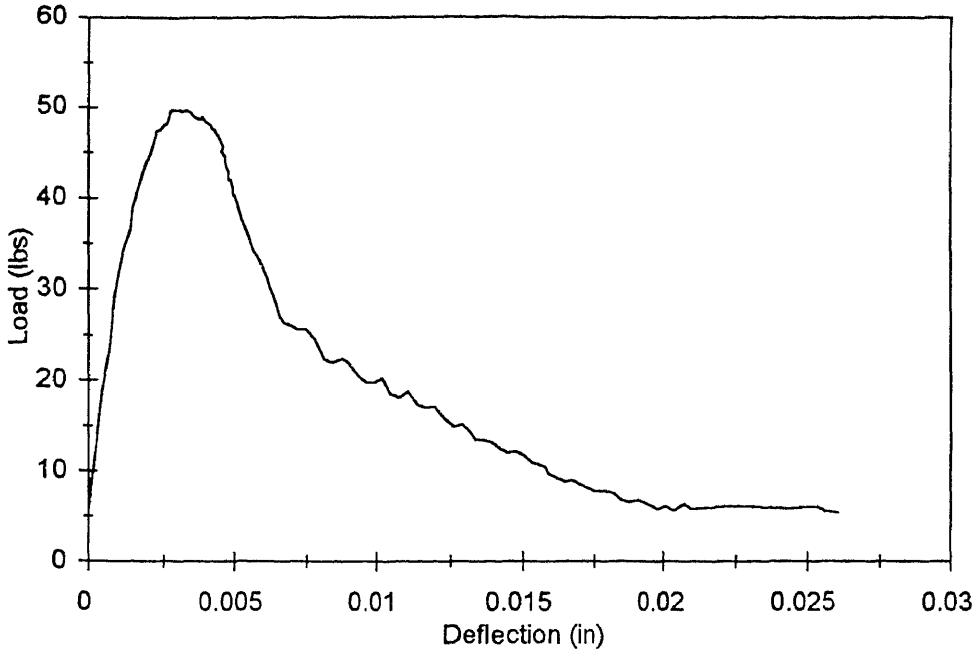

Figure B7c Load versus deflection for size B(T= 23°C, t = 0.56 day)

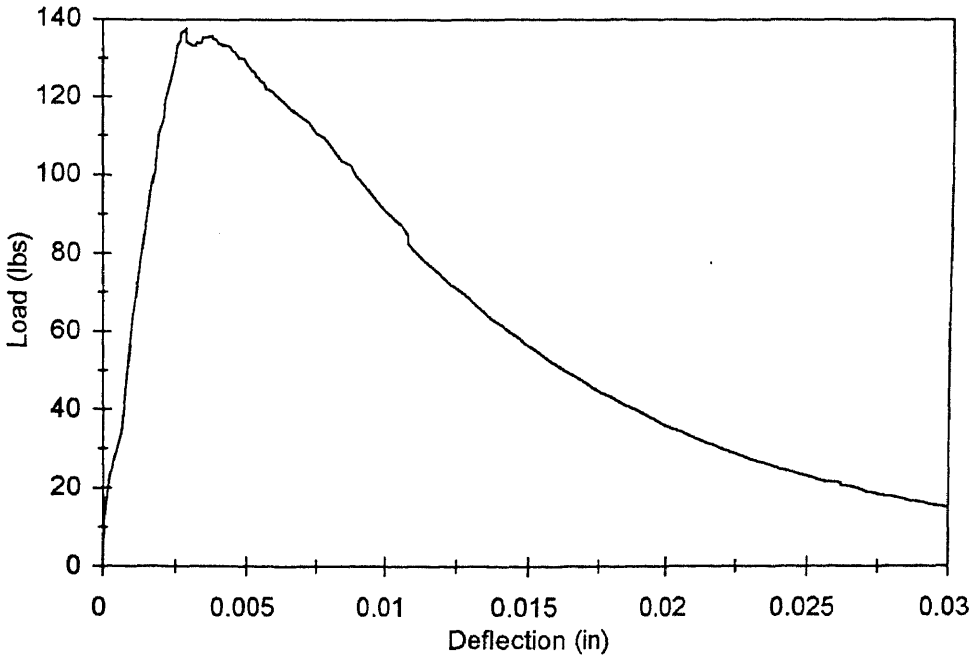

Figure B8a Load versus deflection for size B(T= 23°C, t = 1.21 days)

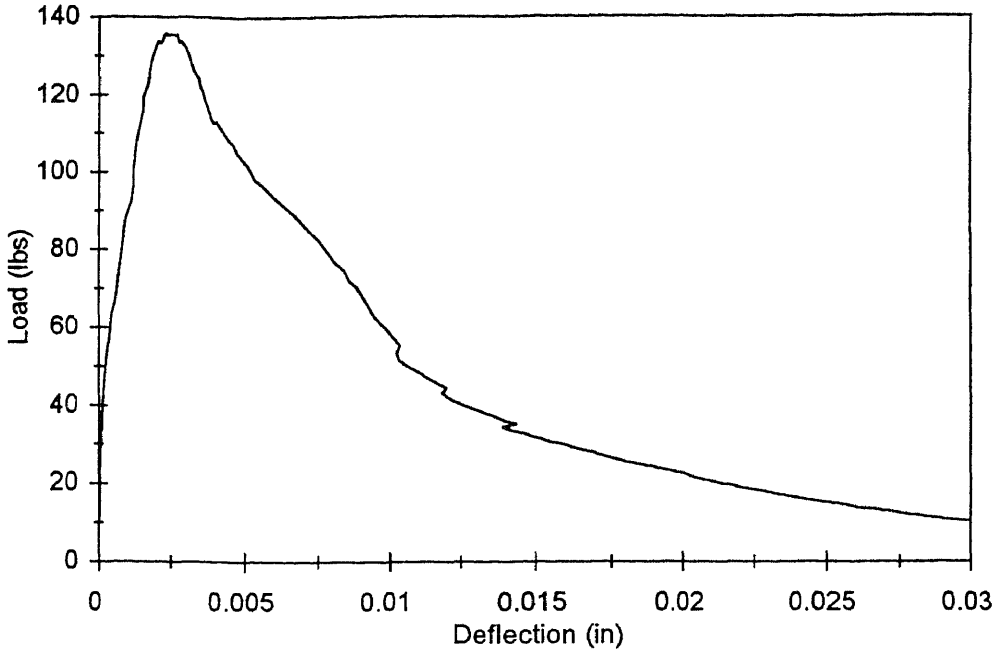

Figure B8b Load versus deflection for size B(T= 23°C, t = 1.21 day)

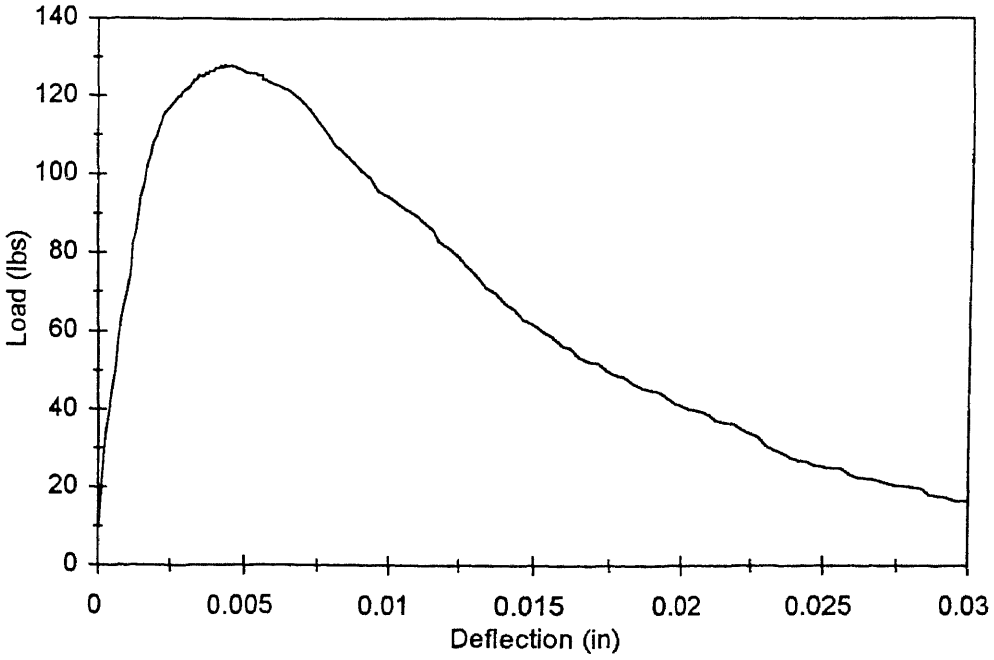

Figure B8c Load versus deflection for size B(T= 23°C, t = 1.21 day)

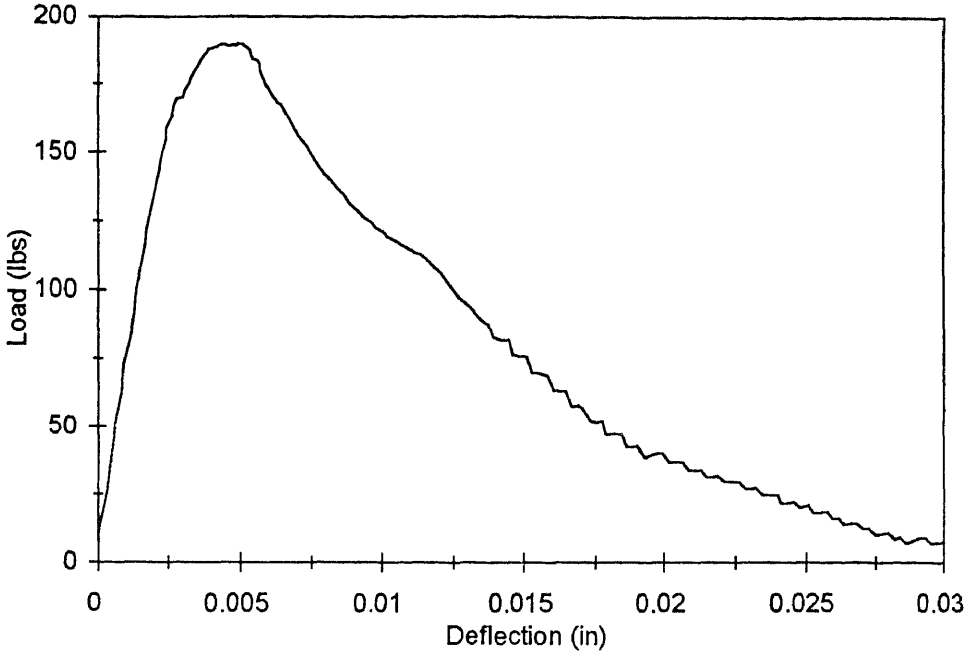

Figure B9a Load versus deflection for size B(T= 23°C, t = 2.95 days)

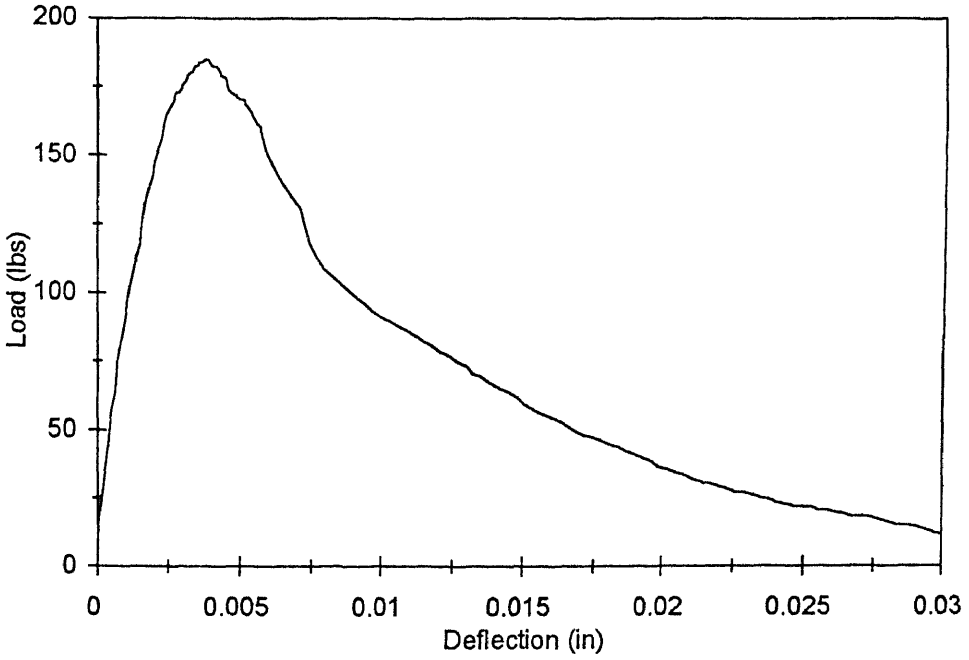

Figure B9b Load versus deflection for size B(T= 23°C, t = 2.95 days)

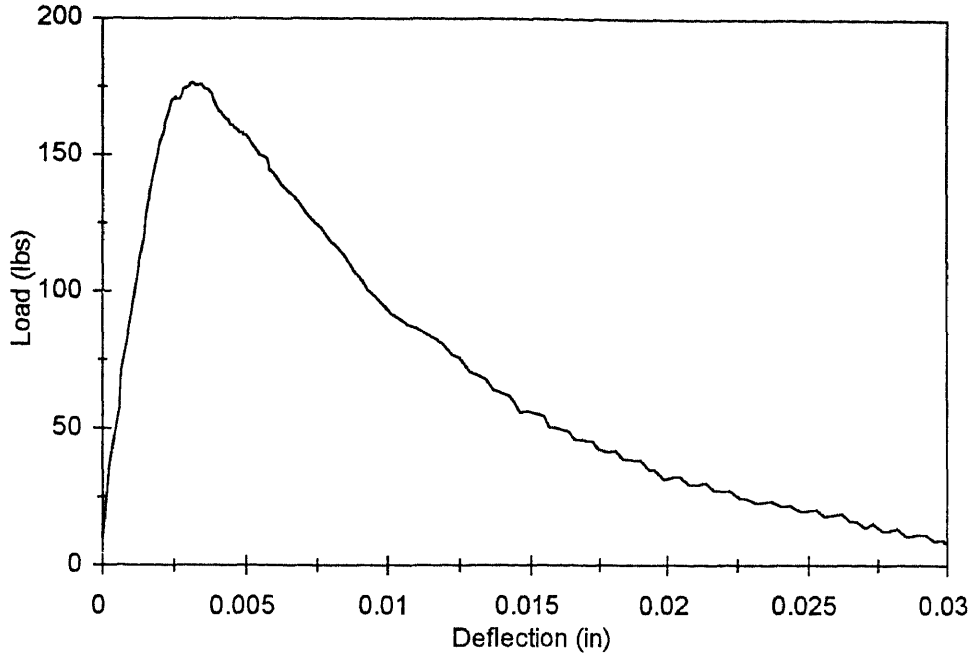

Figure B9c Load versus deflection for size B(T= 23°C, t = 2.95 days)

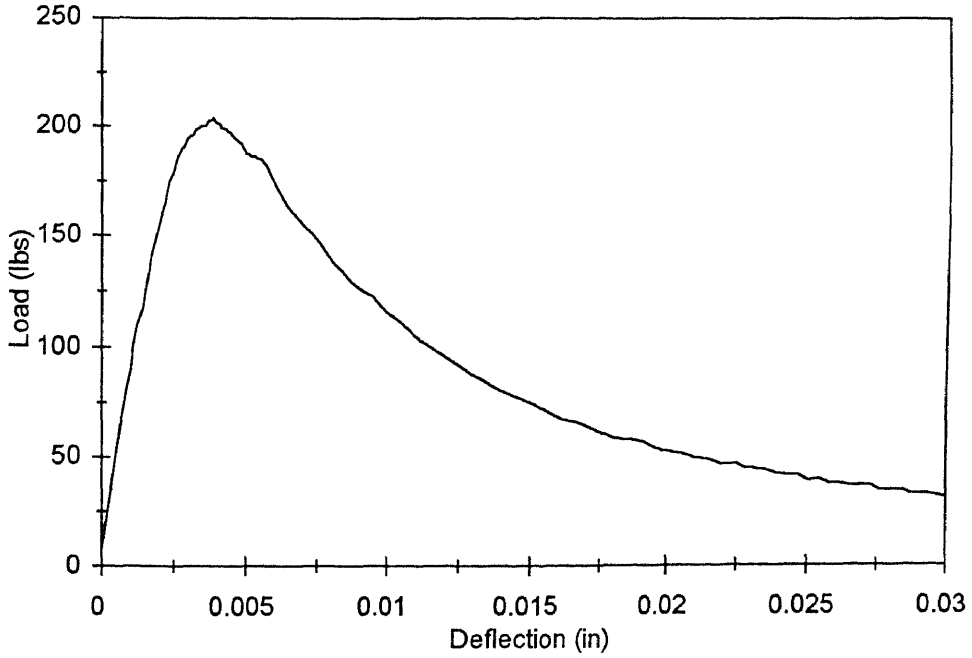

Figure B10a Load versus deflection for size B(T= 23°C, t = 7.16 days)

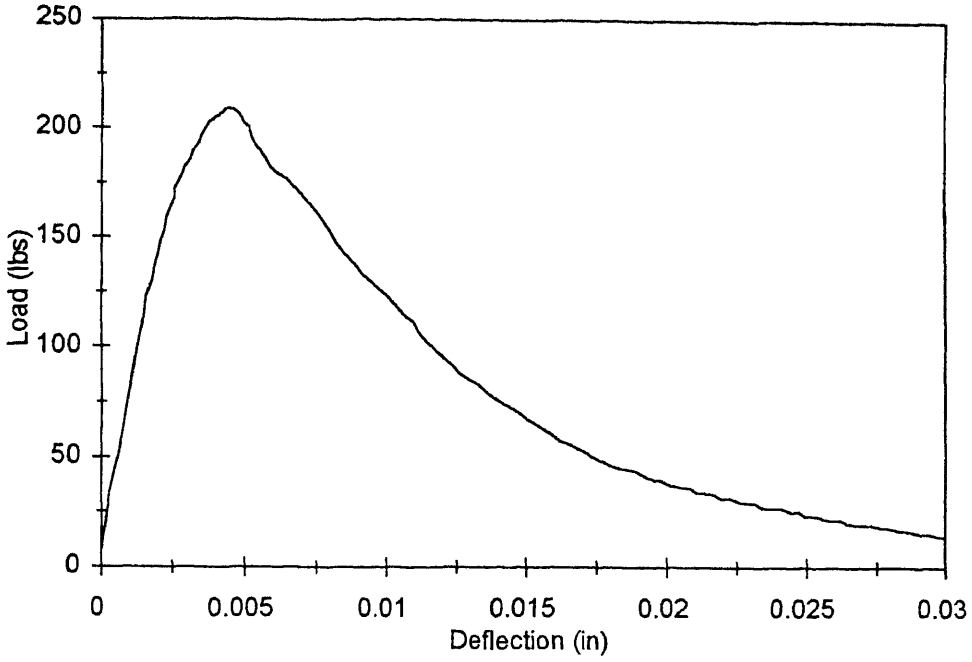

Figure B10b Load versus deflection for size B(T= 23°C, t = 7.16 days)

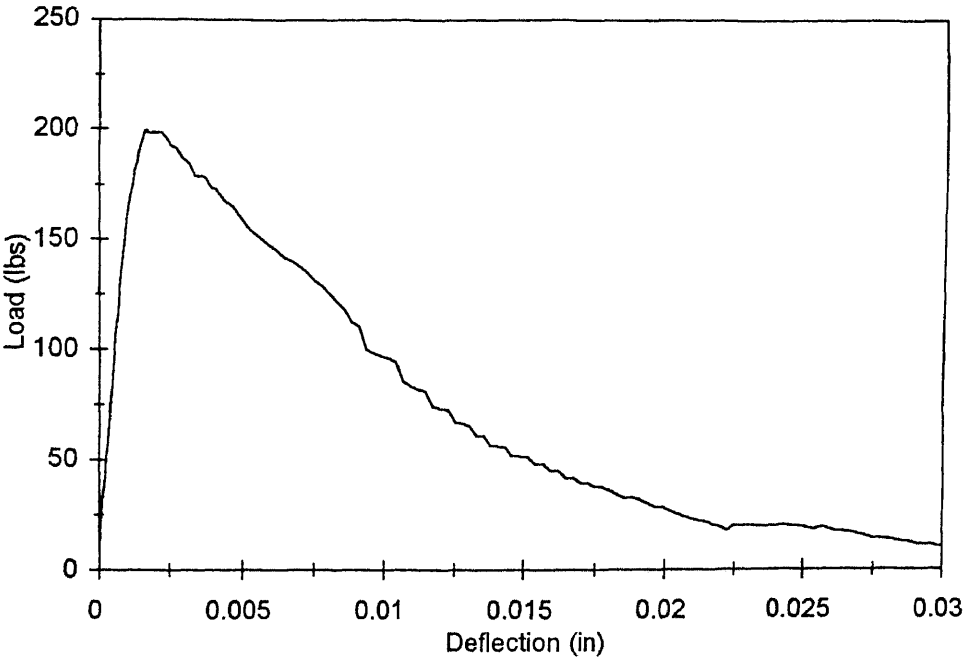

Figure B10c Load versus deflection for size B(T= 23°C, t = 7.16 days)

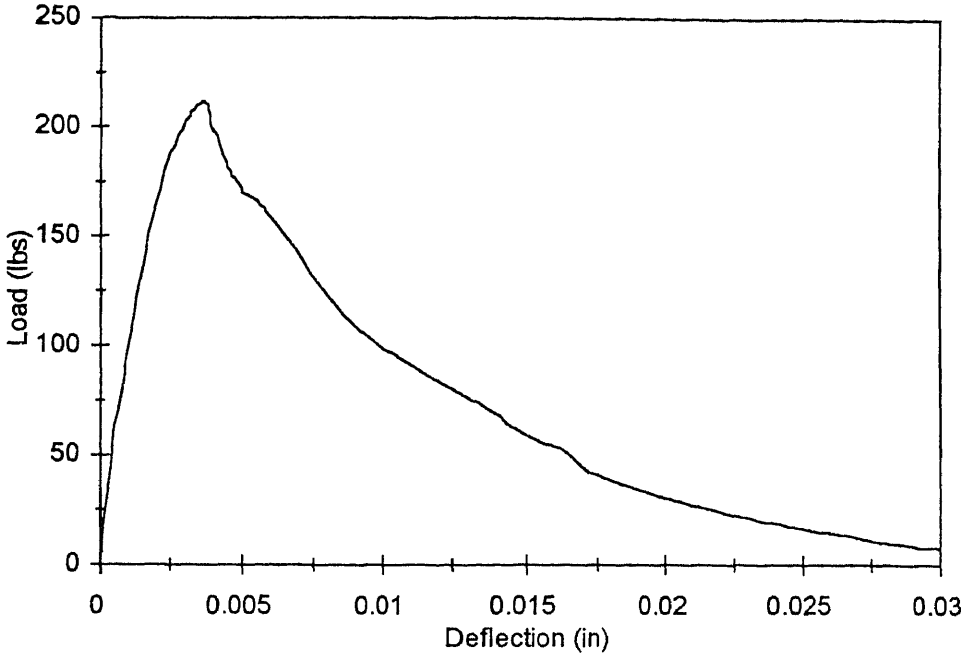

Figure B11a Load versus deflection for size B(T = 23°C, t = 14.02 days)

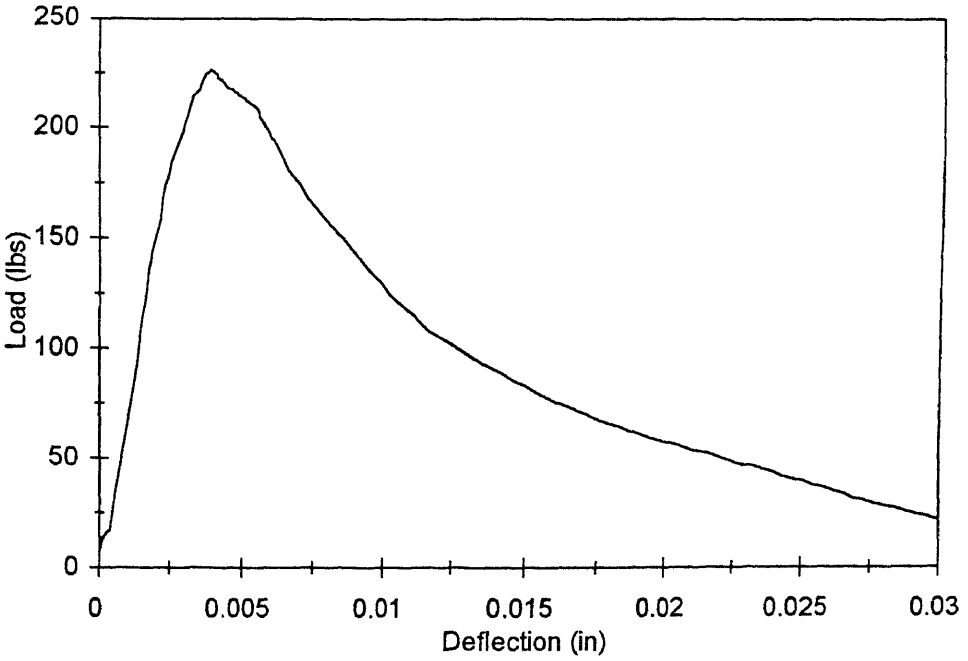

Figure B11b Load versus deflection for size B(T = 23°C, t = 14.02 days)

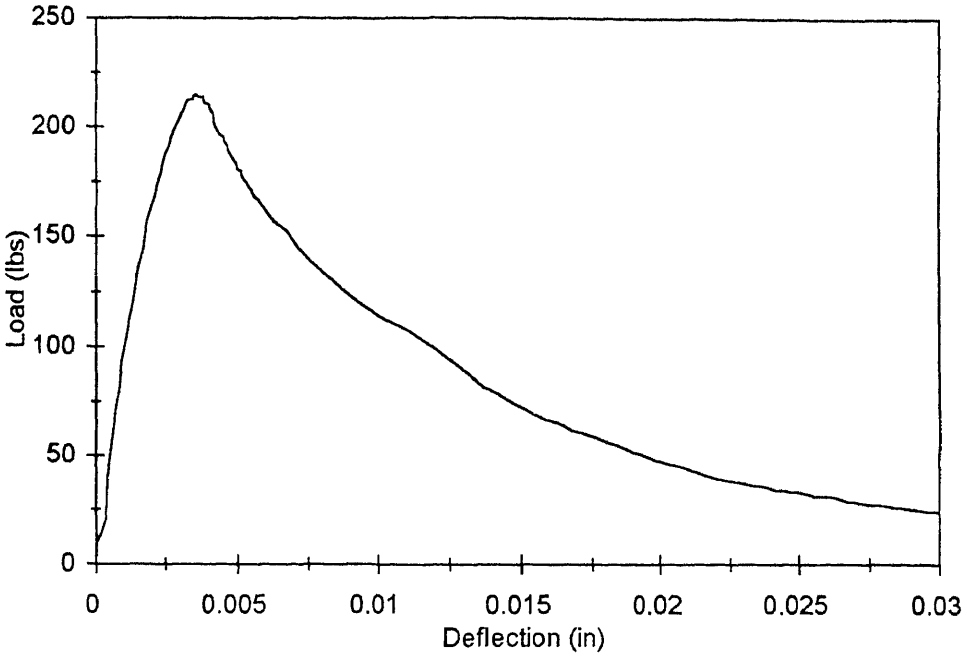

Figure B11a Load versus deflection for size B(T = 23°C, t = 14.02 days)

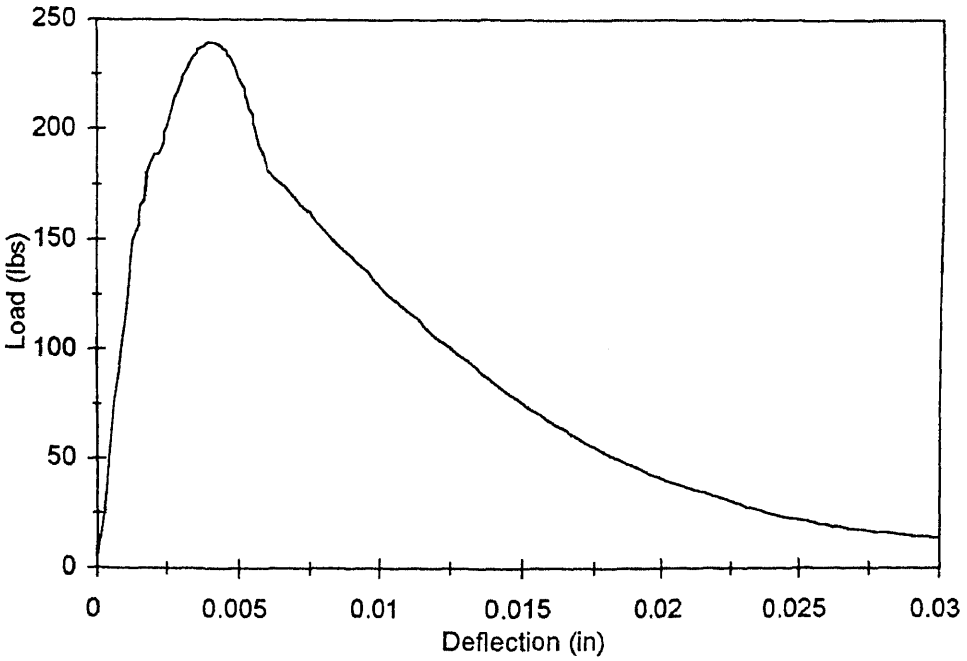

Figure B12a Load versus deflection for size B(T = 23°C, t = 28.0 days)

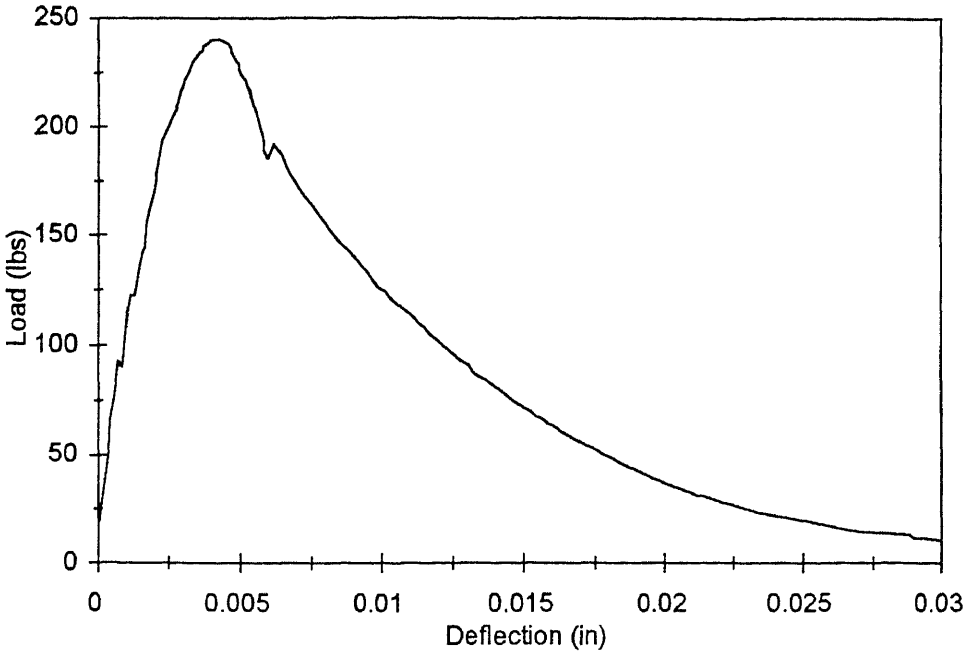

Figure B12b Load versus deflection for size B(T = 23°C, t = 28.0 days)

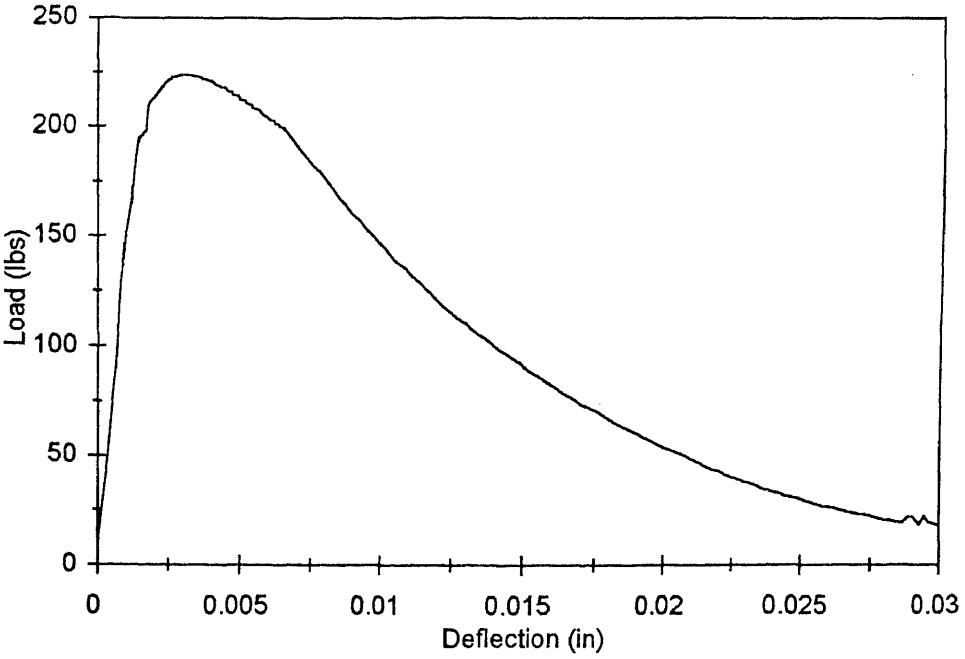

Figure B12c Load versus deflection for size B(T = 23°C, t = 28.0 days)

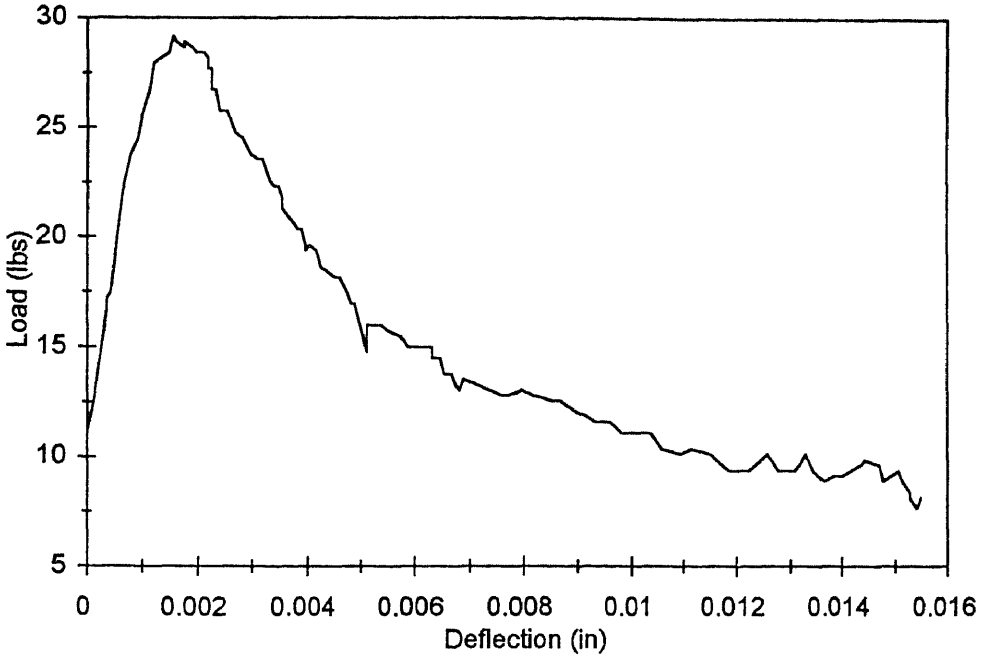

Figure B13a Load versus deflection for size B(T = 35°C, t = 0.25 day)

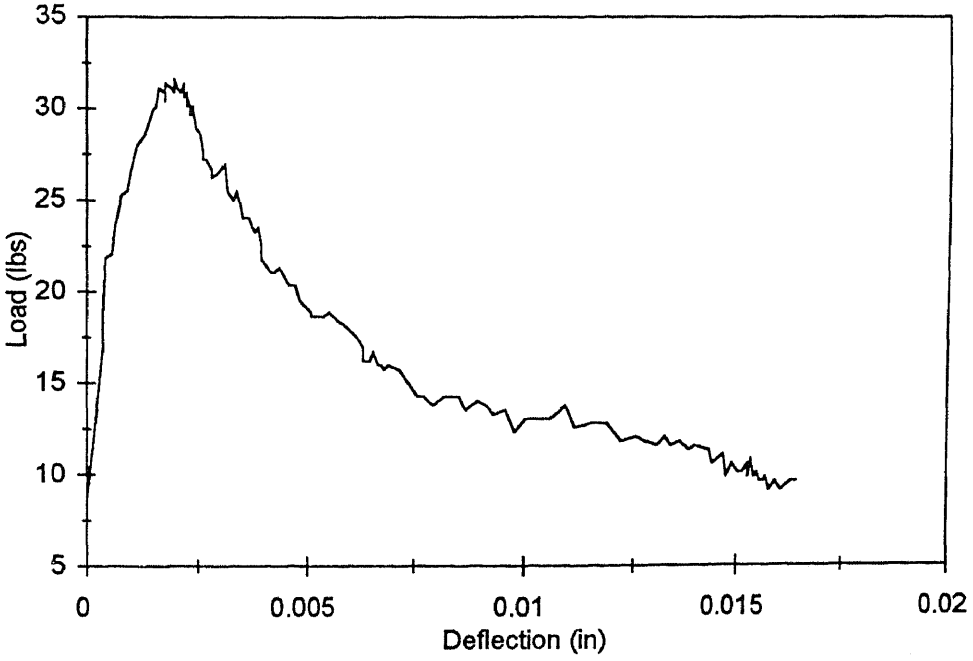

Figure B13b Load versus deflection for size B(T = 35°C, t = 0.25 day)

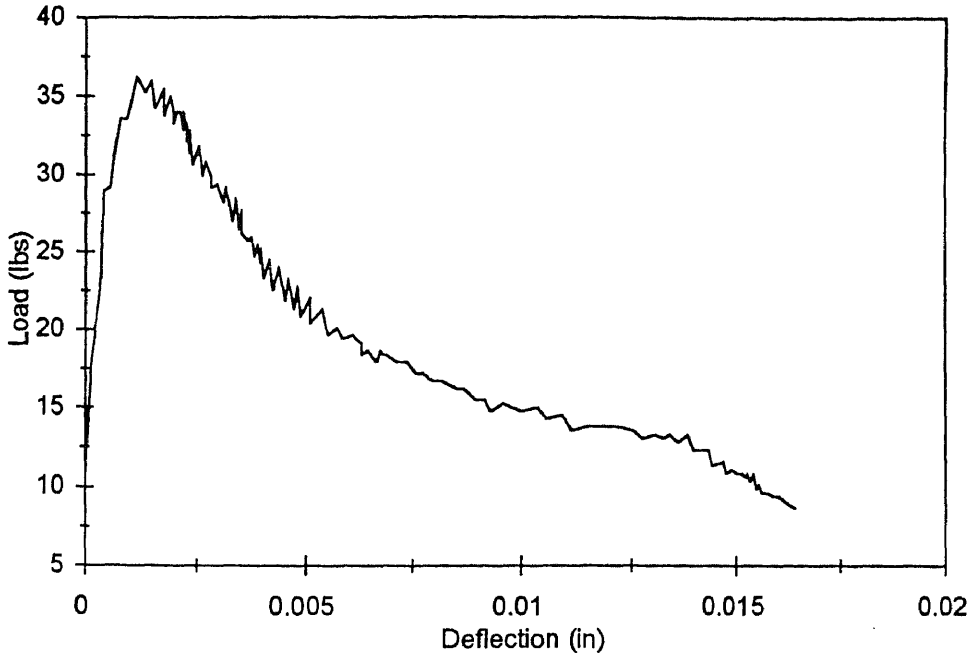

Figure B13c Load versus deflection for size B(T = 35°C, t = 0.25 day)

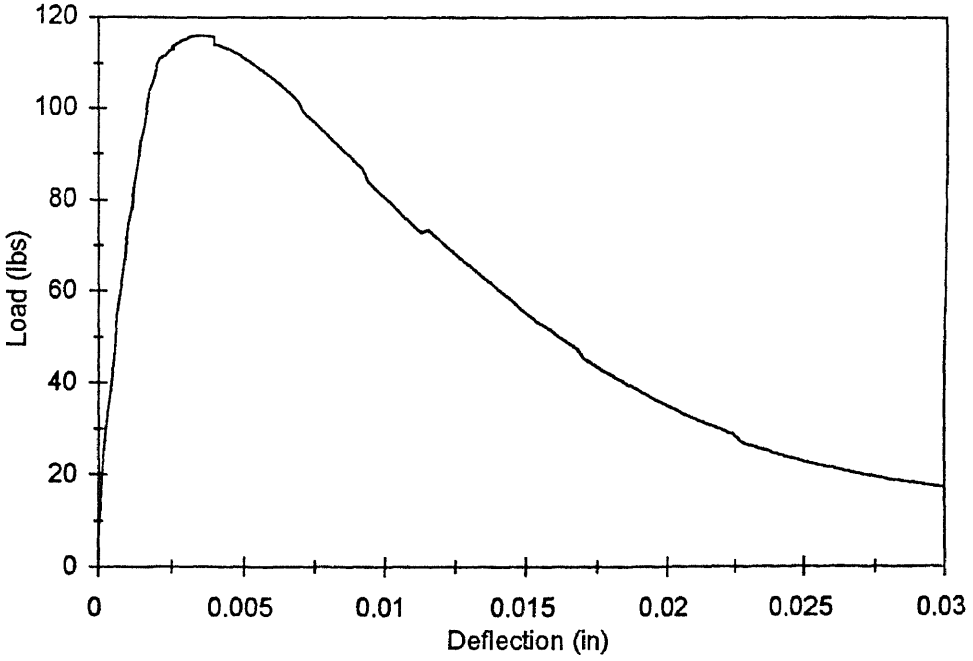

Figure B14a Load versus deflection for size B(T = 35°C, t = 0.55 day)

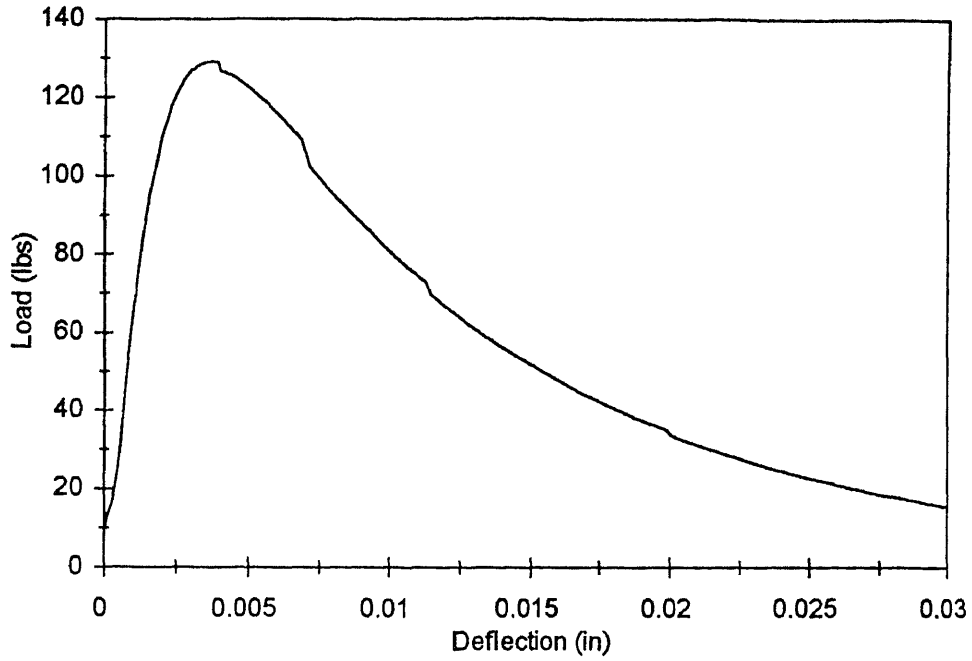

Figure B14b Load versus deflection for size B(T = 35°C, t = 0.55 day)

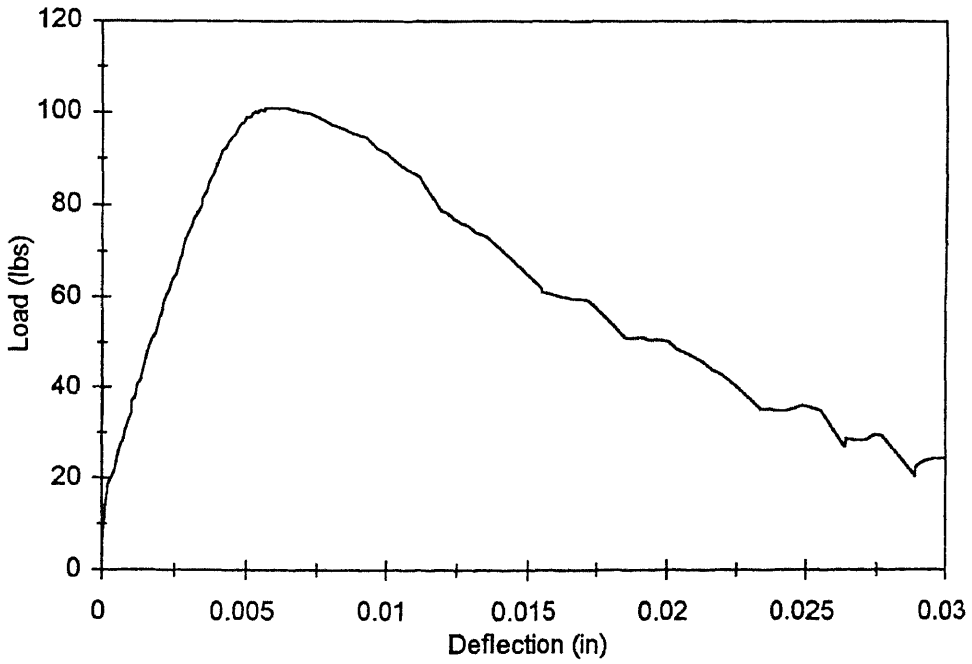

Figure B14c Load versus deflection for size B(T = 35°C, t = 0.55 day)

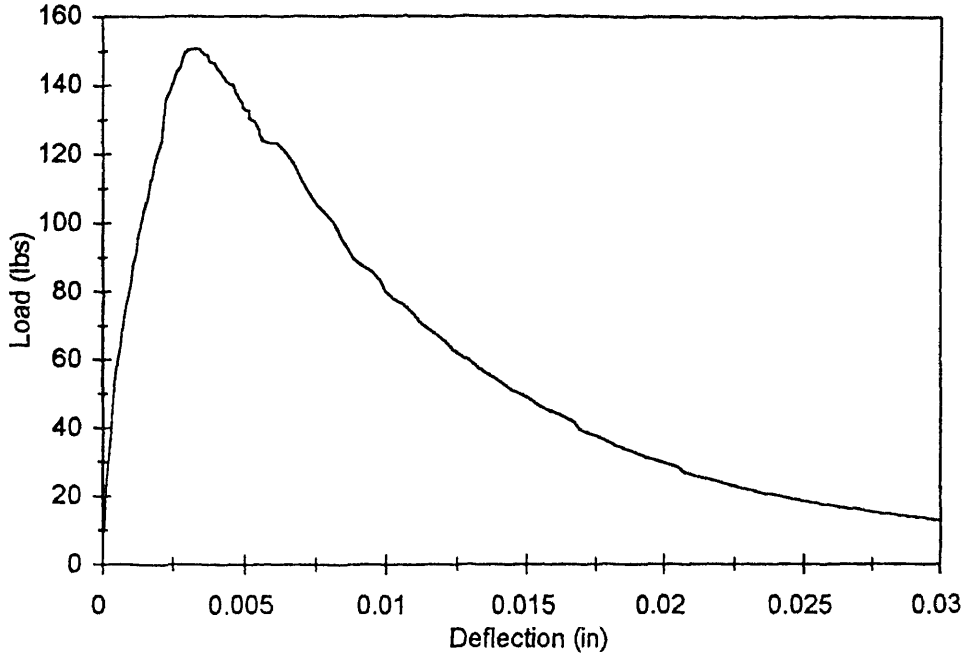

Figure B15a Load versus deflection for size B(T = 35°C, t = 1.55 days)

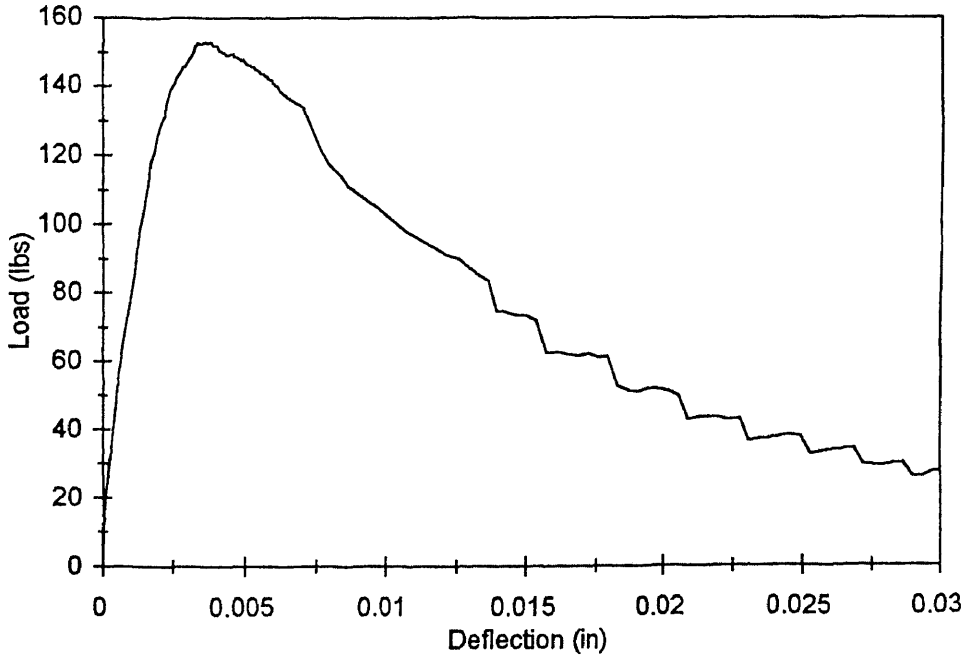

Figure B15b Load versus deflection for size B(T = 35°C, t = 1.55 days)

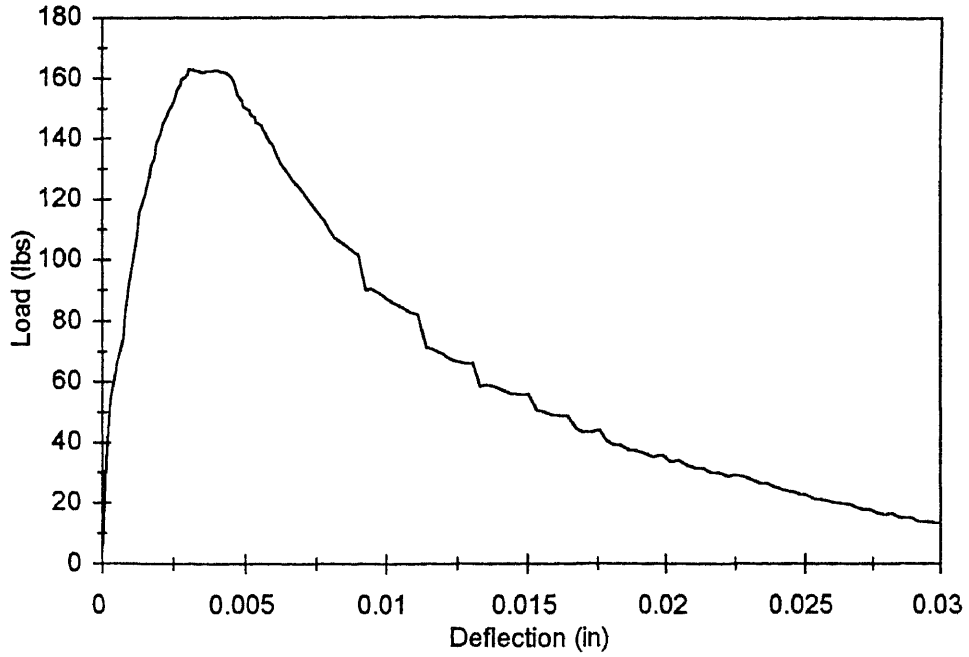

Figure B15c Load versus deflection for size B(T = 35°C, t = 1.55 days)

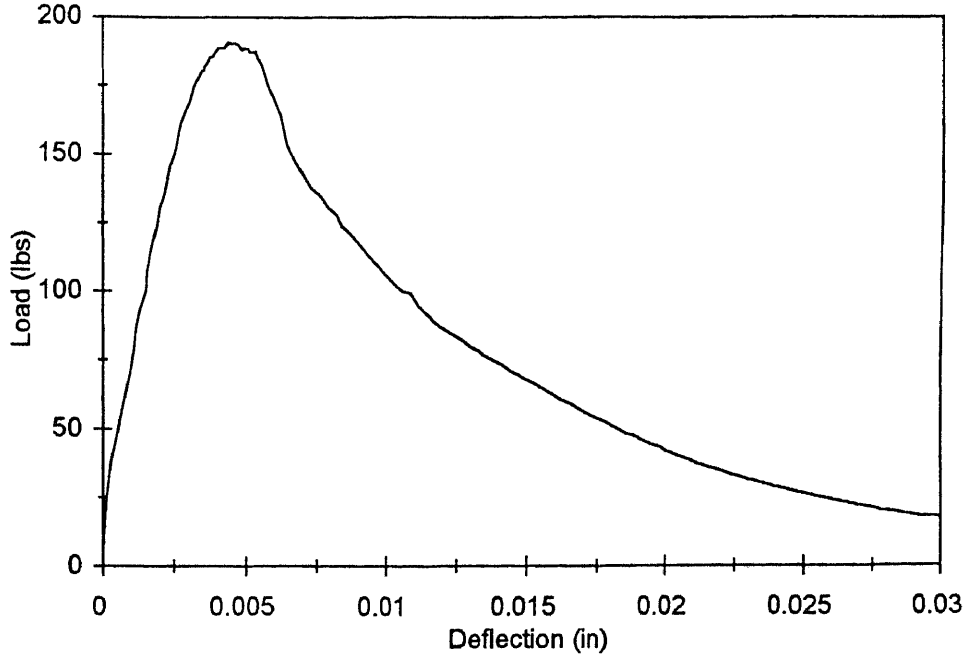

Figure B16a Load versus deflection for size B(T = 35°C, t = 4.26 days)

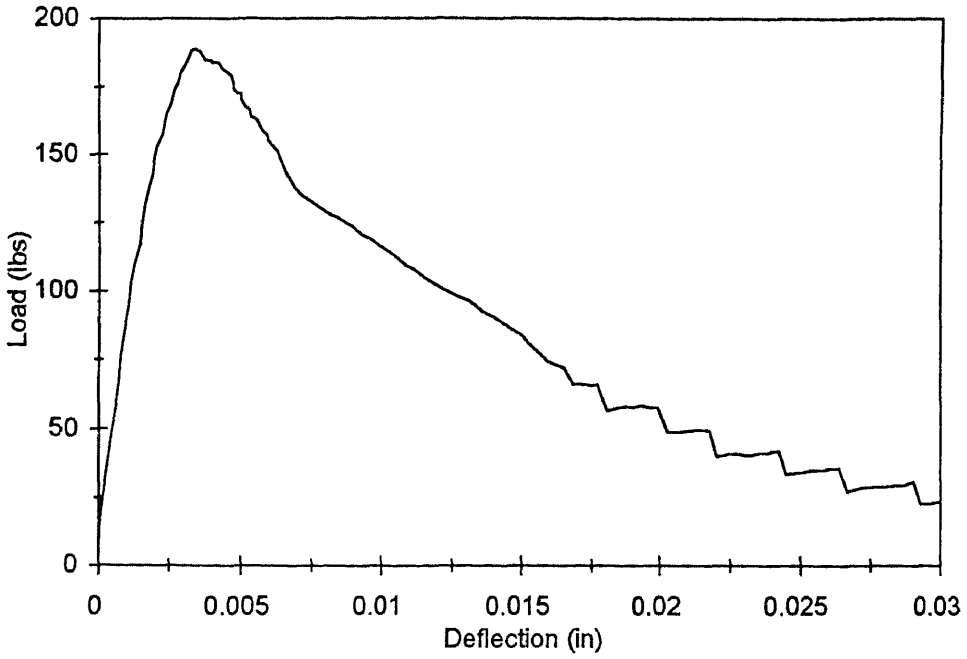

Figure B16b Load versus deflection for size B(T = 35°C, t = 4.26 days)

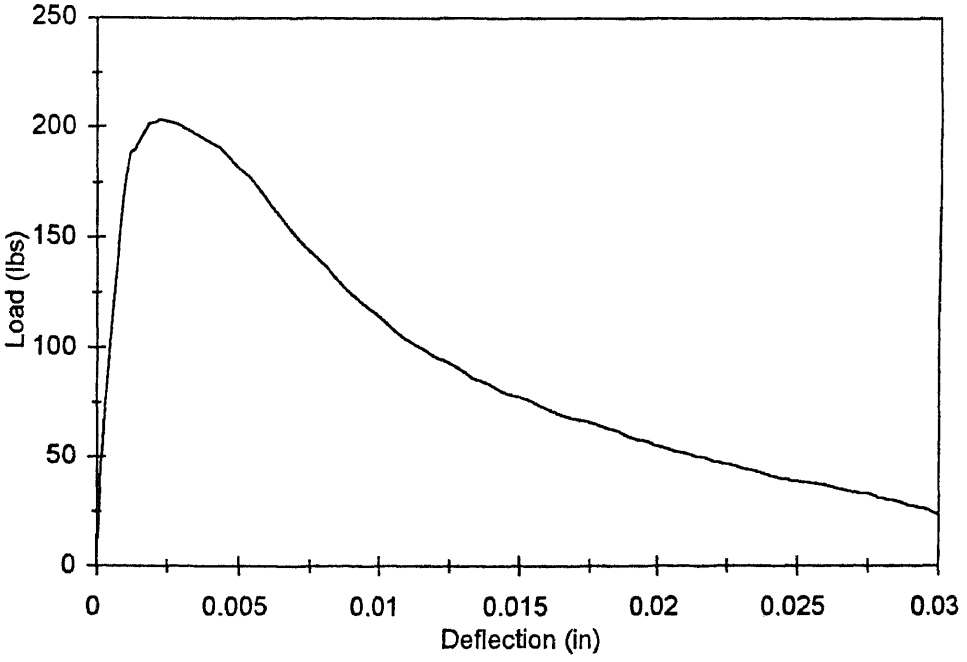

Figure B16c Load versus deflection for size B(T = 35°C, t = 4.26 days)

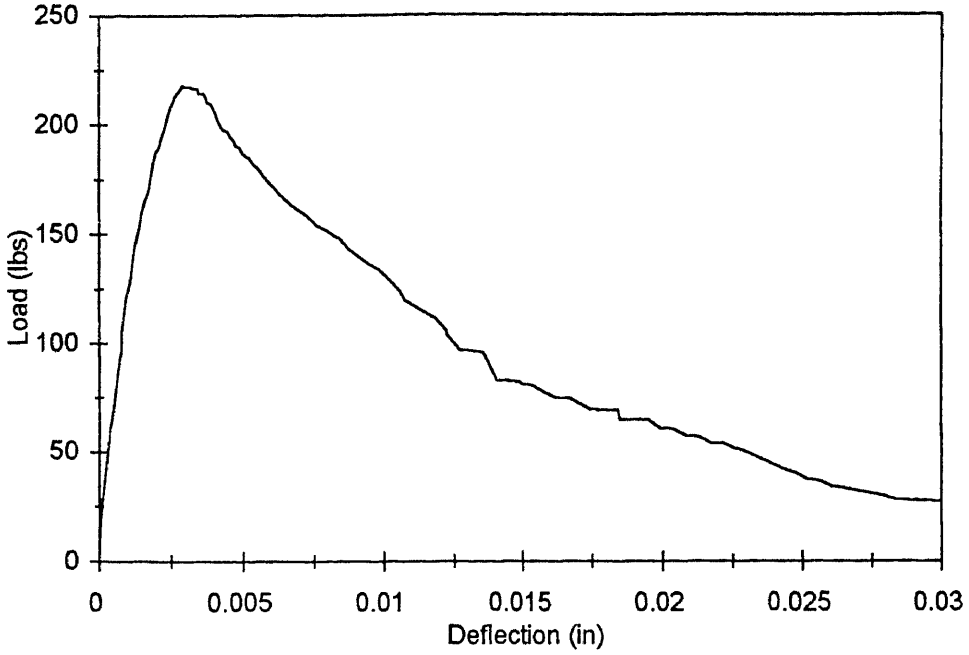

Figure B17a Load versus deflection for size B(T = 35°C, t = 9.05 days)

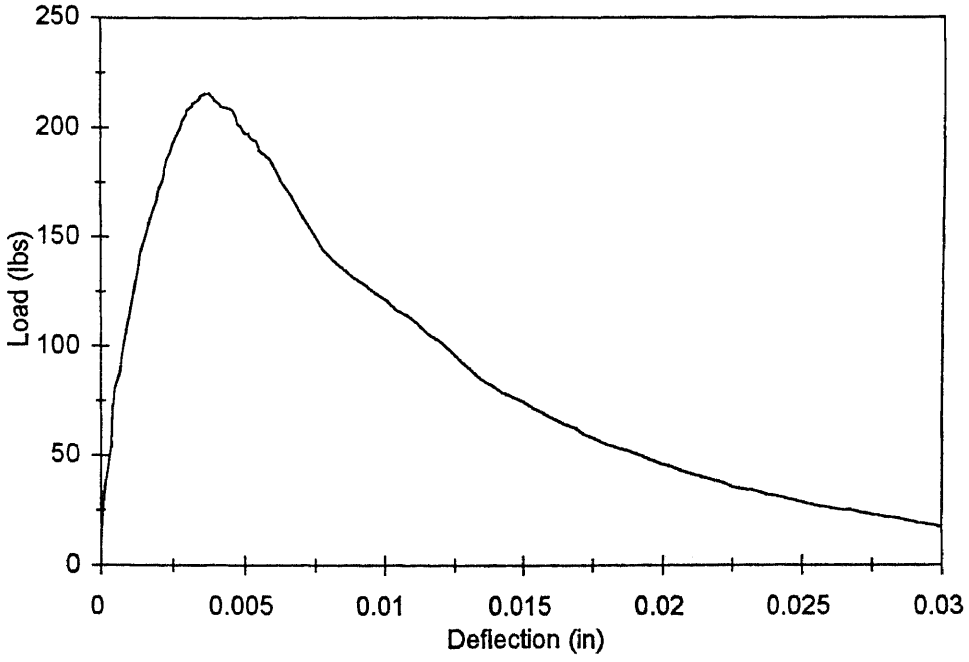

Figure B17b Load versus deflection for size B(T = 35°C, t = 9.05 days)

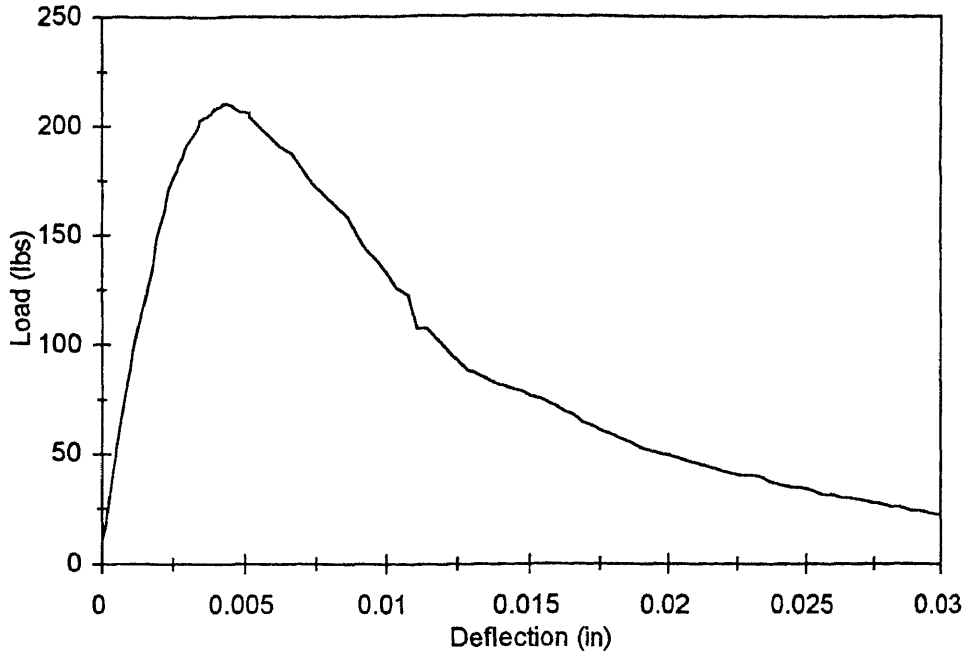

Figure B17c Load versus deflection for size B(T = 35°C, t = 9.05 days)

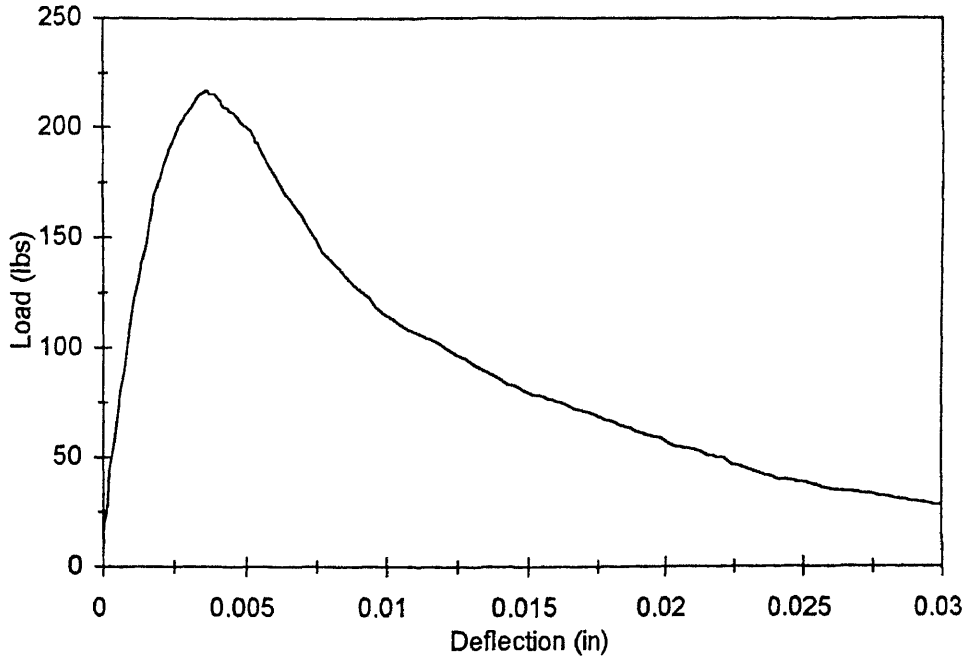

Figure B18a Load versus deflection for size B(T = 35°C, t = 20.2 days)

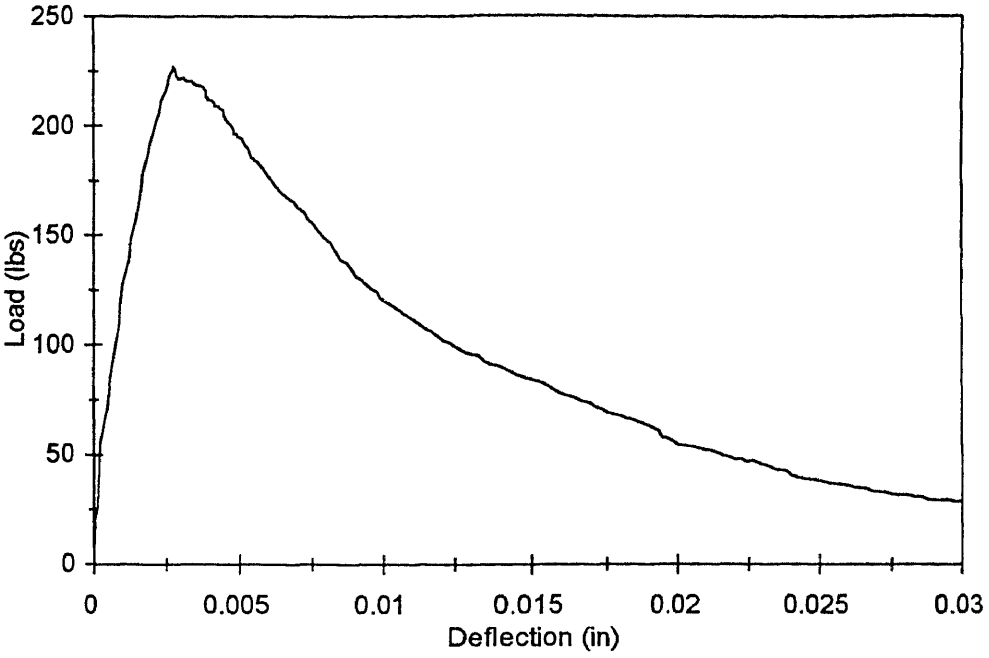

Figure B18b Load versus deflection for size B(T = 35°C, t = 20.2 days)

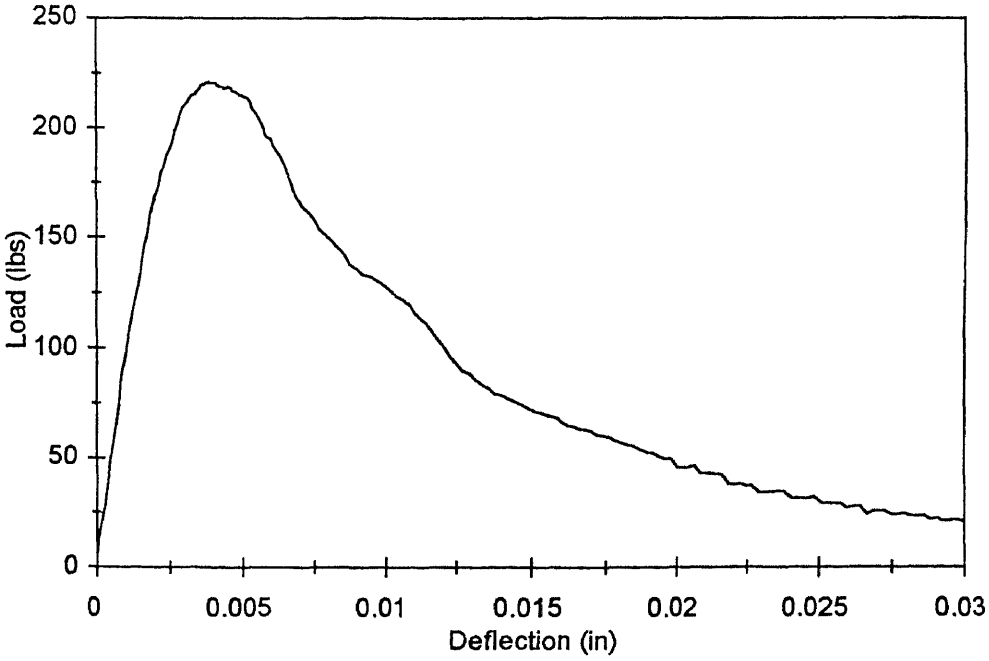

Figure B18c Load versus deflection for size B(T = 35°C, t = 20.2 days)

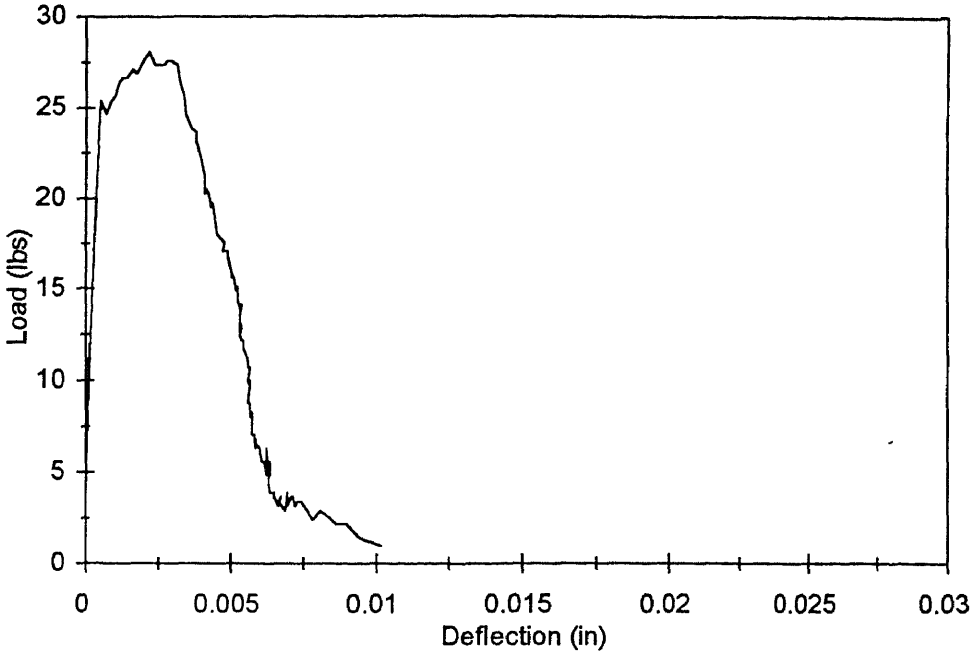

Figure C1a Load versus deflection for size C(T = 14°C, t = 1.1 days)

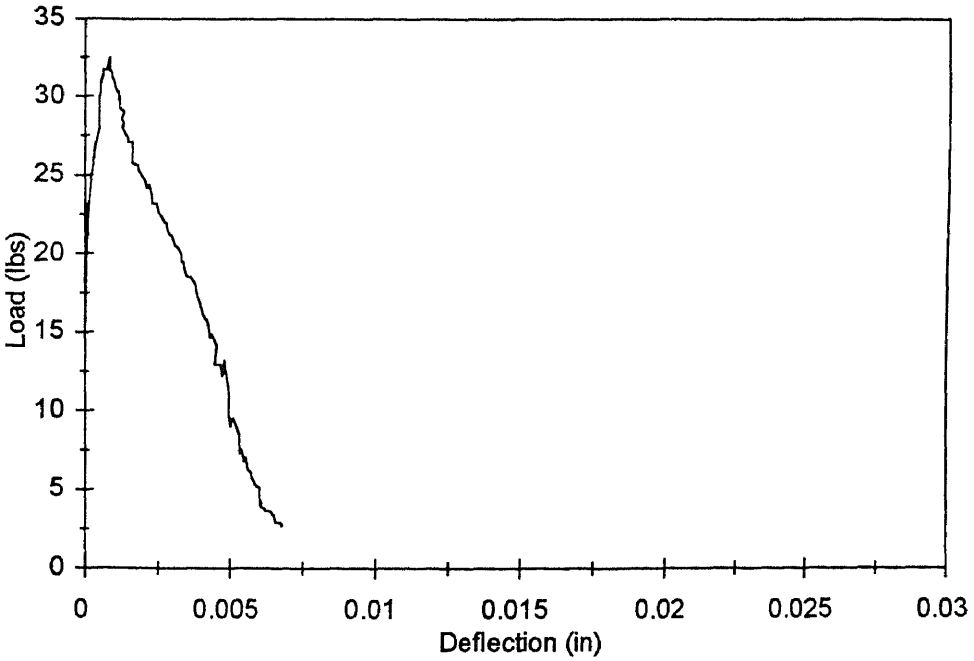

Figure C1b Load versus deflection for size C(T = 14°C, t = 1.1 days)

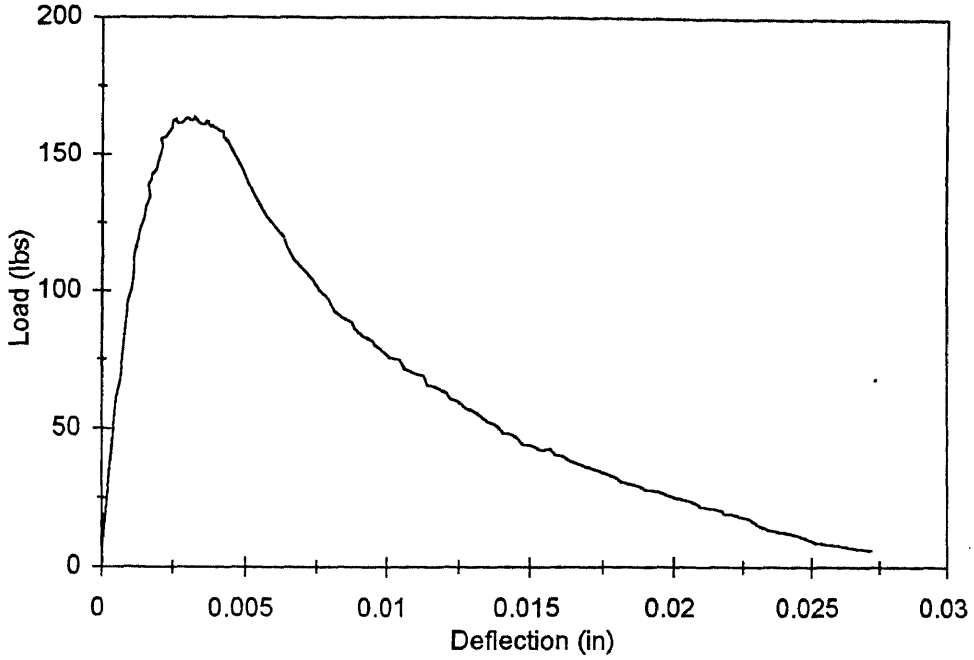

Figure C2a Load versus deflection for size C(T = 14°C, t = 2.1 days)

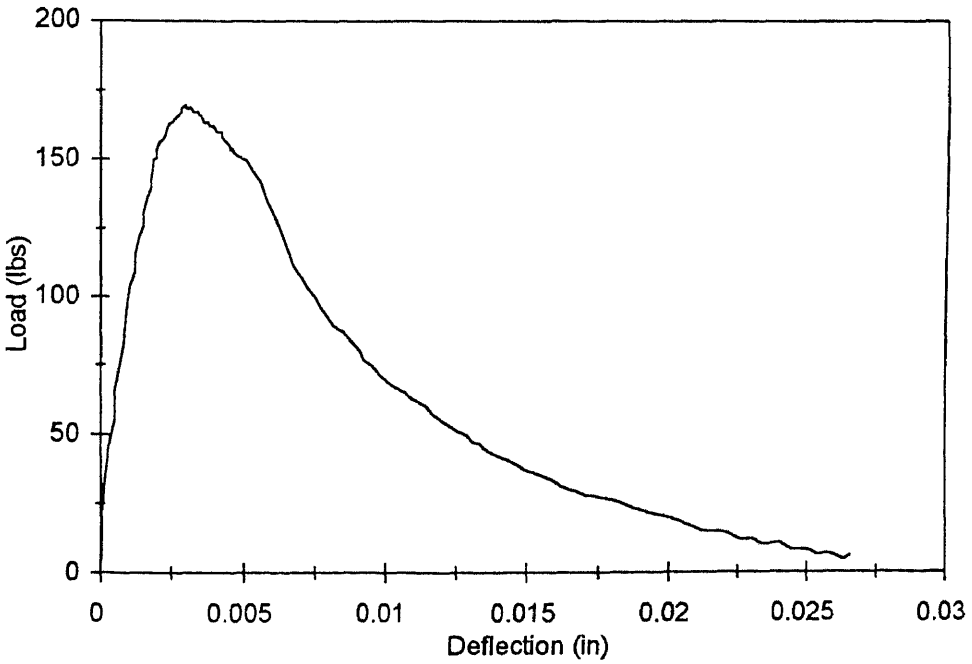

Figure C2b Load versus deflection for size C(T = 14°C, t = 2.1 days)

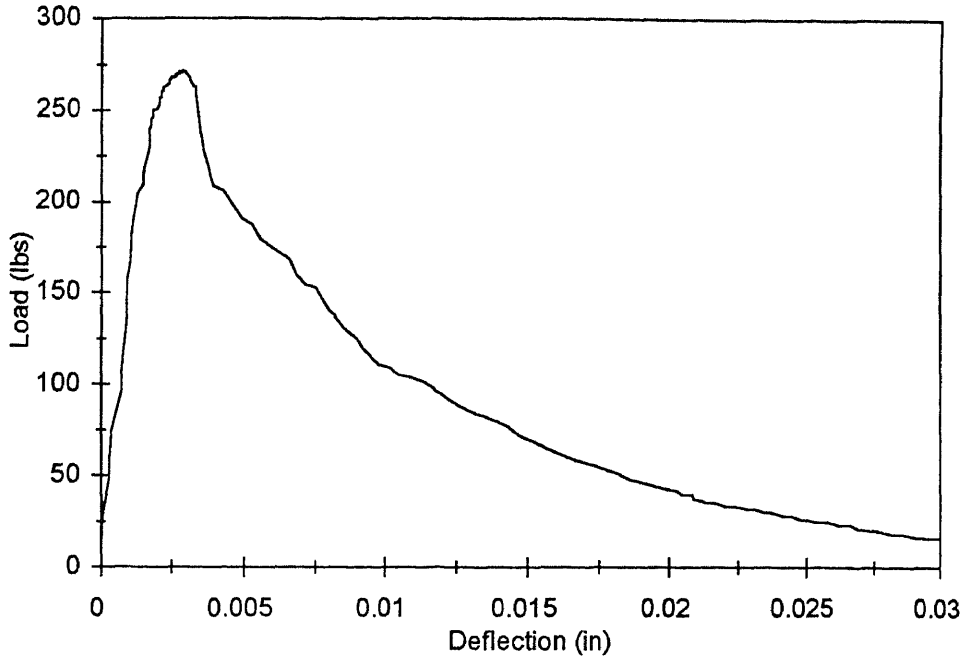

Figure C3a Load versus deflection for size C(T = 14°C, t = 4.0 days)

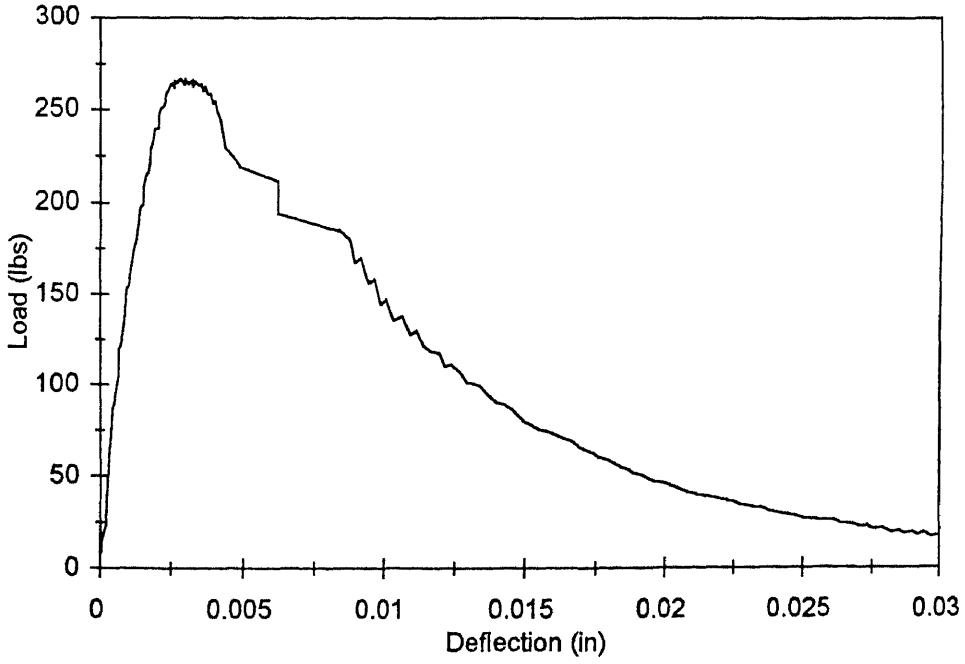

Figure C3b Load versus deflection for size C(T = 14°C, t = 4.0 days)

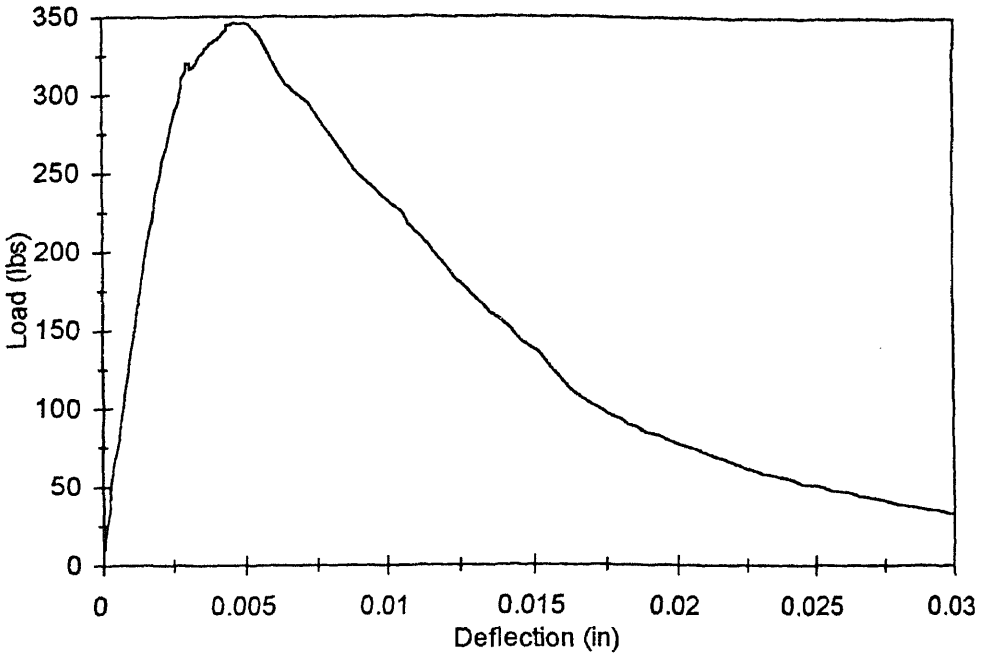

Figure C4a Load versus deflection for size C(T = 14°C, t = 9.0 days)

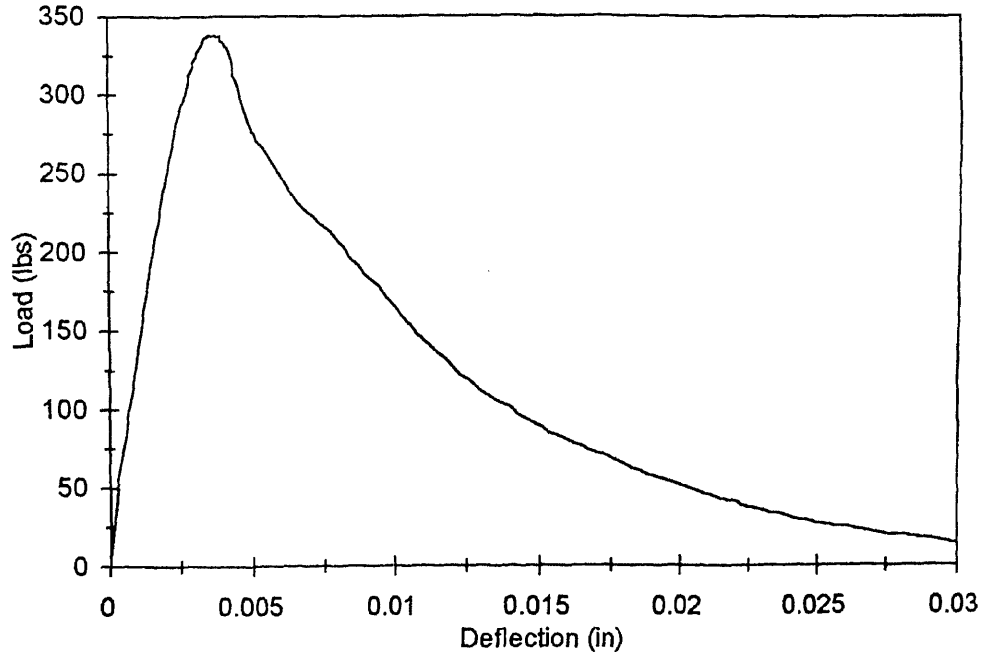

Figure C4b Load versus deflection for size C(T = 14°C, t = 9.0 days)

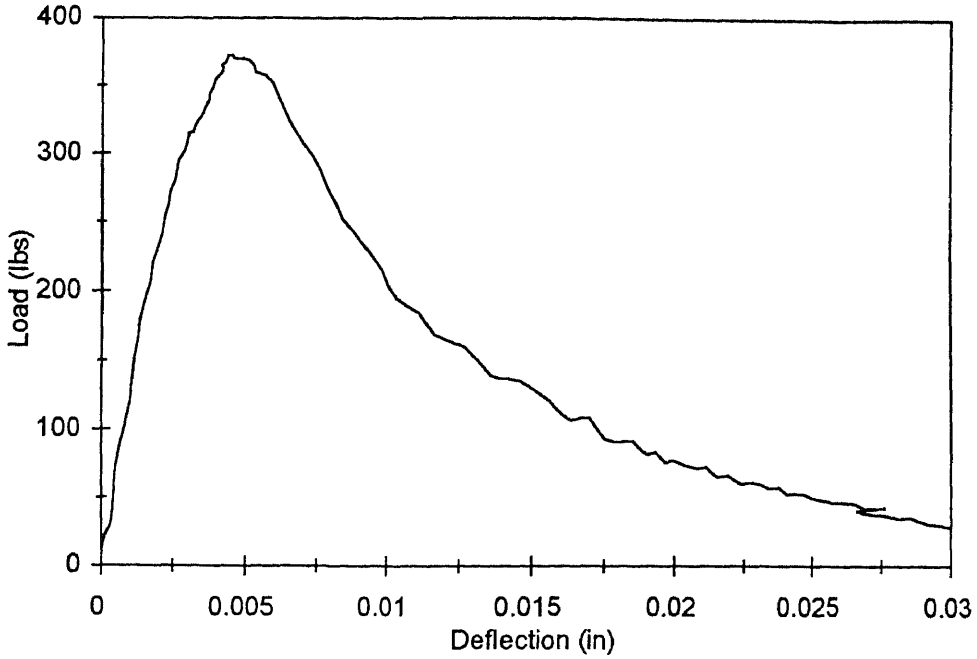

Figure C5a Load versus deflection for size C(T = 14°C, t = 18.0 days)

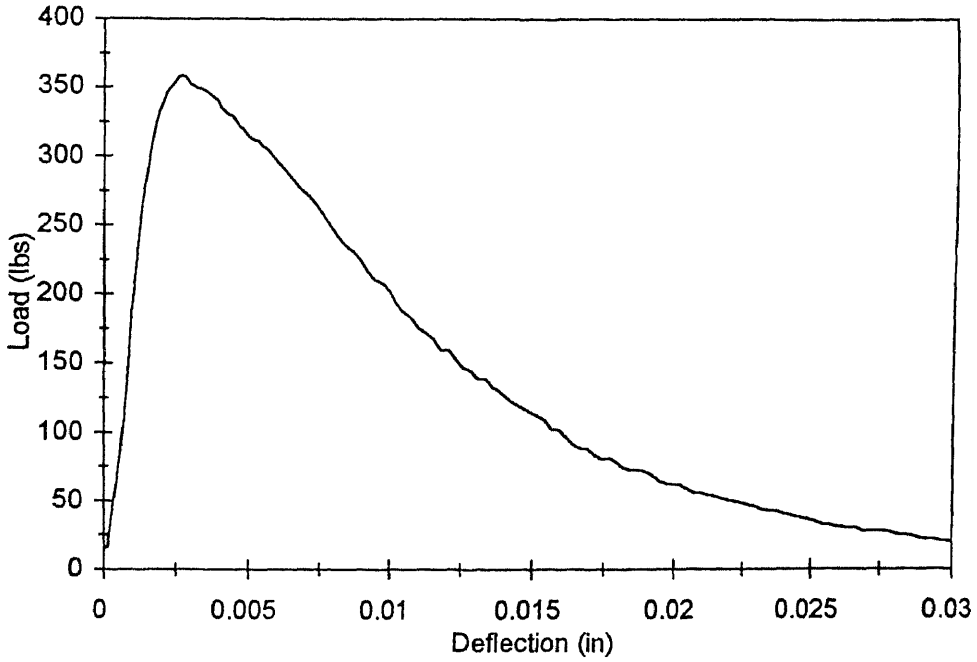

Figure C5b Load versus deflection for size C(T = 14°C, t = 18.0 days)

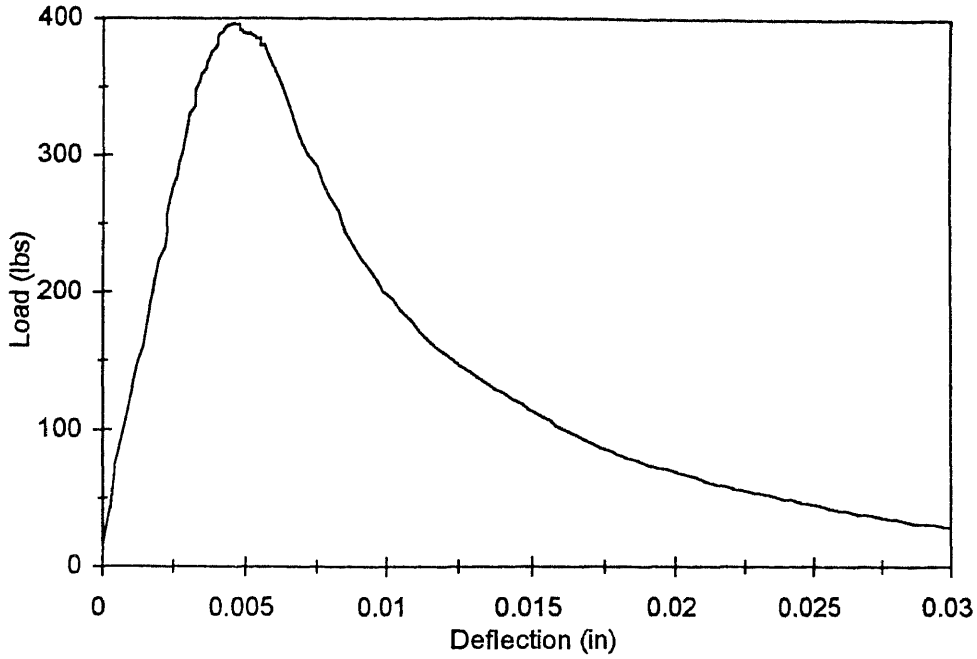

Figure C6a Load versus deflection for size C(T = 14°C, t = 36.0 days)

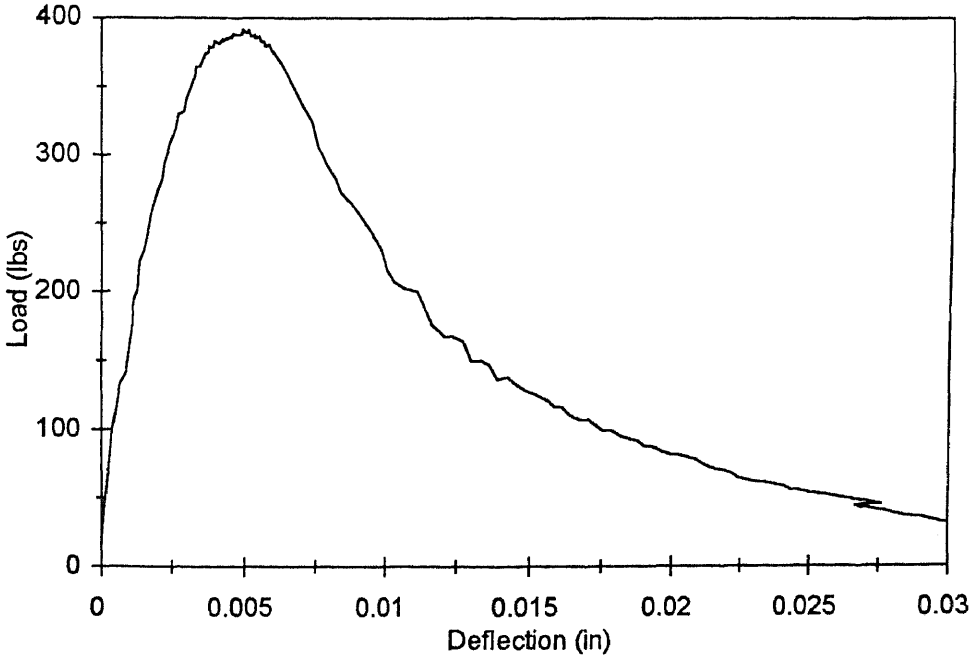

Figure C6b Load versus deflection for size C(T = 14°C, t = 36.0 days)

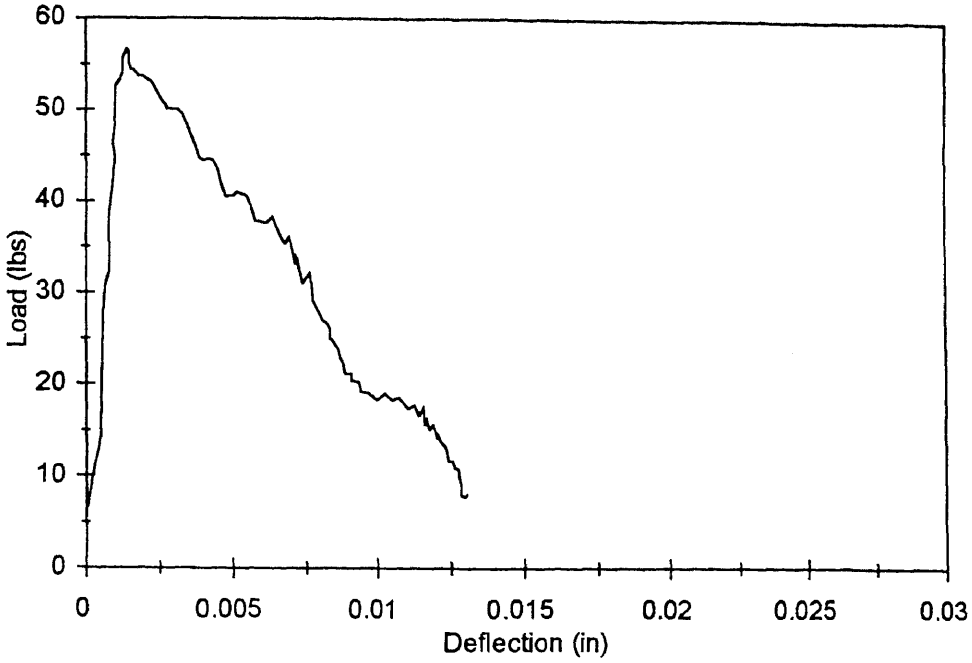

Figure C7a Load versus deflection for size C(T = 23°C, t = 0.65 day)

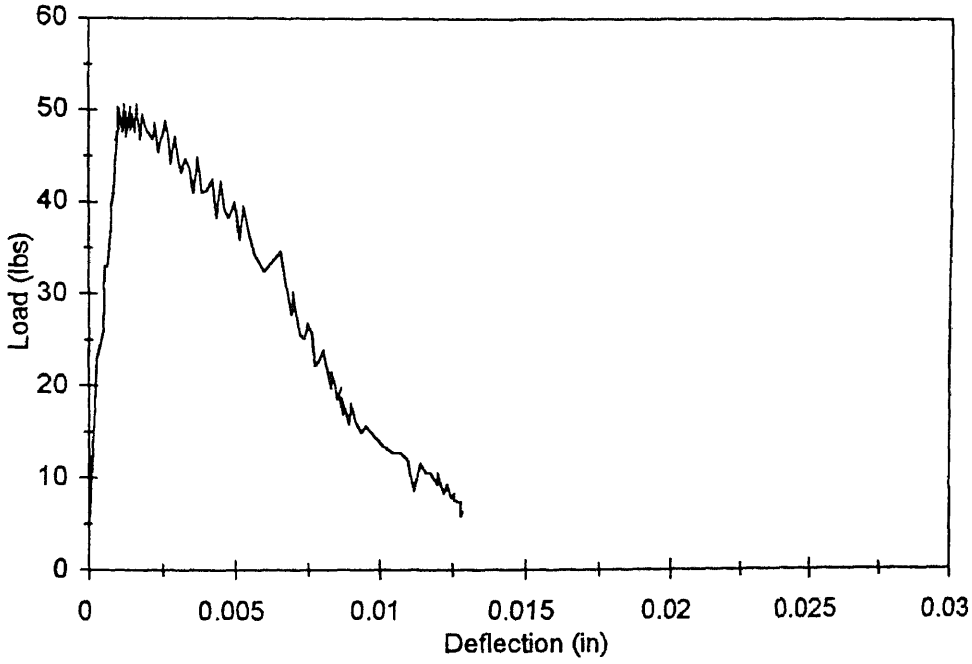

Figure C7b Load versus deflection for size C(T = 23°C, t = 0.65 day)

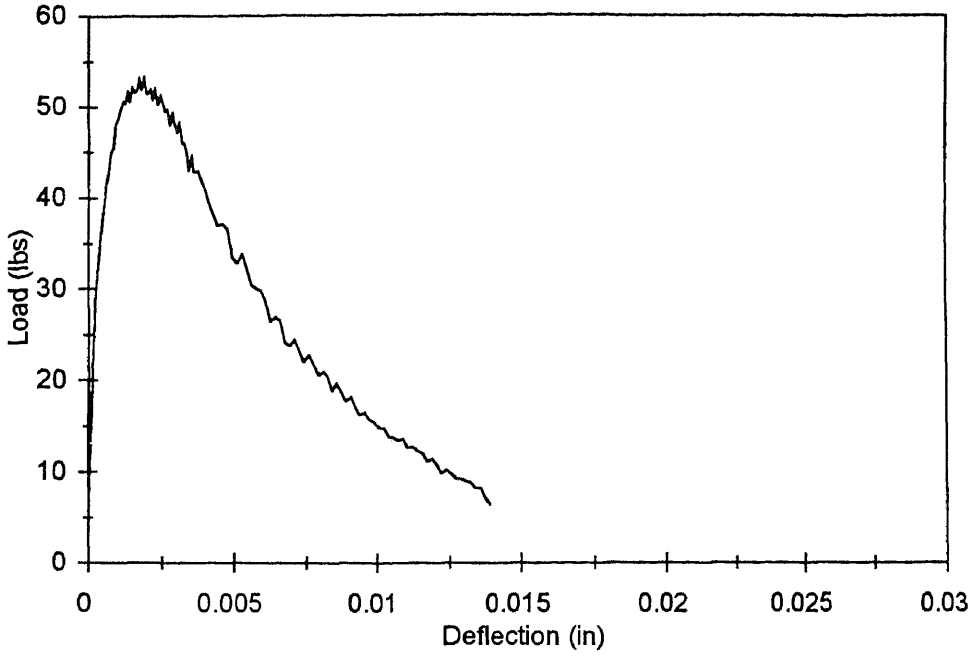

Figure C7c Load versus deflection for size C(T = 23°C, t = 0.65 day)

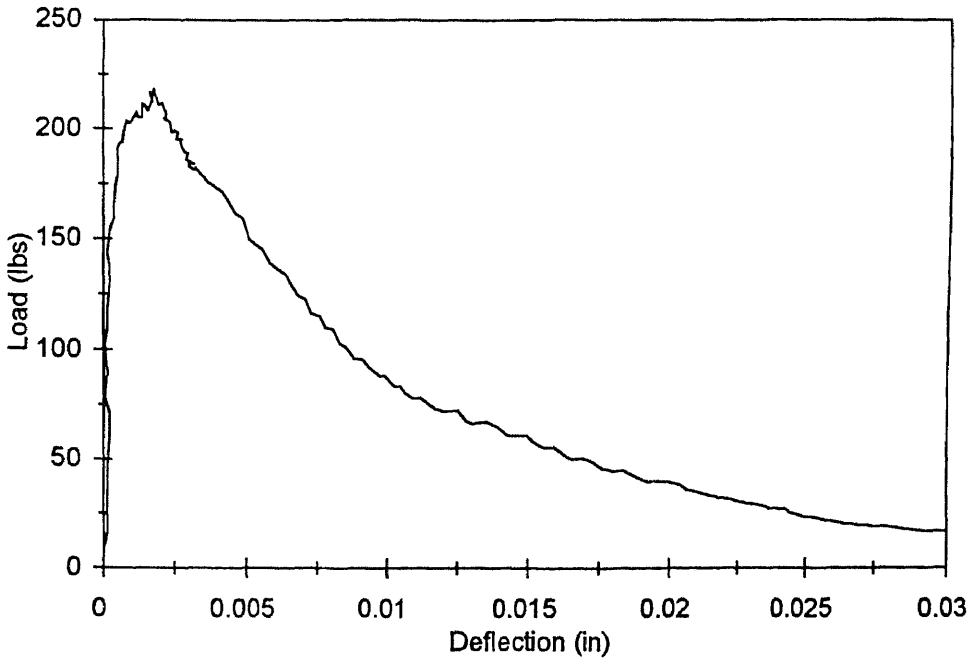

Figure C8a Load versus deflection for size C(T = 23°C, t = 1 day)

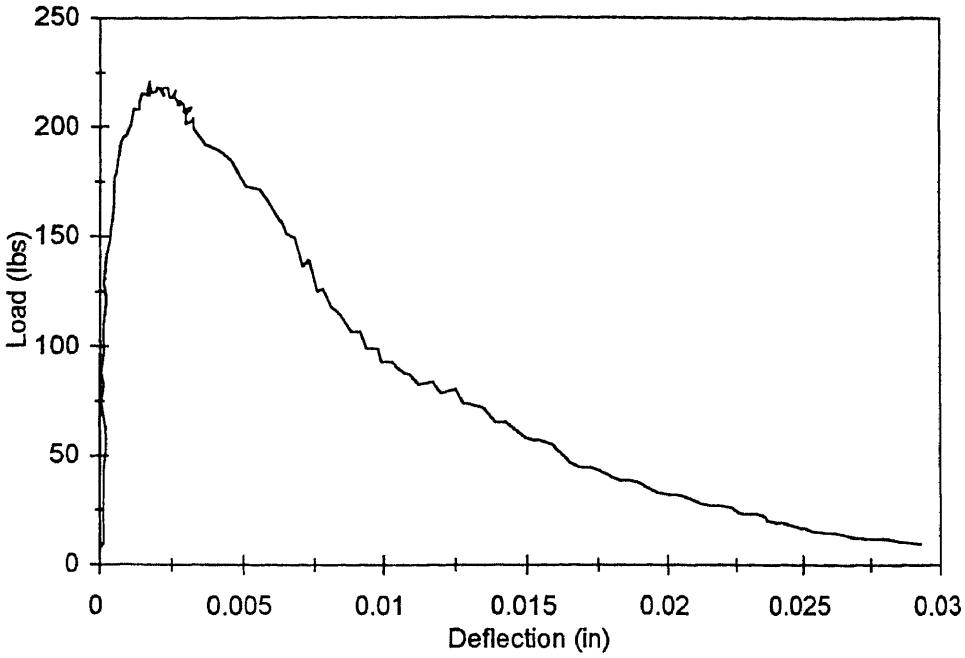

Figure C8b Load versus deflection for size C(T = 23°C, t = 1 day)

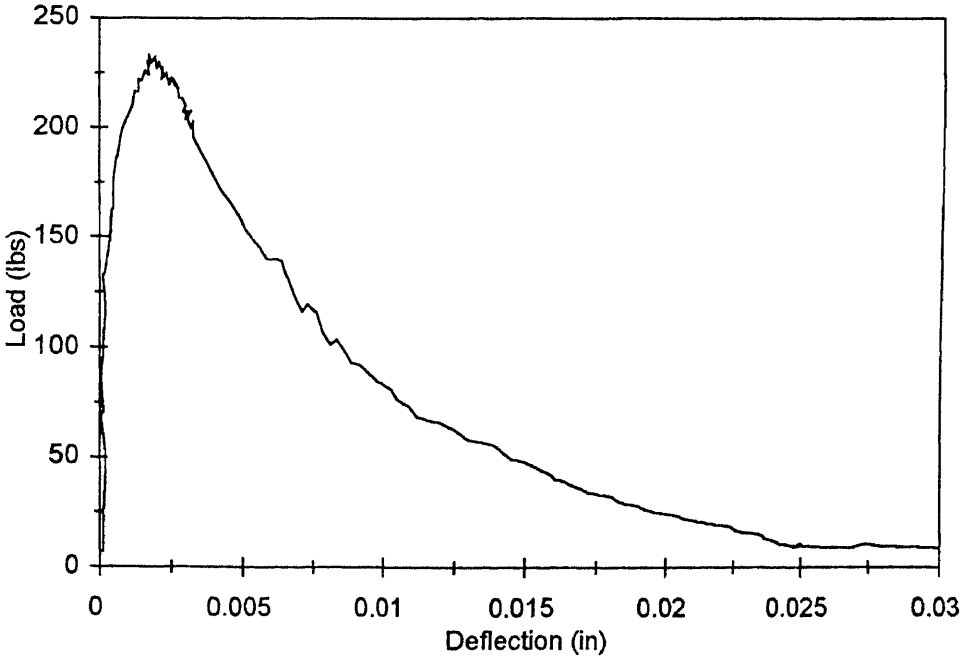

Figure C8c Load versus deflection for size C(T = 23°C, t = 1 day)

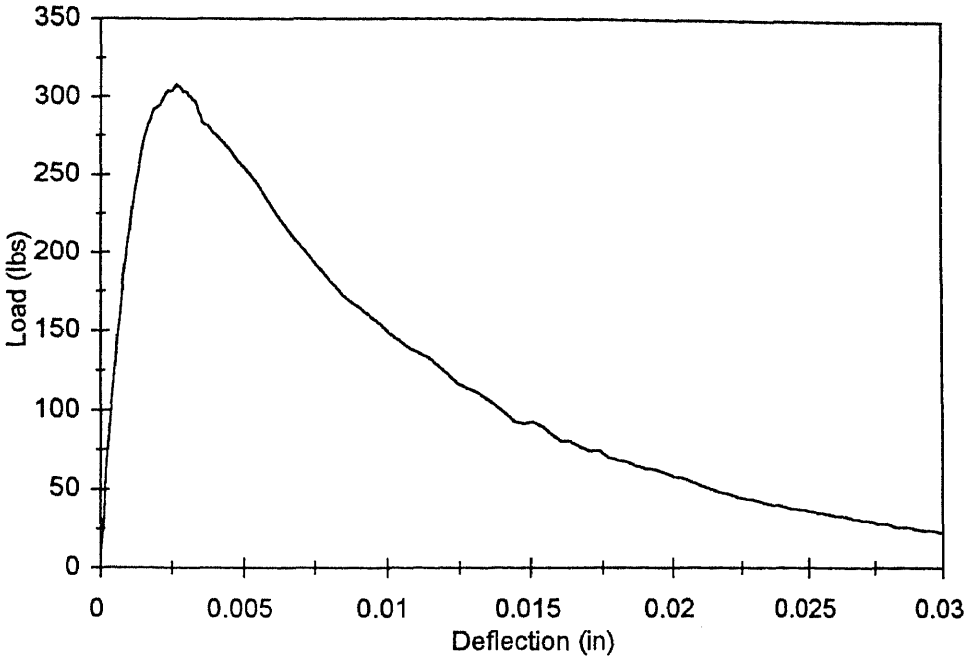

Figure C9a Load versus deflection for size C(T = 23°C, t = 3.0 days)

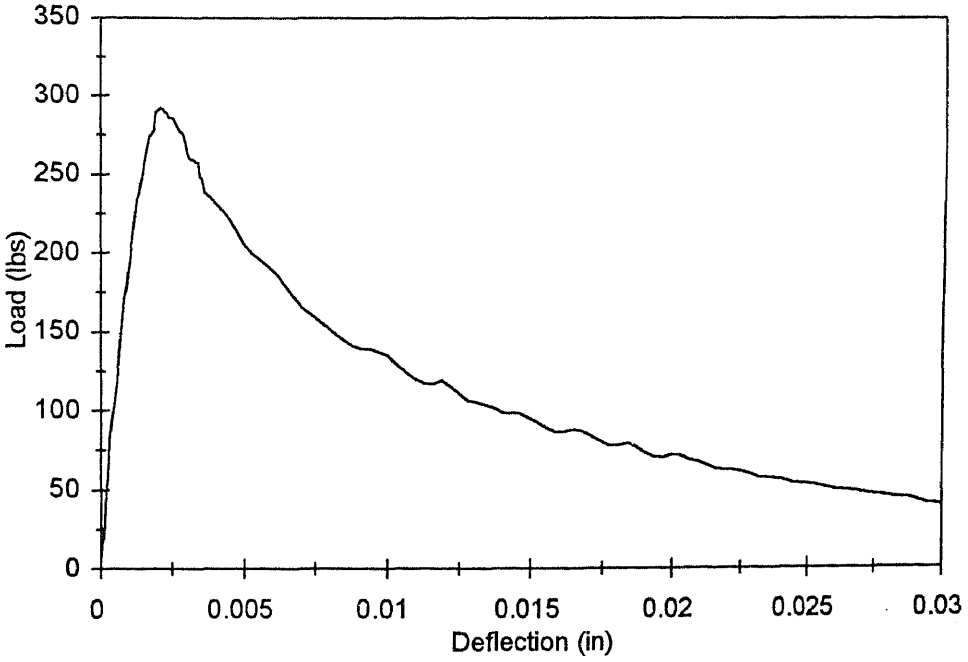

Figure C9b Load versus deflection for size C(T = 23°C, t = 3.0 days)

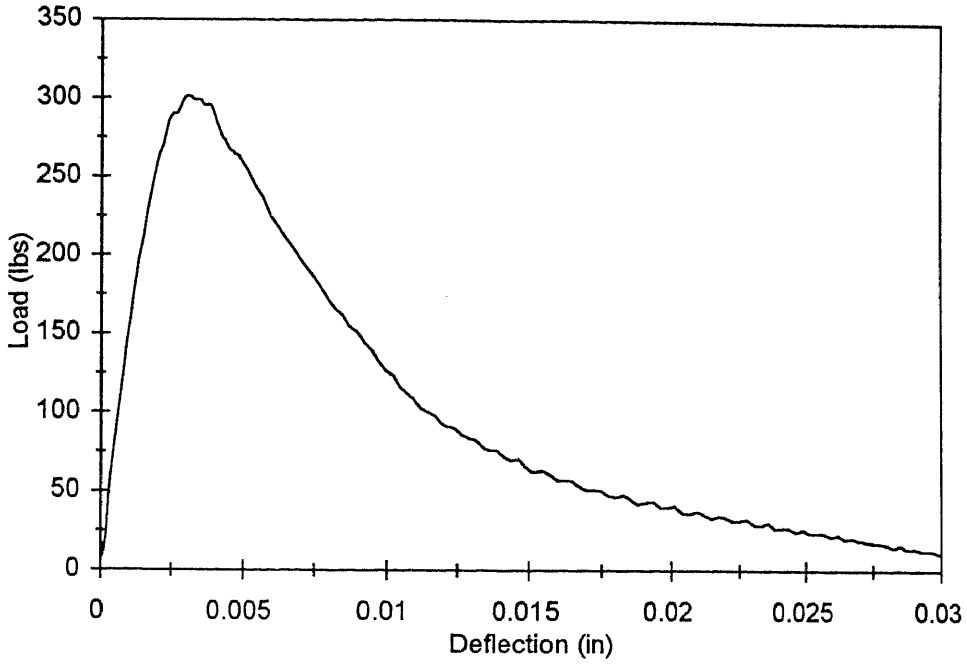

Figure C9c Load versus deflection for size C(T = 23°C, t = 3.0 days)

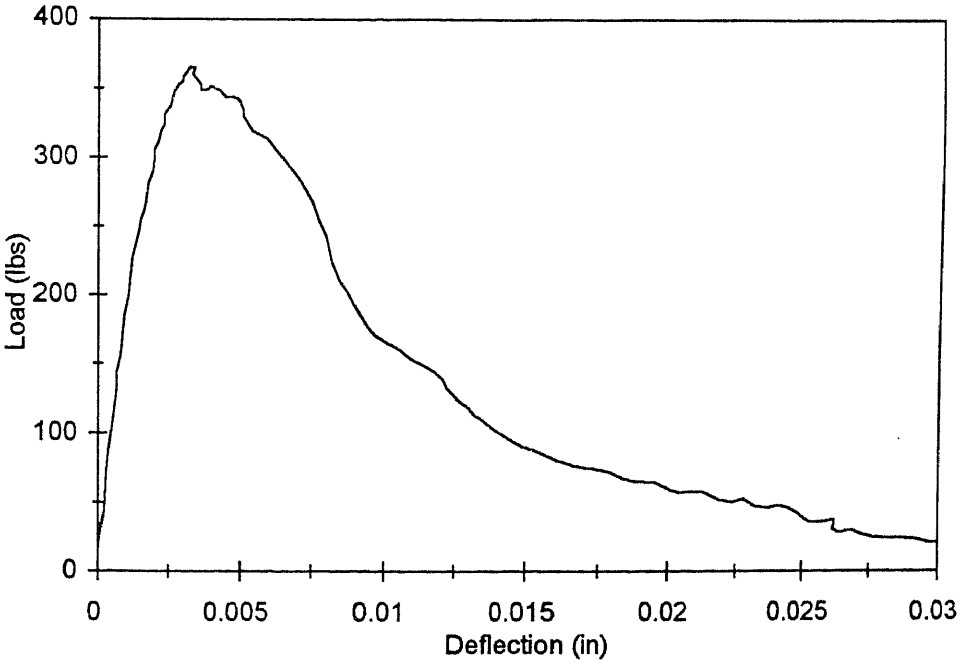

Figure C10a Load versus deflection for size C(T = 23°C, t = 7.0 days)

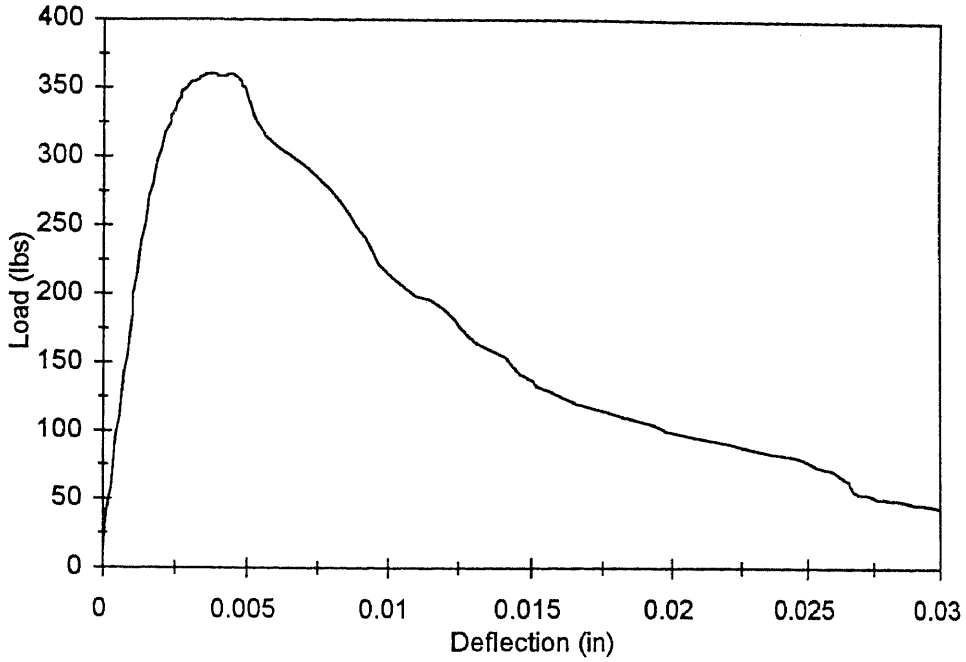

Figure C10b Load versus deflection for size C(T = 23°C, t = 7.0 days)

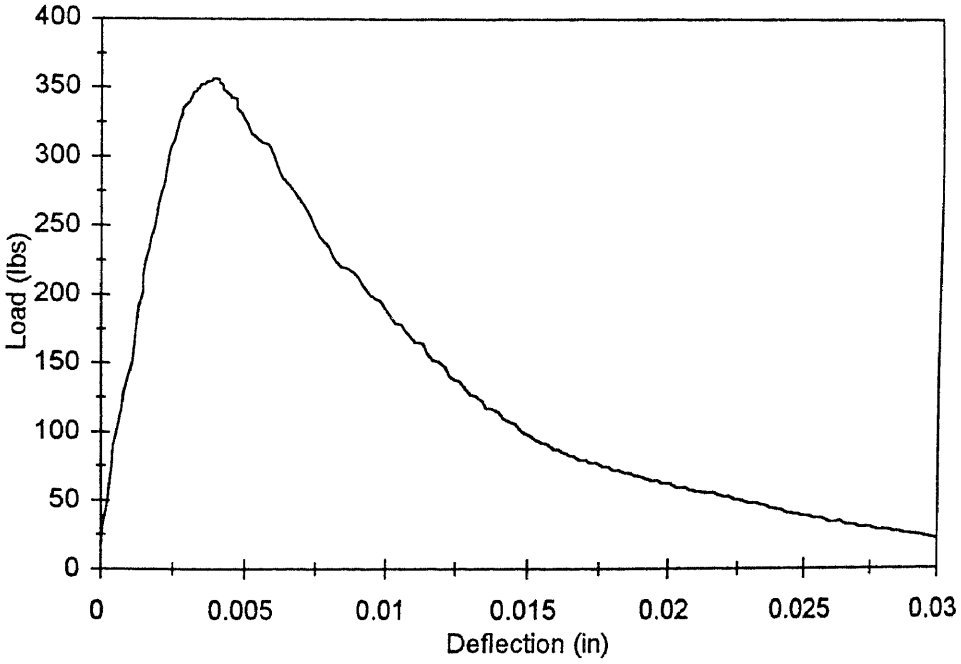

Figure C10c Load versus deflection for size C(T = 23°C, t = 7.0 days)

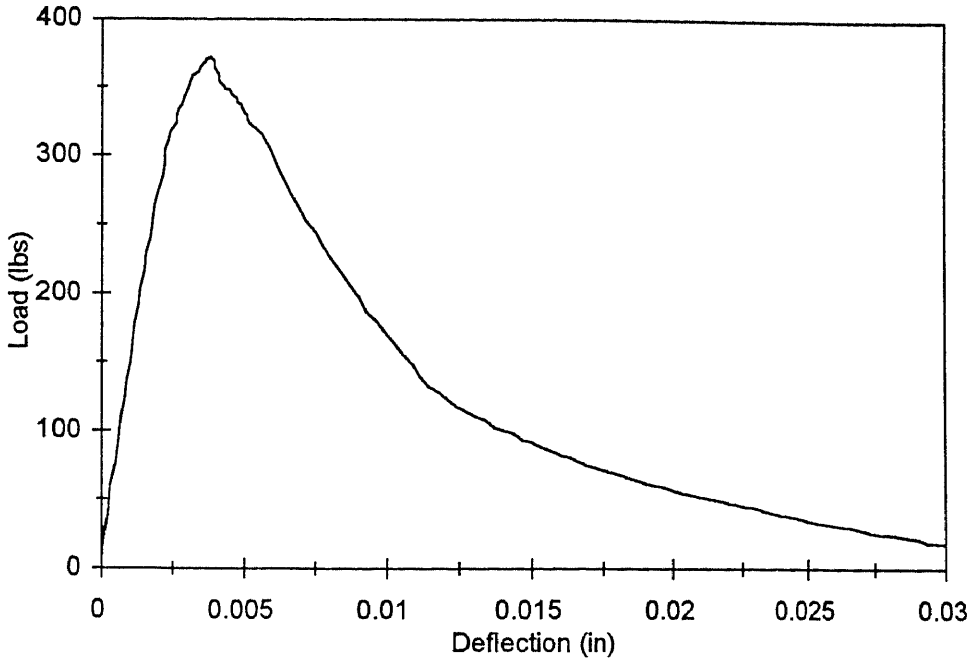

Figure C11a Load versus deflection for size C(T = 23°C, t = 14.0 days)

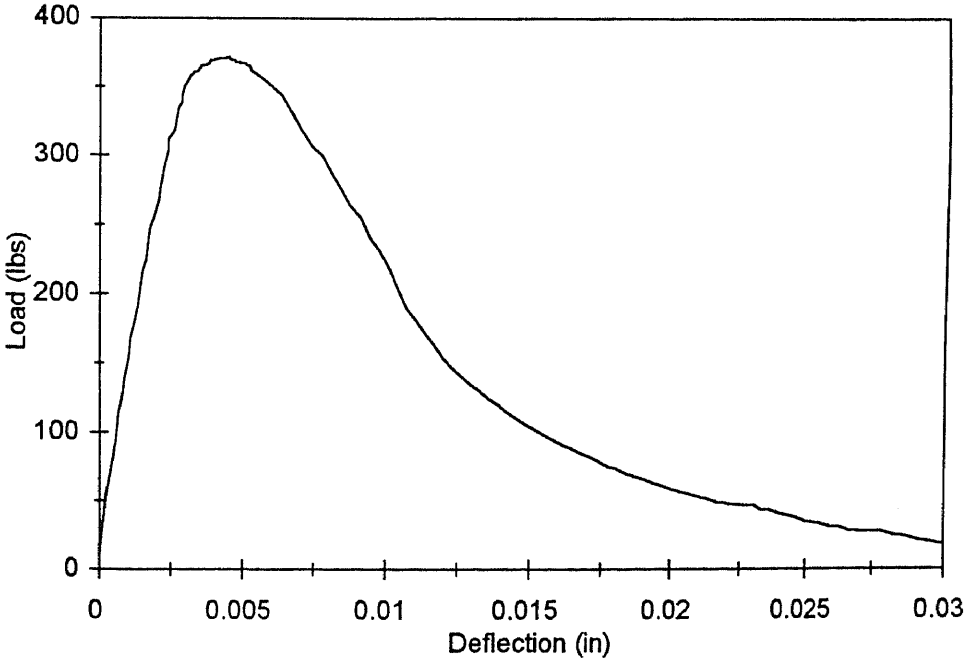

Figure C11b Load versus deflection for size C(T = 23°C, t = 14.0 days)

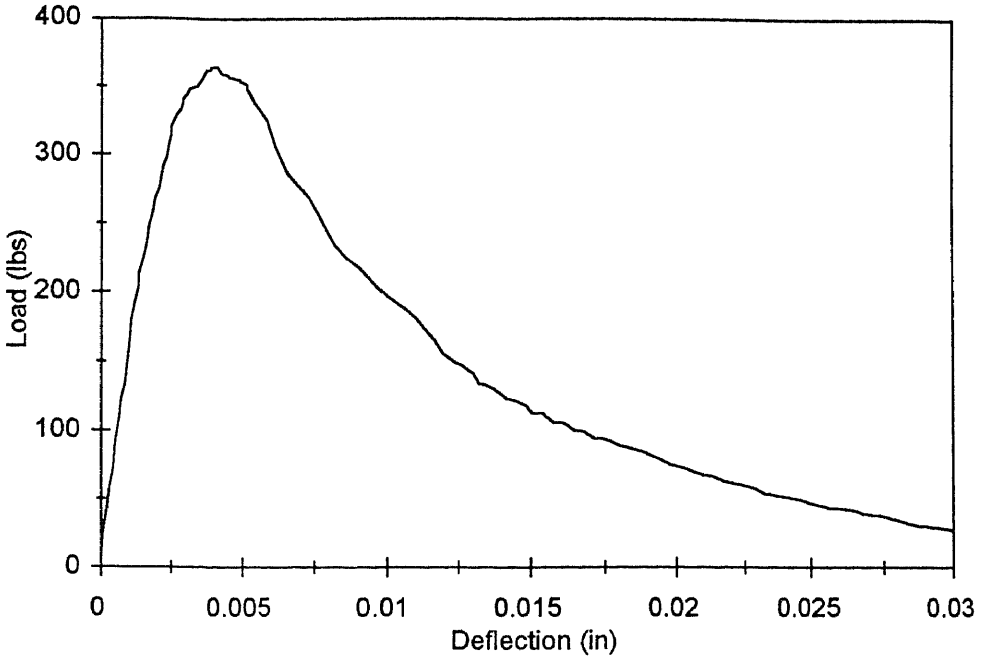

Figure C11c Load versus deflection for size C(T = 23°C, t = 14.0 days)

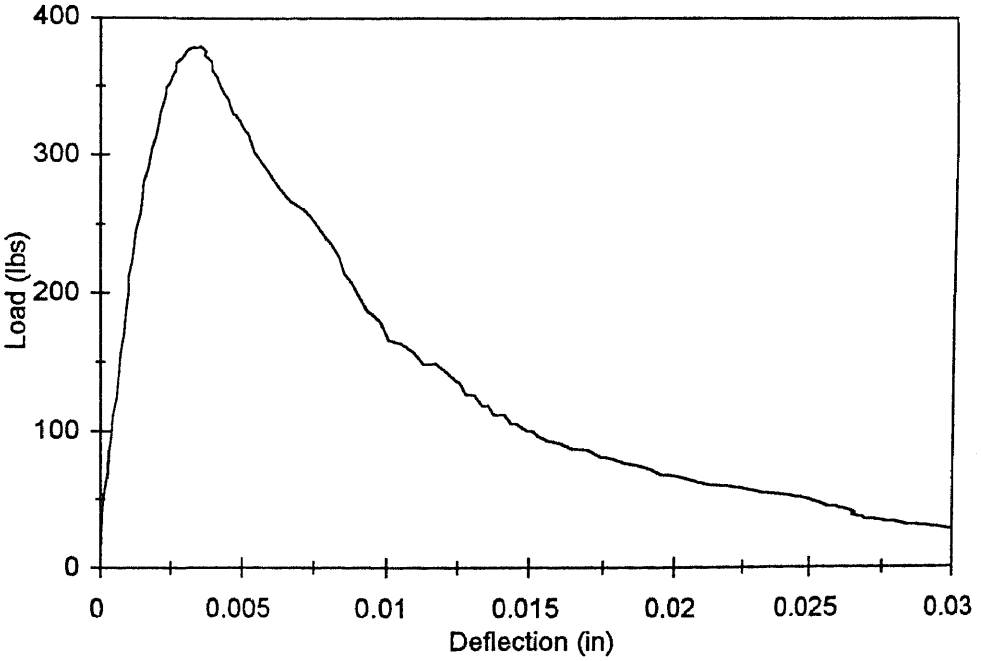

Figure C12a Load versus deflection for size C(T = 23°C, t = 28.0 days)

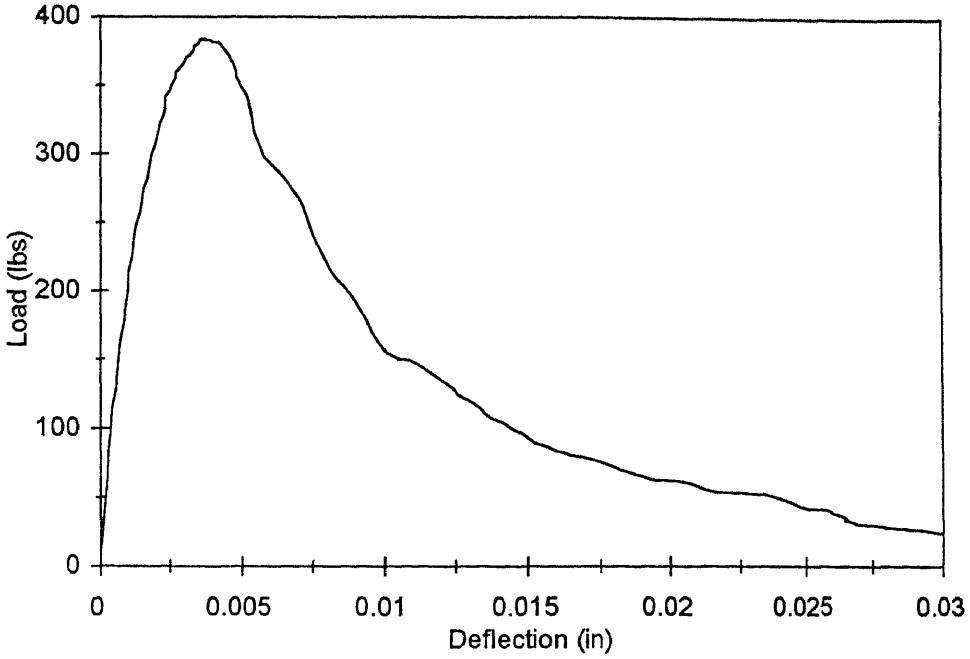

Figure C12b Load versus deflection for size C(T = 23°C, t = 28.0 days)

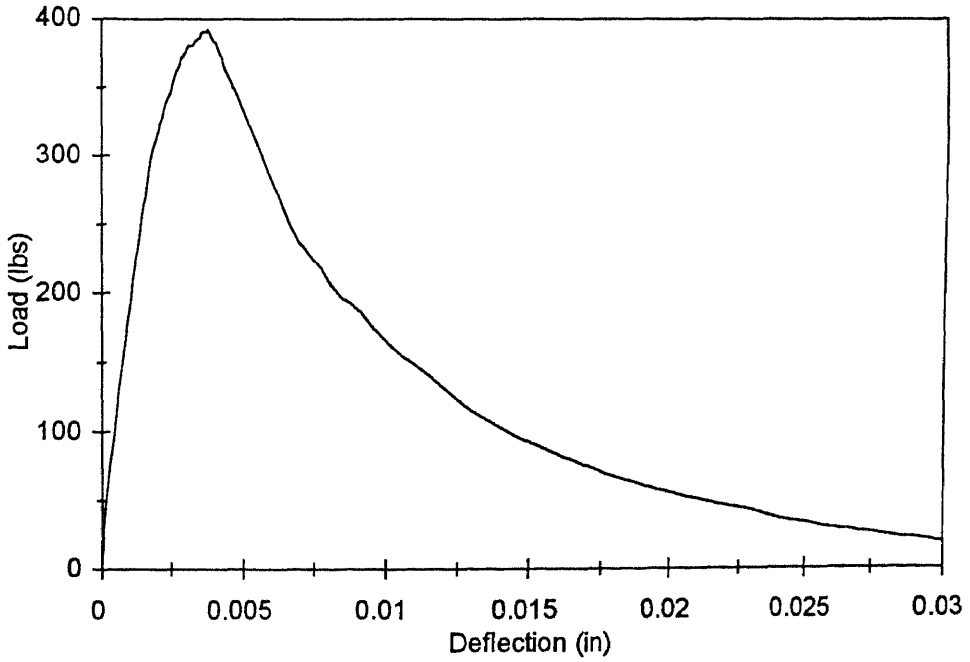

Figure C12c Load versus deflection for size C(T = 23°C, t = 28.0 days)

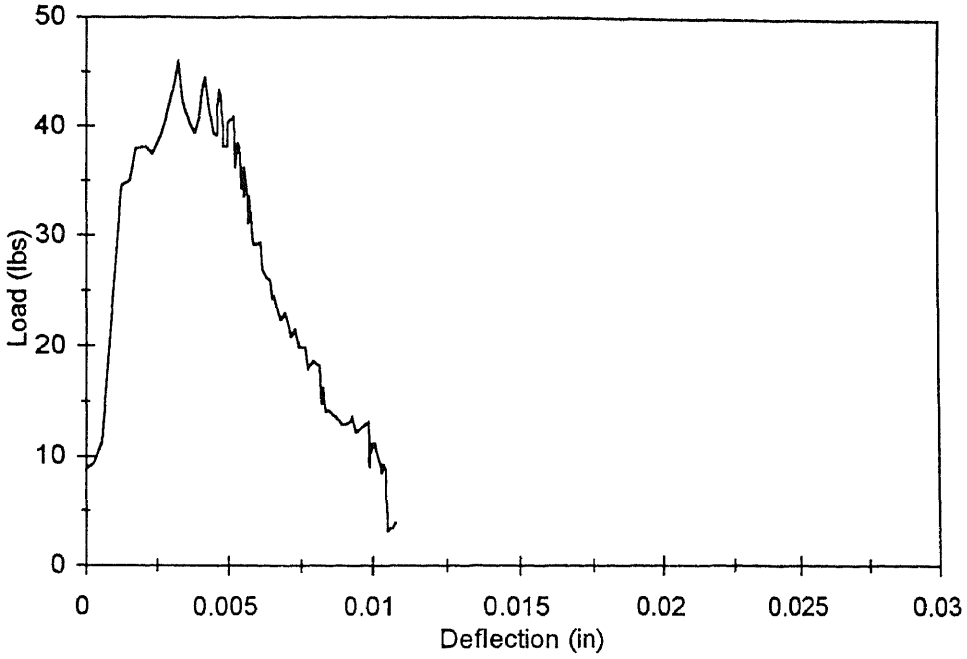

Figure C13a Load versus deflection for size C(T = 35°C, t = 0.29day)

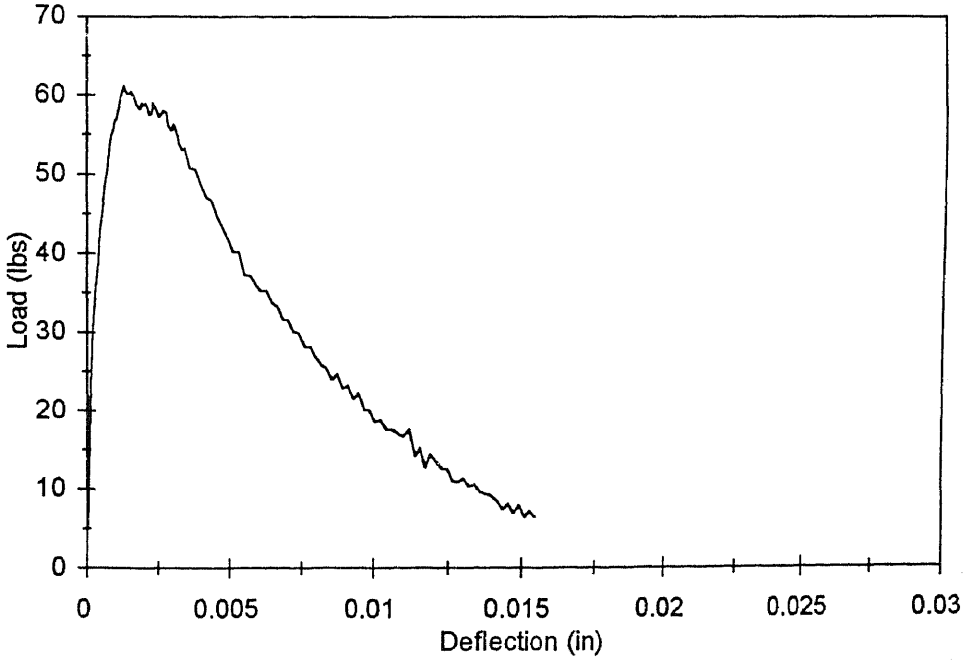

Figure C13b Load versus deflection for size C(T = 35°C, t = 0.29day)

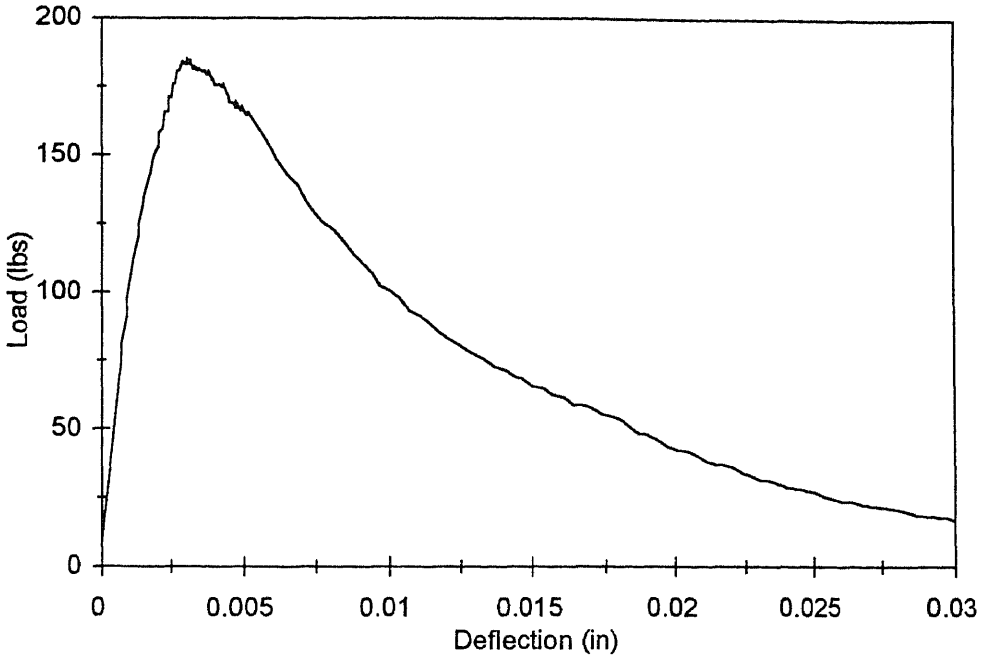

Figure C14a Load versus deflection for size C(T = 35°C, t = 0.51day)

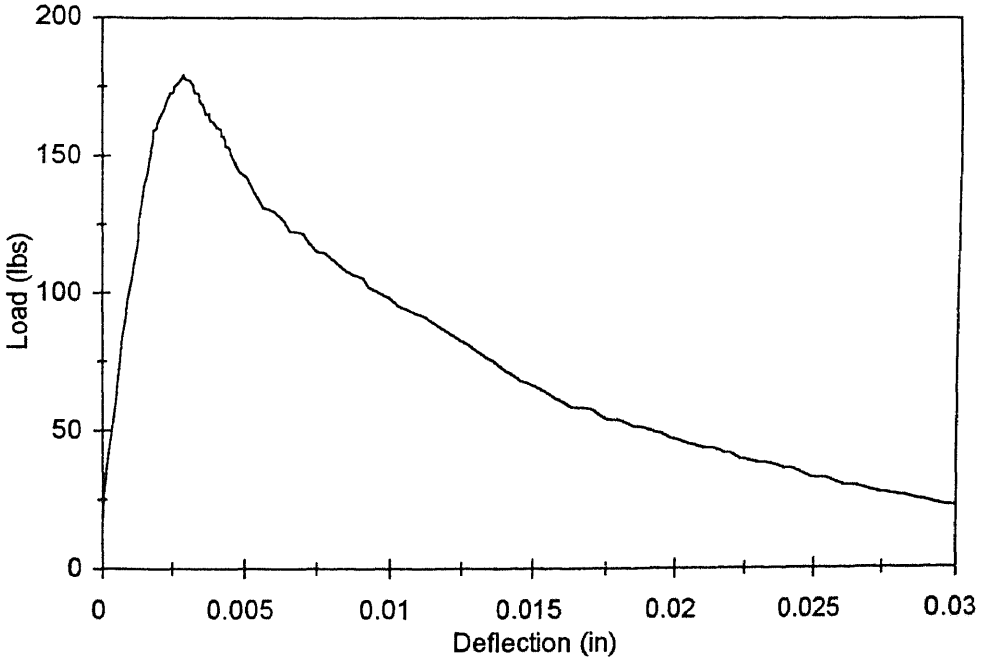

Figure C14b Load versus deflection for size C(T = 35°C, t = 0.51day)

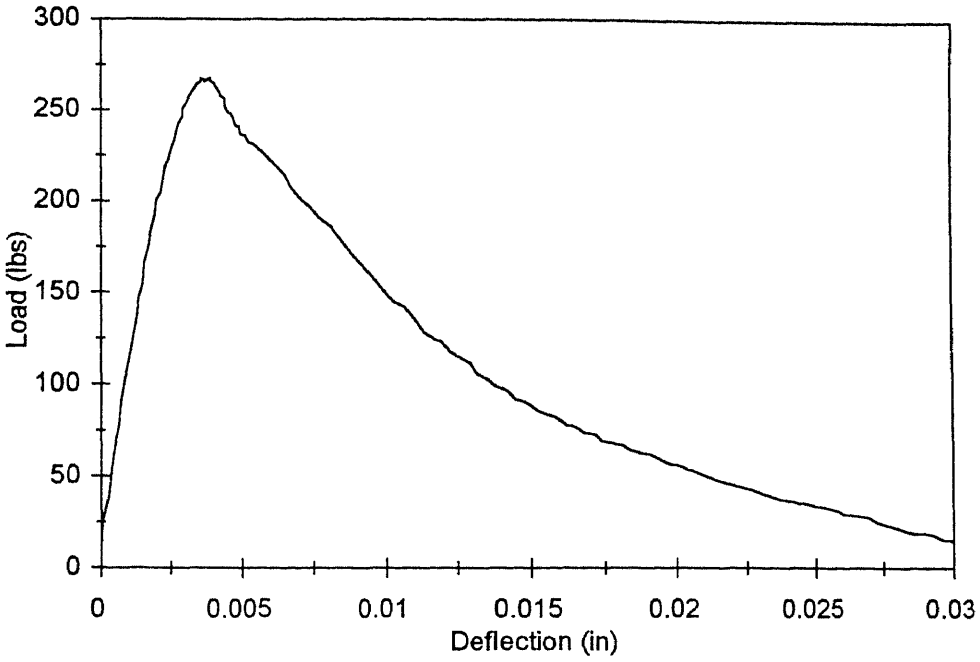

Figure C15a Load versus deflection for size C(T = 35°C, t = 1.03days)

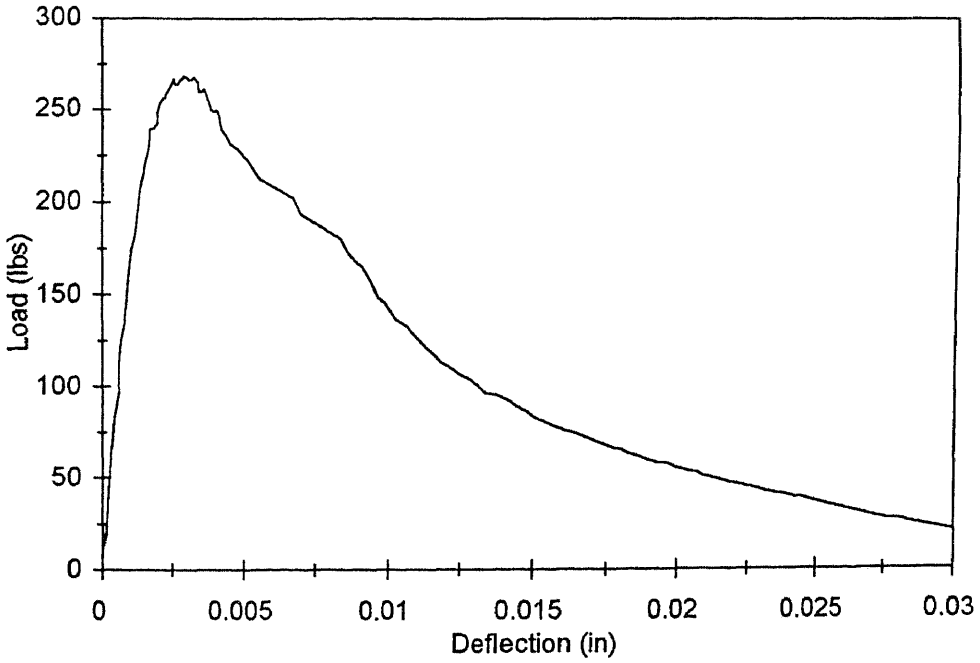

Figure C15b Load versus deflection for size C(T = 35°C, t = 1.03days)

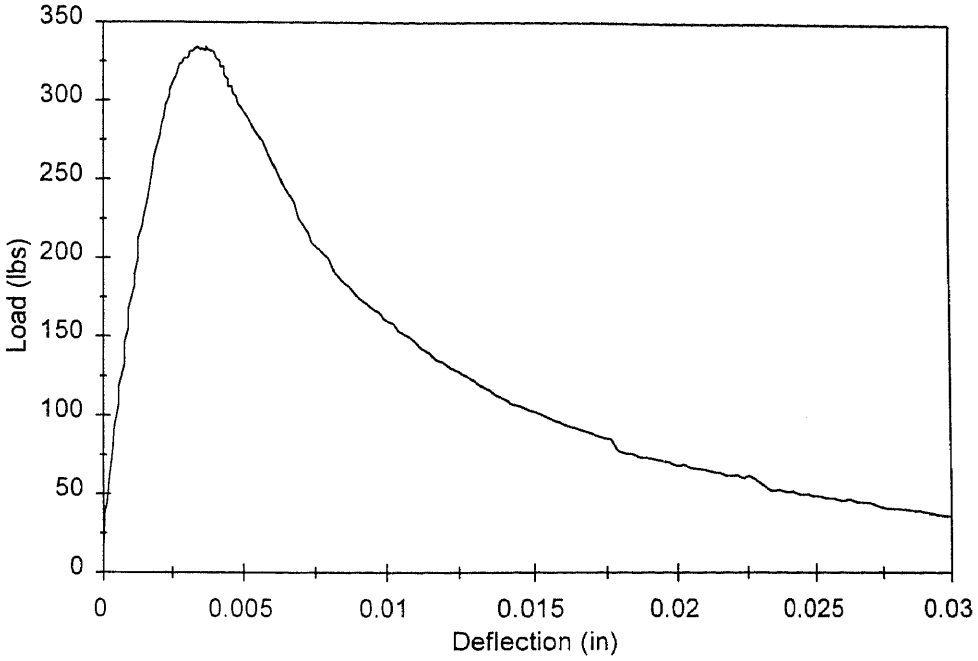

Figure C16a Load versus deflection for size C(T = 35°C, t = 4.28 days)

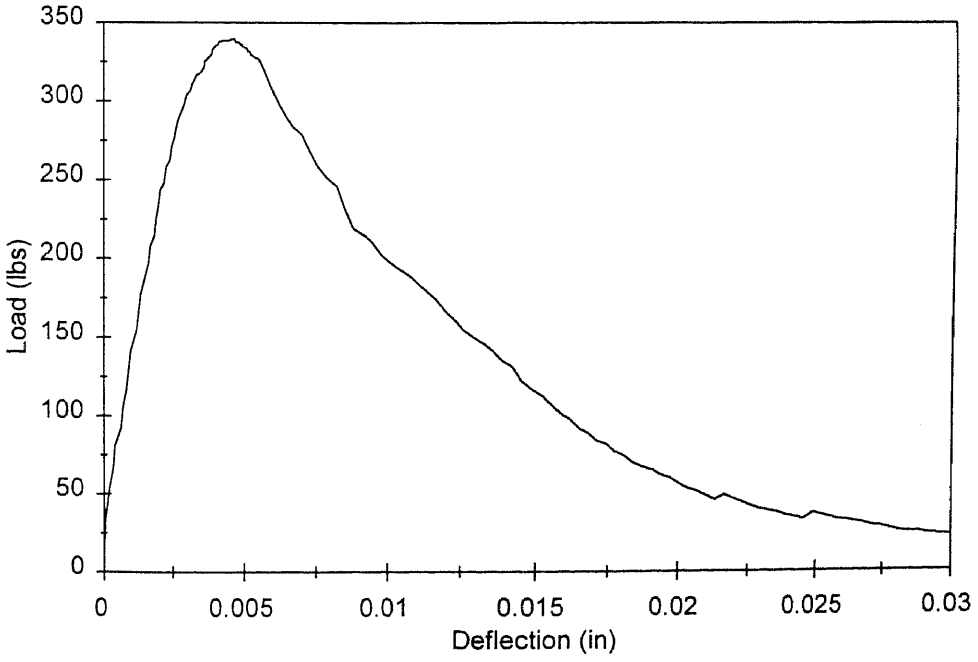

Figure C16b Load versus deflection for size C(T = 35°C, t = 4.28 days)

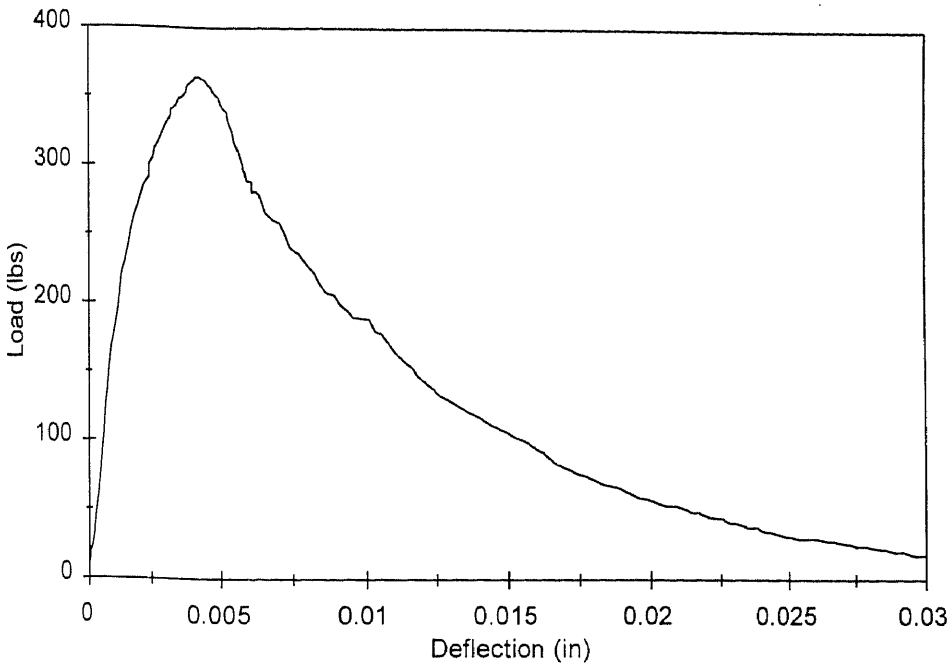

Figure C17a Load versus deflection for size C(T = 35°C, t = 9.0 days)

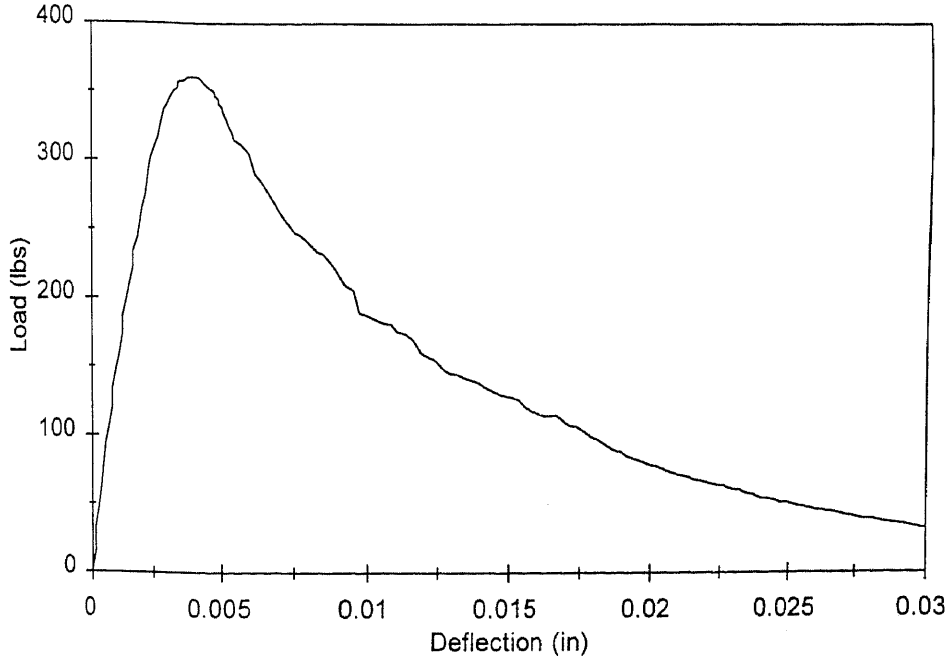

Figure C17b Load versus deflection for size C(T = 35°C, t = 9.0 days)

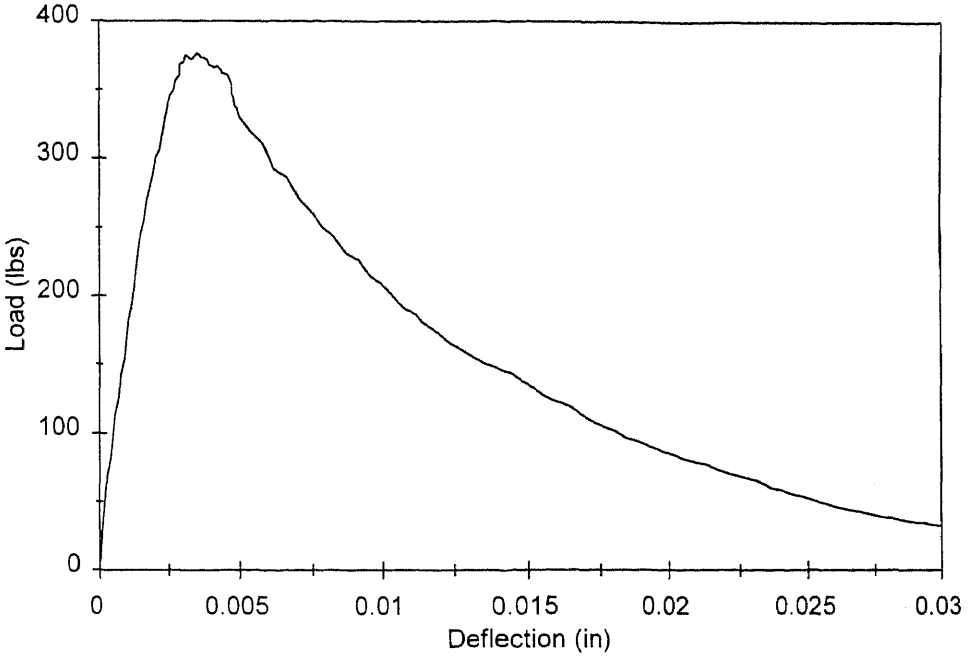

Figure C18a Load versus deflection for size C(T = 35°C, t = 23.01 days)

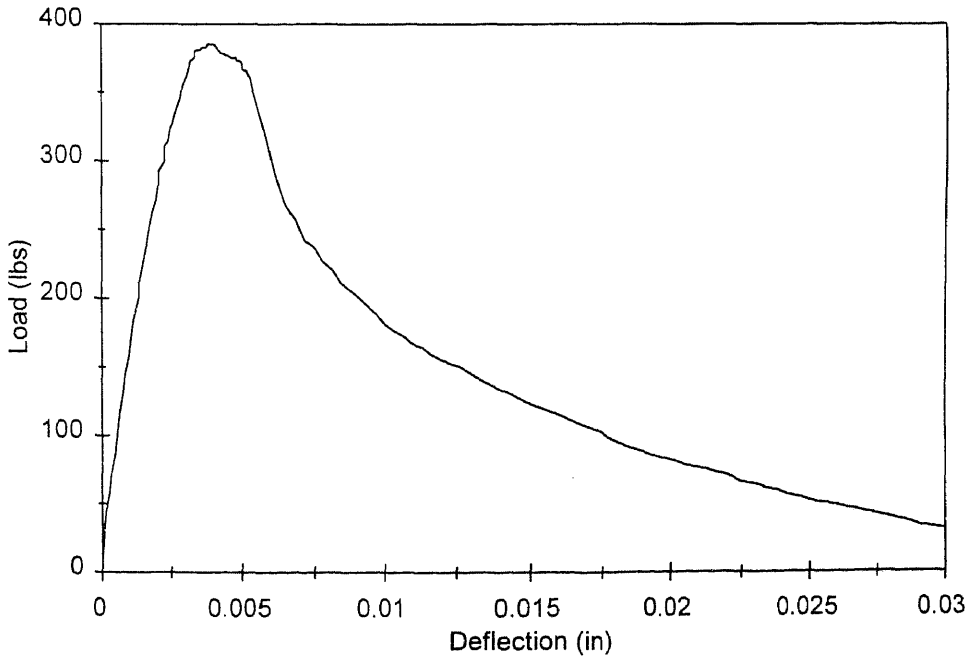

Figure C18b Load versus deflection for size C(T = 35°C, t = 23.01 days)

BIBLIOGRAPHY

ACI Committee 446 (1991), "Fracture Mechanics of Concrete: Concepts, Models and Determination of Material Properties", ACI, Box 19150, Redford Station, Detroit, MI 48219.

ACI Committee 209 (1971), "Prediction of Creep, Shrinkage, and Temperature Effects in Concrete Structures", SP-27, ACI, Box 19150, Redford Station, Detroit, MI, pp. 51-93.

Alexander, K. M., Taplin, J. H., and Wardlaw, J., (1968), "Correlation of strength and hydration with composition of protland cement", Proc. 5th Int. Symp. On the Chemistry of Cement, Cement Association of Japan, Tokyo, 1969, vol. III, 152.

Ananthan, H., Raghuprasad, B. K. and Sundararajaiyengar, K. T., (1990), " Influence of Strain Softening on the Fracture of Plain Concrete Beams", Cement and Concrete Research, vol. 45, pp. 195-219.

Ashby, M. F., and Jones, D. R. H., (1980), Energineering Materials 1 Engineering Department, Cambriege University, England, Pergamon Press, New York.

ASTM C 1074-87 (1989), "Practice for Estimating Concrete Strength by the Maturity Method", Annual Book of ASTM Standards, vol. 04.02 Concrete and Aggregates, pp. 517-523.

Bazant, Z. P. (1984), "Size Effect in Blunt Fracture: Concrete, Rock, Metal", Journal of The Engineering Mechanics Division, ASCE, vol. 110, no. 4, pp. 518-535.

Bazant, Z. P. and Kazemi, M. (1990), "Determination of Fracture Energy, Process Zone Length and Brittlemess Number from Size Effect, with application to rock and concrete", International Journal of Fracture, 44, pp. 111-131.

Bazant, Z. P. and Kazemi, M. (1991), "Size Dependence of Concrete Fracture Energy Determined by RILEM Work-of-Fracture Method", International Journal of Fracture, 51, pp. 121-138.

Bazant, Z. P., and Cedolin, L. (1979), "Blunt Crack Band Propagation in Finite Element Analysis", Journal of The Engineering Mechanics Division, ASCE, vol. 105, no. EM2, pp. 297-315.

Bazant, Z. P., Kim, J. K., and Pfeiffer, P., (1984), "Determination of Nonlinear Fracture Parameters From Size Effect Tests", Proceedings of MATO Advanced Workshop

on Application of Fracture Mechanics to Cementitious Composites, S. P. Shah, Ed., NATO-ARW, Northwesten University.

Bazant, Z. P.,and Oh, B. H. (1983), "Crack Band Theory for Fracture of Concrete", Materials and Structures, vol. 16, no. 93, pp. 155-177.

Bernhardt, C. J., (1956), "Hardening of Concrete at Different Temperatures", Proceedings of the RILEM Symposium on Winter Concreting, Copenhagen, Denmark.

Bocca, P. Carpinteri, A. and Valente, S. (1989), "Evaluation of Concrete Fracture Energy Through A Pull-Out Testing Procedure", Fracture of Concrete and Rock, Edited by S. P. Shah, S. E. Swartz and B. Barr, Elsevier Applied Science Publishers, pp. 347-356.

Brameshuber, W. and Hilsdorf, H. K. (1987), "Development of Strength and Deformability of Very Young Concrete", RILEM, International Conference on Fracture of Concrete and Rock, Houston, Texas, pp. 409-421.

Bresson, J. (1982), "Prediction of Strength of Concrete Products", Proceedings of the RILEM International Conference on Concrete at Early Ages, vol. 1 Paris, pp. 111-115.

Carino, N. J. and Lew, H. S., (1983), "Temperature Effects on Strength-Maturity Relations of Mortar", ACI Journal, Mo. 80-17, pp. 177-182.

Carino, N. J. and Tank, R. C. (1992), "Maturity Functions for Concrete Made with Various Cements and Admixtures ", ACI Materials Journal, vol. 89, no. 2, pp. 188-196.

Carino, N. J., Lew, H. S. and Volz, C. K. (1982), "Early Age Temperature Effects on Concrete Strength Prediction by the Maturity Method", Journal of the ACI, vol. 80, no. 2, pp. 92-101.

Carino, N. J.,(1981), "Temperature Effects on the Strength-Maturity Relation of Mortar", National Bureau of Standards, NBSIR 81-2244, Washington, D.C., pp. 98-121.

Carino, N. J.,(1982a), "Maturity Functions for Concrete", Proceedings of the RILEM International Conference on Concrete at Early Ages, vol. 1, Paris, pp. 123-128.

Carino, N. J.,(1982b), "Application of Maturity Concept to Form Removal and Reshoring Schedule", Proceedings of International Conference on Forming Economical Concrete Builelngs, Portland Cement Association, Skokie, Il, pp. 8.1-8.19.

Carino, N. J.,(1984), "Maturity Method : Theory and Application", Journal of Cement, Concrete, and Aggregates, ASTM, vol. 6, no. 2, pp. 61-73.

Carpinteri, A. (1991), "Size-Scale Transition from Ductile to Brittle Failure: Structural Response vs. Crack Growth Resistance Curve", International Journal of Fracture, 51, pp. 175-186.

Carpinteri, A. , Colombo, G. , Ferrara, G. and Giuseppetti, G. (1987), "Numerical Simulation of Concrete Fracture Through A Bilinear Softening Stress-Crack Opening Displacement Law", Fracture of Concrete and Rock, Edited by S. P. Shah and S. E. Swartz, Springer-Verlag Publishers, pp. 131-141.

Gauthier,E. and Regourd, M. (1982), "The Hardening of Cement in Function of Temperature", Proceedings of the RILEM International Conference on Concrete at Early Ages, vol. 1, Paris, pp. 145-150.

Geiker, M. And Knudsen, T., (1982), "Chemical shrinkage of portland cement pastes" Cement and Concrete Research, 12 (5), 603.

Geiker, M., (1983), "Studies of Portland Cement Hydration by Measurements of Chemical Shrinkage and Systematic Evaluation of Hydration Curves by Means of the Dispersion Model" Ph.D. Dissertation, Technical University of Denmark.

Gjørv, O.E.,Sørensen, S.I. and Arnesen, A. (1977) "Notch Sensitivity and Fracture Toughness of Concrete" Cement and Concrete Research, vol. 7, pp. 333-344.

Gjørv, O.E.,Sørensen, S.I. and Arnesen, A. (1978) "A Discussion of the Paper "Notch Sensitivity and Fracture Toughness of Concrete"" Cement and Concrete Research, vol. 8, pp. 387-388.

Gopalaratnam, V. S. and Shah, S. P., (1985), " Softening Response of Plain Concrete in Direct Tension " ACI Journal, no. 82-27, pp. 310-323.

Goral, M. L., (1956), "Empirical Time-Strength Relations of Concrete", ACI Journal, vol. 53, no. 2, pp. 215-224.

Hansen, A. J. (1981), "COMA-Meter - The Mini Maturity Meter", Nordisk Betong.

Hillerborg, A. (1983), "Analysis of One Single Crack" Fracture Mechanics of Concrete, Edited by Wittmann, F. H., pp. 223-249.

Hillerborg, A. (1985a), "The Theoretical Basis of A Method to Determine the Fracture Energy G_f of Concrete" Materials and Structures, vol. 18, no. 106, pp. 291-296.

Hillerborg, A. (1985b), "Results of Three Comparative Test Series for Determining the Fracture Energy G_f of Concrete" Materials and Structures, vol. 18, no. 107, pp. 407-413.

Hillerborg, A. (1986), "Dimensionless Presentation And Sensitivity Analysis in Fracture Mechanics" Fracture Toughness and Fracture Energy of Concrete, Edited by Wittmann, F. H., pp. 413-421.

Hillerborg, A., Modèer, M. and Petersson, P. E. (1976), "Analysis of Crack Formation and Crack Growth in Concrete by means of Fracture Mechanics and Finite Elements" Cement and Concrete Research, vol. 6, pp. 773-782.

Hilsdorf, H. K. and Brameshuber, W. (1991), "Code-Type Formulation of Fracture Mechanics Concepts for Concrete", International Journal of Fracture, 51, pp. 61-72.

Irwin, G.R., (1958), " Fracture " Handbuch der Physik, vol. VI, ed. Fougge, Springer, pp. 551-590.

Jenq, Y.S. and Shah, S.P. (1984), "Nonlinear Fracture Parameters For Cement Based Composites: Theory and Experiments " Application of Fracture Mechanics to Cementitious Composites, Proceedings of NATO Advanced Workshop on Application of Fracture Mechanics to Cementitious Composites, S. P. Shah, Ed., pp. 319-359.

Jenq, Y.S. and Shah, S.P. (1985a), "A Fracture Toughness Criterion For Concrete" Engineering Fracture Mechanics, vol. 21, no. 5, pp. 1055-1069.

Jenq, Y.S., and Shah, S.P. (1985b), "Two Parameter Fracture Model for Concrete" Journal of Engineering Mechanics, ASCE, vol. 111, no. 10, pp. 1227-1241.

Kaplan, M. F., (1961), "Crack Propagation and the Fracture of Concrete", ACI J., vol. 58, no. 11, pp. 591-610.

Karihaloo, B. L. and Nallathambi, P. (1989), "Fracture Toughness of Plain Concrete from Three-Point Bend Specimens", Materials and Structures, 22, pp. 185-193.

Karihaloo, B. L. and Nallathambi, P. (1990), "Size-Effect Prediction from Effective Crack Model for Plain Concrete", Materials and Structures, 23, pp. 178-185.

Kasai, Y. (1982), "Method of Estimation for Compressive Strength of Concrete at Early Ages", Proceedings of the RILEM International Conference on Concrete at Early Ages, vol. 1 Paris, pp. 157-162.

Knudsen, T., (1980), "On particle size distribution in cement hydration" Proc, 7th Int. Congr. On the Chemistry of Cement, Editions Septima, Paris, vol. II, 170.

Knudsen, T., (1982), "Modelling hydration of portland cement: the effects of particle size distribution" Proc. Engineering Foundation Conf. on Characterization and Performance Prediction of Cement and Concrete, Henniker, NH, 125.

Lew, H. S., and Richard, T. W., (1978a), "Mechanical Properties of Concrete at Early Ages", Journal of the American Concrete Institute, vol. 75, no. 10, pp. 533-542.

Lew, H. S., and Richard, T. W., (1978b), "Prediction of Strength of Concrete from Maturity", SP-56, American Concrete Institute, Detroit, MI. pp. 229-248.

Li, Y. N. and Liang, R. Y., (1991), " Stability Theory of Cohesive Crack Model " Journal of Engineering Mechanics, ASCE, vol.118, no. 3, pp. 587-603.

Llorca, J. L. and Elices, M. (1990), "A Simplified Model to Study Fracture Behaviour in Cohesive Materials", Cement and Concrete Research, vol. 20, pp. 92-102.

Llorca, J. Planas, J. and Elices, M. (1989), "On The Use of Maximum Load To Validate or Disprove Models of Concrete Fracture Behaviour", Fracture of Concrete and Rock, Edited by S. P. Shah, S. E. Swartz and B. Barr, Elsevier Applied Science Publishers, pp. 357-368.

Malhotra, V. M., (1971), " Maturity Concept and the Estimation of Concrete Strength " Information Circular IC 277, Department of Energy, Mines and Resources (Canada), Mines Branch, pp. 43-57.

Malhotra, V. M., (1984), In-situ / Nondestructive Testing of Concrete- A Global Review , ACI SP-82.

Malhotra, V. M. and Carino, N.J., (1991), CRC Handbook on Nondestructive Testong of Concrete

Malvar, L. J., and Warren, G. E. (1988), "Fracture Energy for Three-Point-Bend Tests on Single-Edge-Notched Beams Experimental Mechanics, pp. 266-272.

Mazars, J. Pijaudier-Cabot, G. and Saouridis, C. (1991), "Size Effect and Continuous Damage in Cementitious Materials", International Journal of Fracture, 51, pp. 159-173.

McIntosh, J. D. (1949), "Electrical Curing of Concrete", Magazine of Concrete Research, vol. 1, no. 1, pp. 21-28.

Mihashi, H., Normura, N. and Niiseki, S. (1991), " Influence of Aggregate Size on Fracture Process Zone of Concrete Detected with Three Dimensional Acoustic Emission Technique " Cement and Concrete Research, vol. 21, pp. 737-744.

Mindess Sidney, (1976), "Effect of Notch Width on K_{IC} for Mortar and Concrete" Cement and Concrete Research, vol. 6, pp. 529-534.

Modèer, M, (1979), "A Fracture Mechanics Approch to Failure Analyses of Concrete Matreials", Report TVBM-1001, University of Lund, pp. 120-135.

Nallathambi, P. and Karihaloo, B. L. (1986), "Prediction of Load-Deflection Behavior of Plain Concrete from Fracture Energy" Cement and Concrete Research, vol. 16, pp. 373-382.

Nallathambi, P. and Karihaloo, B. L. (1986), "Prediction of Load-Deflection Behavior of Plain Concrete from Fracture Energy" Cement and Concrete Research, vol. 16, pp. 373-382.

Normura, N., Mihashi, H. and Izumi, M. (1991), "Correlation of Fracture Process Zone and Tension Softening Behavior in Concrete" Cement and Concrete Research, vol. 21, pp. 545-550.

Nurse, R. W. (1949), "Steam Curing of Concrete", Magazine of Concrete Research, vol. 1, no. 2, pp. 79-88.

Oh, B. H. (1987), "Fracture Characteristics of Concrete under Static Loading", Fracture of Concrete and Rock, Edited by S. P. Shah and S. E. Swartz, Springer-Verlag Publishers, pp. 433-441.

Perdikaris, P. C. and Romeo, A., (1992), "Effect of Size and Compressive Strength on the Fracture Energy of Plain Concrete" 1st International Conference on Fracture Mechanics of Concrete Structures, Breckenridge, Colorado.

Petersson, P. E. (1980a), "Fracture Energy of Concrete: Method of Determination", Cement and Concrete Research, vol. 10, no. 1, pp. 79-89.

Petersson, P. E. (1980b), "Fracture Energy of Concrete: Practical Performance And Experimental Results" Cement and Concrete Research, vol. 10, no. 1, pp. 91-101.

Petersson, P. E. (1981), "Crack Growth and Formation of Fracture Zone in Plain Concrete and Similar Materials" Div. of Building Mat., Lnd Inst. of Tech., Report TVBM- 1006.

Planas, J. and Elices, M. (1991), "Nonlinear Fracture of Cohesive Materials", International Journal of Fracture, 51, pp. 139-157.

Portland Cement Association, (PCA), (1988), Design and Control of Concrete Mixtures, 13th Edition, pp. 131-133.

Refai, M. E., and Swartz, S. E. (1988), "Mode I Fracture-Energy Methods for Concrete", Experimental Mechanics, pp. 395-401.

Regourd, M., (1980a), "Structure and behavior of slag portland cement hydrates", Proc. 7th Int. Congr. On the Chemistry of Crment, Paris, Editions Septima, vol. I.

Regourd, M., Mortureux, B., Gauthier, E., Hormain, H., and Volant, J., (1980b), "Characterization and thermal activation of slag cements", Proc. 7th Int. Congr. On the Chemistry of Crment, Paris, Editions Septima, vol. III.

RILEM Commission 42-CEA, (1981), "Properties of Set Concrete at Early Ages, State-of-the-Art-Report", Materials and Structures, vol. 14, no. 84, pp. 399-450.

RILEM DRAFT RECOMMENDATIONS (1985), "Determination of The Fracture Energy of Mortar and Concrete by means of Three-Point Bend Tests on Notched Beams "Materials and Structures, vol. 18, no. 106, pp. 285-290.

RILEM DRAFT RECOMMENDATIONS TC 89-FMT, (1990), "Determination of Fracture Parameters (K_{Ic}^{S} and $CTOD_C$) of Plain Concrete Using Three-Point Bend Tests", Materials and Structures, 23, pp. 457-460.

RILEM DRAFT RECOMMENDATIONS TC 89-FMT, (1990), "Size-Effect Method for Determining Fracture Energy and Process Zone Size of Concrete", Materials and Structures, 23, pp. 461-465.

Roy, D. M. And Idorn, G. M., (1982), " Hydration, Structure, and Properties of Blast Furnace Slag Cements, Mortars and Concrete", Journal of the American Concrete Institute, vol. 79, no. 6, Nov.-Dec. pp. 444-457.

Saul, A. G. (1951), "Principles Underlying the Steam Curing of Concrete at Atmospheric Pressure", Magazine of Concrete Research, vol. 2, no. 6, pp. 127-140.

Seki, S., Kasahara, K., Kuriyama, T., and Kawasumi, M., (1968), "Effects of hydration of cement of compressive strength, modulus of elasticity and creep of concrete", Proc. 5th Int. Symp. On the Chemistry of Cement, Cement Association of Japan, Tokyo, 1969, vol. III, 175.

Shah, S. P., ASCE, A. M. and McGarry, F. J., (1971), " Griffith Fracture Criterion and Concrete ", Journal of the Engineering Mechanics Division , Proceedings of the American Society of Civil Engineers, EM 6, pp. 1663-1676.

Tang, T. Shah, S. P. and Ouyang, C. (1992), "Fracture Mechanics and Size Effect of Concrete in Tension", Journal of Structural Engineering, vol. 118, No, 11, pp. 3169-3185.

Tank, R. C. and Carino, N. J. (1991), "Rate Constant Functions for Strength Development of Concrete", ACI Materials Journal, vol. 88, no. 1, pp. 74-83.

Tank, R. C., (1988), "Rate Constant Model for Strength Development of Concrete", Ph.D. Dissertation, Polytechnic University of New York.

Tada, H., Paris, P. and Irwin, G., (1985), The Stress Analysis of Cracks Handbook, Del Research Corporation, Hellertown, Pennsylvania.

Wittmann, F. H., Roelfstra, P. E., and Mihashi, H., (1987), "Influence of age of loading, water-cement ratio and rate of loading on fracture energy of concrete" Materials and Structures, 20, pp. 103-110.

Ziegeldorf, S., Müller, H. S. and Hilsdorf, H. L., (1980), "A Model Law for the Notch Sensitivity of Brittle Materials "Cement and Concrete Research, vol. 10, pp. 589-599.